Government of Western Australia

Department of
Mines and Petroleum

REPORT
106

GEOCHEMISTRY, GEOCHRONOLOGY, AND PETROGENESIS OF MESOPROTEROZOIC FELSIC ROCKS IN THE WEST MUSGRAVE PROVINCE, CENTRAL AUSTRALIA, AND IMPLICATIONS FOR THE MESOPROTEROZOIC TECTONIC EVOLUTION OF THE REGION

by RH Smithies, HM Howard, PM Evins, CL Kirkland, DE Kelsey, M Hand, MTD Wingate, AS Collins, E Belousova and S Allchurch

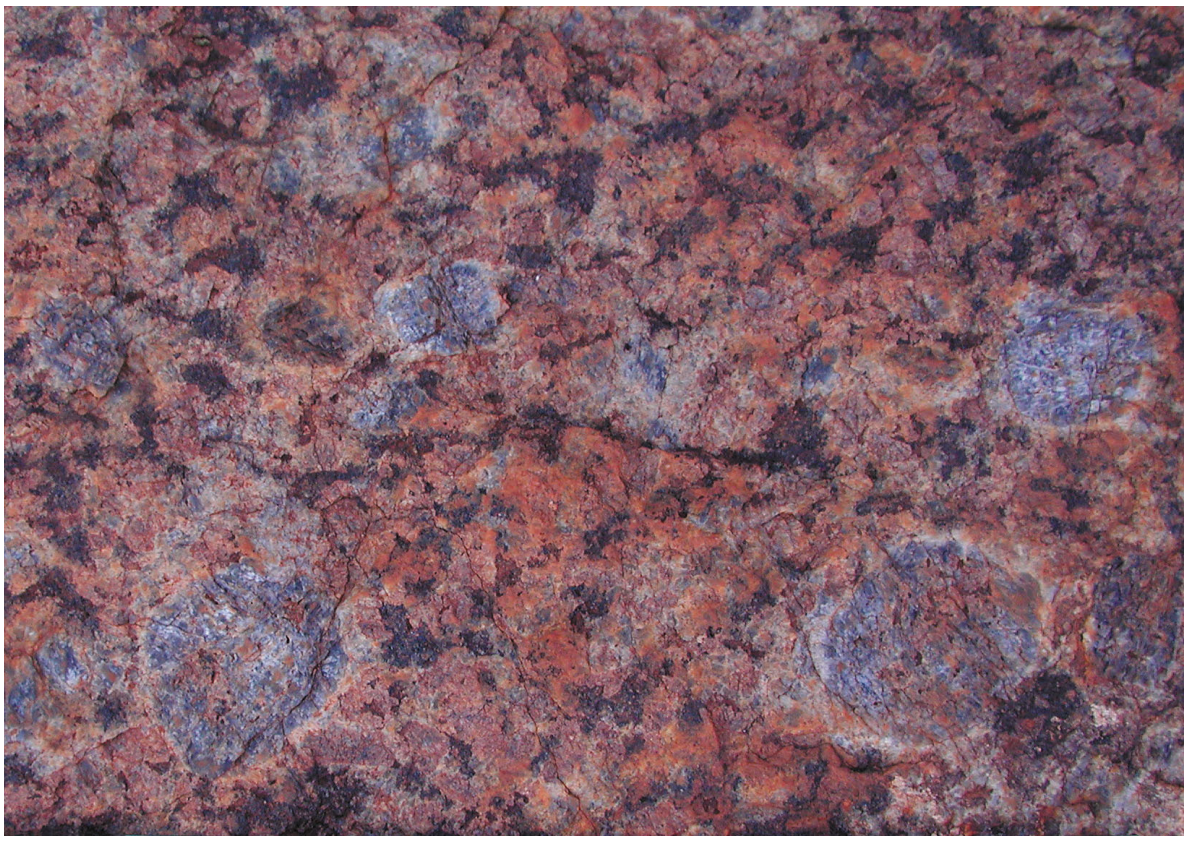

Geological Survey of Western Australia

Government of **Western Australia**
Department of **Mines and Petroleum**

REPORT 106

GEOCHEMISTRY, GEOCHRONOLOGY,AND PETROGENESIS OF MESOPROTEROZOIC FELSIC ROCKS IN THE WEST MUSGRAVE PROVINCE, CENTRAL AUSTRALIA, AND IMPLICATIONS FOR THE MESOPROTEROZOIC TECTONIC EVOLUTION OF THE REGION

by
RH Smithies, HM Howard, PM Evins, CL Kirkland, DE Kelsey[1], M Hand[1], MTD Wingate, AS Collins[1], E Belousova[2] and S Allchurch[2]

[1] **Tectonics, Resources and Exploration Group, School of Earth and Environmental Sciences, University of Adelaide**
[2] **GEMOC, Department of Earth and Planetary Sciences, Macquarie University**

Geological Survey of Western Australia

NGAANYATJARRA COUNCIL (Aboriginal Corporation)

MINISTER FOR MINES AND PETROLEUM
Hon. Norman Moore MLC

DIRECTOR GENERAL, DEPARTMENT OF MINES AND PETROLEUM
Richard Sellers

EXECUTIVE DIRECTOR, GEOLOGICAL SURVEY OF WESTERN AUSTRALIA
Tim Griffin

REFERENCE
The recommended reference for this publication is:
Smithies, RH, Howard, HM, Evins, PM, Kirkland, CL, Kelsey, DE, Hand, M, Wingate, MTD, Collins, AS, Belousova, E and Allchurch, S 2010, Geochemistry, geochronology, and petrogenesis of Mesoproterozoic felsic rocks in the west Musgrave Province, central Australia, and implications for the Mesoproterozoic tectonic evolution of the region: Geological Survey of Western Australia, Report 106, 73p.

National Library of Australia
Cataloguing-in-publication entry

Smithies, RH
Geochemistry, geochronology, and petrogenesis of Mesoproterozoic felsic rocks in the west Musgrave Province, Central Australia, and implications for the Mesoproterozoic tectonic evolution of the region

Bibliography.
ISBN 978 174168 292 2 (pdf)

1. Geochemistry — Australia
2. Geological time
3. Petrogenesis — Australia
4. Australia, Central
I. Geological Survey of Australia
II. (Report. (Series: Report (Geological Survey of Western Australia; Online); 106).

Includes bibliographical references

551.9

ISSN 0508–4741

Grid references in this publication refer to the Geocentric Datum of Australia 1994 (GDA94). Locations mentioned in the text are referenced using Map Grid Australia (MGA) coordinates, Zone 50. All locations are quoted to at least the nearest 100 m.

Copy editor: NS Tetlaw
Cartography: SN Dowsett
Desktop publishing: KS Noonan

Published 2010 by Geological Survey of Western Australia
This Report is published in digital format (PDF)and is available online at www.dmp.wa.gov.au/GSWApublications.
Laser-printed copies can be ordered from the Information Centre for the cost of printing and binding.

Further details of geological publications and maps produced by the Geological Survey of Western Australia are available from:
Information Centre
Department of Mines and Petroleum
100 Plain Street
EAST PERTH, WESTERN AUSTRALIA 6004
Telephone: +61 8 9222 3459 Facsimile: +61 8 9222 3444
www.dmp.wa.gov.au/GSWApublications

Cover photograph:
Rapakivi granite from the Pitjantjatjara Supersuite, on central Bates (MGA 481452E, 7154472N)

Summary

The east-trending Musgrave Province, in central Australia, lies at the convergence of the Proterozoic structural trends which ultimately reflect the Mesoproterozoic amalgamation of the North, West, and South Australian Cratons. The province is dominated by felsic rocks formed, and metamorphosed, during several distinct events within the late Mesoproterozoic. These events correspond to global Grenvillian events and include the 1345–1293 Ma Mount West Orogeny (Wankanki Supersuite), the 1220–1150 Ma Musgrave Orogeny (Pitjantjatjara Supersuite), and the >1078–1026 Ma Giles Event (Warakurna Supersuite). All of these felsic rocks, irrespective of age, were derived from an isotopically and compositionally similar and regionally homogeneous source of basaltic to andesitic bulk composition, which included a felsic component containing material of both Mesoproterozoic and Archean age. Despite a similar source, the compositions of granites from each supersuite differ significantly. Different geographical distribution patterns for these supersuites are also consistent with the recent subdivision of the Musgrave Province, in Western Australia (i.e. the west Musgrave Province), into three zones; the Walpa Pulka Zone, Mamutjarra Zone, and the Tjuni Purlka Tectonic Zone.

Protoliths to rocks of the Wankanki Supersuite comprised hornblende–clinopyroxene–biotite granites (tonalite to syenogranite) that were metaluminous and calcic to calc-alkalic with close compositional similarities to Phanerozoic subduction-related granites of the Andean continental arc. These dominate the bedrock geology of the southwestern part of the west Musgrave Province (the Mamutjarra Zone), but their abundance decreases to the northeast, into the broad northwest-trending Tjuni Purlka Tectonic Zone. Further northeast, in the Walpa Pulka Zone, rocks of the Wankanki Supersuite are absent.

Rocks of the Pitjantjatjara Supersuite dominate the bedrock geology of the Walpa Pulka Zone but their abundance decreases to the southwest, into the Tjuni Purlka Tectonic Zone, and only rare, small intrusions are found in the Mamutjarra Zone. Protoliths to these rocks were relatively anhydrous, orthopyroxene- and biotite-bearing rocks that included rapakivi granites. They were metaluminous, ferroan rocks that range from alkali-calcic to calc-alkalic, with compositional affinities with A-type granites and specifically to Ti- and P-enriched 'charnockite-series' magmas shown elsewhere to have intruded and erupted at temperatures over 1100°C. Very high magmatic temperatures for the Pitjantjatjara Supersuite are indicated by estimates of metamorphic conditions accompanying intrusion (>1000°C), by 'soccer-ball' zonation patterns in zircon within metamorphosed country rock, and from the Zr saturation thermometer (minimum temperatures as high as ~990°C). These ultra-high temperature (UHT) conditions persisted at the level of granite emplacement more or less continuously throughout the ~100 Ma intrusive period of the Pitjantjatjara Supersuite. Eight individual suites are identified in the Pitjantjatjara Supersuite. Two of these — the Walpa and Waratjarra Suites — lie marginal to the boundary of the Tjuni Purlka Tectonic Zone, and show a compositional zonation that parallels that boundary. The other suites show no systematic compositional zonation. One suite, the Tjuni Purlka Suite, is more enriched in incompatible trace elements, and has a slightly less radiogenic Nd-isotopic composition, than the other suites of the Pitjantjatjara Supersuite and is confined to the Tjuni Purlka Tectonic Zone.

The Tjuni Purlka Tectonic Zone is a broad northwest-trending zone of extensive shearing that was a focus of deformation from at least c. 1220 Ma to c. 1050 Ma. The boundaries on either side of the zone have been the main focus for mafic magmatism and associated felsic crustal melts formed during the Giles Event (Warakurna Supersuite), including giant layered troctolite–gabbronorite–gabbro intrusions. Most granites of the Warakurna Supersuite are virtually identical in composition to the granites of the Tjuni Purlka Suite (Pitjantjatjara Supersuite).

The origins of the Wankanki Supersuite, and the tectonic setting of the Mount West Orogeny, are difficult to constrain. Rocks of similar age are observed in the Albany–Fraser Orogen, along the southern coast of Western Australia, and have been attributed to subduction during c. 1300 Ma convergence of the Yilgarn Craton and a southern continental mass. Dehydration melting of lower crust and incorporation into hydrous mantle-derived mafic magmas is consistent with the arc-like geochemistry of the Wankanki Supersuite, but not necessarily evidence of an arc setting. Structures bounding the Tjuni Purlka Tectonic Zone are crustal-scale features, but the basement that formed the source to the later Pitjantjatjara Supersuite, had a similar bulk composition on both sides of that zone. No evidence exists for a c. 1300 Ma suture within the exposed west Musgrave Province. If subduction was involved at this stage in the evolution of the west Musgrave Province then it must have involved a north dipping slab and an unexposed suture to the south.

The main compositional differences between the Wankanki and Pitjantjatjara Supersuites reflect the nature of the reactions through which the felsic crustal component of the bulk source melted, rather than any significant difference in the compositions of the bulk source. While dehydration melting of hornblende was important in the evolution of the Wankanki Supersuite, the formation of the Pitjantjatjara Supersuite involved high-temperature breakdown of F-rich biotite under essentially anhydrous conditions. However, the prevailing UHT conditions and the estimated geothermal gradient

of >40 °C km^{-1} greatly limit the amount of felsic crustal source material available beneath the level of intrusion during the Musgrave Orogeny, because geologically unreasonable crustal temperatures are exceeded within only a few kilometres. The enormous amount of melt generated and the prolonged and extreme thermal input needed to sustain the lower crust at UHT conditions throughout the Musgrave Orogeny require a major thermal and material source contribution from contemporaneous mantle-derived mafic magmas. This is consistent with the high abundance of relatively silica-poor rocks within the supersuite. However, the felsic crust component greatly dominated the incompatible trace element and isotopic budget of the bulk source. Voluminous mafic intraplating during the Musgrave Orogeny heated the lower crust to temperatures above both the liquidus of the mafic magmas and the solidus of the anhydrous country rock. Under such conditions this lower crustal 'hot zone' comprised a mix of partially molten crust and incompletely crystallized mantle-derived magma. These were eventually homogenized within an expanding crystal mush, or MASH (melting, assimilation, storage, homogenization), domain from which the Pitjantjatjara Supersuite was extracted.

The local structural regime was a major control on granite composition during the Musgrave Orogeny. Tapping of active MASH domains throughout the region typically lead to compositionally unzoned suites. Extension along the margins of the Tjuni Purlka Tectonic Zone additionally allowed intrusion of mafic magmas into localized areas of slightly cooled MASH domain. As these domains remelted, the magmas were simultaneously extracted to emplacement level at a rate that prevented further interaction with other melts or country rock. This resulted in suites that show a compositional zonation that parallels the extensional boundary to the Tjuni Purlka Tectonic Zone. Within the Tjuni Purlka Tectonic Zone itself, enhanced faulting allowed crustal melts to ascend before significant interaction with mantle derived magmas, to produce the Tjuni Purlka suite.

The tectonic setting of the Musgrave Orogeny was intracratonic. During the Mesoproterozoic the Musgrave Province evolved at the junction of three cratonic masses, each of which had a significantly greater lithospheric thickness than the Musgrave Province. This ensured that any asthenospheric upwelling was channelled beneath the province. The Pitjantjatjara Supersuite and the associated and prolonged UHT conditions were a response to this massive thermal input. Granites of the Pitjantjatjara Supersuite belong to the same class of very high temperature charnockite-series felsic lavas associated with the Mesozoic break-up of Gondwana. However, whereas some of the thermal responses of an intracontinental rift setting (e.g. very high temperature felsic magmatism) are apparent during the Musgrave Orogeny, they are not accompanied by many of the structural manifestations, such as major extensional deformation and fissure-controlled flood basalt magmatism. We suggest that this was because the Musgrave Province was effectively fixed, or locked, into position between the three bounding cratonic masses. This tectonic regime persisted throughout the Musgrave Orogeny, and likely continued into, and throughout, the Giles Event.

Contents

Appendices

Figures

Table

Geochemistry, geochronology, and petrogenesis of Mesoproterozoic felsic rocks in the west Musgrave Province, central Australia, and implications for the Mesoproterozoic tectonic evolution of the region

by

RH Smithies, HM Howard, PM Evins, CL Kirkland, DE Kelsey[1], M Hand[1], MTD Wingate, AS Collins[1], E Belousova[2] and S Allchurch[2]

Abstract

A dataset comprising more than 150 whole rock geochemical analyses, 28 whole rock Nd isotopic analyses and more than 100 new and previously published age determinations is integrated with the results of recent detailed mapping and thermobarometric studies of peak metamorphic conditions to place new constraints on the petrogenesis and tectonic setting of Mesoproterozoic felsic rocks from the western part of the Musgrave Province, in central Australia.

The oldest exposed felsic meta-igneous rocks, the Wankanki Supersuite, intruded the southwestern part of the west Musgrave Province during the 1345–1293 Ma Mount West Orogeny. These metaluminous and calcic to calc-alkalic hornblende–clinopyroxene–biotite granites are compositionally similar to Phanerozoic subduction-related continental arc granites.

Rocks of the Pitjantjatjara Supersuite formed during the c. 1220–1150 Ma Musgrave Orogeny. They are widespread in the northeastern part of the west Musgrave Province but their abundance decreases to the southwest. These metaluminous and ferroan rocks range from alkali-calcic to calc-alkalic, with affinities with A-type granites, and include orthopyroxene-bearing charnockite. Intrusive ages decrease systematically from c. 1220 Ma in the northeast to c. 1148 Ma in the southwest. High-grade metamorphism continued to c. 1120 Ma. The anhydrous, Ti- and P-enriched compositions of the granites, coupled with Zr saturation thermometric estimates of intrusion temperatures, thermometric estimates of peak metamorphic conditions, and 'soccer-ball' zonation patterns in zircon within metamorphosed country rock, all point to sustained ultra-high temperature (UHT) conditions (temperatures >1000°C), even at the exposed level of granite emplacement, throughout the ~100 Ma of the Musgrave Orogeny. The composition of the granites and the thermal regime in which they evolved reflect a significant mantle contribution in terms of both heat and source material. A lower crustal MASH (melting, assimilation, storage, homogenization) domain, in which crustal melts and mantle-derived magma mixed into a crystal mush zone, provided the source region for the Pitjantjatjara Supersuite. During the Musgrave Orogeny, an intracratonic tectonic setting in which the Musgrave Province was rigidly fixed at the junction of three cratonic masses, each with a significantly greater lithospheric thickness, ensured that any asthenospheric upwelling was focussed beneath the province, providing both heat and mantle-derived magma. Thus, whereas some of the thermal responses of an intracontinental rift setting are apparent (e.g. very high temperature felsic magmas, as displayed in the Pitjantjatjara Supersuite), they are not accompanied by many of the structural manifestations, such as major extensional deformation and fissure-controlled flood basalt magmatism. This tectonic regime persisted throughout the Musgrave Orogeny, and likely continued throughout the subsequent >1078–1026 Ma Giles Event.

KEYWORDS: Musgrave Province, Pitjantjatjara Supersuite, Wankanki Supersuite, granite, geochemistry, geochronology, Mesoproterozoic, tectonic evolution, ultra-high temperature (UHT)

[1] Tectonics, Resources and Exploration Group, School of Earth and Environmental Sciences, Universitry of Adelaide
[2] GEMOC, Department of Earth and Planetary Sciences, Macquarie University

Introduction

Proterozoic belts stitch together older lithospheric fragments that form the fundamental building blocks of continents (e.g. Windley, 1977). These belts are almost always multiply deformed and metamorphosed terrains produced during periods of intense magmatic and thermal flux (e.g. Cawood and Korsch, 2008), and this severely challenges attempts to chronicle their tectonic evolution and their history of crust–mantle interaction. Many Proterozoic belts are dominated by felsic magmas which show a wide range in both composition and inferred source regions. Such rocks are commonly easy to date, and their geochemical and isotopic compositions are able to provide an indelible record of source composition and melting conditions. This allows constraints on both tectonic setting and geodynamic evolution of a region. As a result, the geochemical, isotopic, and geochronological study of granites provides one of the most rewarding avenues in deciphering Proterozoic crustal history.

The Mesoproterozoic to Neoproterozoic Musgrave Province*, in central Australia, is geophysically expressed as an east-trending belt up to 800 km long and 350 km wide, bounded to the north and south by Neoproterozoic to Paleozoic basins (Fig. 1). The province lies at the convergence of Australia's main Proterozoic structural trends which ultimately reflect the Mesoproterozoic amalgamation of the North, West, and South Australian Cratons (Fig. 2). As such, this triple-point is one of the most important links in the reconstruction of Proterozoic Australia, and beyond that, the late Proterozoic supercontinent Rodinia. However, because of the geographical remoteness and cultural sensitivity of the region, the Musgrave Province remains Australia's least-studied exposed Proterozoic terrane. Apart from geological surveys which have established

* Previously referred to in Western Australia as the Musgrave Complex (Myers et al., 1996).

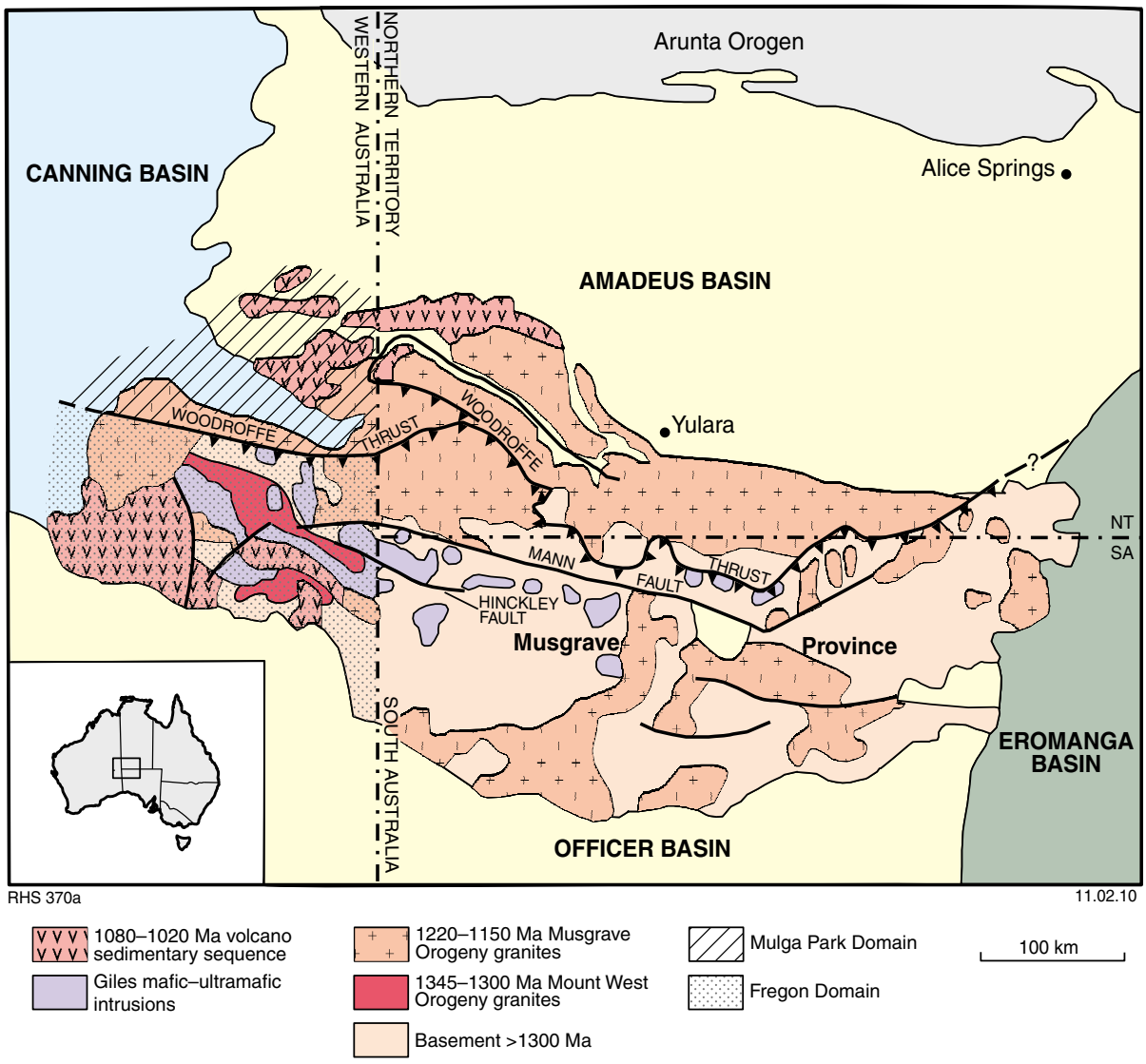

Figure 1. Regional geological sketch of the Musgrave Province (modified from Glikson et al., 1996 and Edgoose et al., 2004).

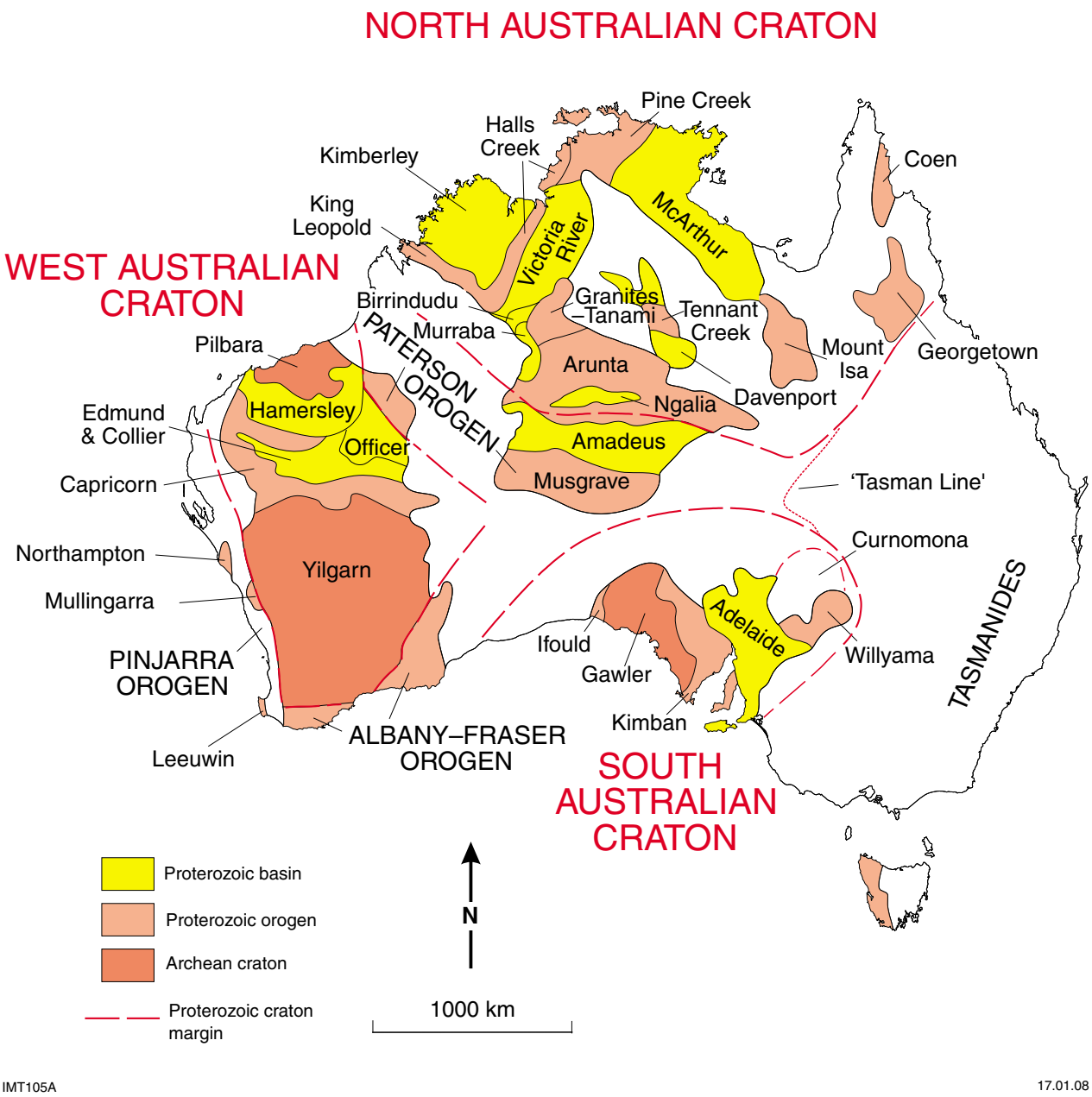

Figure 2. Location of the Musgrave Province with respect to the North, South, and West Australian Cratons (modified from Myers et al., 1996).

a broad lithological framework (Daniels, 1974; Glikson et al., 1996; Edgoose et al., 2004), an assessment of what this province represents within a wider Proterozoic evolutionary context has hinged on a few targeted studies (e.g. Goode, 1970; Gray, 1971; Maboko, 1988; Camacho, 1997; White, 1997; Edgoose et al., 2004; Wade et al., 2008; and several derivative publications). The studies by White (1997) and Wade et al. (2008) have been particularly important in establishing temporal links to other regional Proterozoic terranes, and in identifying potential basement and granite source-terranes within the province. Until recently, however, the regionally extensive geochemical, isotopic, and geochronological datasets required to further chronicle and constrain the tectonic evolution of this region, have been lacking.

In 2004, the Geological Survey of Western Australia (GSWA) began a new program of geological investigation within the portion of the Musgrave Province that lies in the state of Western Australia (herein referred to as the 'west Musgrave Province'; Fig. 1). This has provided a large and regionally extensive dataset of new geochemical, isotopic, and geochronological data, underpinned by detailed geological mapping (Fig. 3).

This Report concentrates primarily on the felsic igneous rocks (including their metamorphosed equivalents) that dominate outcrop within the west Musgrave Province. These formed during several distinct events within the late Mesoproterozoic that are associated with global Grenvillian events; the 1345–1293 Ma Mount West

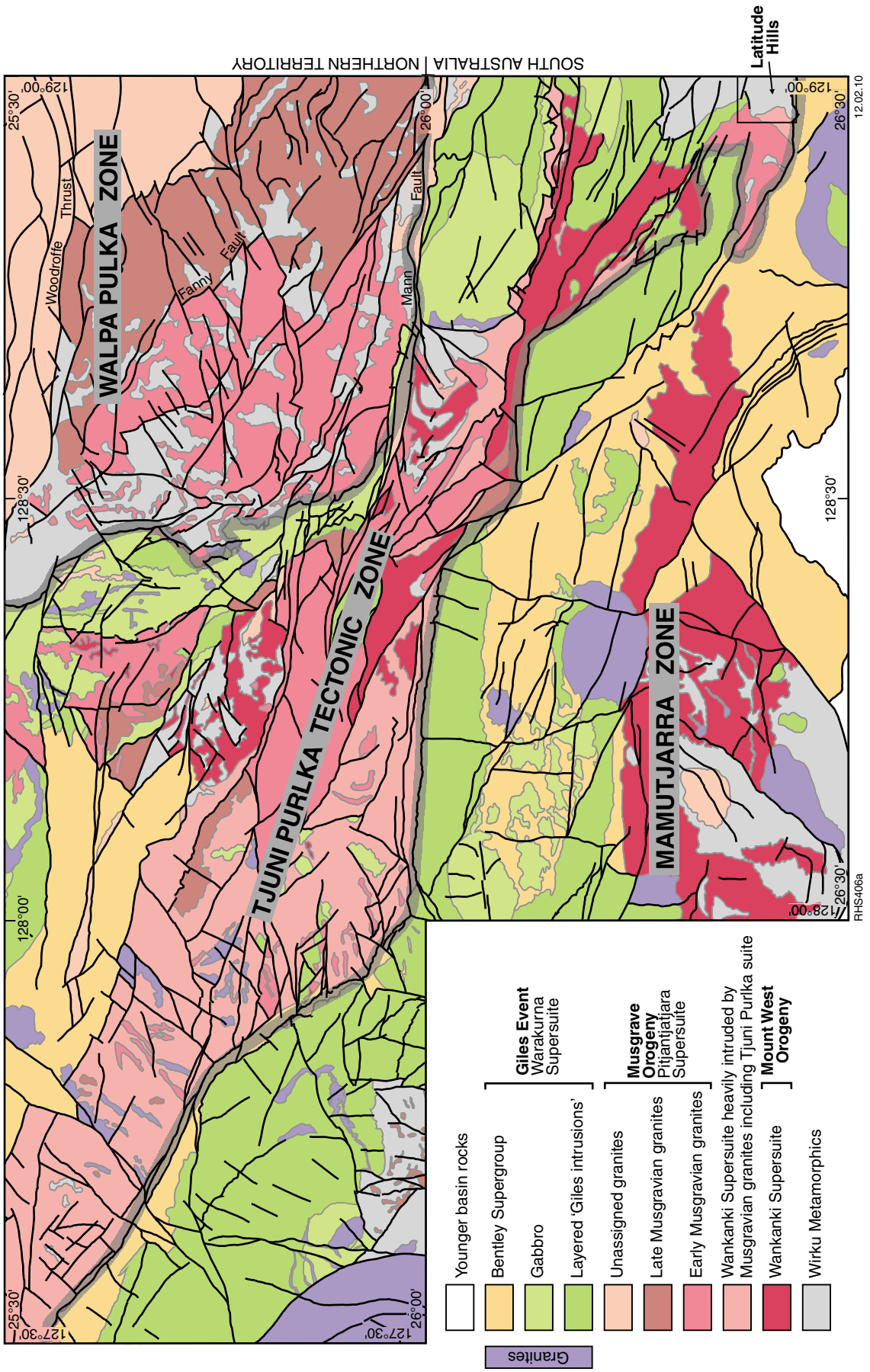

Figure 3. Simplified geological map of the eastern portion of the west Musgrave Province showing the three lithotectonic zones.

Orogeny, the 1220–1150 Ma Musgrave Orogeny, and the >1078–1026 Ma Giles Event. We present new geochemical, isotopic, and geochronological data and use these to place constraints on the range of processes and source compositions that contributed to this felsic magmatism, and on the possible tectonic environments in which it may have occurred. Felsic magmatism generated in this region spans a wide compositional range from calcic and calc-alkalic compositions during the Mount West Orogeny to calc-alkalic and alkali-calcic magmatism during the Musgrave Orogeny and Giles Event. Despite this change most granites, regardless of their age, contain a large mantle component and share a common crustal source component, although they vary in the proportions of these source components, and in the ways in which they blend.

Regional geology

Previous regional studies led Camacho (1989) to subdivide the Musgrave Province into the Mulga Park Domain, to the north, and the Fregon Domain, separated by the south-dipping Woodroffe Thrust (Fig. 1) which developed during the intracratonic, c. 550 Ma, Petermann Orogeny. Both domains apparently share similar lithologies and geological histories (i.e. they are not exotic), but differ significantly in metamorphic grade as a result of Petermann-age exhumation along the Woodroffe Thrust, which juxtaposed sub-eclogite facies crust to the south against amphibolite facies crust to the north (Camacho, 1989; Edgoose et al., 2004).

The west Musgrave Province lies almost entirely within the Fregon Domain (Fig. 1), which has now been redefined and further subdivided (Smithies et al., 2009a; Evins et al., in prep.). A broad zone of multi-generational shearing extends in a northwest direction across the west Musgrave Province and is referred to as the Tjuni Purlka Tectonic Zone (Fig. 3). This was a focus for deformation from at least c. 1220 to c. 1050 Ma. To the north, the Walpa Pulka Zone (Fig. 3) is a deep-crustal domain dominated by c. 1220–1150 Ma high-K granite plutons generated during the Musgrave Orogeny. Widespread high-pressure metamorphic assemblages are preserved through rapid exhumation along east and east-northeast trending mylonites and migmatitic shear zones related to the c. 550 Ma Petermann Orogeny (Scrimgeour and Close, 1999; Camacho et al., 1997; Raimondo et al., 2009). To the south of the Tjuni Purlka Tectonic Zone, the Mamutjarra Zone (Fig. 3) is dominated by c. 1345–1293 Ma calc-alkaline granites related to the Mount West Orogeny. Here, high-K granites formed during the Musgrave Orogeny are less voluminous than they are to the north, typically forming small dykes and plugs. However, the effects of prolonged high-temperature, low- to moderate-pressure metamorphism during the Musgrave Orogeny are widespread and include extensive migmatization of supracrustal units and of the 1345–1293 Ma calc-alkaline granites. The effects of the Petermann Orogeny in this zone are minimal.

The boundaries on either side of the Tjuni Purlka Tectonic Zone have been the focus for mafic magmatism and associated felsic crustal melts between c. 1080 and

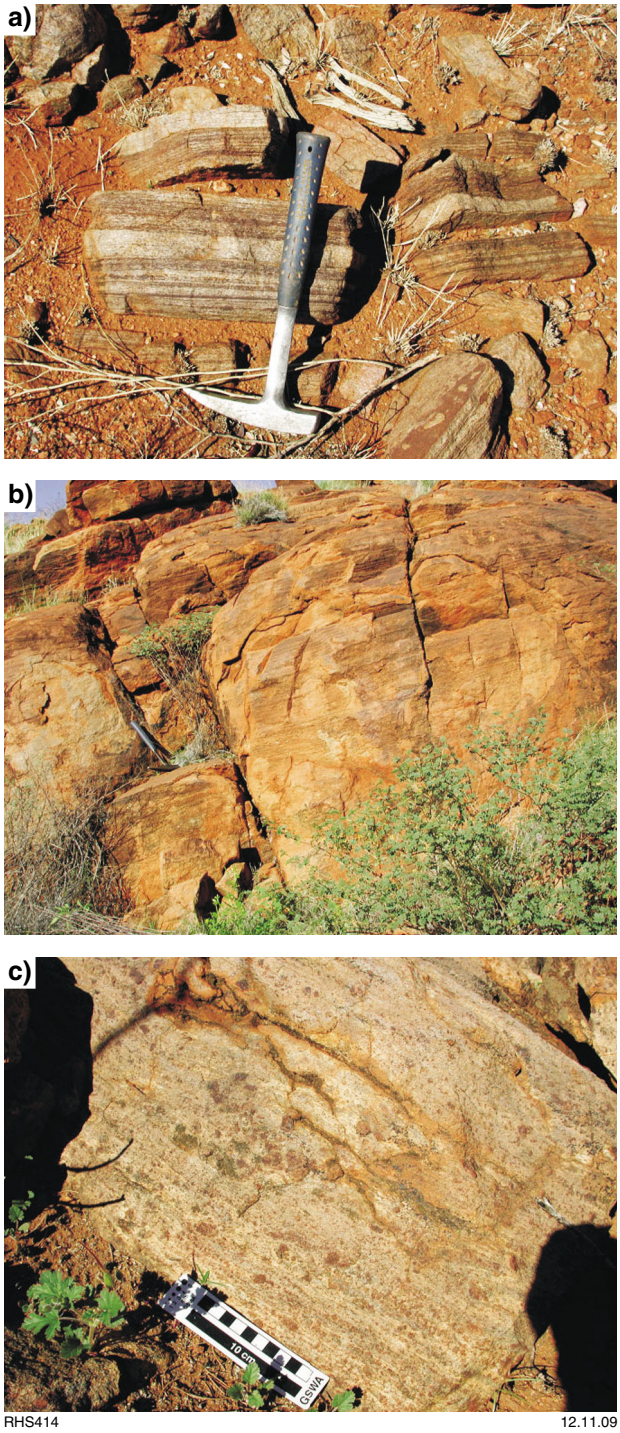

Figure 4. Outcrop photographs of the Wirku Metamorphics: a) thinly interbedded arkosic metasandstone; b) laminated arkosic metasandstone; c) pelitic (garnet–sillimanite–hercynite–cordierite) gneiss.

c. 1050 Ma (broadly referred to as the Giles Event). Giant layered troctolite–gabbronorite–gabbro intrusions mark the southwestern edge of the zone, whereas a thick zone of syn-tectonic and co-mingled gabbro and granite marks the northeastern edge (Evins et al., in press).

Banded gneiss (Fig. 4a), mainly preserved as rafts in granite, locally forms a significant component of the west Musgrave Province (Gray, 1971, 1978; Stewart 1995;

Howard et al., 2006, 2007; Smithies et al., 2009a), and is found in all three zones. Several studies report pre-Musgrave ages for these gneisses, which are typically interpreted as being derived from volcanic, volcaniclastic, and clastic protoliths (e.g. Gray, 1971, 1978; Gray and Compston 1978; Edgoose et al., 2004). Some gneisses from the eastern Musgrave Province are thought to have a granitic protolith with crystallization ages as old as 1590 ± 25 Ma (Edgoose et al., 2004). Evins et al. (in prep), however, showed that the oldest intrusive or extrusive felsic material exposed in the west Musgrave Province (and likely throughout much of the eastern part of the province as well) was formed between c. 1345 and 1300 Ma. Older ages from this part of the Musgrave Province appear almost invariably to reflect detrital zircon populations in paragneisses now assigned to the Wirku Metamorphics (elsewhere referred to as the 'Birksgate Complex' (Major and Conor, 1993) or 'Musgravian gneiss' (Edgoose et al., 2004)).

The Wirku Metamorphics are interpreted to have protoliths of sedimentary and lesser volcaniclastic and volcanic origin, based on locally continuous layering (Fig. 4 a,b), the presence of pelitic (Fig. 4c), arkosic (Fig. 4b), and near-orthoquartzitic interlayers, and on complex zircon age spectra. The detrital zircon age-spectra for these rocks varies from region to region (Fig. 5). Most paragneisses in the Tjuni Purlka Tectonic Zone are dominated by detrital zircon age peaks between 1560 and 1470 Ma and significant age components between c. 1360 and 1310 Ma. However, in a small and isolated area within the southeastern part of this zone (Latitude Hills area; Fig. 3), the paragneisses appear significantly different, with several prominent detrital zircon age peaks between c. 3200 and 2630 Ma and between 1790 and 1590 Ma (Fig. 5). A unifying feature, however, is that youngest detrital zircons indicate maximum depositional ages between c. 1360 and 1307 Ma, whereas intrusive contacts with granites of the Mount West Orogeny provide a minimum depositional age of 1345–1293 Ma.

In the western part of the Mamutjarra Zone, the Wirku Metamorphics is dominated by banded to laminated pelitic to psammitic paragneiss. In the east of this zone, the rocks are dominantly psammitic, compositionally very similar to granites related to the Mount West Orogeny, and are likely derived from volcanic or volcaniclastic protoliths. These rocks preserve very few detrital zircons, but show virtually unimodal zircon age populations that are best interpreted as reflecting primary deposition during the c. 1345–1293 Ma Mount West Orogeny (Evins et al., in prep.).

In the Walpa Pulka Zone, detrital zircon age peaks in rocks of the Wirku Metamorphics differ slightly from those in the Tjuni Purlka Tectonic Zone, with a main peak at c. 1570 Ma and several smaller peaks between 1650 and 1500 Ma (Fig. 5). Here, detrital zircons in the c. 1360–1307 Ma age range, which define the maximum depositional age of sediments in the Tjuni Purlka Tectonic Zone, are virtually absent, as are granites related to the Mount West Orogeny. The relationship between the paragneisses in the different zones is not yet clear; we cannot rule out the possibility that they simply represent slightly different tectonostratigraphic packages within a single depositional basin that evolved between c. 1360 and c. 1307 Ma.

The Mount West Orogeny and the Wankanki Supersuite

Gray (1971), Sun et al. (1996), and White (1997) identified isolated outcrops of felsic gneiss in the central part of the Tjuni Purlka Tectonic Zone with protolith ages between c. 1330 and 1300 Ma. Intrusive rocks of this age are now known to form a significant component within the zone and represent the most voluminous pre c. 1100 Ma magmatic component of the Mamutjarra Zone (Fig. 3; Howard et al., 2007; Smithies et al., 2009a,b; Evins et al., 2009). At the current level of exposure, these granites can locally be shown to have intruded their own volcanic carapace. The crystallization age range of the granitic and volcanic rocks is from c. 1345 to c. 1293 Ma (Fig. 5; White et al., 1999; Bodorkos and Wingate, 2008a,b; Bodorkos et al., 2008a–e; Kirkland et al., 2008a–g; Smithies et al., 2009a), with most occurring within a narrow interval between c. 1326 and 1312 Ma. Howard et al. (2007) grouped these granitic and volcanic rocks into the Wankanki Supersuite and termed the crustal event during which they were produced the Mount West Orogeny.

Rocks from the Wankanki Supersuite have been metamorphosed to granulite facies and show a wide textural range, from moderately foliated porphyritic rocks to layered gneisses showing incipient to advanced migmatization. Weakly metamorphosed examples preserve an igneous mineralogy that includes hornblende>biotite, with clinopyroxene cores to hornblende.

On a regional basis, White (1997) showed that the magmatic and thermal histories of the Musgrave Province and the Albany–Fraser Orogen, along the southern margin of Western Australia, were similar between c. 1330 and 1170 Ma, inviting speculation of structural links which equated c. 1330–1300 Ma magmatism in the Musgrave Province to what is believed to have been a subduction setting in the Albany–Fraser Orogen at that time (e.g. Condie and Myers, 1999; Bodorkos and Clark, 2004).

The Musgrave Orogeny and the Pitjantjatjara Supersuite

The dominant northwest structural trend of the west Musgrave Province (Fig. 3) reflects a crustal architecture established during or before the Musgrave Orogeny that was locally modified and reactivated during the Musgrave Orogeny, Giles Event, and the Petermann Orogeny. The Musgrave Orogeny is the oldest orogenic event to have clearly affected all areas of the west Musgrave Province and involved intense deformation and widespread granulite facies crustal reworking. Edgoose et al. (2004) place the orogeny between c. 1200 and 1160 Ma, and grouped syn- to post-tectonic granite magmas into the Pitjantjatjara Supersuite. There is no regional evidence for collisional or accretionary tectonics associated with the prolonged Musgrave Orogeny, which appears to have been essentially intracratonic (Wade et al., 2008).

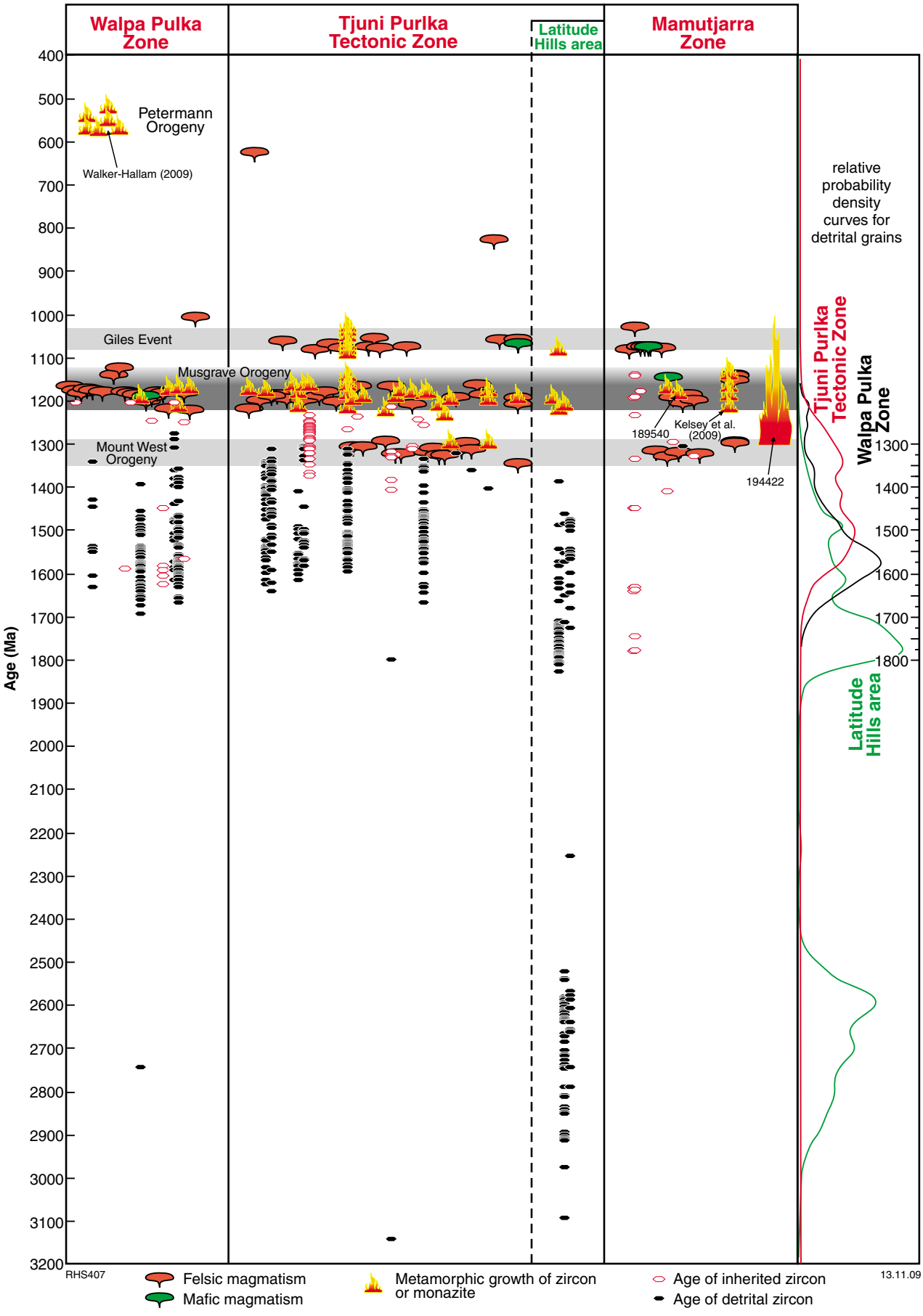

Figure 5. Time-space plot of SHRIMP U–Pb zircon ages (see Appendix 1 for data).

Most rocks of the Pitjantjatjara Supersuite have been metamorphosed at granulite facies conditions, in some cases as a result of thermal peaks late in the Musgrave Orogeny, but also during the c. 1080–1030 Ma Giles Event (Clarke et al., 1995; Fig. 5). In addition, parts of the region were deeply buried beneath Neoproterozoic sedimentary basins, and rapid differential uplift of the Walpa Pulka Zone during the c. 550 Ma Petermann Orogeny has exposed metamorphic assemblages reflecting pressures as high as 10–14 kbar (Scrimgeour and Close, 1999). The metamorphosed granites of the Pitjantjatjara Supersuite range from statically recrystallized and unfoliated (Fig. 6a–c), to strongly foliated and mylonitized (Fig. 6f). Whereas the primary mineralogy of these granites was essentially anhydrous (quartz, plagioclase, K-feldspar, orthopyroxene, clinopyroxene, biotite), retrograde recrystallization is locally directly associated with foliation development and has resulted in partial to near-complete alteration of pyroxene to hornblende, actinolite, and biotite.

Granites of the Pitjantjatjara Supersuite can be broadly subdivided into three lithological groups. The first and most voluminous typically ranges from granodiorite to syenogranite (although the full range is from monzodiorite to alkali-feldspar granite), and where primary igneous textures are preserved, includes rounded rapakivi-textured feldspar phenocrysts up to 5 cm in diameter (Fig. 6d). Many of these rocks retain evidence of primary orthopyroxene-bearing mineralogy and on that basis can be classified as charnockites (e.g. Frost and Frost, 2008). The porphyritic granodiorite–syenogranite group dominates the Walpa Pulka Zone as large composite plutonic bodies, and forms smaller plutons and dykes in the Tjuni Purlka Tectonic Zone (Fig. 3). These rocks are mostly restricted to dykes and minor intrusions within the Mamutjarra Zone; although in the northwest of that zone they form a widespread but non-continuous collection of small intrusions.

This first group of Pitjantjatjara Supersuite granites typically does not contain abundant enclaves, and whereas other evidence for mixing or mingling (e.g. dykes terminating in chains of lobate inclusions) is locally present (Fig. 7a), there is no field evidence for significant physical interaction between individual granite intrusions, or between these and any other magma batches, at the present level of exposure. Several broad styles of intrusions are identified. Most exposures show significant variation in texture (from seriate to porphyritic to megacrystic; Fig. 6) and in grain size (Fig. 7c–d) on a scale of one metre to many tens of metres, suggesting that larger bodies are typically composite intrusions of numerous individual dykes and sills. Geochemical data (see '**Granite geochemistry**') show that individual intrusions, or collections of intrusions (forming individual granite suites) are either compositionally heterogeneous throughout (e.g. the Mirturtu, and Ilurpa; Fig. 8), or show a systematic compositional variation that parallels the northwest trend of major shear zones (e.g. Walpa and Waratjarra). Other suites (Pirntirri and Punuwarra) are of more texturally and compositionally homogeneous granites.

The second group of Pitjantjatjara Supersuite granites is entirely restricted to the Tjuni Purlka Tectonic Zone and comprises locally schlieric, biotite–orthopyroxene leucogranites (Tjuni Pulka suite) typically in the monzogranite to syenogranite compositional range. These form veins and sheets that cut and engulf earlier rocks of the Wirku Metamorphics and Wankanki Supersuite.

The third group of Pitjantjatjara Supersuite granites are locally derived anatectic melts that formed highly leucocratic sheets and veins which engulfed all earlier lithologies and formed throughout the entire duration of the Musgrave Orogeny. These granites range from metaluminous to peraluminous, are strongly depleted in rare earth elements (REE) and high field strength elements (HFSE), and typically enriched in large ion lithophile elements (LILE), and are not considered further here.

Igneous events and geographic trends

A compilation of new secondary ionization mass spectrometry (SIMS) U–Pb dates on zircons (by sensitive high-resolution ion microprobe (SHRIMP)) from >100 samples (Fig. 9; Appendix 1) includes ages interpreted to reflect crystallization of the granite magma as well as ages of zircon rims, interpreted to reflect growth during metamorphism. In the Walpa Pulka Zone, the combined age populations can be divided into two broad but distinct groups; an older group reflecting magmatism and metamorphism between c. 1220 and 1200 Ma, and a younger group reflecting magmatism and metamorphism between c. 1190 and 1150 Ma (Fig. 9). These two groups bracket events referred to as 'early Musgravian' and 'late Musgravian' respectively (Smithies et al., 2009a). The oldest early Musgravian granite so far identified is dated at 1219 ± 12 Ma (GSWA 174737; Bodorkos et al., 2008d) and was foliated before or during intrusion of, and metamorphism by, late Musgravian anatectic melt veins at 1180 ± 6 Ma (GSWA 174736; Bodorkos et al., 2008c). The youngest late Musgravian granite from the Walpa Pulka Zone has been dated at 1157 ± 9 Ma (GSWA 189254; preliminary data) and is an unfoliated granite dyke that cuts an early Musgravian foliation. Zircons from early Musgravian granites commonly have rims with ages reflecting growth (or regrowth) during late Musgravian events.

Based on the crystallization ages of granites, the Walpa Pulka Zone can be broadly divided into two areas separated by the northwest-trending Fanny Fault. Early Musgravian granites (mainly the Walpa suite) are restricted to the western area (Fig. 8) and range in composition from quartz monzodiorite and granodiorite to monzogranite. Late Musgravian granites form the eastern area (Mirturtu and Kapi-Parra suites) and range in composition from monzogranite to syenogranite.

Most granites of the Pitjantjatjara Supersuite in the Mamutjarra Zone have late Musgravian intrusive ages between 1179 ± 10 Ma (GSWA 189452) and 1148 ± 6 Ma (GSWA 189522).

The northeastern part of the Tjuni Purlka Tectonic Zone contains deformed plutons of granites with early Musgravian ages (Pirntirri and Ilurpa suites; Figs 8 and 9) similar to those in the western part of the adjacent

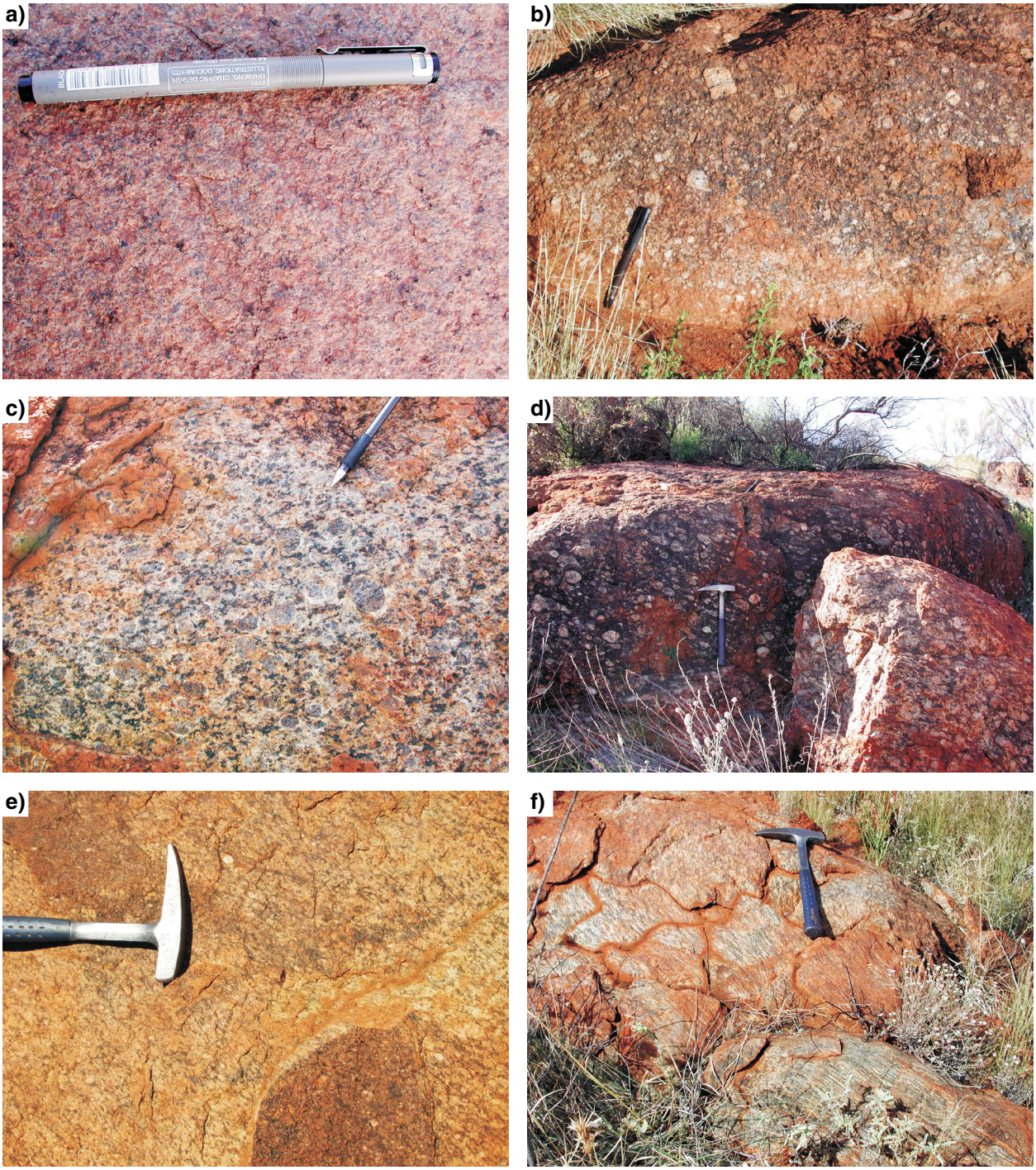

Figure 6. Various textural manifestations of the Pitjantjatjara Supersuite: a) massive and equigranular; b) massive and seriate textured; c) massive, with large rapakivi-textured feldspar; d) weakly foliated, with large rapakivi-textured feldspar; e) foliated; f) mylonitic.

Walpa Pulka Zone. In the southwest, the Tjuni Purlka Tectonic Zone contains late Musgravian granites similar to those in the adjacent part of the Mamutjarra Zone. Apart from these, Pitjantjatjara Supersuite granites in the Tjuni Purlka Tectonic Zone are schlieric biotite–orthopyroxene leucogranites (Tjuni Purlka suite), which intruded throughout the Musgrave Orogeny, and are dated from 1200 ± 5 Ma (GSWA 185339) to 1156 ± 3 Ma (GSWA 183509).

Mafic magmatism did not form a significant component of the Musgrave Orogeny, at present outcrop level. Mafic dykes of this age are extremely rare, and the granites themselves do not typically contain mafic enclaves. Nevertheless, rare leucogabbro intruded the Walpa Pulka Zone during the late Musgravian at 1190 ± 7 Ma (GSWA 174594; GSWA preliminary data) and rare norite dykes cut the Mamutjarra Zone at 1149 ± 10 Ma (GSWA 194376; GSWA preliminary data).

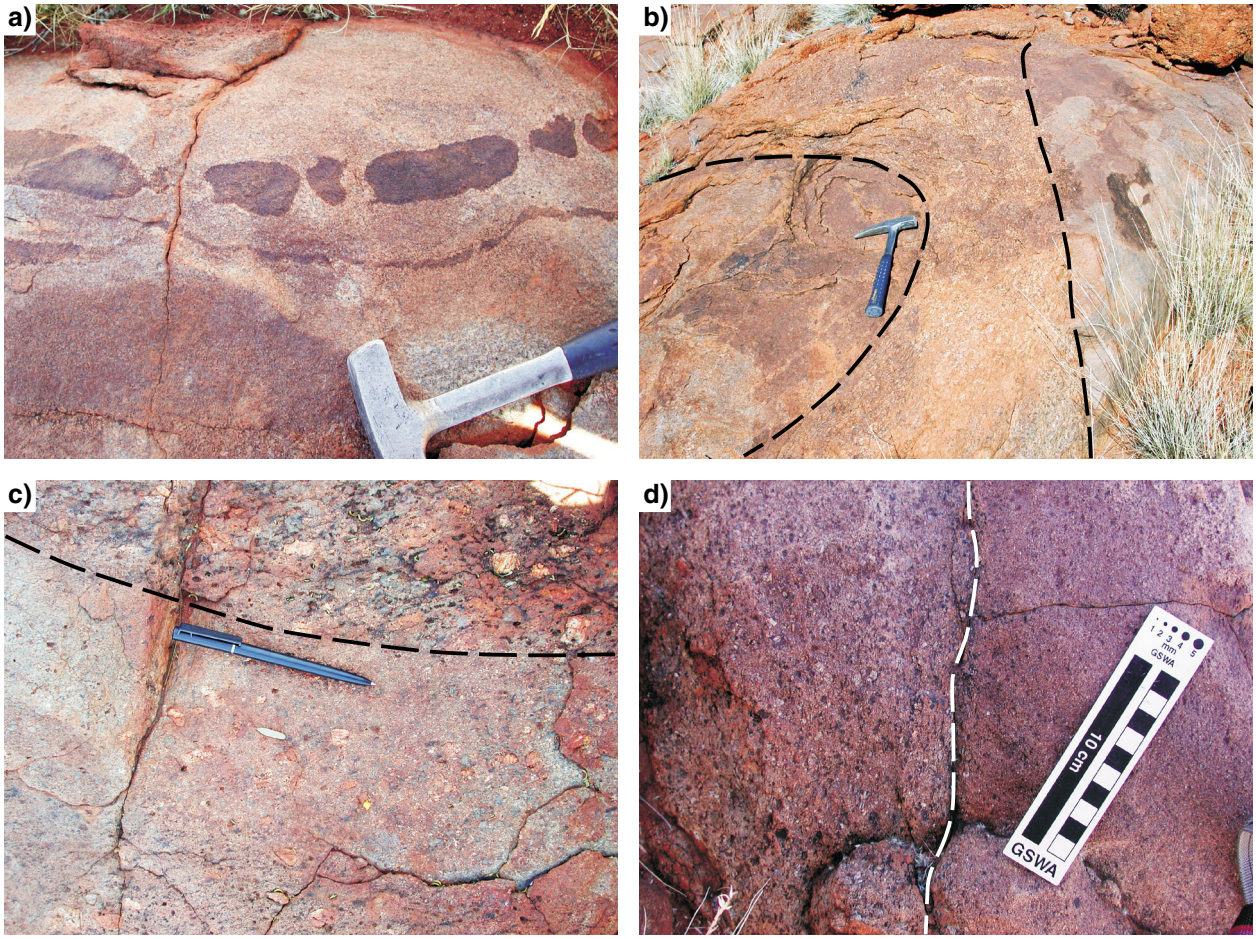

Figure 7. Various large-scale textural features of the Pitjantjatjara Supersuite: a) disrupted syn-magmatic dioritic dyke; b–d) various internal intrusive contacts (marked with dashed line) between texturally different intrusive phases, demonstrating the composite nature of the granite bodies.

There is a broad geographical trend in the crystallization ages of Pitjantjatjara granites, including the schlieric biotite–orthopyroxene leucogranites (Tjuni Purlka suite) of the Tjuni Purlka Tectonic Zone. However, only late Musgravian granites lie northeast of the Fanny Fault. To the southwest of the Fanny Fault, crystallization ages decrease from c. 1220 Ma in the northeast to c. 1150 Ma in the southwest (Mamutjarra Zone). These observations reflect a migration of either the locus of melting or the locus of intrusion, or both.

There is also a clear antithetic relationship in the relative geographical distribution of granites of the Pitjantjatjara and Wankanki Supersuites (Fig. 8), with Pitjantjatjara granites dominating in the northeast (to the total exclusion of Wankanki granites in the Walpa Pulka Zone) and Wankanki granites dominating in the southwest.

Metamorphic conditions and level of magmatic emplacement

Thermobarometry

In the Walpa Pulka Zone, metamorphic assemblages developed in pelitic gneisses that are intruded by granites of the Pitjantjatjara Supersuite have been overprinted by high-pressure granulite assemblages formed during burial beneath Neoproterozoic basins and exhumed during the Petermann Orogeny. However, pelitic rocks located far south of the areas significantly affected by Petermann Orogeny metamorphism preserve mineral assemblages that reflect pressure–temperature (P–T) conditions achieved during the Musgrave Orogeny (e.g. King, 2008; Kelsey et al., 2009). These conditions were estimated by King (2008) and Kelsey et al. (2009) using THERMOCALC v3.0 and v3.1 (Powell and Holland, 1988). Bulk chemical compositions used for the calculation of P–T pseudosections were estimated by integrating the abundance of minerals in a specific reaction microstructure with the measured mineral chemistry (measured from electron microprobe). The pseudosections were calculated in the model chemical system Na_2O–CaO–K_2O–FeO–MgO–Al_2O_3–SiO_2–H_2O–TiO_2–O (NCKFMASHTO, where 'O' represents ferric iron) as this model chemical system closely resembles the major element composition of the metapelitic rocks of interest. Calculated P–T pseudosections are used rather than classic thermobarometry as they provide a graphical representation of mineral assemblages in P–T space, and can be used to define a paragenetic sequence, and thus a P–T path, based upon the petrographic observations.

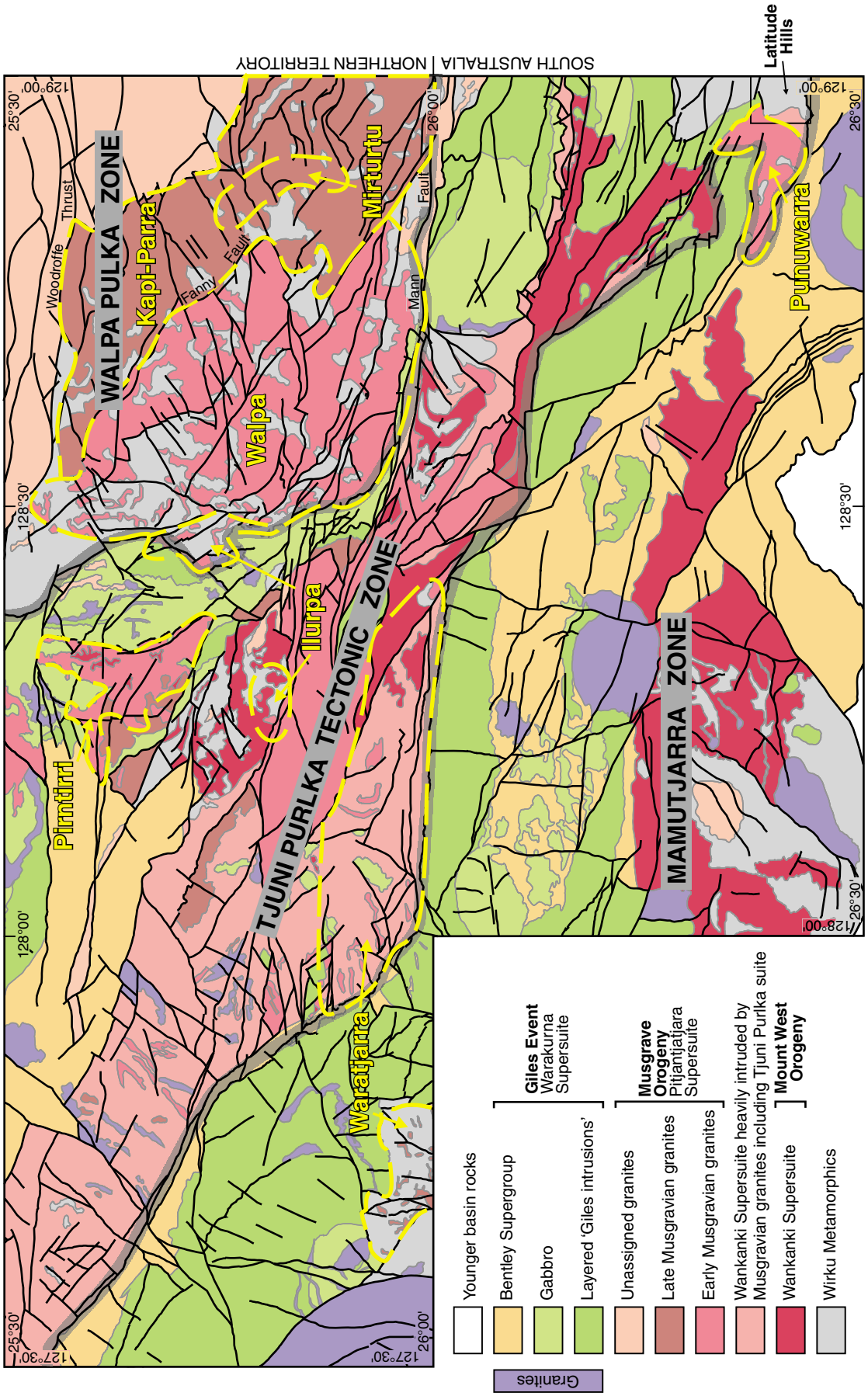

Figure 8. Simplified geological map of the eastern portion of the west Musgrave Province showing the location of various geochemically and geochronologically constrained granite suites within the Pitjantjatjara Supersuite.

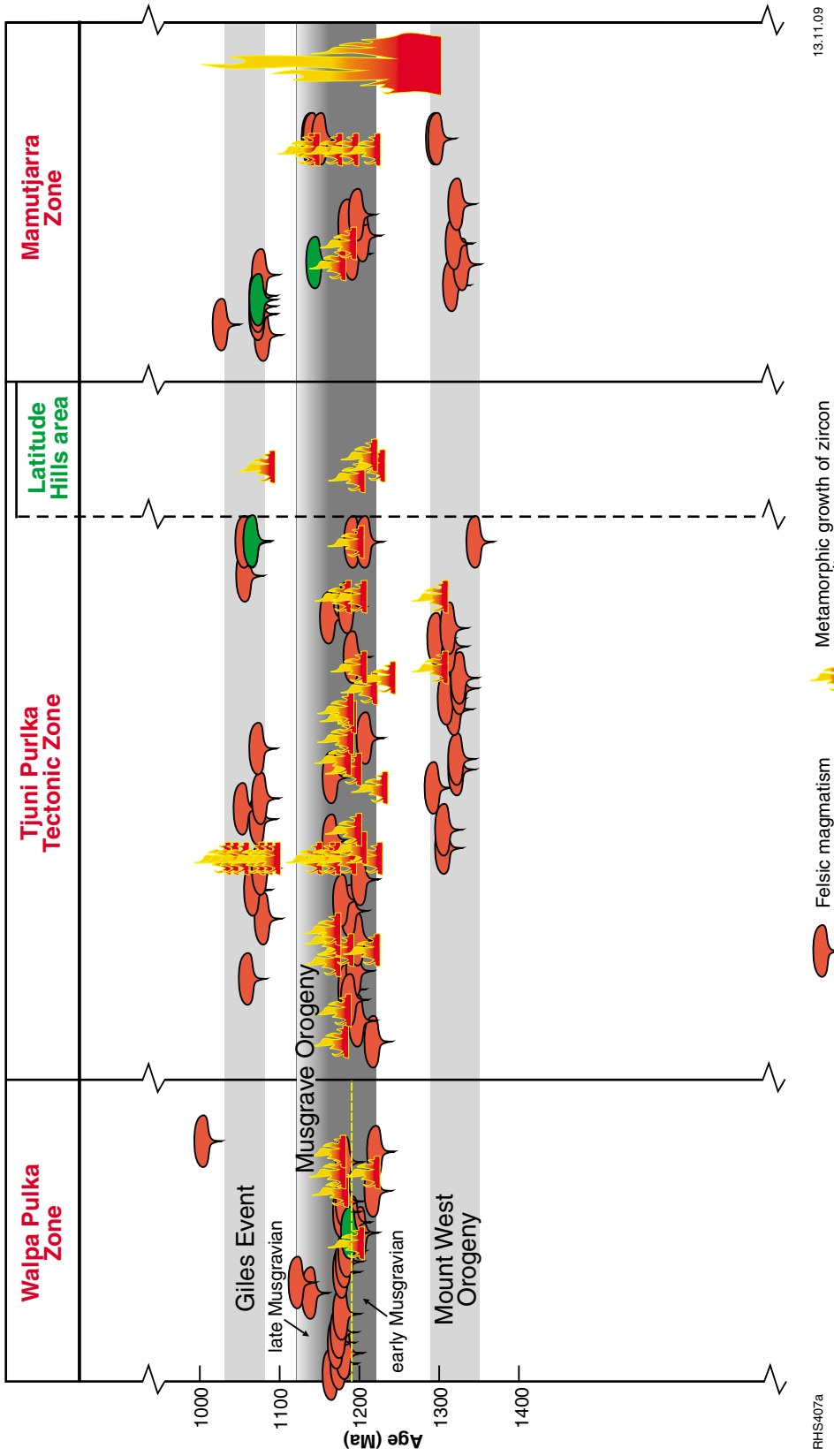

Figure 9. Detailed time-space plot of SHRIMP U–Pb zircon ages covering the period between c. 1400 Ma and 1000 Ma.

In the southeastern parts of the Tjuni Purlka Tectonic Zone, King (2008) and Kelsey et al. (2009) established that metapelites with the coarse-grained peak mineral assemblage of garnet–sillimanite–spinel–quartz equilibrated at conditions of 900–1000+°C and 6–8 kbars (e.g. sample GSWA 183460) at 1211 ± 13 Ma (U–Pb zircon). In the west of the Mamutjarra Zone, Kelsey et al. (2009) show that similar coarse-grained peak assemblages equilibrated at conditions of ≥1000°C and 7–8 kbars at 1211 ± 7 Ma (U–Pb monazite). Such conditions reflect ultra-high temperature (UHT) metamorphism, the most thermally extreme type of crustal metamorphism, characterized by temperatures >900°C (Harley, 1998; Kelsey et al., 2004; Kelsey, 2008) and a geothermal gradient >>20°C km^{-1} (Brown, 2007a). In the case of the west Musgrave Province, the P–T estimates define an apparent geothermal gradient of >40°C km^{-1}.

As the studied metapelites are essentially anhydrous, probably as a consequence of melt loss, no constrained information can be gleaned about the prograde history of these rocks. In contrast, the post-peak segment of the P–T path is constrained by the symplectic and coronitic reaction microstructures. Cordierite–spinel symplectites, cordierite coronae, and rare garnet coronae mantle coarse-grained garnet, sillimanite, and spinel (Fig. 10). In conjunction with calculated P–T pseudosections, these post-peak reaction products define a P–T path that is dominated by cooling from >1000°C and involves little decompression.

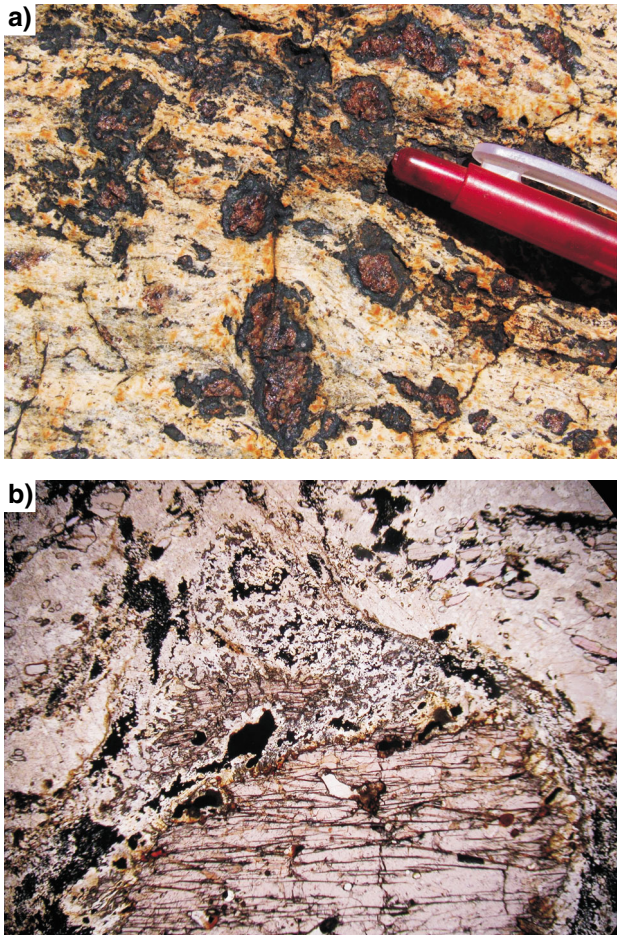

Figure 10. a) Coarse garnet porphyroblasts mantled by coronae of spinel + cordierite intergrowths; b) photomicrograph of reaction microstructure involving the breakdown of garnet and sillimanite (sillimanite in the upper right hand corner) to a cordierite + spinel intergrowth.

Temperature inferences from metamorphic zircon

Studies of metamorphic zircons from two samples of pelitic gneiss from the Mamutjarra Zone further elucidate the UHT metamorphic history of the Musgrave Orogeny. Interpretation of 'metamorphic' zircons is challenging due to the numerous different mechanisms that zircon can grow in a metamorphic environment, including subsolidus reactions that liberate zirconium (e.g. Fraser et al., 1997; Degeling et al., 2001; Moeller et al., 2003), crystallization from partial melts during high grade metamorphism (anatectic melts, e.g. Vavra et al., 1999; Schaltegger et al., 1999), or by dissolution–reprecipitation of pre-existing zircon with metamorphic fluids (e.g. Ashwal et al., 1999; Hoskin and Black, 2000). More than one of these crystallization mechanisms may operate in the same rock at essentially the same time (Kirkland et al., 2009). Nonetheless, for rocks of the west Musgrave Province, the ages of grains interpreted to have grown during metamorphism (e.g. analyses of unzoned zircon rims overgrowing concentrically zoned igneous zircon in granites of the Pitjantjatjara Supersuite and of unzoned rims truncating detrital zircon cores in rocks of the Wirku Metamorphics) closely correspond to known ages of igneous intrusion (Fig. 9).

GSWA 194422: quartzite, Cohn Hill

Dated samples from the western part of the Mamutjarra Zone (Cohn Hill) include sample GSWA 194422 (Kirkland et al., 2010a); a medium-grained (retrogressed) sillimanite-bearing quartzite, with two textural varieties of zircon (Fig. 11): Type 1 with inherited cores and Type 2 with no distinct cores. Type 1 comprises colourless, spheroidal to ellipsoidal grains ranging from 50 to 200 µm in diameter. Under cathodoluminescence (CL), Type 1 zircons display a distinctive zonation pattern consisting of high-CL response cores, some with sector zoning or oscillatory zoning, overgrown by numerous homogenous overgrowths with low-CL response. Type 2 grains are colourless, spheroidial, and up to 300 µm in diameter. Under CL, they are either homogeneous, with little CL response, or are sector-zoned ('soccer-ball') zircons (Fig. 11), thought to signify high-grade metamorphism at a deep crustal level (e.g. Vavra et al., 1999). Many of the crystals display numerous overgrowths.

Sixty of 59 crystals indicate $^{207}Pb^*/^{206}Pb^*$ dates ranging from 1266 to 1072 Ma, for analyses >95% concordant (Fig. 12). A weighted mean of all concordant $^{207}Pb^*/^{206}Pb^*$ dates yields an apparent age of 1142 ± 14 Ma (MSWD = 3.2), although the scatter is greater than can be ascribed to analytical uncertainties alone, implying a prolonged

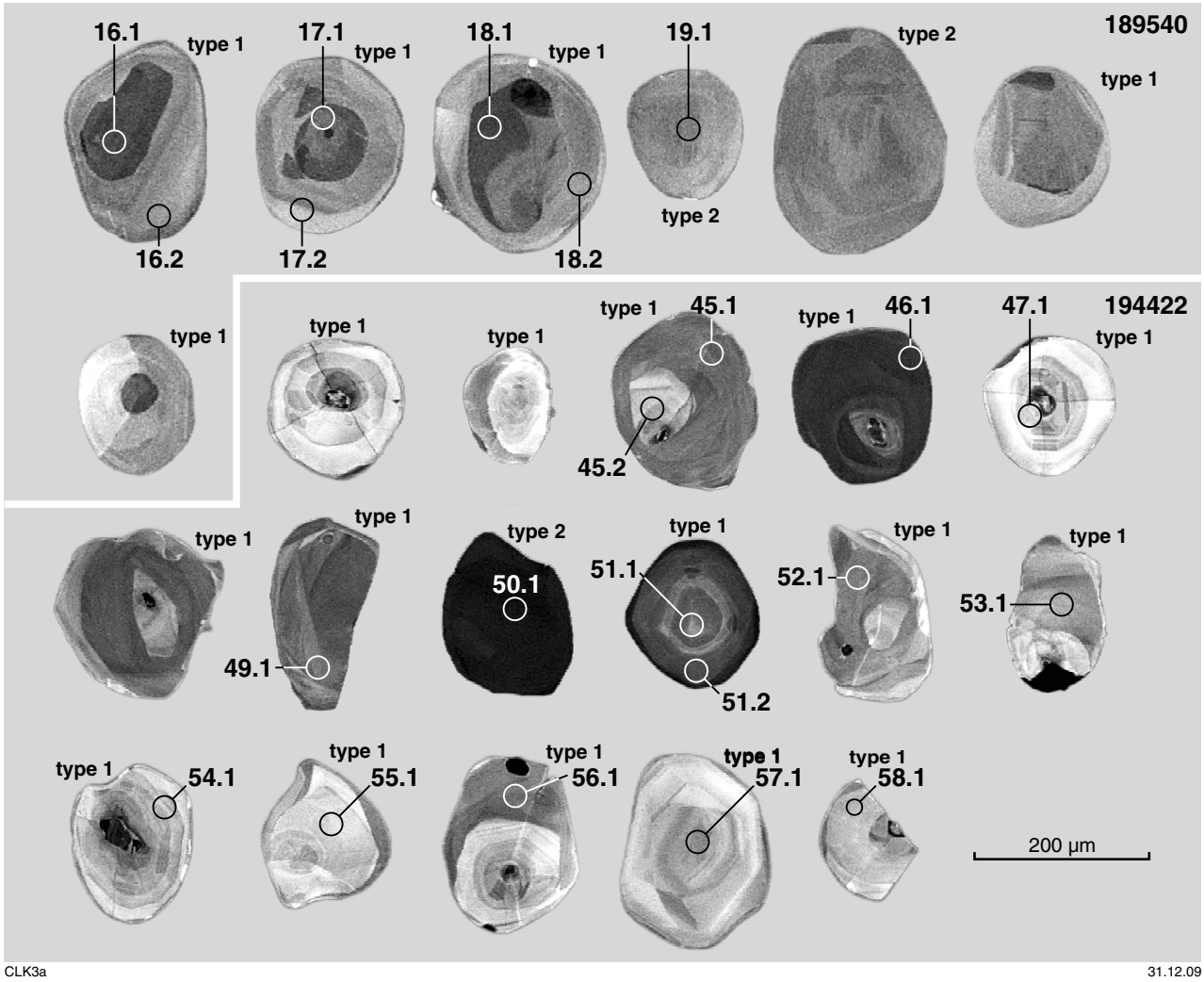

Figure 11. Cathodoluminescence (CL) images of selected zircon grains from GSWA 194422 and 189540. Ellipses indicate the approximate positions of the analytical sites, labelled with the grain spot identification corresponding to that given in Appendix 2. Type 1 zircons contain cores with oscillatory zoning typical of magmatic crystallization or growth during high-grade metamorphism and anatexis; Type 2 zircons are discrete grains with characteristic faint sector zoning ('soccer ball') textures or are homogeneous and are interpreted to have grown during high-grade metamorphism.

process or inheritance. Twenty analyses of both rims and cores (of Type 1 and 2) yield a concordia age of 1119 ± 7 Ma (MSWD = 0.90). The data for both cores and rims spans essentially the same age range, with no correlation between zircon type and date. The zircon textures are compatible with an interpretation in which neocrystallization of rims occurred synchronously with radiogenic-Pb loss in pre-existing cores. The alternative interpretation of continuous crystallization related to in-situ melting accompanied by metamorphic zircon growth is incompatible with the mineralogy of this sample, which does not contain any feldspar. Furthermore, a Pb-loss interpretation is supported by faded oscillatory textures in the Type 1 cores, implying original magmatic growth for Type 1 zircons and their presence in this rock as a detrital phase.

In sample GSWA 194422, the growth of zircon rims appears to have been contemporaneous with radiogenic-Pb loss from cores over a protracted period, spanning 1266 to 1072 Ma. Many of the grains have low U concentrations and all grains have a low calculated alpha radiation dose, corresponding with a 'crystalline' structure (Murakami et al., 1991). Furthermore, there is no correlation between age and U content. This implies temperatures fluctuating in excess of 1000°C (i.e. UHT conditions), required to permit Pb diffusion in the crystalline zircon cores (Williams, 1992; Cherniak and Watson 2001).

GSWA 189540: pelitic gneiss, Mount Blyth

Another example of similar zircon morphology is from sample GSWA 189540 (Kirkland et al., 2010b), a pelitic gneiss from the eastern part of the Mamutjarra Zone (Mount Blyth). Again, two textural varieties of zircon exist: Type 1 with older cores, displaying a truncation of earlier textures, and Type 2, discrete homogeneous grains. Type 1 grains are a minor population and comprise colourless to light brown, spheroidal crystals, up to 400 µm in diameter. In CL, Type 1 zircon displays low-CL

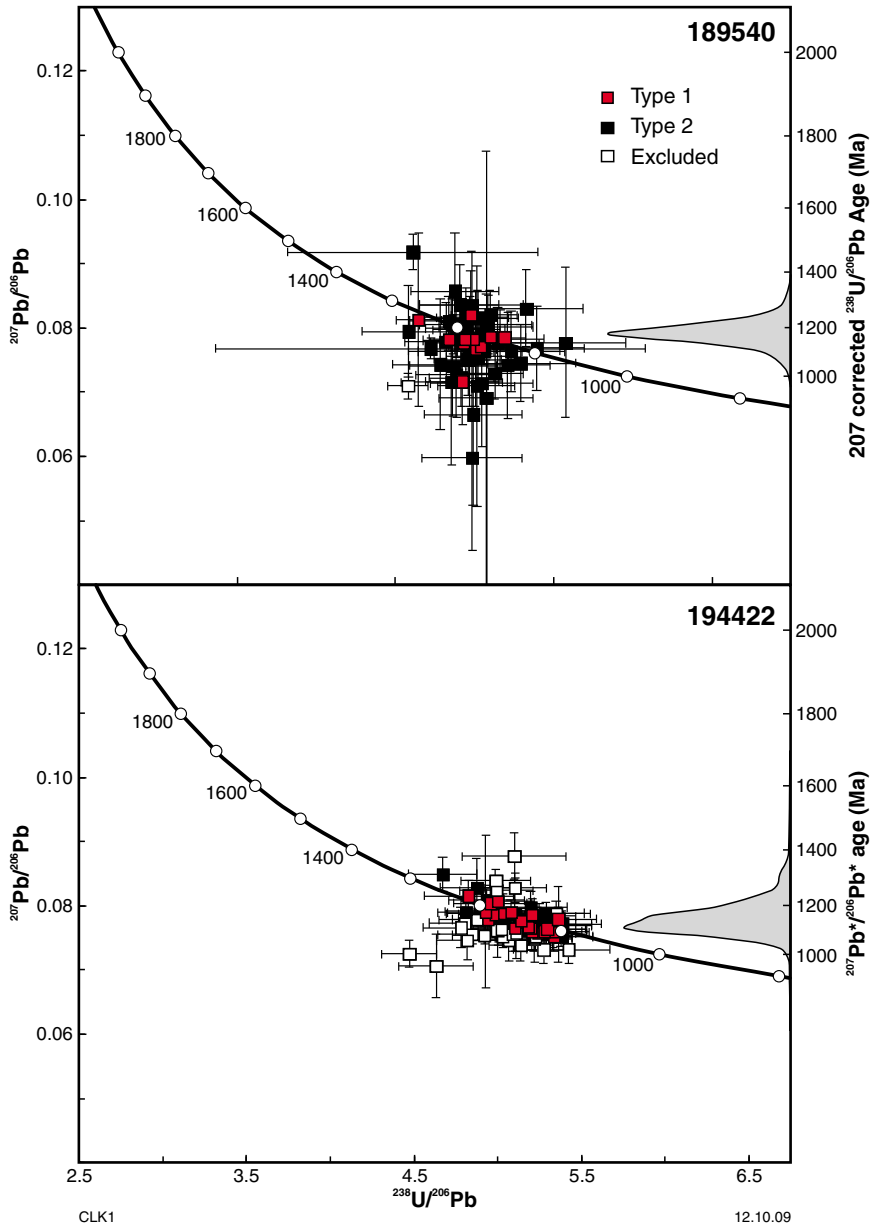

Figure 12. U–Pb analytical data for GSWA 194422 and 189540. Error ellipses are shown at the 2σ level. Age probability plots are displayed on the right Y axis.

response cores, some with faint indications of oscillatory zoning, overgrown by numerous homogenous, moderate-CL response rims. Type 2 zircons are the dominant population, are also spheroidal, and have a moderate CL response with faint sector zoning ('soccer ball'). This sample has notably fewer grains with potential cores than GSWA 194422.

Fifty-five analyses, both from cores and rims of Type 1 zircons and from Type 2 zircons, yield a weighted mean 207-corrected $^{238}U/^{206}Pb^*$ date of 1175 ± 8 Ma (MSWD = 1.5), interpreted as the age of a high-grade metamorphic event. One analysis of Type 1 zircon (zircon 27.1) yields a somewhat older date of 1258 ± 40 Ma (1σ).

All Type 2 grains in GSWA 189540 have low to very low U contents (typically <20 ppm). No indication of older ages is retained within the core domains of Type 1 zircons. All analyses indicate calculated alpha radiation dosages corresponding with a 'crystalline structure' and no correlation is evident between U content and date. Hence, the 1175 Ma date is interpreted to primarily reflect neocrystallization of zircon during a high-grade metamorphic event. Zircon cores yield an identical age to rims and imply that radiogenic-Pb loss was occurring synchronously with neocrystallization of rims. This also requires temperatures in excess of the Pb diffusion temperature in crystalline zircon (i.e. >1000 °C).

Magmatic temperatures at emplacement level

Magmatic temperatures at which the granites of the Pitjantjatjara Supersuite were emplaced can be

estimated using the Zr-saturation thermometer of Watson and Harrison (1983) and fall in the range 746–993°C with an average of 868°C. These temperatures are slightly lower than the inferred and calculated metamorphic temperatures (above), but reflect minimum temperatures because the primary magmas were undersaturated with Zr, as shown by the lack of zircon inheritance.

The Pitjantjatjara Supersuite granites show very close compositional and mineralogical similarities to a series of anhydrous, Ti- and P-rich charnockitic intrusive and extrusive rocks described by Kilpatrick and Ellis (1992) from a range of Paleozoic to Proterozoic terrains. In unmetamorphosed examples of 'charnockite series' granites and volcanic rocks, the presence of inverted pigeonite and the application of two-pyroxene thermometry confirm extremely high crystallization temperatures, in some cases greater than 1100˚C (e.g. Garland et al., 1995; Ewart et al., 2004a).

Because voluminous Pitjantjatjara magmatism was more or less continuous throughout the Musgrave Orogeny (Fig. 9), it appears likely that UHT conditions also persisted more or less continuously at that crustal level throughout the roughly100 Ma period of the Musgrave Orogeny. Given the voluminous nature of Pitjantjatjara magmatism at the exposed level of emplacement, these ultra-high temperatures appear to support the suggestion that charnockite plutonism can be a major driving force for granulite facies metamorphism (e.g. Frost and Frost, 2008). However, metamorphic temperatures in the west of the Mamutjarra Zone are estimated to have reached 1000+°C at c. 1211 Ma (Kelsey et al., 2009), whereas the most voluminous Pitjantjatjara granite intrusion in this region occurred c. 70 Ma later. Hence, UHT conditions at the current level of exposure are not necessarily tied to the regionally synchronous intrusion of Pitjantjatjara granites, although both reflect even more extreme metamorphic conditions at depth (see below). It also follows that the broad southwest trend to younger crystallization ages for Pitjantjatjara granites more likely reflects a migration in the locus of intrusion rather than in the locus of melting or of maximum heat flux.

Although the spread of ages attributable to UHT events (c. 1220–1120 Ma) is interpreted to reflect sustained ultra-high temperatures throughout the Musgrave Orogeny, the crystallization of the Pitjantjatjara Supersuite granite intrusions themselves, the preservation of planar internal contact relationships within these granite bodies, and the P–T paths interpreted from post-peak reaction microstructures, all indicate that, in detail, temperatures periodically fluctuated below the liquidus temperatures of these granites. Nevertheless, a 100 Ma history of at least periodic episodes of UHT metamorphism (e.g. King, 2008), including more or less continuous high-temperature charnockitic magmatism (Smithies et al., 2009a) chronicles an extremely unusual tectonothermal regime almost certainly involving extensive crust–mantle interaction.

The Giles Event — Warakurna Supersuite

Igneous rocks of the Warakurna Supersuite crop out across approximately 1.5 million km^2 of central and western Australia, forming the Warakurna large igneous province (Fig. 13; Wingate et al., 2004; Morris and Pirajno, 2005). In the Musgrave Province, this supersuite incorporates giant layered mafic–ultramafic intrusions (Giles intrusions), mafic dykes, granites, and remnants of a bimodal (basalt and rhyolite) volcanic succession (Bentley Supergroup).

Smithies et al. (2009a) and Evins et al. (in press) showed that mafic and felsic rocks originally attributed to the c. 1075 Ma Giles Event, in the west Musgrave Province, are actually part of a complex sequence of magmatic and tectonic events punctuated over a span of at least 50 Ma This sequence consists of at least seven magmatic episodes with hiati of up to ~10 Ma (Evins et al., in press).

Giant layered mafic–ultramafic bodies (Giles intrusions) — the largest probably initially more than 170 km long, 25 km wide, and up to 10 km thick — intruded the boundary between the Mamutjarra and Tjuni Purlka Tectonic Zones (Fig. 3) between c. 1120 Ma and 1078 Ma (Smithies et al., 2009a; Evins et al., in press). Large bodies of massive, unlayered gabbro form a near-continuous feature focused along syn-magmatic shear zones that mark the northeastern boundary of the Tjuni Purlka Tectonic Zone (Fig. 3) at c. 1075 Ma, and are locally characterized by extensive zones of co-mingling with felsic magmas. Mafic and felsic magmatism continued to be channelled along the boundaries of the Tjuni Purlka Tectonic Zone until eruption of felsic lavas of the Tollu Group from c. 1075 to 1026 Ma (e.g. GSWA 187177). In the Tjuni Purlka Tectonic Zone and the Mamutjarra Zone, felsic intrusions range from dykes and sheets to plutons up to 12 km in diameter (Tollu pluton), and mostly intruded between c. 1075 and c. 1062 Ma (Evins et al., in press). These range from monzogranite to quartz syenite and include rapakivi varieties, typically with mafic mineral assemblages of clinopyroxene–hornblende(–biotite).

The age of the Giles Event and of the Warakurna large igneous province is close to the timing of the assembly of the Rodinia supercontinent (c. 1000–1100 Ma). They have been interpreted to be related to a mantle plume which impacted the lithosphere beneath the Musgrave Province at c. 1075 Ma (Wingate et al., 2004; Morris and Pirajno, 2005), although a geodynamic setting more complex than a single mantle plume appears most likely (Smithies et al., 2009a; Evins et al., in press).

Previous studies supported by geochronological data have identify only the main, spaced, thermal peaks, resulting in the Musgrave Orogeny and the Giles Event being regarded as distinctly separate tectonothermal entities. However, Evins et al. (in press) have shown that the Giles Event occurred over a period of at least 60 Ma and formed a failed intracontinental rift system called the Ngaanyatjarra Rift. Furthermore, our extensive geochronological dataset (Smithies et al., 2009; GSWA Geochronology

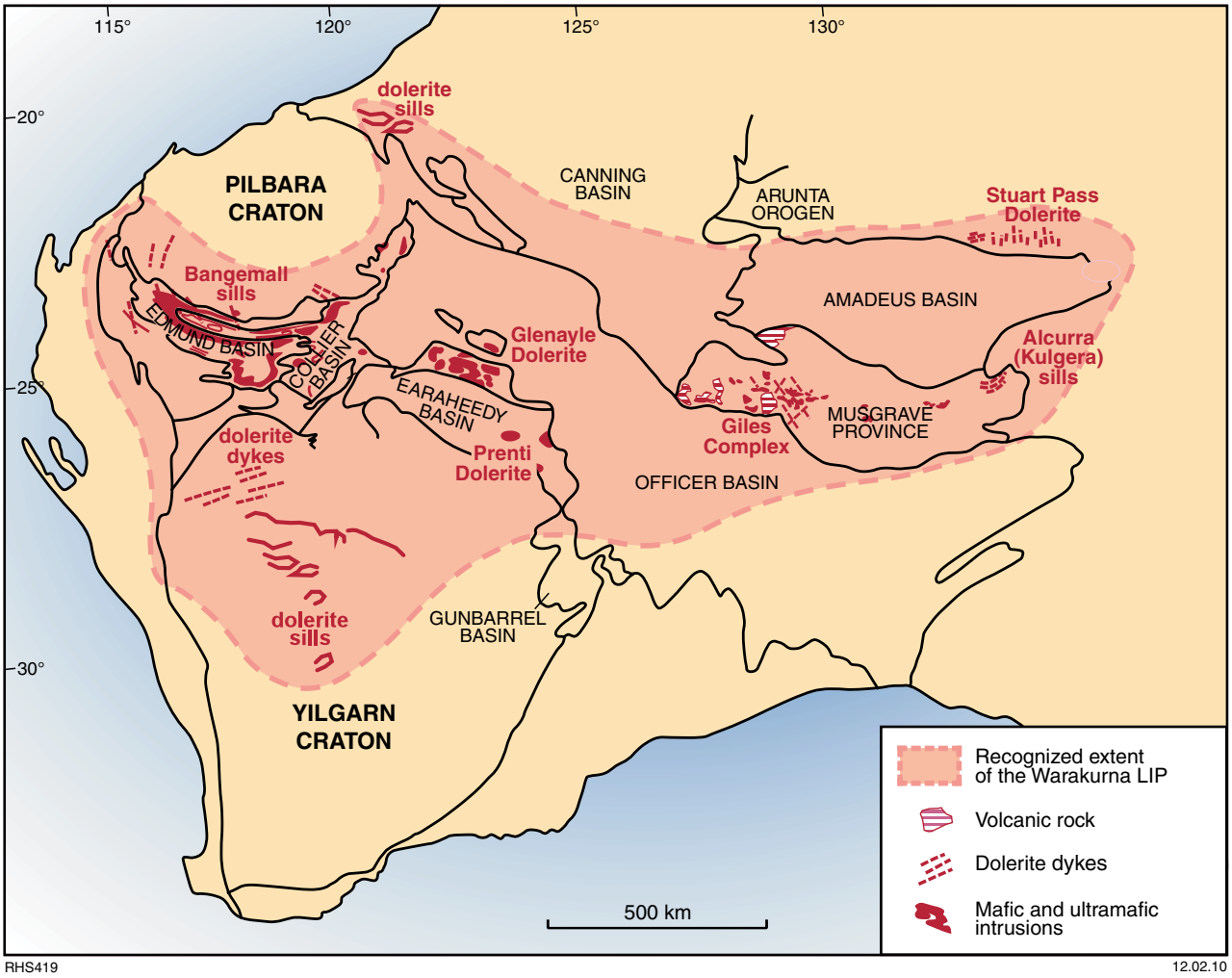

Figure 13. Map of central and western Australia showing the regional extent of extrusive and intrusive rocks attributed to the Warakurna Large Igneous Province (modified from Wingate et al., 2004).

Record Series) shows that thermal events related to the Musgrave Orogeny span a roughly 100 Ma period down to a minimum age of c. 1119 ± 7 Ma, which overlaps the maximum possible intrusive age of the giant layered mafic–ultramafic bodies of the Giles Event (Fig. 5). Accordingly, it might be legitimate to regard the Giles Event as a late component of the Musgrave Orogeny — forming a combined high-temperature metamorphic and magmatic period spanning about 200 Ma.

Younger tectonism

The Musgrave Province was again deformed during the c. 550 Ma Petermann Orogeny, which coincides with the global 'Pan-African' period of plate reorganization that marks the assembly of Gondwana. The Petermann Orogeny appears to have been essentially intracratonic with very little, if any, production of new crust. Granulites and high-grade gneisses of the Musgrave Province were thrust northwards, over or into rocks of the Neoproterozoic basins (Camacho, 1997; Flöttmann and Hand, 1999; Edgoose et al., 2004), in a process that involved intracontinental channel flow (Raimondo et al., 2009). Significant vertical displacements juxtaposed lower-crustal near-eclogite facies rocks against amphibolite facies rocks along the west to west-northwest trending Mann Fault in the south and the Woodroffe Thrust in the north (Camacho et al., 1997).

Granite geochemistry

Analytical details for whole-rock geochemical and Nd isotopic analyses, as well as Hf isotopic analyses of zircon, are presented in Appendix 2. Whole rock geochemical data are presented in Appendix 3 and Nd and Hf isotopic data are presented in Appendices 4 and 5 respectively.

Effects of metamorphism on geochemistry

All rocks of the Wankanki and Pitjantjatjara Supersuites have been recrystallized at granulite facies. Rocks with

a strong gneissosity or with visible migmatitic melt veinlets or melt patches were avoided during sampling. Nevertheless, granites within the west Musgrave Province show a wide range in Th/U (Fig. 14), possibly reflecting element mobility related to such processes as metamorphic dehydration, separation of a migmatitic melt fraction, or hydrothermal alteration. The range for the older rocks of the Wankanki Supersuite is particularly wide, with most values >10 and up to ~60. In addition, many geochemical variation diagrams for the Wankanki Supersuite (and less so for the Pitjantjatjara Supersuite) show several points with anomalous concentrations (outliers), and this is particularly evident for CaO, Na_2O, K_2O, Sr, and Ba. While it is generally the same samples that show anomalous concentrations of these elements, these data have not been removed from the geochemical variation diagrams, except in cases where their inclusion results in scales that obscure trends in the remaining data.

Regardless, geochemical trends for most elements and for all supersuites, show surprisingly little scatter, which is not improved by separating rocks into textural (i.e. gneissic, massive) groups. This is true even for some of the strongly incompatible large ion lithophile elements (LILE) including Rb and Pb, both of which show surprisingly well constrained variations for rocks of both the Wankanki and Pitjantjatjara supersuites, particularly given the high temperature and prolonged metamorphic history of these rocks.

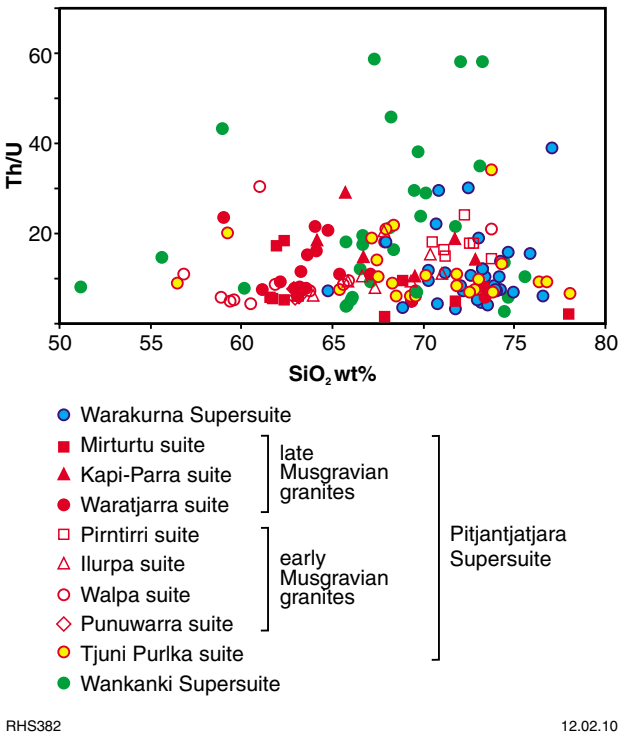

Figure 14. Plot of Th/U versus SiO_2 for granites of the west Musgrave Province.

Wankanki Supersuite

Rocks from the Wankanki Supersuite show a large range in SiO_2 from 51.2 to 75.6 wt%, although there is a significant gap in that range, from 60.3 to 65.8 wt%, which separates rare tonalites and granodiorites from more abundant monzogranites and syenogranites (Fig. 15). The compositions are typically metaluminous (ASI = 0.6–1.02) and calcic to calc-alkalic. With increasing SiO_2 there are systematic decreases in Al_2O_3 (17.8–12.8 wt%), CaO (11.2–0.92 wt%), Fe_2O_3T (total Fe as Fe_2O_3 = 11.2–1.0 wt%), MgO (7.4–0.15 wt%), $Mg^{\#}$ * (56–22), TiO_2 (1.19–0.09 wt%), and P_2O_5 (0.29–0.03), and corresponding increases in K_2O (0.63–6.60 wt%) and K_2O/Na_2O (0.21–1.98; not shown).

The LILE (e.g. Sr, Ba, Rb, and Pb) show reasonably well constrained trends (Fig. 16); both Pb (6–51 ppm) and Rb (23–230 ppm) increase with increasing SiO_2, whereas Ba (and possibly Sr) initially increases (Ba from 271 to 1118 ppm) to an inflection point within the silica gap, and then decreases (to 292 ppm Ba). Small variations can be seen in Rb/Sr (0.06 to ~1.1) and K/Rb (~350 to ~200) over the full silica range and Sr/Ba decreases (0.65 to 0.13).

Rocks from the Wankanki Supersuite have low concentrations of high field strength elements (HFSE e.g. Nb, Zr, Hf, REE, and Y; Fig. 17). The light rare earth elements (LREE; e.g. La and Ce) and Ta show small increases in concentration with increasing silica, whereas the middle- and heavy rare earth elements (MREE; e.g. Sm, Eu, Gd: HREE; e.g. Yb, Lu), Nb and Zr either decrease slightly or remain constant. The result of variations in Nb and Ta is a small decrease in Nb/Ta ratios with increasing SiO_2 or decreasing $Mg^{\#}$. Incompatible trace element ratios such as La/Yb, La/Sm, and La/Nb (Fig. 18), also remain low and constant, or increase slightly with increasing silica, up to the silica gap, and then show a range to higher values. Mantle normalized REE patterns (Fig. 19) show moderate LREE enrichment, with weak negative Eu anomalies, and reasonably flat trends for the middle- to heavy REE (M-HREE).

Nd-isotopic data for the Wankanki Supersuite (Fig. 20; Appendix 4) show a narrow range of rather juvenile to moderately evolved εNd values from -0.56 to -2.39 with the rocks from the southeastern part of the Mamutjarra Zone, in particular, showing a very narrow range from -0.56 to -1.17. Depleted mantle model ages (T_{DM2} — denotes the two-stage Nd-evolution model of Liew and Hofmann, 1988) typically lie with a range from 1900 to 2040 Ma.

The Hf-isotopic value of zircons within rocks of the Wankanki Supersuite (Appendix 6) also span a range of moderately juvenile values that plot consistently between primitive and depleted (εHf from +1 to +5) mantle, but form age clusters that lie on trends that reflect crustal $^{176}Lu/^{177}Hf$ ratios of ~0.015 (Fig. 21). Magmatic zircon cores (c. 1321 Ma) and metamorphic rims (c. 1200 Ma) from a sample of Wankanki Supersuite granite (GSWA 183496) yield a mean crustal model age [T_{DM}^{c}(Hf)] of ~1840 Ma, which is very close to the whole-rock T_{DM2}(Nd) of 1900 Ma. Similarly, zircon xenocrysts in a granite of the Pitjantjatjara Supersuite (Tjuni Purlka suite; GSWA 185339) have Wankanki Supersuite ages and also yield a very narrow range of T_{DM}^{c}(Hf) values (from c. 1850 to 2000 Ma) with a mean T_{DM}^{c}(Hf).

* $Mg^{\#}$ is the molecular ratio of MgO/(MgO+FeO) with all Fe calculated as Fe^{2+}

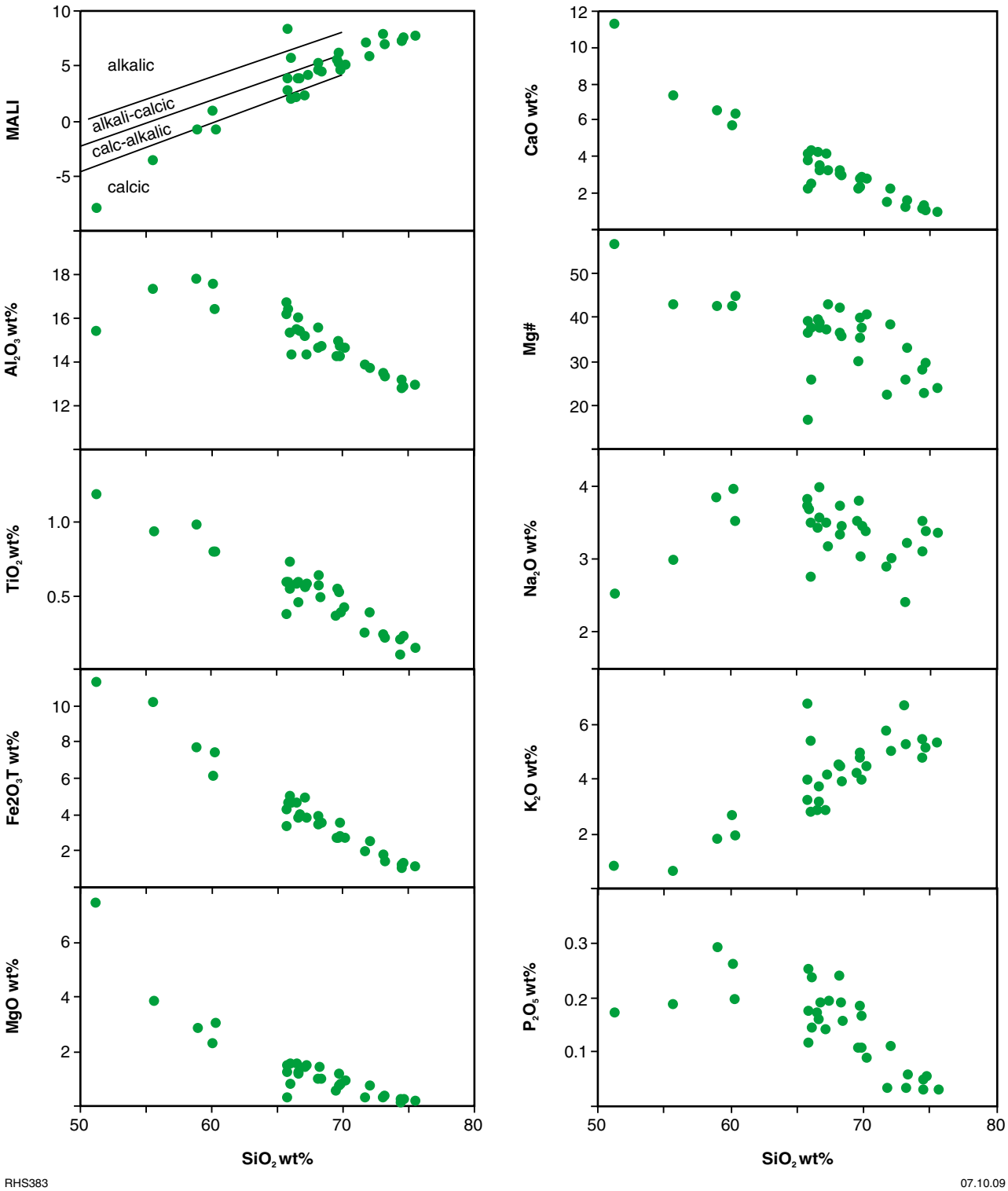

Figure 15 Plot of major elements versus SiO_2 for granites of the Wankanki Supersuite. Modified alkali-lime index (MALI = Na_2O+K_2O-CaO) and fields for alkalic, alkali-calcic, calc-alkalic, and calcic rocks are from Frost et al. (2001).

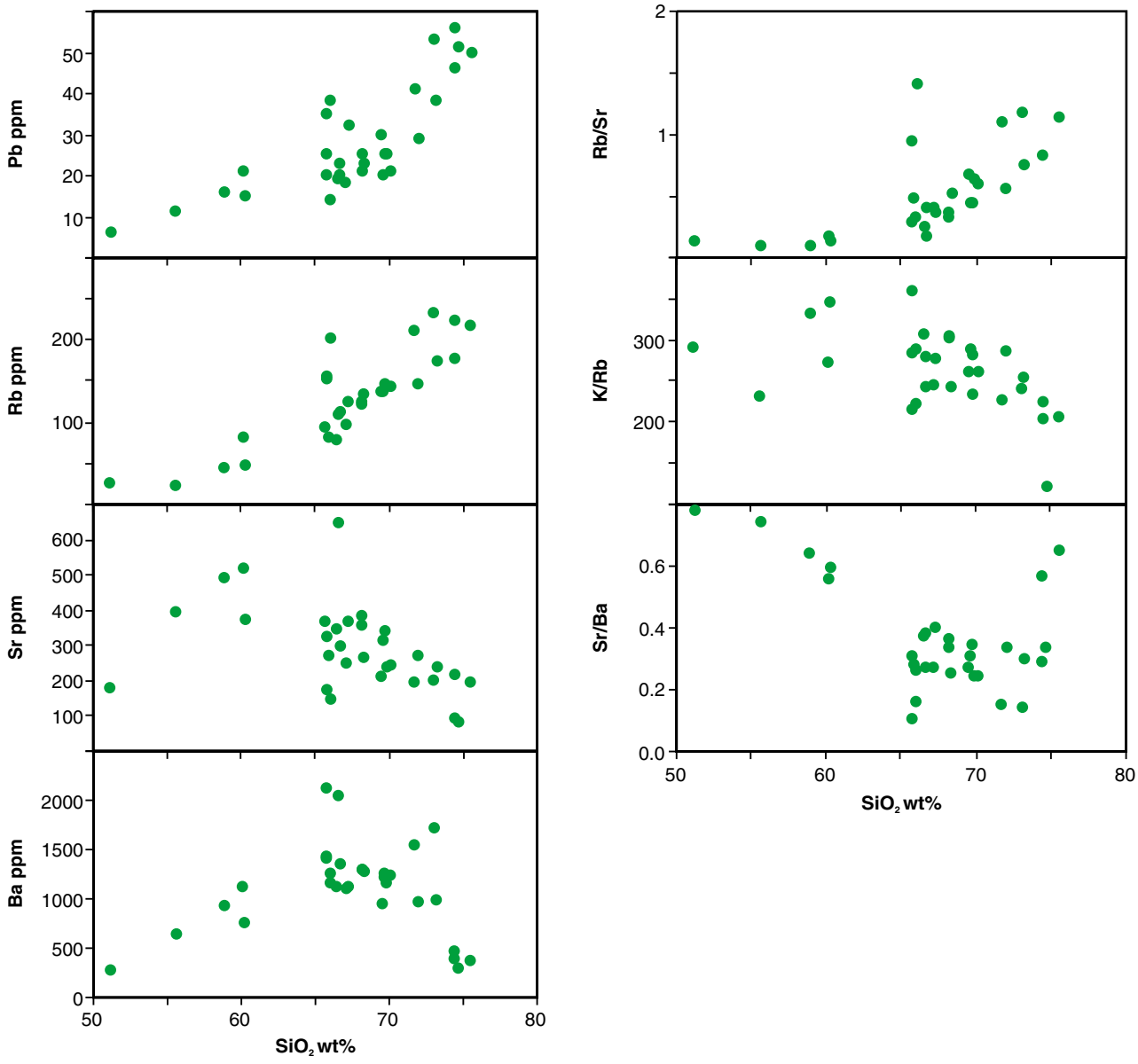

Figure 16. Plot of Pb, Rb, Sr, Ba, Rb/Sr, K/Rb and Sr/Ba versus SiO_2 for granites of the Wankanki Supersuite.

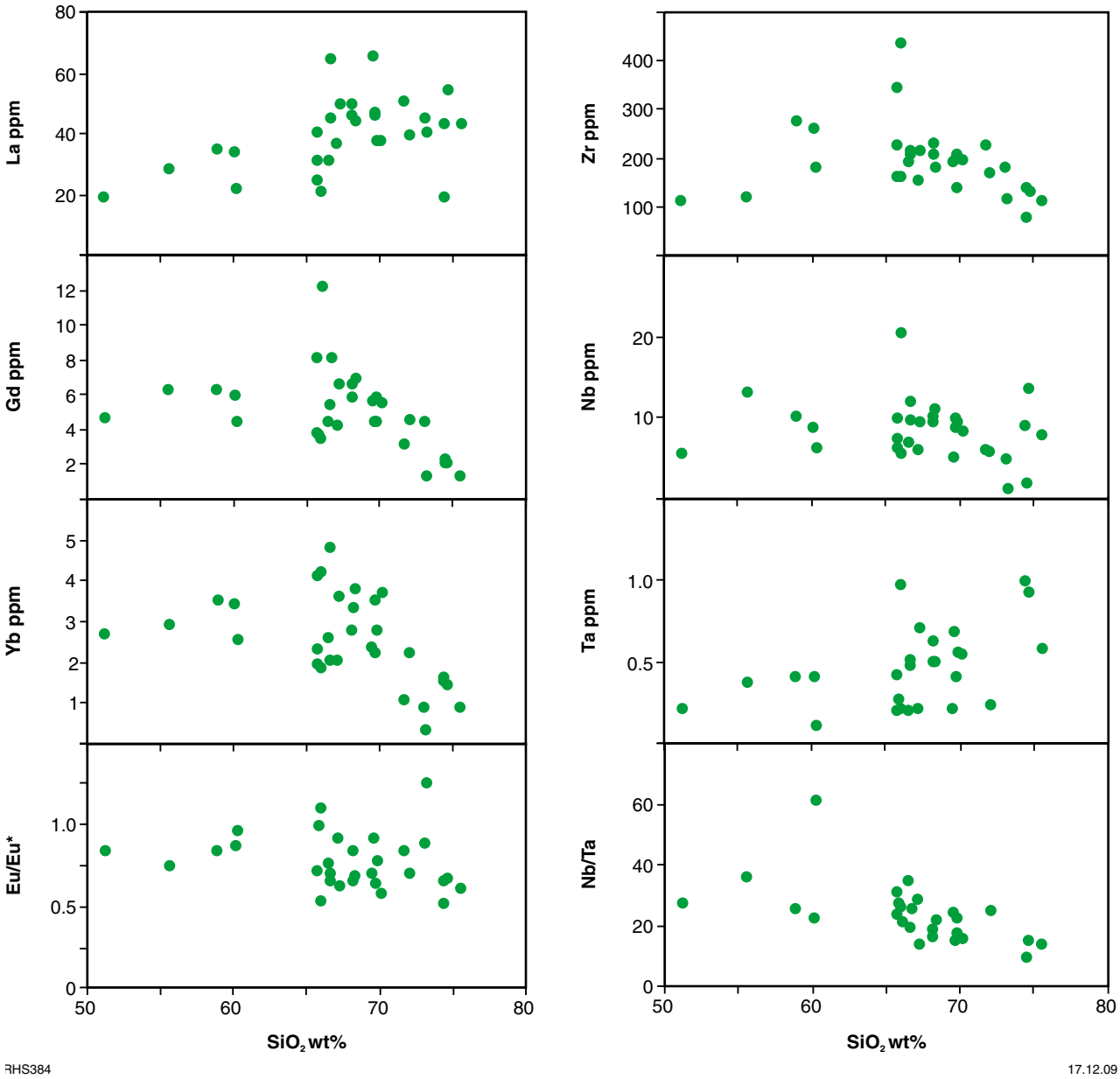

Figure 17. Plot of La, Gd, Yb, Eu/Eu*, Zr, Nb, Ta and Nb/Ta versus SiO_2 for granites of the Wankanki Supersuite.

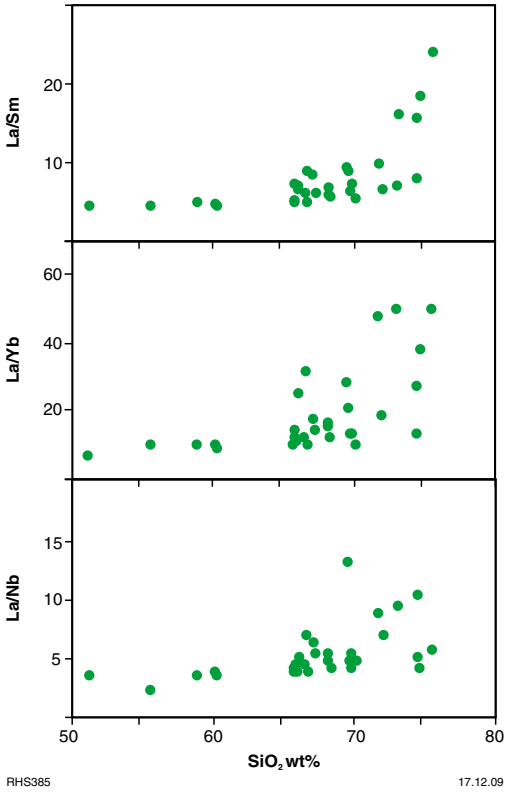

Figure 18. Plot of La/Sm, La/Yb and La/Nb versus SiO_2 for granites of the Wankanki Supersuite.

Figure 19. (below) Multi-element and REE spider diagrams for granites of the west Musgrave Province (normalization factors from Sun and McDonough, 1989).

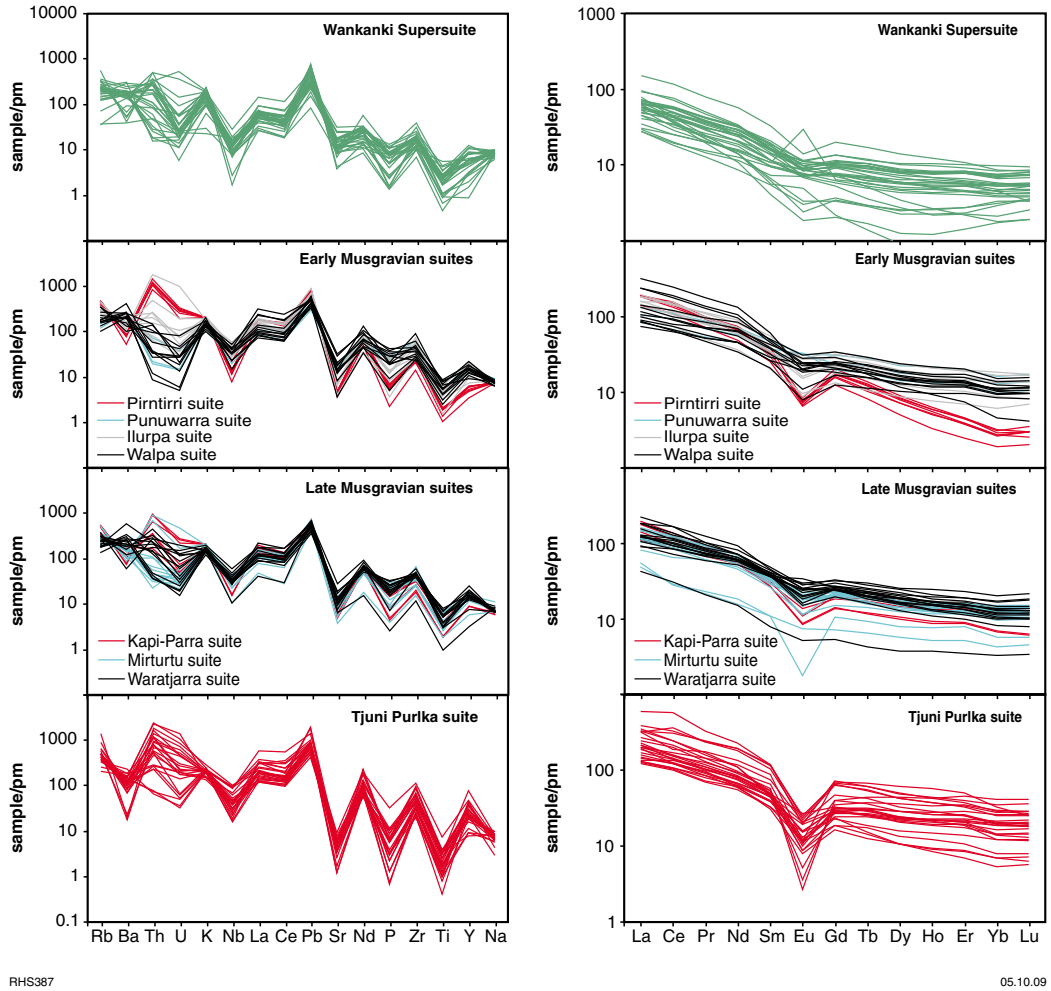

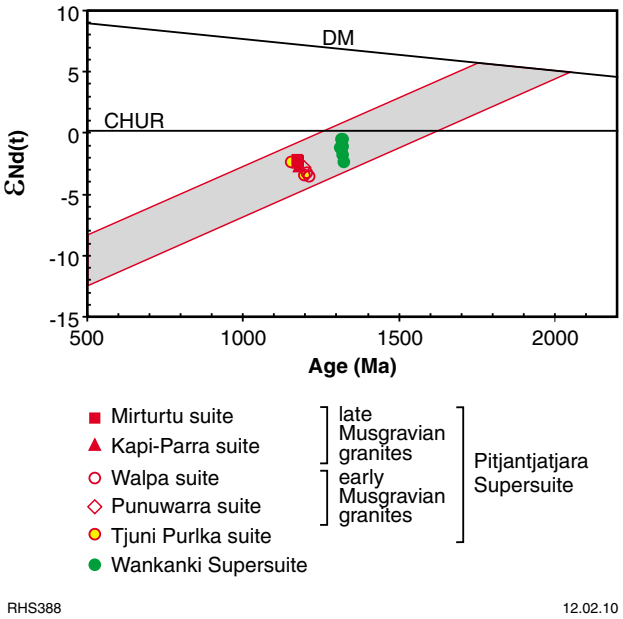

Figure 20. **ε_{Nd} evolution diagram for granites of the Wankanki and Pitjantjatjara Supersuites showing the isotopic evolution field for rocks of the Wankanki Supersuite. DM= depleted mantle; CHUR = bulk silicate earth (chondritic uniform reservoir). All model ages reside between 1700 and 2000 Ma.**

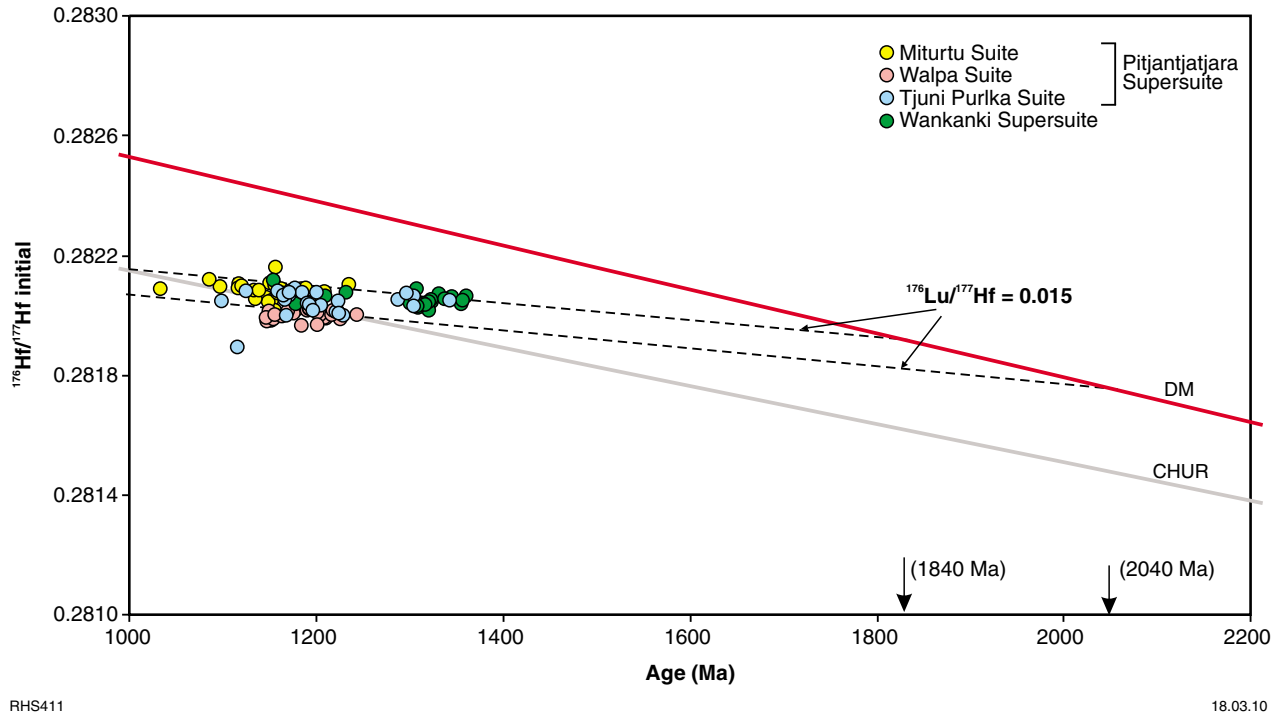

Figure 21. Initial Hf evolution diagram for granites of the Wankanki and Pitjantjatjara Supersuites.

Pitjantjatjara Supersuite

As a group, the Pitjantjatjara Supersuite granites can be readily distinguished geochemically from the Wankanki granites. Both supersuites are metaluminous and cover a similarly wide range in silica, but compared to the Wankanki granites, the Pitjantjatjara granites at equivalent silica concentrations generally range to lower Al_2O_3, CaO, Na_2O, ASI, Sr, MgO, Eu/Eu*[*], and $Mg^{\#}$ (not shown) and higher K_2O, TiO_2, Fe_2O_3, P_2O_5, Pb, Rb, REE, and HFSE (Figs 22–24). Very high concentrations of TiO_2, P_2O_5, and HFSE and low concentrations of Sr, in particular, separate most granites of the Pitjantjatjara Supersuite from those of the Wankanki Supersuite. The Pitjantjatjara Supersuite granites are strongly ferroan and typically alkali-calcic.

With increasing SiO_2, rocks of the Pitjantjatjara Supersuite collectively show a systematic decrease in Al_2O_3 (17.25 – 11.74 wt%), CaO (6.18 – 0.62 wt%), Fe_2O_3T (total Fe as Fe_2O_3 = 10.48 – 0.98 wt%), MgO (2.35 – 0.07 wt%), $Mg^{\#}$ (35–12), TiO_2 (1.86 – 0.09 wt%) and P_2O_5 (0.92 – 0.01). Concentrations of K_2O show a weak trend to higher values (2.85 – 6.00 wt%) with increasing silica, and K_2O/ Na_2O (not shown) increase (0.82 – 2.56). The LILE show moderately well constrained trends, with Sr (672–15 ppm) and Ba (3000–33 ppm) decreasing and Rb (65–639 ppm) and Pb (19–67 ppm) increasing with decreasing SiO_2 but with only modest variations in Rb/Sr (0.15 to 3.96) and K/Rb (383 to 65). Concentrations of REE, and HFSE either remain constant or decrease with increasing silica, with small increases in La/Nb, La/Yb, and La/Gd (not shown) and decreases in Gd/Yb and Eu/Eu* (1.05 – 0.17; Figs 24–25).

Individual suites

In the west Musgrave Province, rocks of the Pitjantjatjara Supersuite can be subdivided into eight suites (Fig. 26) based on geochemical similarities within groups of similar age and limited geographical extent.

One early Musgravian (Walpa) and two late Musgravian (Mirturtu and Kapi-Parra) suites are recognized in the Walpa Pulka Zone. A series of northwest-trending faults separate the older rocks, to the west, from the younger rocks. The early Musgravian Walpa suite has a large range in silica (56.89 – 73.8 wt%), and K_2O (2.85 – 5.83 wt%), high concentrations of Sr (to ~670 ppm) and Ba (to ~3000 ppm), and correspondingly high K/Rb and low Rb/Sr ratios. The late Musgravian Mirturtu suite ranges to higher silica values (61.59 – 78.02 wt%) and is also slightly depleted in P_2O_5 and has higher $Mg^{\#}$ (not shown) than the Walpa suite at equivalent silica contents. Compared with these suites, intrusions that form the Kapi-Parra suite have a narrow silica range (64.14 – 72.87 wt%) but show similar trends and similar concentrations at equivalent silica values, with the exceptions of the LREE and Th, both of which increase significantly with decreasing silica (La increases from 76 to 137 ppm; Th increases from 16 to 91 ppm). The La/Sm and La/Gd ratios (not shown on figure) also have a more significant increase in the Kapi-Parra suite and HFSE are marginally more enriched, at a given silica content, compared with the rocks of the Mirturtu suite.

One late Musgravian suite (Waratjarra) is recognized in the western part of the Mamutjarra Zone, straddling the boundary with the southeastern part of the Tjuni Purlka Tectonic Zone. These rocks are geochemically similar to the late Musgravian Mirturtu suite from the Walpa Pulka Zone, but typically range to higher concentrations of HREE, Y (not shown), and Zr.

Two early Musgravian suites (Pirntirri and Ilurpa) form plutons within the northeastern part of the Tjuni Purlka Tectonic Zone, and another early Musgravian suite (Punuwarra) lies in the southeast. The Pirntirri suite has a very limited range of high silica values (70.5 – 73.7 wt%), and is characterized by high LREE (La ~130 ppm), Th (80–133 ppm) and Pb (~60 ppm), low HREE (Yb = 1.54 – 0.95 ppm) concentrations and high La/Yb (~100) La/Nb (~15) and Nb/Ta (24–66) ratios. The Ilurpa suite has a wider silica range, but at lower concentrations (63.92 – 70.99 wt%), and while it shows many compositional similarities to the Mirturtu suite and to the Waratjarra suite, it is distinctly enriched in P_2O_5 , Nb, and HREE, at a given silica content. The mesocratic charnockites of the Punuwarra suite have a very narrow silica range (62.85 – 63.14 wt%), but at equivalent silica contents, are geochemically similar to the late Musgravian Mirturtu suite from the Walpa Pulka Zone. However, they have higher concentrations of Al_2O_3 (15.09 – 16.59 wt%), CaO (4.51 – 4.94 wt%), Na_2O (3.10 – 3.52 wt%), and Eu (5.33 – 5.65 ppm; not shown) reflecting the abundance of feldspar phenocrysts, which comprise up to 40% of the rock.

Perhaps the most conspicuous suite of Pitjantjatjara granites within the west Musgrave Province is the Tjuni Purlka suite of schlieric biotite–orthopyroxene leucogranites. These rocks are confined to the Tjuni Purlka Tectonic Zone where they form locally voluminous veins, dykes, and sheets with crystallization ages spanning from the early to late Musgrave Orogeny. This suite is relatively silicic (SiO_2 mostly >67 wt%) but within that range, has generally higher Na_2O (to 3.89 wt%), Fe_2O_3T, Rb, Th (to 217 ppm), U (to 30 ppm; not shown), HFSE (Nb to 69 ppm; Zr to 1060 ppm), REE (La to 404 ppm; Ce to 1006 ppm), and particularly the MREE and HREE (Gd to 43 ppm; Yb to 17 ppm), but lower values for TiO_2, P_2O_5, $Mg^{\#}$ (to 7), Sr, and Ba than other Pitjantjatjara granites. HFSE and REE in these rocks decrease in concentration with increasing SiO_2.

Nd-isotopic data for the Pitjantjatjara magmas (Appendix 4) show a very limited range in εNd values from -2.2 to -3.6, with T_{DM2} typically from 1900 to 2040 Ma. The early Musgravian magmas in the Tjuni Purlka Tectonic Zone and Walpa Pulka Zone account for the less radiogenic analyses (εNd values of -2.5 to -3.6), while the late Musgravian magmas from the Walpa Pulka Zone lie within a very narrow εNd range from -2.2 to -2.7, reflecting an extremely isotopically homogeneous source. Significantly, the Nd-isotopic data for the Pitjantjatjara Supersuite lie entirely within a narrow isotopic evolution

[*] Eu/Eu* is primitive mantle normalized concentration of Eu divided by the hypothetical value for the normalized concentration of Eu obtained by extrapolation between the normalized concentrations of Sm and Gd — i.e. it is a measure of the Eu anomaly on a normalized REE profile.

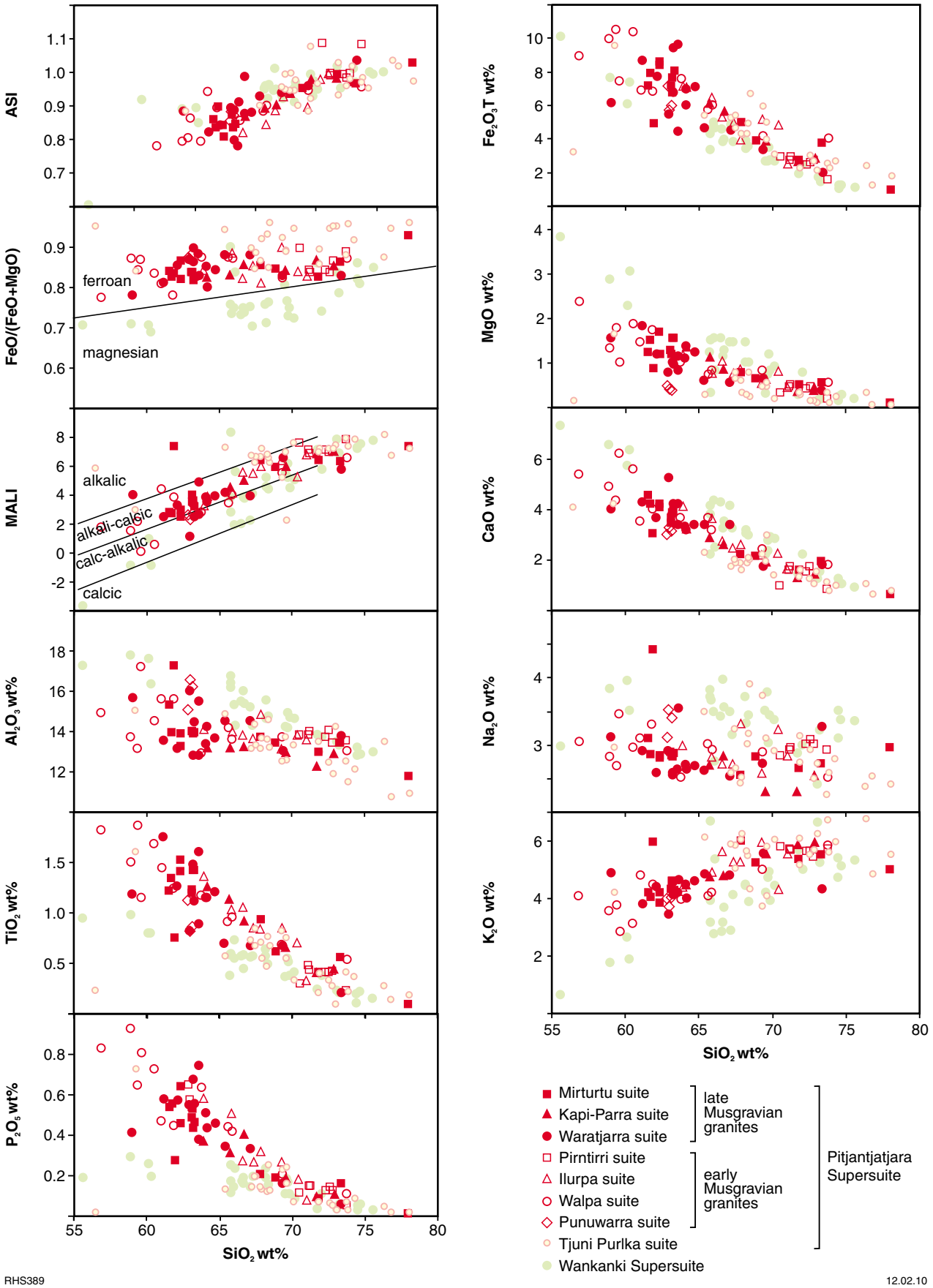

Figure 22. Plot of major elements versus SiO_2 for granites of the Pitjantjatjara Supersuite. Modified alkali-lime index (MALI = $Na_2O+K_2O–CaO$), fields for alkalic, alkali-calcic, calc-alkalic and calcic rocks and for ferroan and magnesian rocks are from Frost et al. (2001). Rocks of the Wankanki Supersuite are plotted for comparison in light green.

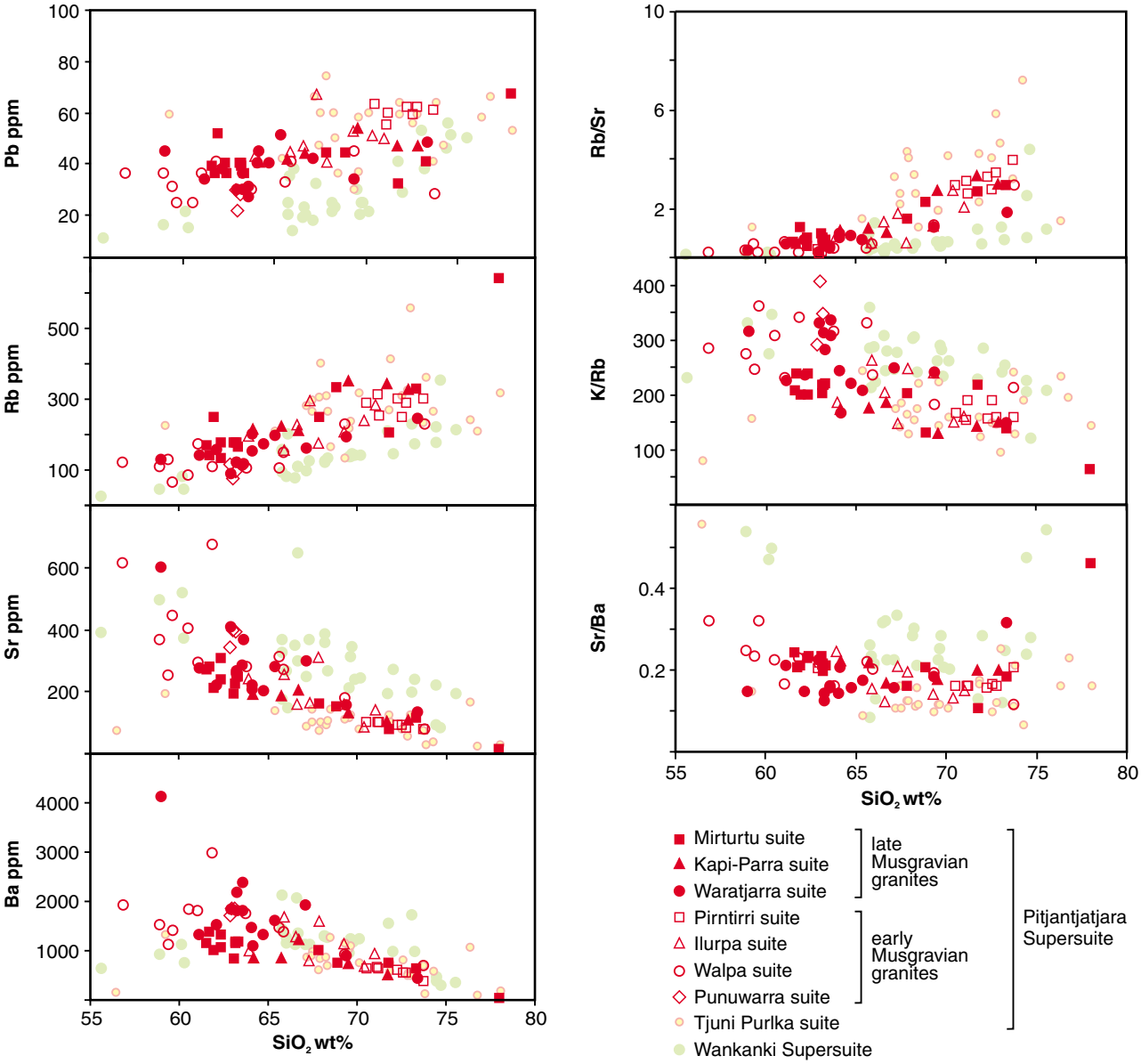

Figure 23. Plot of Pb, Rb, Sr, Ba, Rb/Sr, K/Rb and Sr/Ba versus SiO_2 for granites of the Pitjantjatjara Supersuite. Rocks of the Wankanki Supersuite are plotted for comparison in light green.

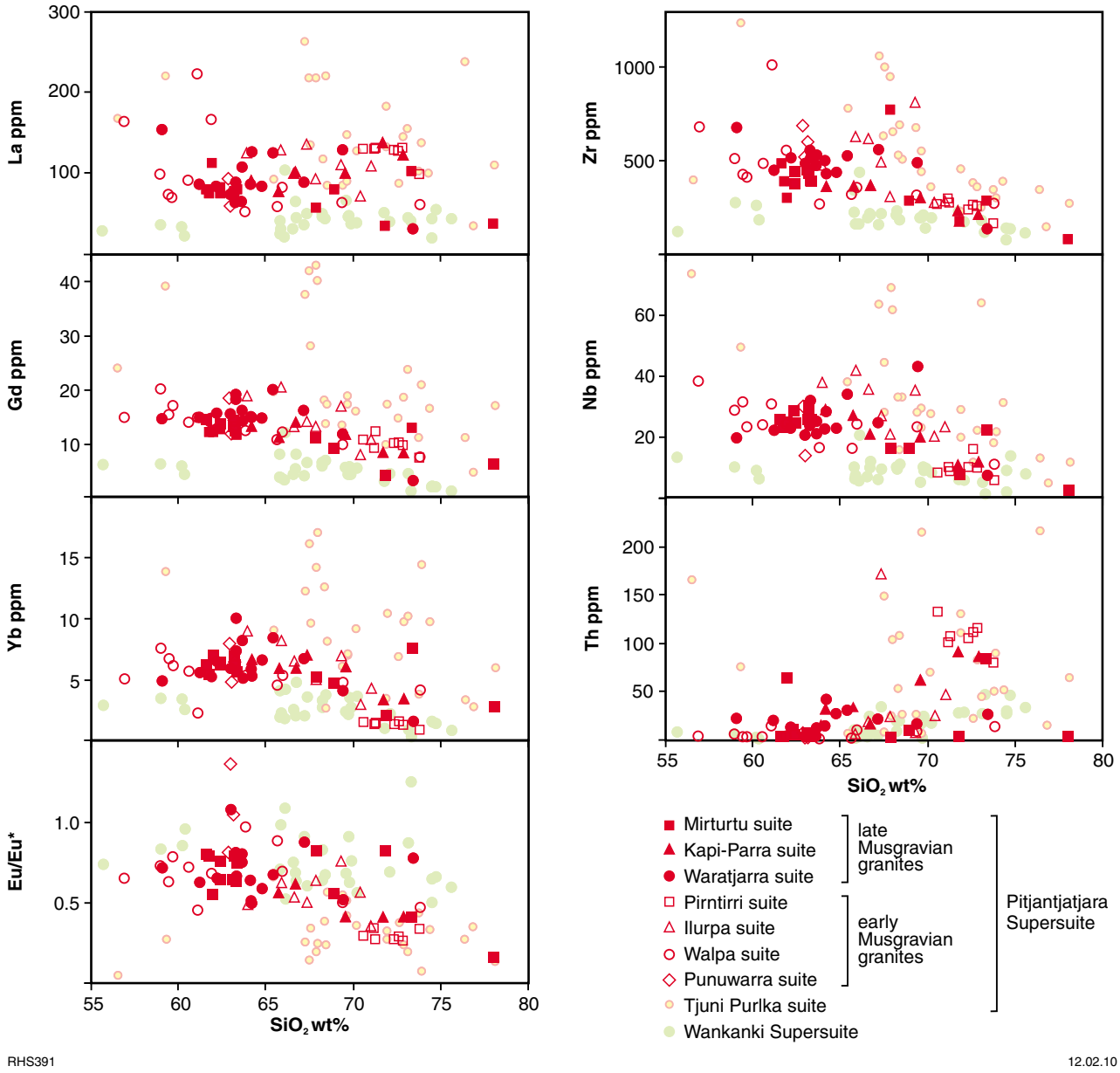

Figure 24. Plot of La, Gd, Yb, Eu/Eu*, Zr, Nb, and Th versus SiO_2 for granites of the Pitjantjatjara Supersuite. Rocks of the Wankanki Supersuite are plotted for comparison in light green.

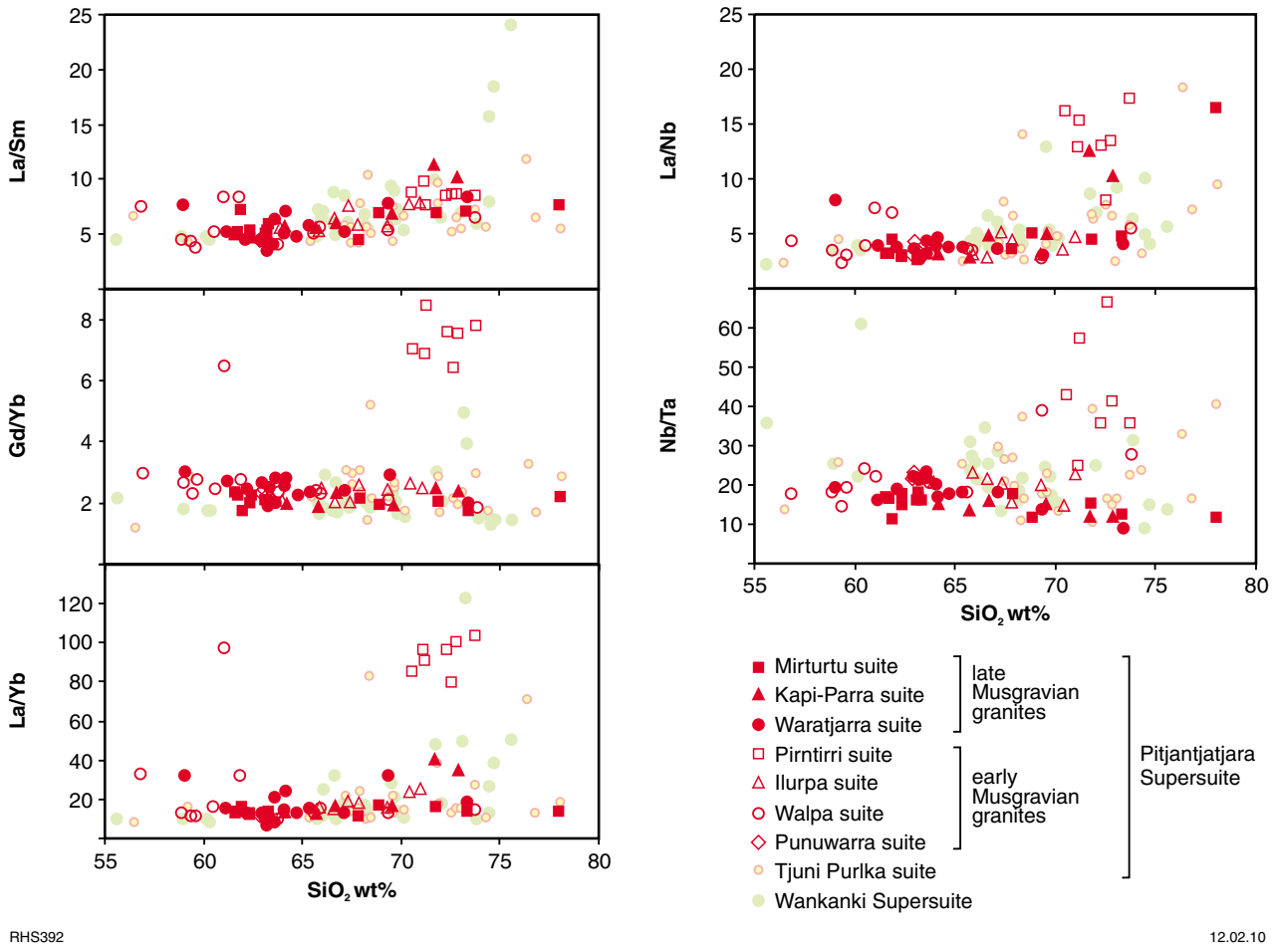

Figure 25. Plot of La/Sm, Gd/Yb, La/Yb, La/Nb and Nb/Ta versus SiO_2 for granites of the Pitjantjatjara Supersuite. Rocks of the Wankanki Supersuite are plotted for comparison in light green.

envelope defined by the rocks of the earlier Wankanki Supersuite (Fig. 20).

Like those from granites of the Wankanki Supersuite, the Hf-isotopic value of zircon within rocks of the Pitjantjatjara Supersuite (Appendix 6) span a range of rather juvenile values that plot consistently between primitive and depleted mantle, and form age clusters that lie on trends with crustal $^{176}Lu/^{177}Hf$ ratios of ~0.015 (Fig. 21). The Hf-isotopic value of zircons was obtained from two samples of Pitjantjatjara granites from the Walpa Pulka Zone. Zircons from a sample of the Walpa Suite (GSWA 174558) show a very narrow range of εHf values (from +0.7 to -2.5) and yield a mean T_{DM}^{c}(Hf) of c. 2040 Ma, while those from a sample of the Mirturtu Suite (GSWA 180256) show a slightly higher contribution from a juvenile component (εHf from -1.3 to +4) and yield a mean T_{DM}^{c}(Hf) of c. 1880 Ma, both overlapping with the whole-rock T_{DM2}(Nd) range of 1900–2040 Ma.

The range in Hf-isotopic values of zircons from two Pitjantjatjara granites (Tjuni Purlka suite) from the Tjuni Purlka Tectonic Zone (GSWA 185339 and 183509) is greater than that in the other individual samples of Pitjantjatjara or Wankanki granite. However, the model ages (1840–2040 Ma) span the same range as that from the other suites.

Geographically and temporally related compositional variations

The Walpa and Waratjarra suites show several systematic compositional trends related to their geographical position. Figure 27 orders the granites in terms of their relative position, in a northeast–southwest direction, perpendicular to the structural trend of the Tjuni Purlka Tectonic Zone, and of other major shear zones within the region. In the southwest of the Walpa Pulka Zone, the early Musgravian Walpa suite shows a southwestward increase in La/Yb (not shown), La/Sm, La/Gd, and Gd/Yb ratios, $Mg^{\#}$, as well as an increase in concentrations of LREE, Nb, Ta, and F, and a decrease in Yb and Fe_2O_3T concentrations over a distance of ~25 km. In the northeast of the Mamutjarra Zone, the late Musgravian Waratjarra suite shows the same southwestward trends over a distance of ~50 km.

Both the Walpa and Waratjarra suites also show a marked systematic southwestward increase in minimum magmatic temperature (Fig. 28), corresponding to increasing $Mg^{\#}$. Magmatic temperatures, estimated from the Zr-saturation thermometer of Watson and Harrison (1983), appear to be typically ~10 to 50ºC higher within the Tjuni Purlka Tectonic Zone than in surrounding zones. Although less pronounced than the temperature increases shown

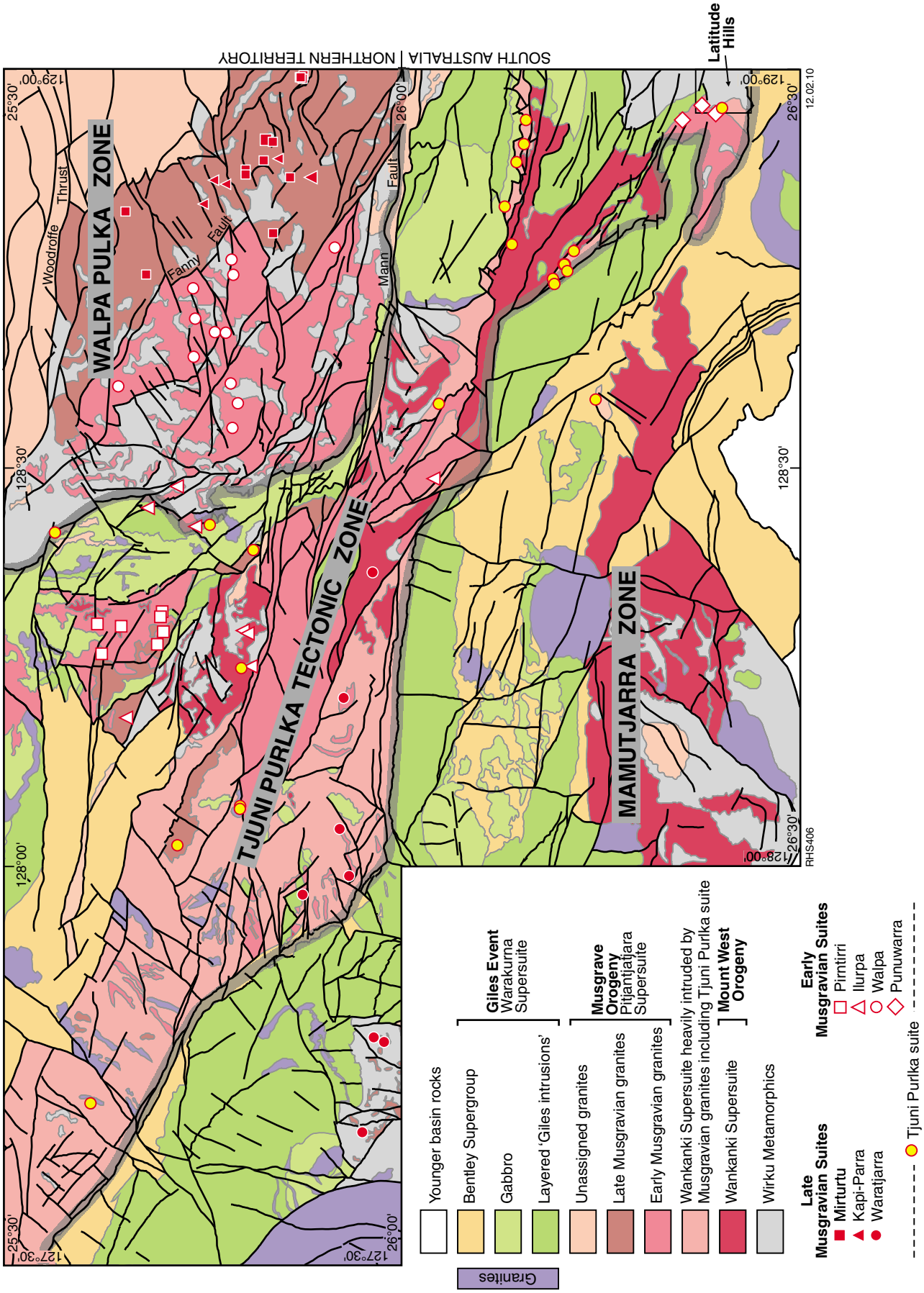

Figure 26. Simplified geological map of the eastern portion of the west Musgrave Province showing the location of geochemical samples within various granite suites of the Pitjantjatjara Supersuite.

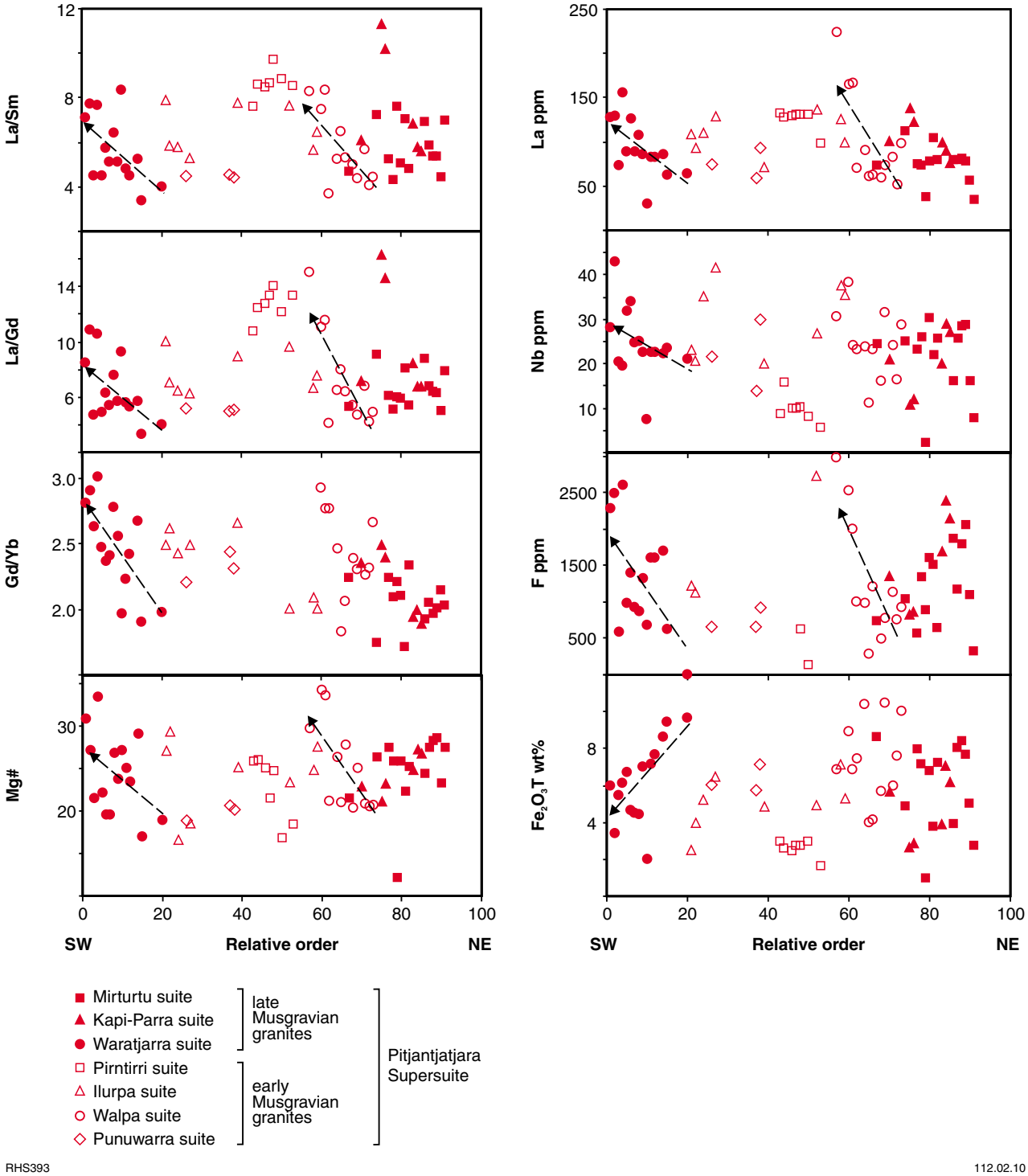

Figure 27. Geographical compositional variation within the Pitjantjatjara Supersuite. Samples have been ordered in terms of their position projected on to a northeast trending line across the west Musgrave Province (i.e. 100 being the most northeasterly sample and 0 the most southwesterly). Arrows show computer-fitted trend-lines for each data population.

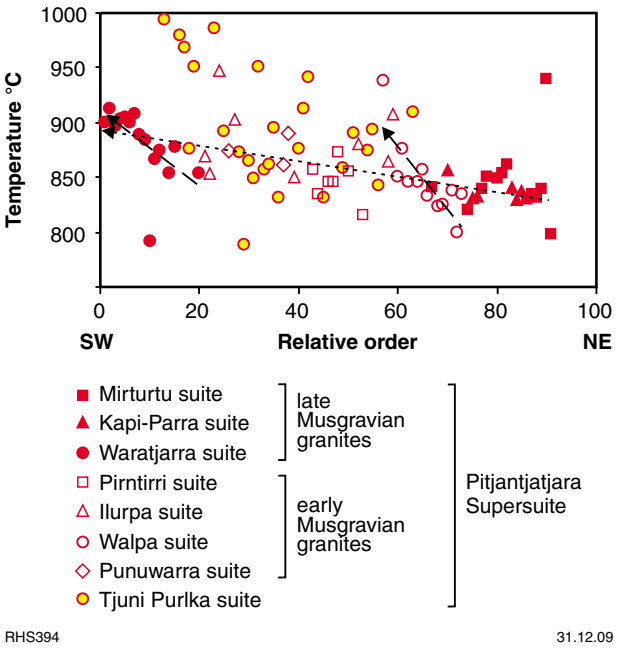

Figure 28. Geographical variation in intrusive temperature for the Pitjantjatjara Supersuite.

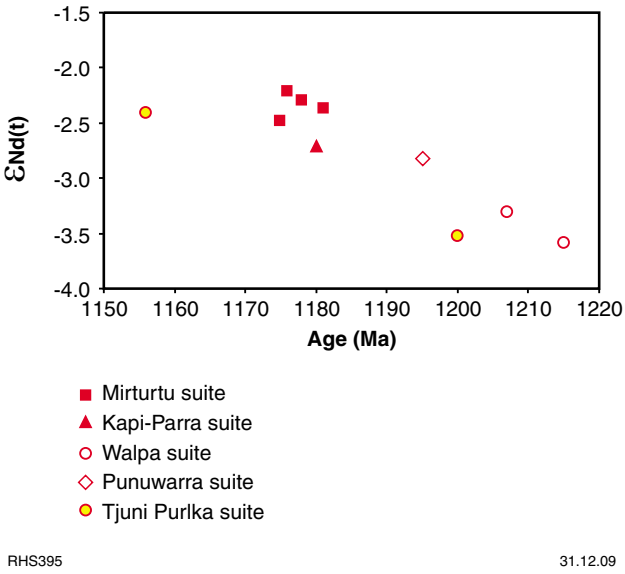

Figure 29. Detailed plot of ε_{Nd} versus time for granites of the Pitjantjatjara Supersuite.

individually by the Walpa and Waratjarra suites, the combined Pitjantjatjara granite population also shows a slight but systematic southwestward increase in magmatic temperature (Fig. 28).

Figure 29 plots all dated samples for the Pitjantjatjara Supersuite granites that have accompanying Nd-isotopic data. Treating these as a group, a trend is defined that shows systematically more radiogenic Nd isotopic compositions with decreasing age, with εNd values decreasing from -3.6 to -2.2. Two samples from the leucogranite of the Tjuni Purlka suite both have εNd values ~0.5 units lower than the trend defined by the remainder of the supersuite.

Warakurna Supersuite

Felsic rocks of the Warakurna Supersuite examined here comprise locally rapakivi-textured, syenogranites, quartz syenites, and monzogranites intruded mainly along the tectonic margins of the Tjuni Purlka Tectonic Zone between c. 1075 and c. 1062 Ma. These leucocratic rocks — referred to here as the Warakurna granites — are compositionally almost identical to the rocks of the Tjuni Purlka suite (Fig. 30). The Nd isotopic evolution envelope for both granites also coincides, indicating that

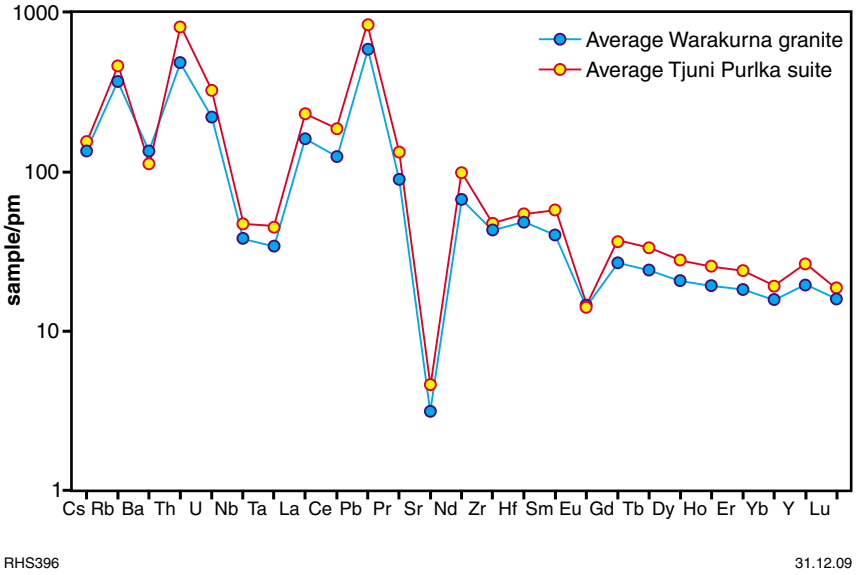

Figure 30. Compositional comparison between averaged Tjuni Purlka suite and Warakurna granite.

they are derived from an isotopically equivalent source region. The Warakurna granites are, however, usually easily identified in the field because they commonly show intrusive relationships with mafic rock emplaced during the Giles Event. They are also typically less deformed and only weakly metamorphosed, compared with rocks of the Pitjantjatjara Supersuite.

Petrogenesis of the felsic rocks

Wankanki Supersuite

The Wankanki Supersuite comprises metaluminous calcic to calc-alkalic rocks (Fig. 15). They show a strong compositional similarity to the Phanerozoic granites of the Andean continental-arc, including strong enrichment in Ba and relative depletion in Nb (e.g. high La/Nb ratios), although they are dominated by more silica-rich rocks, with most Wankanki granites containing >65 wt% SiO_2 (Fig. 31). Not surprisingly, rocks of the Wankanki Supersuite consistently fall within the field for volcanic arc granites in tectonic discrimination diagrams (e.g. Pearce et al., 1984; Fig. 32), and they differ in this respect from most other granites in the west Musgrave Province, which lie within the field of within-plate granites.

A significant decrease in Ba (and possibly Sr) concentration possibly suggests removal of plagioclase and K-feldspar, the main phenocryst minerals, as a mode of compositional variation although these trends are not accompanied by a clear decrease in Eu/Eu* (Figs 16–17). The trends for Nb/Ta (Fig. 17) suggest extensive removal of hornblende ($D_{Nb}>D_{Ta}$; e.g. Foley et al., 2002), the main mafic mineral in these rocks, or the incomplete removal of this mineral during melting of the source. Either process would also explain increasing La/Nb (Fig. 31) and decreasing Dy/Yb ratios with increasing SiO_2 (not shown).

In terms of their Nd-isotopic compositions (Fig. 20), the granites of the Wankanki Supersuite are the most juvenile granites in the west Musgrave Province. This is also supported by predominantly positive εHf values (up to +5) recorded in zircons from these granites. However, their ε_{Nd} values (-0.56 to -2.39), along with depleted mantle model ages (T_{DM2} from 1900 to 2040 Ma) that are ~600–700 Ma older than the crystallization age, require the involvement of at least small amounts of older felsic crustal material. The T_{DM2} ages indicate that the bulk source included crustal components with a significant crustal residence time, but with a narrow (weighted average) age range. A weak negative correlation between SiO_2 and ε_{Nd} (Fig. 33) possibly implicates assimilation-fractional crystallization (AFC) processes in the evolution of these rocks, although if this was a dominant process then there was very little isotopic contrast between primary magmas and assimilated crust.

Arc-like geochemical characteristics do not necessarily imply magma genesis in an arc setting. The Nd-isotopic data, in particular, allow for an alternative suggestion that the 'arc-signature' in the Wankanki Supersuite was inherited through incorporation of a crustal component, itself possibly produced in an earlier convergent plate margin setting, into a mantle derived melt in a non-subduction environment.

Pitjantjatjara Supersuite

In the terminology of Frost et al. (2001), all rocks of the Pitjantjatjara Supersuite are ferroan, and range from alkali-calcic to calc-alkalic (Fig. 22). They fall into the within-plate granite field on the tectonic discrimination diagrams of Pearce et al. (1984), and the A-type fields of Whalen et al. (1987) and Frost et al. (2001; Fig. 32). With the exception of the Tjuni Purlka suite, the Pitjantjatjara Supersuite granites show very close compositional similarities to anhydrous, Ti- and P-rich charnockite series magmas described by Kilpatrick and Ellis (1992; Fig. 34). Although such rocks are now generally regarded as part of the A-type spectrum (e.g. Bonin, 2007; Frost and Frost, 2008), the combination of high K_2O, TiO_2, P_2O_5, and $Mg^{\#}$ make them distinct within that group. In contrast, rocks of the Tjuni Purlka suite are generally more typical of A-type granite suites, having higher Si and Fe and lower Ti and P than other suites of the Pitjantjatjara Supersuite (Fig. 22).

At a given silica value, there is very little compositional distinction between most of the individual suites of the Pitjantjatjara Supersuite (Figs 22–25). Rocks of the Tjuni Purlka suite are an exception (see below). This limited compositional variation extends to the narrow range in Nd-isotopic compositions (ε_{Nd} = -2.2 to -3.6) and T_{DM2} model ages (1900–2040 Ma; Fig. 20), and likely indicates that the individual suites were derived from compositionally similar sources through a similar range of petrogenetic processes. A very narrow range of εHf values in zircon strongly supports this conclusion. Given the present surface extent of the granites (at least 15 000 km^2 in the Western Australian section of the province alone and up to 60 000 km^2 to the east), this compositionally homogenous source is of regional significance. However, the systematic geographical variations in composition shown by (in particular) the Walpa and Waratjarra suites (Figs 27–28), must also reflect a local systematic variation in conditions under which those suites evolved.

The field evidence that most granite suites of Pitjantjatjara Supersuite form composite intrusions of numerous individual dykes and sheets also suggests that little compositional evolution occurred at the level of emplacement. This is a common conclusion for composite, or incrementally constructed, felsic magma chambers (e.g. Brown, 2007b; Shaw and Flood, 2009). In the case of the Walpa and Waratjarra suites, however, it also suggests that systematic geographical variations in composition relate to variations in process that operated either at the source or in deep crustal staging chambers.

The Punuwarra and Pirntirri suites (Fig. 26) are unlike the other suites in that they form isolated, geographically distinct, and compositionally and texturally homogenous bodies. Some rocks of the comparatively Sr-rich Punuwarra suite have slightly positive Eu-anomalies consistent with feldspar accumulation and this is supported by observations that 1–2 cm size plagioclase phenocrysts form up to 40% of the rock. In contrast, rocks of the Pirntirri suite are relatively Sr-poor and have the lowest Eu/Eu* ratios, consistent with separation of significant amounts of feldspar. They also have a limited, but high, silica range, the most extreme La/Yb ratios (85–105), and amongst the highest Rb/Sr ratios. In

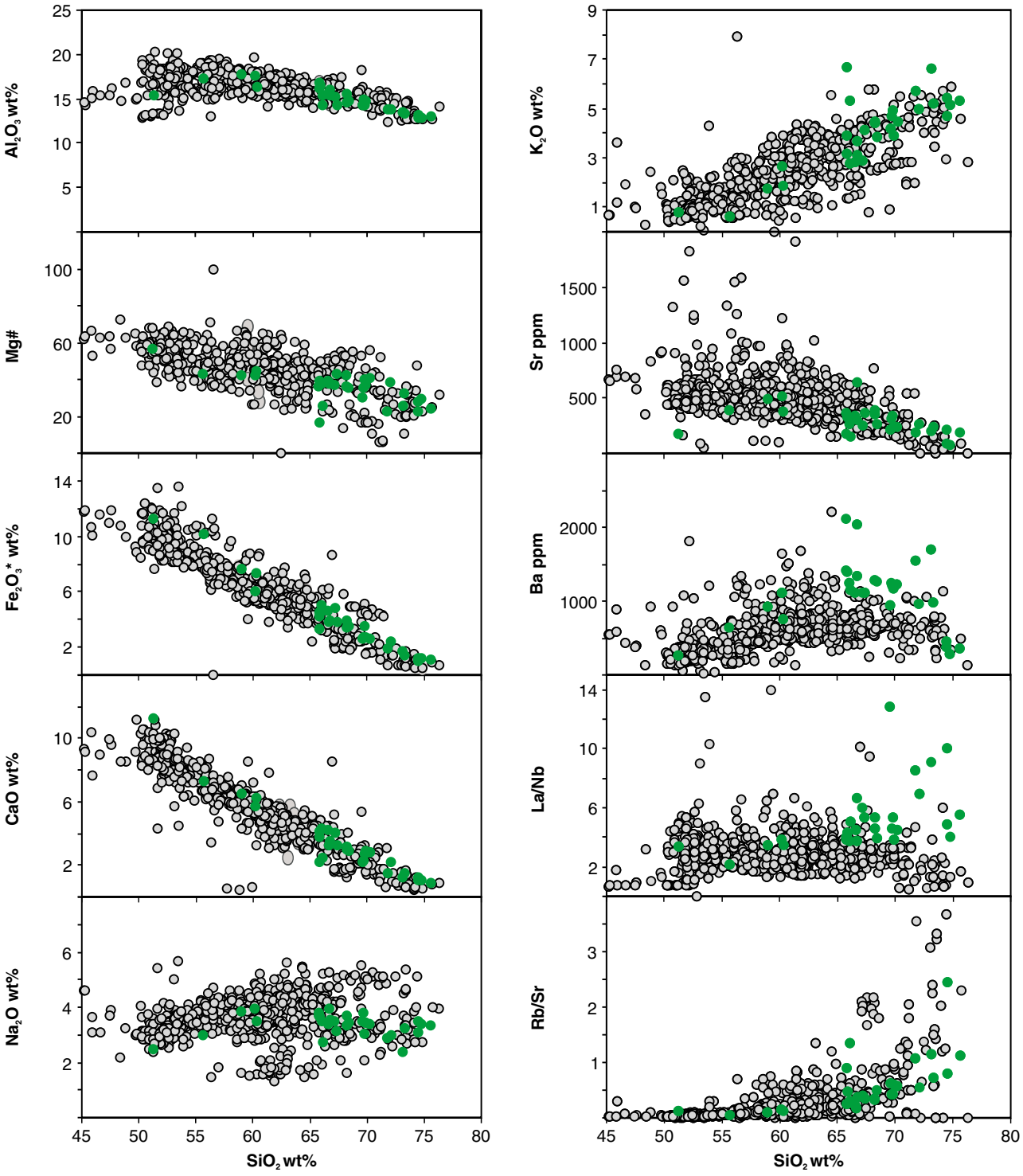

Figure 31. Plot comparing the composition of the Wankanki Supersuite with Andean granites (grey dots). Data for Andean rocks is from the GEOROC database — http://georoc.mpch-mainz.gwdg.de/.

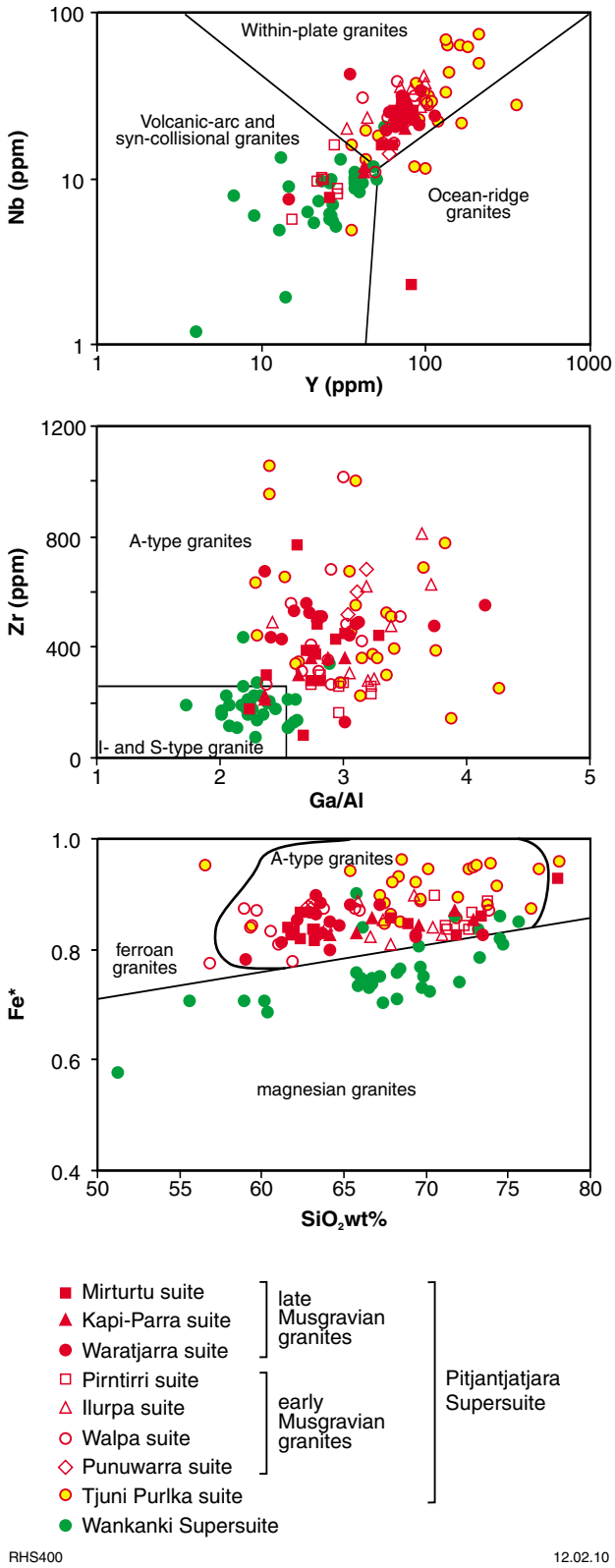

Figure 32. Tectonic discrimination diagrams for granites of the west Musgrave Province. Nb versus Y after Pearce et al. (1984), Zr vs Ga/Al after Whalen et al. (1987), and Fe* vs SiO_2 after Frost et al. (2001).

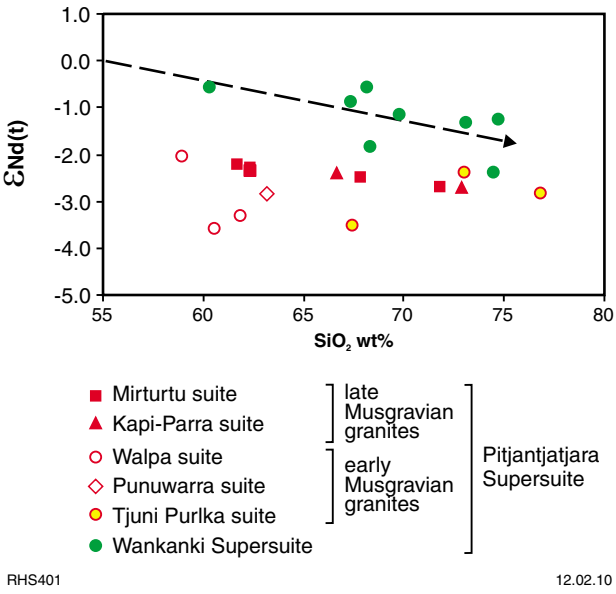

Figure 33. Plot of ε_{Nd} versus SiO_2 for granites of the Wankanki and Pitjantjatjara Supersuites.

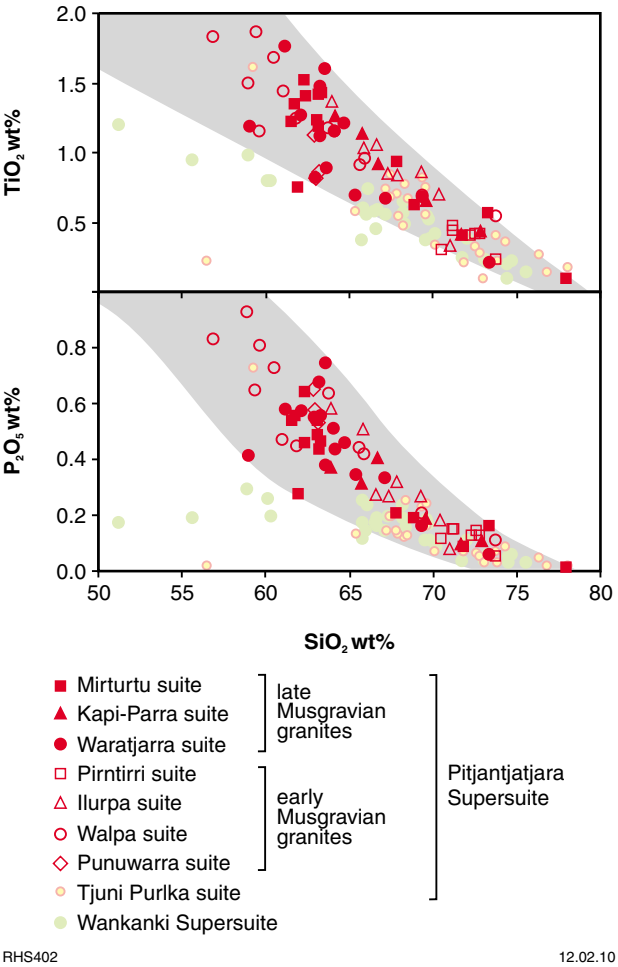

Figure 34. Plot comparing the composition of the Pitjantjatjara Supersuite with charnockite-series granites (grey field — from Kilpatrick and Ellis, 1992).

both cases, the geochemistry clearly reflects the effects of significant physical separation of melt and crystals. It is also likely that rocks of the Mirturtu suite, and possibly also the Kapi-Parra, and Ilurpa suites (Fig. 26), which include rocks with generally high Rb and Th concentrations and that range to relatively high Rb/Sr and low K/Rb ratios, have also undergone significant crystal-melt separation.

Least-squares modelling was carried out to see if a realistic hypothetical fractionating assemblage could account for the compositional differences between an average low-silica (~61.6 wt% SiO_2) and high-silica (~73.4 wt% SiO_2) Pitjantjatjara Supersuite granite. The metamorphic destruction of the primary mineralogy necessitated the use of end-member mineral compositions and published actual mineral compositions (see Table 1 — we used Fe-rich orthopyroxene, Fe-rich clinopyroxene, ilmenite, apatite, plagioclase (An37), Or, and Ab). A mathematically excellent result ($\Sigma r^2 = 0.0002$) was obtained for a hypothetical fractionating assemblage (Table 1) containing plagioclase (~43%) and orthopyroxene (~18%) with minor ilmenite (~4%) and apatite (~2%). The calculated fraction of melt remaining (F = 0.44) closely matches the maximum value predicted from enrichments in Rb (F = 0.43), assuming Rb was perfectly incompatible. However, the wide range of published partition coefficients appropriate for rocks of this silica range (GERM database: http://earthref.org) ensures that removal of this assemblage can account for the modelled trace element variations, and although averaged D values predict trace element variation trends reasonably similar to the observed trends, very little significance can be attached to these models. It must also be noted that the required fraction of melt remaining for most models is significantly below that predicted either by least squares modelling of by changes in concentrations of Rb (Fig. 35).

Concentrations of HFSE and REE in granites of the Pitjantjatjara Supersuite (Fig. 24) either remain constant or decrease slightly with increasing silica, but the trends are not strongly developed. Correlations between these trace elements and other indices of compositional evolution such as $Mg^{\#}$, Rb, or K_2O (Figs 22–23) are also very poorly defined and likely suggest that some of the observed compositional variation is not via a simple process of low-pressure fractional crystallization alone. In some of the suites (Walpa, Waratjarra), the typically rather low Rb/Sr and high K/Rb, and only modest variations in these ratios, as well as the scattered values for Eu/Eu* which show either no trend or a slight decrease with increasing silica (Fig. 24), also suggests that they are not strongly fractionated rocks. This contrasts to some extent with the findings of Landenberger and Collins (1996), Smith et al. (1999), and Tollo et al. (2004), that the effects of fractionation in A-type magmas typically overprint those of earlier processes.

A feature of the compositionally zoned Walpa and Waratjarra suites, as well as the fault-emplaced Kapi-Parra suite, is a positive correlation between $Mg^{\#}$ and F (Fig. 36), and both show a geographical trend to systematically higher concentrations to the southwest (Fig. 27). The crystallizing assemblage throughout most of the primary cooling history in these rocks does not include minerals that concentrate F; it was anhydrous, and variations in F

Table 1. Least squares modelling

	Primitive magma	*Evolved magma*	*Or*	*Ab*	*Plagioclase*	*Orthopyroxene*	*Clinopyroxene*	*Ilmenite*	*Apatite*
SiO_2	61.65	73.46	63.81	46.14	58.65	49.81	49.56	0.00	0.00
TiO_2	1.44	0.41	0.00	0.00	0.00	0.24	0.47	52.08	0.00
Al_2O_3	15.37	13.16	19.44	46.14	25.90	0.50	1.99	0.00	0.00
FeOtot	7.33	2.65	0.00	0.00	0.11	37.81	19.32	47.92	0.00
MgO	1.57	0.46	0.00	0.00	0.00	10.27	5.07	0.00	0.00
CaO	4.57	1.60	0.50	0.00	7.88	1.37	21.47	0.00	56.70
Na_2O	3.22	2.80	0.80	7.52	7.15	0.00	2.10	0.00	0.00
K_2O	4.22	5.35	15.45	0.21	0.31	0.00	0.00	0.00	0.00
P_2O_5	0.61	0.10	0.00	0.00	0.00	0.00	0.00	0.00	43.30
Total	100.00	100.00	100.00	100.00	100.00	100.00	100.00	100.00	100.00

Potential fractionating assemblage

Mineral	*Amount removed (% of initial magma)*	*Amount as % of fractionating assemblage*
Or	-11.72	20.85
Ab	-3.97	7.07
Plagioclase	-20.55	36.57
Orthopyroxene	-10.23	18.20
Clinopyroxene	-6.09	10.83
Ilmenite	-2.32	4.12
Apatite	-1.32	2.35
Total relative to initial magma		56.19%
Sum of residuals squared (Σr^2)		0.0002

NOTES: Primitive and evolved magmas = average of six lowest and highest silica Pitjantjatjara Supersuite magmas
Mineral compositions from Deer et al (1966)

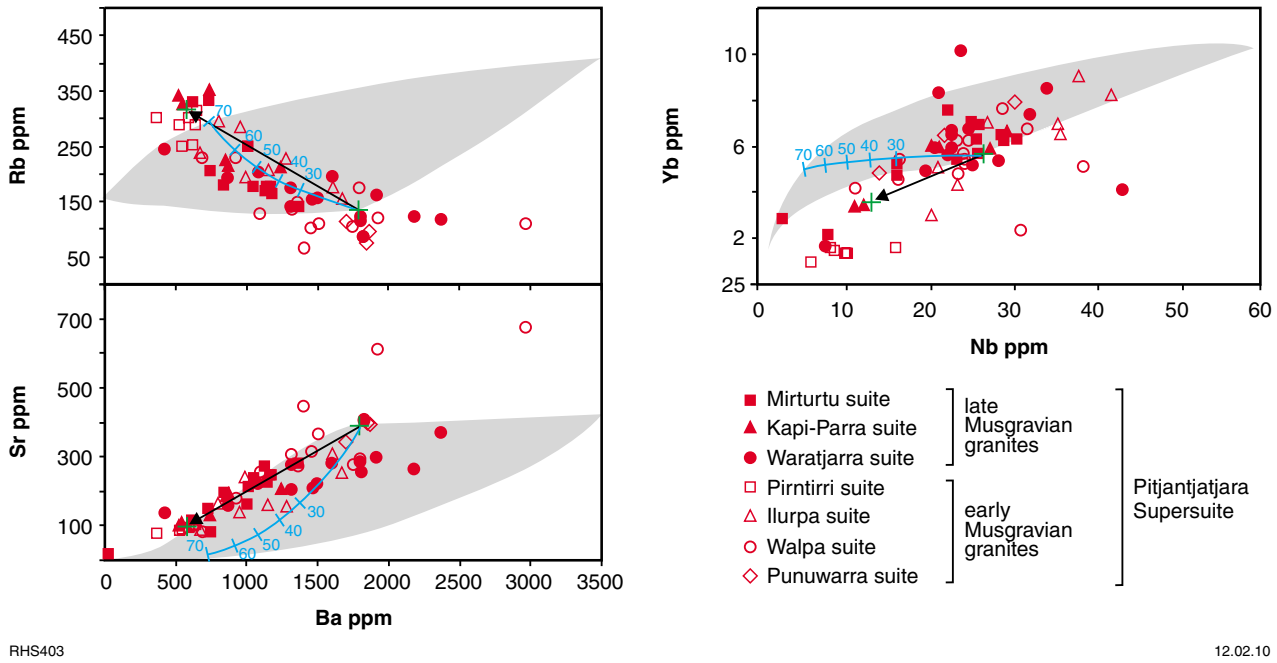

Figure 35. Trace-element fractional crystallization models for granites of the Pitjantjatjara Supersuite. Black arrow connects the average composition of least evolved granites to the average composition of the most evolved granites. Blue line shows compositional evolution for up to 70% fractional crystallization of the assemblage predicted through least squares modelling (see text for details) using an average value for mineral-melt distribution coefficients from the GERM database (http://earthref.org). Grey field encloses all possible solutions for up to 70% equilibrium or fraction crystallization employing the full range of available mineral-melt distribution coefficients appropriate for the modelled fractionating mineral assemblage and the magmas compositions under consideration.

are not correlated with P_2O_5 (Fig. 36) and so cannot be attributed to a F-rich apatite phase. Therefore, fractional crystallization should result in negatively correlated F and $Mg^{\#}$. However, Muñoz (1984), Peterson et al. (1991), and Icenhower and London (1997) showed that the $D_F^{Bt/melt}$ is strongly positively correlated with the $Mg^{\#}$ of biotite, and that during partial melting of granulites, F is strongly concentrated into increasingly Mg-rich residual biotite. This is consistent with the recognition that biotite in high-grade terranes is F-rich (Guidotti, 1984). It might be argued that during alteration or retrograde metamorphism, F is preferentially retained in the assemblages that stabilize the most biotite. The lack of a correlation, however, between F and LOI or elements strongly partitioned into a volatile phase (e.g. Cs, U; Fig. 36), and reasonable correlations with HFSE (Fig. 36; see below), argues against this for the Pitjantjatjara Supersuite. Thus, we suggest that the $Mg^{\#}$–F trends in these three suites (at least) are best explained in terms of varying degrees of partial melting, controlled by biotite breakdown.

It has been shown that the substitution of both F and Ti stabilize biotite to significantly higher temperatures (Muñoz, 1984; Peterson et al., 1991; Skjerlie and Johnston, 1993) such that vapour-absent melting of rocks containing F- and Ti-rich biotite might be restricted to ultra-high temperatures (Peterson et al., 1991; Brown, 2007b). These ultra-high temperatures are entirely consistent with those suggested for the formation of high P- and Ti- charnockitic magmas in general (Kilpatrick and Ellis, 1992), for the Pitjantjatjara Supersuite itself (*minimum* intrusive temperatures up to 993°C), and with metamorphic conditions known to have prevailed during emplacement of the Pitjantjatjara Supersuite.

Interestingly, for some suites, the HFSE and REE also correlate positively with F (Fig. 36) and with $Mg^{\#}$. In lower crustal granulites, these trace elements are typically hosted within accessory phases such as zircon, allanite, apatite, rutile, etc. which themselves are commonly included in biotite and/or amphibole. In this way, these trace elements are shielded from incorporation in low-degree partial melting (e.g. Bea, 1996), particularly if the biotite (or amphibole) is F-rich. Hence, the concentrations of HFSE and REE in the Walpa and Waratjarra suites, and possibly in other suites of the Pitjantjatjara magmas, could also be strongly influenced by the amount of biotite participating in melt reactions (e.g. Brown, 2007b; Bea, 1996; Collins et al., 1982). In this case, the trends to lower HFSE and REE with increasing SiO_2 and decreasing F and $Mg^{\#}$ reflect *decreasing* degrees of partial melting.

This is obviously an over-simplification, and significant increases in La/Sm ratios with increasing Rb (Fig. 37), even within the Walpa and Waratjarra suites (although not as well defined as for the other suites), show the clear effects of mineral/melt trace-element fractionation. Both variable degrees of partial melting and subsequent fractional crystallization may have played important roles in the compositional evolution of the Pitjantjatjara Supersuite. Other processes that must also be considered here, particularly for those suites that show no systematic spatial variation in composition, include MASH (melting, assimilation, storage, homogenization; Hildreth and

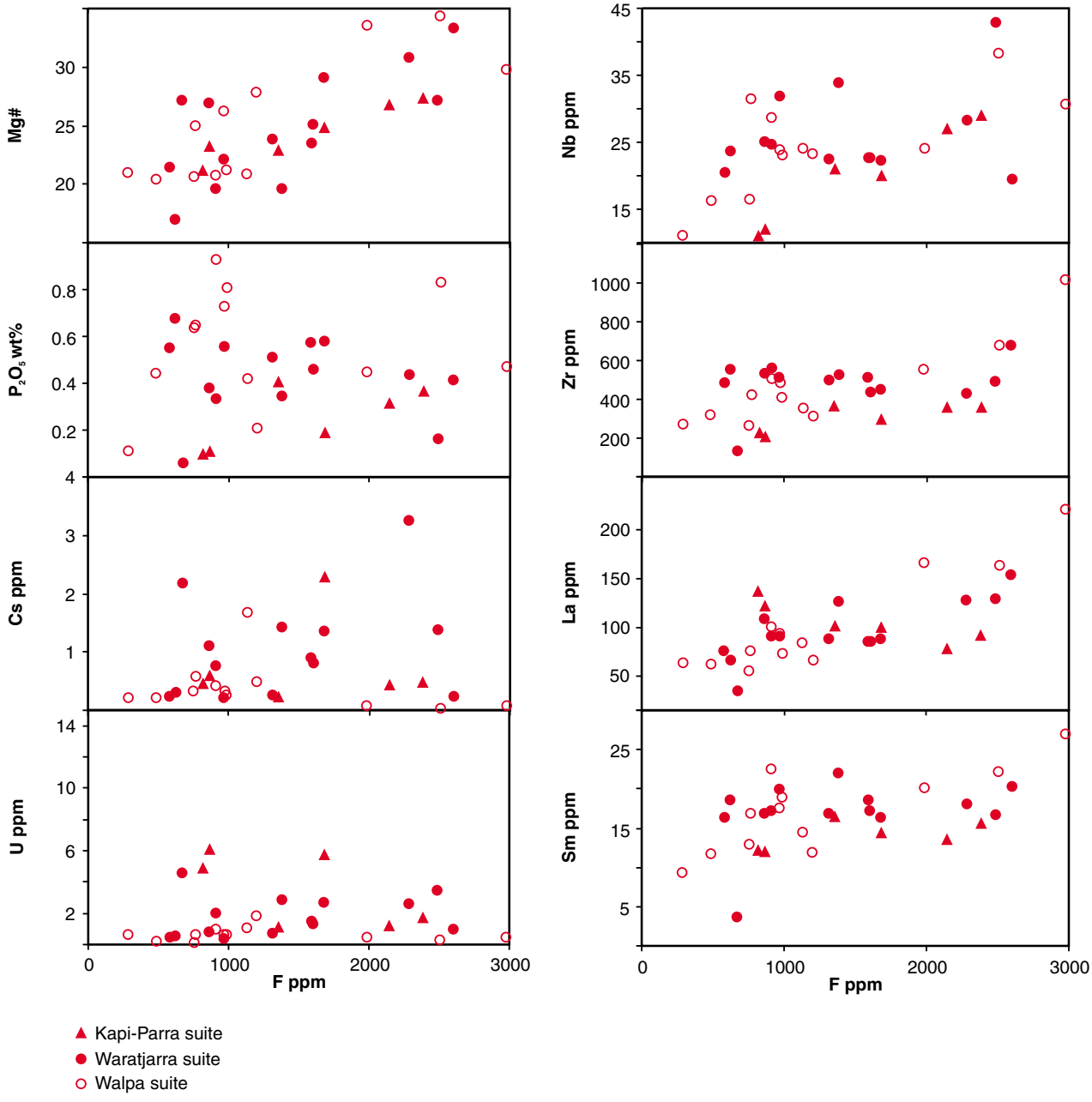

Figure 36. Plot of various elements and ratios versus F for granites of the Kapi-Parra, Waratjarra, and Walpa suite (Pitjantjatjara Supersuite).

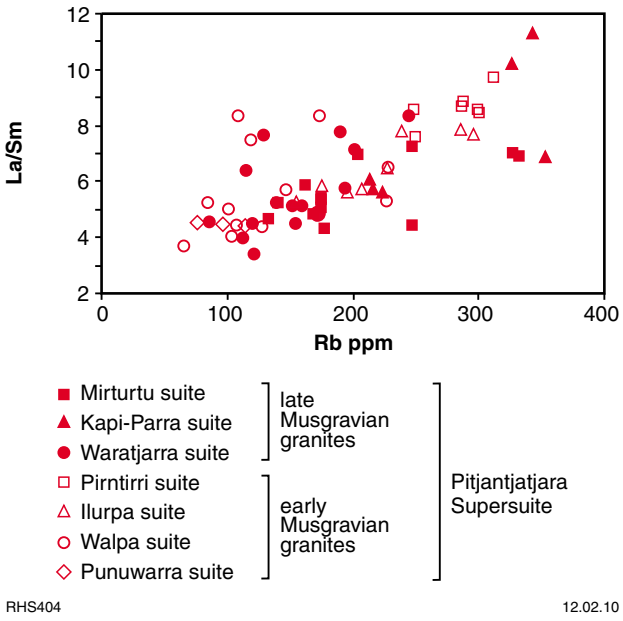

Figure 37. Plot of La/Sm versus Rb for granites of the Pitjantjatjara Supersuite.

Moorbath, 1988) and dynamic mixing of evolving melt sheets within deep crustal hot zones (e.g. Annen et al., 2006). Both processes can result in the kinds of linear geochemical arrays displayed by most suites of the Pitjantjatjara Supersuite.

Thus, compositional variation within the Pitjantjatjara Supersuite appears to be controlled by melt generation, extraction, and emplacement history and is strongly reflected in the style of intrusion. Varying degrees of high-temperature partial melting of a rather compositionally homogeneous source exerted a significant control over compositional variation in some of the parental magmas, and in cases where there was little subsequent fractional crystallization or mixing of magma batches, was the dominant cause of compositional variation. The geographical variations in composition shown by the compositionally zoned Walpa and Waratjarra suites (Fig. 27) resulted from the incremental amalgamation of successive magma pulses that systematically varied according to the degree of partial melting, with higher degrees of partial melting yielding higher magmatic temperatures, $Mg^{\#}$, and concentrations of F. These pulses were possibly also each extracted to emplacement level at a rate that precluded further compositional evolution. Such high rates of extraction may have reflected more active stages in the tectonic history of the Musgrave Orogeny. It is perhaps not coincidental that both suites lie along the boundary to the Tjuni Purlka Tectonic Zone with the observed compositional gradients possibly reflecting the direction of local extension.

It is also likely that compositional variation during migration of Walpa and Waratjarra magmas was limited by very short melt-migration distances. The Pitjantjatjara granites typically have significant mantle-normalized depletions in Sr (Fig. 19), even in the least evolved rocks (e.g. SiO_2 <60 wt%), as well as high concentrations of Yb (>5 ppm; Fig. 24), Y (Fig. 19), and low La/Yb ratios (Fig. 25). Such compositions suggest a source with residual plagioclase but not garnet, and constrain pressures of melting to <10 kbar (e.g. Wolf and Wyllie, 1994; Rapp and Watson, 1995), only ~2 kbar higher than calculated metamorphic pressures at the emplacement level. Thus, at the beginning of the Musgrave Orogeny (c. 1220 Ma), the distance separating the melting level from the level of emplacement was as little as ~7 km. Moreover, we consider this to be a maximum possible thickness of crust below the current level of emplacement, because extrapolation of the apparent geothermal gradient (>40°C km^{-1} for the early part of the Musgrave Orogeny at least) to depth rapidly implicates geologically unreasonable crustal temperatures (see later).

Other suites (Mirturtu, Pirntirri, Punuwarra, and Ilurpa), show evidence that factors other than variable degrees of source melting have had a major control on compositional variation. For some of these suites, marked increases in Rb and Th concentrations and Rb/Sr ratios at higher silica levels (Figs 23–24) suggest a role for fractional crystallization. However, these suites typically show a narrower range in magmatic temperatures, with no systematic geographical variation in temperature or composition. Magmas that form these suites were perhaps extracted at slower rates than those forming the zoned suites, and their intrusion history likely included periods of storage during less active stages in the tectonic history of the Musgrave Orogeny.

At similar silica values, rocks of the Tjuni Purlka suite are relatively depleted in TiO_2 and P_2O_5 compared with typical high P-, Ti-charnockitic magmas (Figs 22 and 34). Large depletions in Sr and Ba, very well developed negative Eu-anomalies (Eu/Eu* 0.66 to 0.06), and significant enrichments in Rb, Th, REE, and HFSE (Figs 23–24) suggest that the Tjuni Purlka suite represent more evolved magmas than those that the other Pitjantjatjara granite suites crystallized. Moreover, the strong enrichments in REE and HFSE, at equivalent silica contents, do not permit a direct genetic link between the Tjuni Purlka suite and the other Pitjantjatjara granite suites through any simple process of fractional crystallization or partial melting. This is also indicated by the Nd isotopic signature of the Tjuni Purlka suite (Fig. 20), which is marginally less radiogenic than that of other Pitjantjatjara granites at an equivalent age, and requires some variation in the bulk source composition.

Discussion

Constraints on the source of the granites of the Pitjantjatjara Supersuite.

Implicit in the suggestion that compositional variation of the early Musgravian Walpa suite (1215–1207 Ma) and the late Musgravian Waratjarra suite reflects variable degrees of partial melting of a biotite-bearing source, is that melting (at least for those suites) occurred at crustal levels. This means that, for these suites, a *direct* material

contribution to granitic magmas from contemporaneous mantle-derived mafic magmas was minor; i.e. they did not evolve via a dominantly liquid line-of-descent involving fractionation of mantle-derived magmas, with or without assimilation of crust. A further constraint is that the source region for all of the granite suites was rather compositionally homogeneous on a regional scale, although, as noted above (and discussed further below), there is a small but systematic progression to a bulk source with slightly more radiogenic Nd with decreasing crystallization age, as well as a contribution of a slightly greater amount of less radiogenic crust within the bulk source of the Tjuni Purlka suite at a given time (Fig. 20).

In all samples from both the Pitjantjatjara and Wankanki Supersuites, the Hf-isotopic value of zircon spans a common, narrow range and is strongly coupled to whole rock Nd-isotopic compositions. Nd-isotopic compositions that are less radiogenic than bulk earth (εNd down to ~-4.0), a consistent coincidence of maximum T_{DM}^{c}(Hf; in zircon) and T_{DM2}(Nd) values at ~2040 Ma, and the tight T_{DM} age range (1840–2040 Ma) that is 700–900 Ma older than the crystallization age, indicate that the isotopic budget for granites of the Pitjantjatjara Supersuite was overwhelmingly dominated by an old 'crustal' component. They also indicate that the bulk source of these granites was regionally isotopically homogeneous. This isotopically enriched 'crustal' source component was almost certainly also enriched in a range of incompatible trace elements (i.e. in addition to Hf, Zr, and REE), and was likely to be K-rich and felsic in composition.

Nevertheless, the T_{DM}^{c}(Hf) and T_{DM2}(Nd) model ages are unlikely to reflect (or bracket) the true age of the crustal component because regional age data from magmatic zircons, rare zircon xenocrysts in granites, and from detrital zircons include no significant populations (i.e. no crystallization ages) of this age (Fig. 5). Because the exposed emplacement level of the Pitjantjatjara Supersuite does not appear to be significantly displaced from the zone of magma generation (i.e. <7 km), it might be expected that over the area of the west Musgrave Province, some physical evidence of that source be exposed. Zircon xenocrysts in granites and detrital zircons from the west Musgrave Province mainly show age populations between 1650 and 1340 Ma or are Archean (Fig. 5). This suggests that the enriched felsic crustal component in the source of the Pitjantjatjara and Wankanki Supersuites itself comprised several components, at least one between c 1345 Ma (maximum age of the Wankanki Supersuite) and c. 1650 Ma, and another of Archean (>2600 Ma) age.

Furthermore, this enriched combined felsic component was unlikely to be the sole, nor possibly even the most voluminous, source component for these granites. Given that several granites of both the Pitjantjatjara and Wankanki Supersuites have silica values <60 wt%, the bulk source most likely had a basaltic to intermediate silica range, and must have included a significant mafic component. Kilpatrick and Ellis (1992) drew similar conclusions about the source requirements for charnockite series granites in general.

Petrogenesis of A-type magmas, including charnockite-series magmas

Felsic magmas that can be broadly classified as A-type, including charnockite-series magmas, are typically related to extension, or to the extensional phases of a range of tectonic environments (e.g. continental rifts, rifted arcs, and back arcs; see reviews in Bonin, 2007, and Frost and Frost, 2008). Here, lithospheric thinning, and under- and intra-plating of mantle-derived rocks, lead to lower-crustal temperatures that can reach, or exceed, 1000°C and to the evolution of relatively anhydrous magmatic systems that range from directly mantle derived to purely crustal in origin. In areas where a range of spatially and temporally related granites of contrasting compositions occur, trends to more A-type characteristics are typically accompanied by increasingly juvenile isotopic compositions (e.g. Kemp et al., 2005). This emphasizes the important role that mantle-derived magmas have in the petrogenesis of most A-type magmas through a range of processes including direct differentiation of mantle derived melts, with or without the affects of variable assimilation of crustal material (AFC or MASH processes; e.g. Turner et al., 1992; Anderson et al., 2003; Frost and Frost, 1997, 2008; Frost et al., 2001; Ewart et al., 2004a; Bonin, 2007), including assimilation of juvenile mafic crust related to the same mantle magmatic event (e.g. Vander Auwera et al., 2008).

Models that invoke a dominantly crustal origin for A-type magmas typically call for a granulitic source that was dehydrated and melt-depleted during a prior high-temperature event (e.g. Collins et al., 1982; Clemens et al., 1986). However, Kilpatrick and Ellis (1992) suggested that the generally enriched geochemical compositions of high P and Ti charnockite-series magmas, like those of the Pitjantjatjara Supersuite, reflected a dehydrated but fertile source. Melting of a dehydrated basalt underplate was discounted because of difficulties in deriving the high K_2O contents of charnockites from basalt (although it has since been shown that the Mesozoic high P and Ti (HPT) basalts of both the Etendeka and Karoo flood basalt provinces have up to 3.5 wt% K_2O; e.g. Ewart et al., 2004a and b). However, a mixed lower-crustal source of intermediate bulk composition, comprised of dry, but fertile (e.g. high F), felsic granulites and dry mafic granulite, derived through dehydration of basalt underplated during a previous tectonic event, was considered appropriate (Kilpatrick and Ellis, 1992).

High P- and Ti-charnockitic granites share close geochemical and mineralogical similarities with anhydrous high-Ti latites and quartz latites from continental flood basalt provinces (Kilpatrick and Ellis, 1992), and in particular, from the Karoo and Paraná-Etendeka provinces associated with the Mesozoic break-up of Gondwana. Kilpatrick and Ellis (1992) considered these volcanic rocks to be the extrusive equivalents of charnockite series granites. High-Ti latites are typically temporally and spatially associated with low-Ti latites as well as with voluminous HPT and low P and Ti (LPT) basalts, and the felsic rocks had an eruption temperature in excess of 1050°C (e.g. Garland et al., 1995; Ewart et al., 2004a). The two mafic-felsic series (high-Ti and low-Ti) are generally not regarded as being directly related genetically. Low-Ti

latites are widely accepted as the result of AFC processes involving LPT basalt parental melts and felsic lower crust (Hawkesworth et al., 1988; Garland et al., 1995; Ewart et al., 2004a). However, the origin of the high-Ti latites is more contentious, with opinion divided as to whether they form through remelting of underplated HPT basalt (e.g. Garland et al., 1995; Miller and Harris, 2007) or through AFC processes involving HPT parent melts and felsic lower crust (e.g. Ewart et al., 2004a). For example, Ewart et al. (2004a, b) provided numerical models showing that it was theoretically possible to produce the high-Ti latites and quartz latites of the Cretaceous Etendeka flood basalt province from K-rich HPT basalts through AFC processes involving associated low-Ti latite crust. These authors, however, concede that their modelling cannot rule out re-melting of underplated HPT basalt as a source of high-Ti latites and quartz latites. Regardless, a direct, or at least young (i.e. rapidly re-cycled) mantle component clearly dominates the petrogenesis of HPT latite, and all components are essentially anhydrous.

Our data for the Pitjantjatjara Supersuite invites similar petrogenetic elements; a felsic granulitic component with a significant crustal residence time dominating the incompatible trace-element budget of all the granites, and a mantle-derived mafic component. Importantly, and like the Mesozoic Karoo and Paraná-Etendeka HPT latites (e.g. Ewart et al., 2004b), granites of the Pitjantjatjara Supersuite might then represent a significant juvenile contribution to the crust.

The thermal and material contribution from mafic magmatism

The evidence presented above is that all suites of the Pitjantjatjara Supersuite formed from the same range of source components mixed in similar proportions (i.e. an isotopically and geochemically homogeneous bulk source). While a *direct* material contribution into the magmas that crystallized some granite suites of the Pitjantjatjara Supersuite was probably negligible, an incompatible trace-element poor mafic component formed a significant proportion of the bulk source. However, physical evidence for mafic magmatism during the Musgrave Orogeny is conspicuously lacking. Throughout the ~100 Ma intrusive history of the supersuite, mafic magmas reached the presently exposed crustal levels only twice, at c. 1190 Ma and at c. 1150 Ma, and were even then only a minor component of the magmatism (at that intrusive level) at those times. A possible third event relates to a regionally extensive swarm of dolerites — the Marda Moorn dyke swarm — dated at c. 1210 Ma, that virtually rims the entire Archean Yilgarn Craton (e.g. Wingate et al., 2000; Wingate et al., 2005). Emplacement of this dyke swarm is synchronous with the early Pitjantjatjara Supersuite, and although no dykes of this age are yet known from the Musgrave Province itself, the trend of the swarm, prior to its geophysical trace being lost under Phanerozoic cover, is towards the Musgrave Province.

Despite this lack of physical evidence for mafic magmatism, our data show that the Musgrave Orogeny involved more or less continuous UHT metamorphism and felsic magmatism for about 100 Ma The estimated metamorphic temperatures, at the level of granite emplacement, are already at the limit that can be achieved in the lowest crust through conduction of mantle heat alone — even assuming total removal of lithospheric mantle (e.g. ~1000°C — Stüwe, 2002; Brown, 2008). However, because our data also require an enriched felsic component in the bulk source for the granites of the Pitjantjatjara Supersuite, and that melting for at least some suites likely occurred at crustal levels, a significant amount of crust must have existed below the exposed level of emplacement. This crust would have been at temperatures that demanded an extensive contribution of heat (particularly considering the apparent geothermal gradient of >40°C km^{-1} for the early part of the Musgrave Orogeny at least) both directly conducted from the mantle and introduced via intra- and underplating of mantle-derived magmas.

In this regard, there may be some analogies with the Mesozoic Chon Aike Province of Patagonia and the Antarctic Peninsula, a felsic large igneous province related to the break-up of Gondwana and temporally equivalent to Karoo-Ferrar mafic magmatism (Pankhurst et al., 2000; Riley et al., 2001). These felsic magmas are also believed to be crustal melts, but whereas associated mafic magmatism is rare, crustal melting resulting in the Chon Aike Province is attributed to mafic underplating, lithospheric thinning, and the impact of the Discovey–Shona–Bouvet group of plumes (Pankhurst et al., 1998, 2000; Riley et al., 2001). In the case of the Pitjantjatjara Supersuite, however, we suggest that contemporaneous mafic magmatism not only provided a heat source, but that estimates of the amounts of pre-existing crust available to contribute to the source of these granites actually requires that mantle-derived magmatism made a major material contribution (the voluminous trace-element poor mafic component) to the bulk source, via hybridization or some form of MASH process.

The estimated distance separating the melting level from the level of emplacement during the Musgrave Orogeny was ~7 km. However, this is likely to be a maximum possible thickness of crust below the current level of emplacement, because extrapolation of the apparent geothermal gradient (>40°C km^{-1} for the early part of the Musgrave Orogeny at least) to depth implicates geologically unreasonable crustal temperatures after only a few kilometres (i.e. lower-crustal temperatures that greatly exceeded 1100°C). Either the crustal thickness below the exposed emplacement level of the Pitjantjatjara Supersuite was considerably less than 7 km or that crust contained a high proportion of melt (e.g. in a MASH zone) — or both. The volume of magmas produced during the Musgrave Orogeny is difficult to estimate, but granites of the Pitjantjatjara Supersuite are inferred to form >80% of the bedrock geology throughout the entire Walpa Pulka Zone. Given that this region is interpreted to comprise a series of shallowly southwest-dipping fault slices (Howard et al., 2006; Raimondo et al., 2009), the true thickness of the granite layer almost certainly significantly exceeds 5 km. We can take a very conservative estimate of the volume of Pitjantjatjara magmatism (excluding any possible volcanic equivalents), as forming the equivalent of a regional layer ~4 km thick. Even if we assume that the primary Pitjantjatjara granite magmas reflect as much

as 25% partial melting, a 7 km column of source material can only produce a 1.75 km thick column of granite. Additional source material needs to have been available, but was not a component of the <7 km crustal column beneath the current granite emplacement level until at least the beginning of the Musgrave Orogeny. Thus, voluminous mantle melt must have continuously been fed into the source region during the Musgrave Orogeny, and the material contribution this ultimately made to the Pitjantjatjara granites themselves (directly or indirectly) must have greatly exceeded 50%.

The role of the Tjuni Purlka suite granites and the significance of the felsic rocks of the Warakurna Supersuite.

The highly silicic, and REE- and HFSE-enriched compositions of the Tjuni Purlka suite distinguish these rocks clearly from all other rocks of the Pitjantjatjara Supersuite, and it is unlikely that any simple process of fractional crystallization or partial melting can relate the two groups. The rocks of the Tjuni Purlka suite and the Warakurna granites, however, are geochemically and isotopically virtually identical (Fig. 30) and almost certainly evolved in the same way and from a compositionally equivalent source. Most Warakurna granites intruded the structural boundaries defining the Tjuni Purlka Tectonic Zone and are directly associated temporally and spatially with voluminous gabbro and gabbronorite intrusions. The granites have a narrow range of Nd isotopic compositions (εNd =-2.9 to -4.3) whereas the mafic rocks show a wide range (εNd = +1.0 to -3.8; Fig. 38) that reflects variable mixing with, and contamination by, crustal components, including the granite melts. This is consistent with field evidence for magma mingling and mixing (Smithies et al., 2009a). However, a significant silica gap separating the granites and gabbro also precludes a direct genetic link between the two rock types. Instead, the Warakurna granites most likely reflect direct melting of felsic lower crust during emplacement of the mantle-derived magmas that produced the gabbro and gabbronorite intrusions. If granites of the Tjuni Purlka suite are also melts of a lower crustal source, the geochemical and isotopic differences between these and other granites of the Pitjantjatjara Supersuite suggest that this source had a more felsic and non-radiogenic bulk composition.

If this is the case, and in view of the fact that normal granites of the Pitjantjatjara Supersuite geographically and temporally overlap with granites of the Tjuni Purlka suite, we need to consider how both granite types and their sources may have coexisted and interacted. In the following section, we develop a model that integrates the thermal and magmatic history of the west Musgrave Province to account for the systematic geographical, temporal, and compositional trends within the granites of the Pitjantjatjara Supersuite, and the antithetic relationship between the Wankanki and Pitjantjatjara Supersuites. We then discuss the implications for general models of 'A-type' granite petrogenesis and the tectonic implications for the Proterozoic evolution of central Australia.

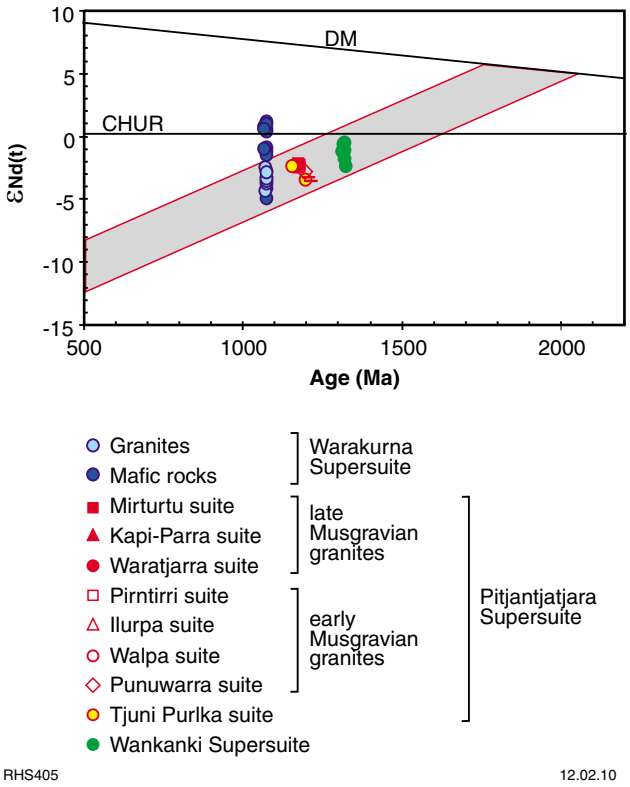

Figure 38. ε_{Nd} evolution diagram for granites of the west Musgrave Province.

An integrated model

Our suggestion that voluminous mantle-derived magmatism contributed both heat and source material to the petrogenesis of the Pitjantjatjara Supersuite is consistent with recent models for the generation of large-volume felsic magmas in all tectonic environments (e.g. Annen et al., 2006; Bachmann and Bergantz, 2008). However, the processes that produce this material contribution may be varied, and in the case of the Walpa and Waratjarra suites, which reflect in-situ partial melting, must have involved homogenization of the mafic component into the bulk source as well as cooling, prior to re-melting. Numerical thermal modelling suggests that large-scale crustal melting requires unusually high heat flow (e.g. Petford and Gallagher, 2001; Annen and Sparks, 2002; Dufek and Bergantz, 2005). This applies even in the case of dehydration melting, and so the production of relatively dry magmas like those of the Pitjantjatjara Supersuite presents an even greater problem, particularly given the enormous volume of felsic melt required to produce this regionally dominant lithological feature. In this respect, the evolution of the Walpa and Waratjarra suites might not be typical of the Pitjantjatjara Supersuite in general, although the source components and bulk source compositions might be the same.

Bachmann and Bergantz (2008) argue that most evolved felsic magmas form within, and are extracted from, long-lived crystallizing mush zones periodically fed by mantle-derived magmas (Fig. 39). Partial melting of crust is considerably less important, but is coupled to

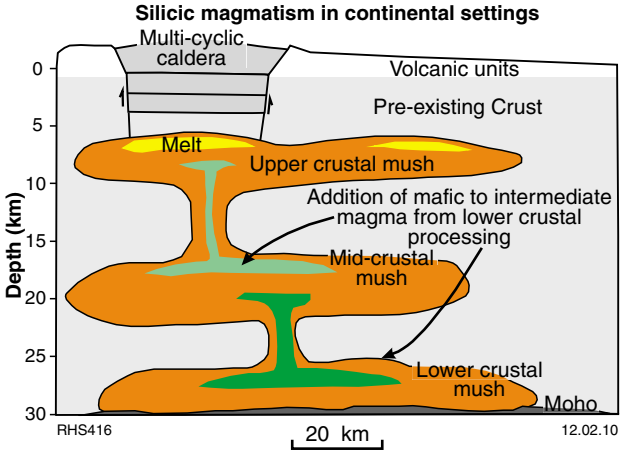

Figure 39. Schematic model of an intracontinental magma mush zone (modified after Bachmann and Bergantz, 2008).

emplacement of mush zones, and allows for the transfer of crustal compositional attributes to the interstitial mush magmas. Such models are heavily based on the MASH hypothesis, which attributes large scale homogeneity in the lower crustal source regions of granites to the formation of extensive and long-lived crystal-melt mush, or MASH, domains. These are produced when mantle-derived mafic underplated and intraplated magmas mix with, and assimilate, local crustal components (typically as melts of country rock), producing crystal-rich mush chambers that undergo dynamic homogenization as well as periodic magma recharge, (e.g. Hildreth and Moorbath, 1988; Hildreth and Wilson, 2007; Riley et al., 2001).

A model that also incorporates aspects of the MASH hypothesis is that of granite formation in deep crust 'hot zones' (Annen et al., 2006; Fig. 40). This model was developed to explain the genesis of subduction-related felsic magmas, but is equally applicable to a range of tectonic environments, including rift settings where basaltic magmas are relatively hot and dry compared with typical arc-related mafic magmatism. According to this model, deep crustal hot zones formed through extensive basaltic intraplating. A high intrusion rate can lead to a situation where each successive intrusion adds more heat to the lower crust than is conducted away. The model of Annen et al. (2006), predicts that within this emerging 'hot zone', ambient temperatures may eventually exceed the solidus temperature of both the basalt and of the country rock. Under such conditions, the country rock may partially melt, whereas the basaltic sills will retain a residual melt fraction (i.e. they will not fully crystallize). The relative proportion and composition of the residual melt fraction will depend on the extent to which ambient temperatures exceeded the solidus (higher temperatures lead to more residual melt and of a more mafic composition), and the duration that this residual fraction remains melt will depend on how long the imposed thermal gradient is sustained. Mixing between partial melt (of country rock) and residual melt fractions produces a range of magmatic compositions.

Combining aspects of models for mush zones, MASH domains, and lower crustal hot zones, we propose the following petrogenetic model for felsic magmatism associated with the Mesoproterozoic Musgrave Orogeny.

The Musgrave Orogeny began with extensive underplating and intraplating of hot and dry basaltic sills into the lower crust. According to Ewart et al. (2004b), Mesozoic flood basalts of the Etendeka Province erupted at temperatures between 1100°C and 1250°C. Given the compositional similarities between these charnockite-series magmas (Kilpatrick and Ellis, 1992) and the Pitjantjatjara Supersuite, and the metamorphic conditions that accompanied emplacement of the Pitjantjatjara granites, we suggest a similar, or slightly higher, range of deep crustal temperatures during the Musgrave Orogeny. A high intrusive rate and large intrusive volume elevated lower crustal ambient temperatures above the solidus of

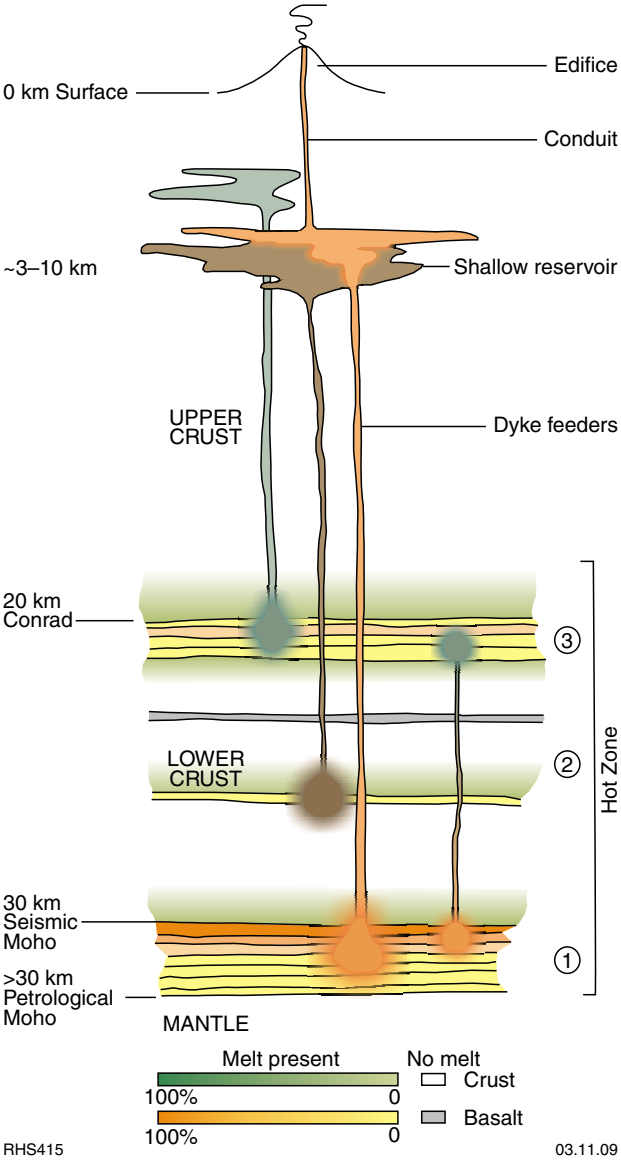

Figure 40. Schematic model of a lower crustal hot zone (modified after Annen et al., 2006).

both high-K, biotite-bearing, felsic granulite (country rock), and of the invading mafic sills.

The maximum temperature at which totally dry (i.e. no free, or grain boundary H_2O and no H_2O structurally bound in minerals) crust will begin to melt can be constrained (at 10 kbar) to between the dry solidus for granite (1080°C) and for basalt (1140°C; e.g. Thompson, 1992) and would be considerably lowered by addition of even small amounts of water (or other fluxes — e.g. F). Melting experiments on 'relatively dry' ($H_2O^+ < 0.5$ wt%) granodioritic gneiss and dioritic charnockite (Beard et al., 1993) produced 25 to 50% melt at pressures of 6.9 kbar and temperatures between 950°C and 1000°C. K-feldspar was consumed early during melting of the dioritic charnockite and the resulting melts share the metaluminous, K- and Ba-rich compositions of the Pitjantjatjara granites. The experimental conditions used by Beard et al., (1993) are comparable to estimates of the UHT conditions (King, 2008; Kelsey et al. 2009) that prevailed at the time and at emplacement level of the Pitjantjatjara Supersuite.

We suggest that as a result of this extensive underplating and intraplating, lower crustal felsic granulite partially melted to yield large amounts of metaluminous, high-K melt (e.g. Beard et al., 1993). When ambient temperatures eventually exceeded the basalt solidus, the mafic sills only partially crystallized to leave residual melt fractions ranging in composition from rhyolite to andesite depending on ambient temperature (Fig. 41a — inset). Mixing of small amounts of this residual melt fraction into the lower crustal partial melts was locally facilitated by the formation of dilational zones during deformation, particularly within the Tjuni Purlka Tectonic Zone, and resulted in Tjuni Purlka suite-type granite magmas (Fig. 41a — inset). These have the strongest 'crustal' geochemical and isotopic compositions of all Pitjantjatjara Supersuite granites. Within the Tjuni Purlka Tectonic Zone, movement along northwest-trending faults allowed these Tjuni Purlka suite magmas to segregate, accumulate in dilatant zones, and ascend the short crustal interval to the current level of exposure. However, these felsic hybrid rocks are too silicic and geochemically evolved to be either parental to the other suites of the Pitjantjatjara Supersuite or to be their source.

To produce the main suites of the Pitjantjatjara Supersuite, we suggest that sustained high heat flux allowed partial melt, residual melt fraction and felsic hybrid magma to accumulate and mix with fresh inputs of basaltic magma (Fig. 41b). This occurred mainly in areas of relatively subdued tectonic activity, away from the Tjuni Purlka Tectonic Zone. As intraplating continued, these intermediate hybrid magmas merged and the lower crust progressed from a hot zone phase to a MASH phase (Fig. 41c). These homogenous MASH domains became the source for granites of the Pitjantjatjara Supersuite. Each individual suite of Pitjantjatjara granites likely reflects a separate MASH domain, with slightly different compositions.

One of the key aspects of the lower crustal hot zone hypothesis is that once hot zones develop, they provide a impenetrable physical barrier to mantle-derived magmatism (Annen et al. 2006), and this provides an

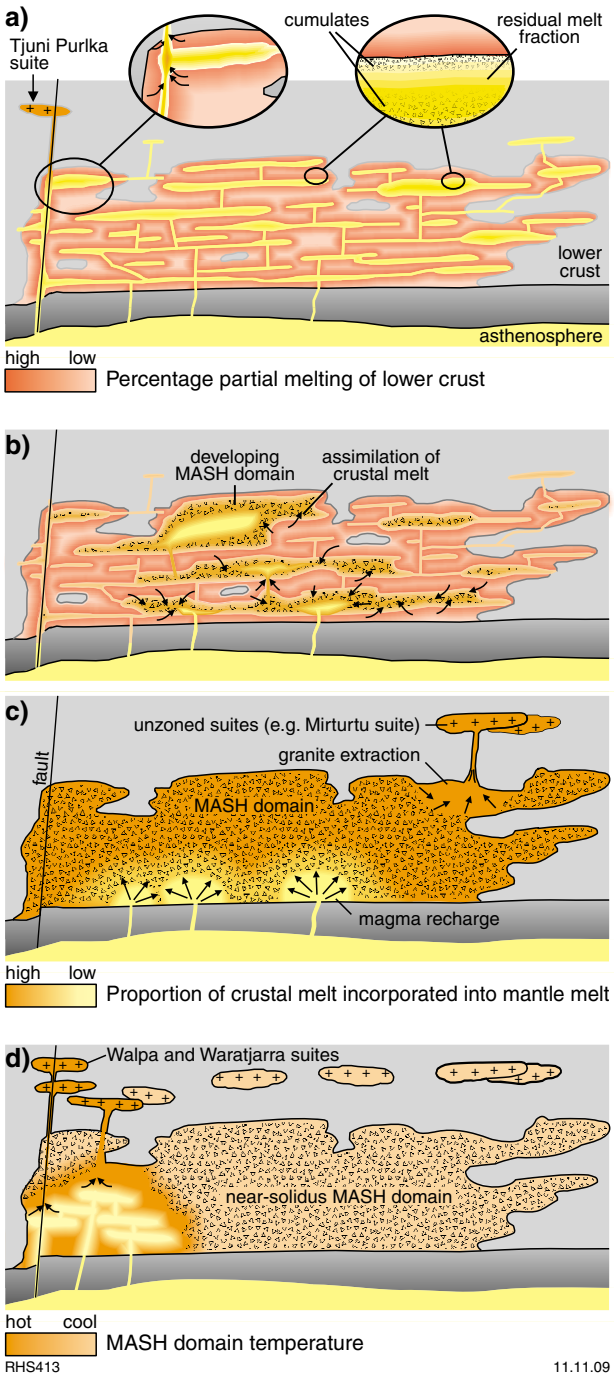

Figure 41. Schematic model for the evolution of the Pitjantjatjara Supersuite — see text for details.

explanation for the virtual absence of mafic magmas, at the current level of exposure, throughout the Musgrave Orogen.

Another key aspect of the MASH hypothesis, and of hot zones, is that the components of such systems (crystals and melt) can be stored for long periods (theoretically indefinitely) without further compositional differentiation, as long as the thermal gradient is preserved (Annen et al., 2006). This promotes compositional homogenization (e.g. Hildreth and Moorbath, 1988; Riley et al., 2001). For the

west Musgrave Province, the high thermal gradient was potentially preserved for up to 100 Ma. In detail, however, variations in heat-flux probably ensured periods where temperatures in MASH domains dropped below the solidus and where the zones effectively solidified (Fig. 41d).

There were certainly periods where hot MASH domains were directly tapped, yielding felsic magmas either as crystal-poor segregations in dykes or as mush columns. These ascended the short distance to the present level of exposure to produce the composite unzoned bodies of the Pitjantjatjara Supersuite (e.g. Mirturtu, Ilurpa, Pirntirri suites; Fig. 41c). However, the evidence that varying degrees of partial melting controlled compositional variation of the Walpa and Waratjarra suites rules out extraction of these suites from an active MASH domain. Instead, we suggest that these suites formed through remelting of a cooled MASH domain produced during under- and intra-plating events at earlier stages of the Musgrave Orogeny. Although cooled, such domains hovered at near-solidus conditions, and were rapidly remobilized into an active MASH domain by subsequent intrusion of basaltic sills. Both the Walpa and Waratjarra suites lie against, or straddle, the boundary to the Tjuni Purlka Tectonic Zone. Here, extension along crustal-scale shear zones allowed the rapid injection of mantle material into cooled MASH domains and also facilitated the effective extraction of the resulting partial melts into the zoned composite intrusions with strong systematic gradients in emplacement temperatures (Fig. 41d). As in the case of the Tjuni Purlka suite magmas, the prevailing structural regime exerted a strong control on magma formation, magma composition, and pluton construction.

Partial melting renders the crust refractory, or less fertile, and incapable of yielding further melt without further increases in temperature and/or fluxing. In this sense, the crustal component (high-K, biotite-bearing, felsic granulite) incorporated into the MASH domains was non-replenishable, but the basalt component must have been periodically replenished (Hildreth and Moorbath, 1988; Hildreth and Wilson, 2007; Bachmann and Bergantz, 2008) simply to sustain the thermal gradient. Over time, magmas extracted from MASH domains should then become isotopically more juvenile. Samples for which we have both precise intrusive ages and Nd-isotopic data are mainly from the northeastern part of the west Musgrave Province, and these data do indeed show a systematic trend to more radiogenic Nd isotopic compositions with decreasing age (Fig. 29), consistent with progressively less crustal material in successively younger magmas.

The relationship between the Wankanki and Pitjantjatjara Supersuites

It was shown earlier that the granites of the Wankanki Supersuite have calcic to calc-alkalic compositions that closely match those of continental arc magmas, leading to a suggestion that formation of these granites during the Mount West Orogeny could have occurred in a setting similar to the Phanerozoic North American Andean arc. Subduction processes introduce significant amounts of water into the sub-arc mantle, and a portion of this is inevitably transferred, through magmatism into the lower crust. There is limited geochronological evidence for high-grade metamorphism or crustal melting in the period between the Mount West Orogeny and the Musgrave Orogeny (Fig. 5). Hence, the evidence for a dry lower crust during the Musgrave Orogeny possibly requires that all hydrous components of a Mount West (Wankanki) subduction system be removed before the end of the Mount West Orogeny and that the lower crust remained dehydrated.

An alternative suggestion is that the homogeneous bulk source for the Wankanki Supergroup formed during an earlier event (perhaps during 1600–1500 Ma subduction along the northern margin of the Musgrave Province (e.g. Wade et al., 2008) or during the earliest stages of the Mount West Orogeny ~1345 Ma) and underwent dehydration melting to produce the hornblende-bearing Wankanki granites.

If the similarities in the Nd- and Hf-isotopic compositions of the Pitjantjatjara and Wankanki Supersuites do reflect common source components, then the significant major-element differences between the calcic to calc-alkalic Wankanki Supersuite and the calc-alkalic to alkali-calcic Pitjantjatjara Supersuite could mainly relate to differences in the a_{H2O} of the bulk source and its effect on melt reactions and residual mineralogy, or on crystallising assemblages (e.g. Frost and Frost, 1997). We suggest that the Wankanki granites formed as high-K, biotite- and hornblende-bearing, felsic amphibolite or granulite (country rock) was intruded by basaltic magmas, underwent dehydration melting, and was incorporated into those mafic magmas. Compositional control is via hornblende- and biotite-dehydration melting reactions, reflecting high a_{H2O} conditions in which plagioclase solubility was enhanced.

A variation in the a_{H2O} of a common source also explains the antithetic relationship in outcrop distribution between the Pitjantjatjara and Wankanki Supersuite granites. Extraction of calcic to calc-alkalic melts during the Mount West Orogeny would have rendered the lower crust in the southwestern parts of the west Musgrave Province both dehydrated *and* melt-depleted, and incapable of further voluminous melt production during subsequent thermal events. The progressive northeasterly decrease in abundance of Wankanki granites (and their eventual absence) (Figs 3 and 8) suggests that, during the Mount West Orogeny, the lower crust to the northeast underwent progressively less melt-depletion, and was eventually simply dehydrated at granulite facies.

Implications for the tectonic evolution of Mesoproterozoic central Australia

The Musgrave Province lies at the convergence of Australia's main Proterozoic structural trends, which ultimately reflect the amalgamation of the North, West, and South Australian Cratons (Fig. 2). To the north of the Musgrave Province, the Arunta Orogen lies along the southern margin of the North Australian Craton and is dominated by protolith ages in the range of c. 1880–

1700 Ma (e.g. see Cawood and Korsch, 2008). Along the southern margin of the Arunta Orogen lies the Warumpi Province, with protolith ages between 1690 and 1630 Ma (Close et al., 2003). The Warumpi Province has been interpreted as a continental arc related to a south-dipping subduction zone that developed outboard of the northern part of the Arunta Orogen (Close et al., 2003, 2006; Scrimgeour et al., 2005; Cawood and Korsch, 2008). Rocks with a similar age and Nd-isotopic composition also form part of the Biranup Zone of the Albany–Fraser Orogen (Spaggiari et al., 2009), to the southwest of the Musgrave Province.

Wade et al. (2006, 2008) provided some new insights into how the Musgrave Province may have evolved within the context of Proterozoic central Australia. Pivotal to that study is the suggestion that basement to the province was juvenile arc-related crust formed at 1600 to 1540 Ma during subduction along the southern edge of the Warumpi Province, and that this juvenile crust ultimately formed the intracratonic source for the Pitjantjatjara Supersuite. This suggestion of a subduction setting was based upon the juvenile Nd-isotopic composition and subduction-like geochemical signature of gneisses, interpreted to be meta-igneous rocks with 1600 to 1540 Ma protolith ages (Glikson et al., 1996; Wade et al., 2006, 2008). Many of those rocks have been reinterpreted as either paragneisses dominated by 1600–1540 Ga detritus, and with more realistic depositional ages younger than 1400 Ma, or as Pitjantjatjara Supersuite granites with emplacement-level contamination by paragneiss. However, it is also clear that the eastern part of the Musgrave Province does contain rare igneous rocks with 1600–1540 Ma magmatic ages (Evins et al., in prep). In addition, the presence throughout the Musgrave Province of paragneiss with protolith depositional ages between c. 1345 and 1300 Ma, with a dominance of c. 1600–1540 Ma detritus and with ε_{Nd} values (at c. 1400 Ma) between ~+3 and -2 (Wade et al., 2006, 2008; Evins et al., in prep), provides good evidence supporting the presence of a regional source of c. 1600–1540 Ma juvenile felsic material. These paragneisses, along with the rocks of the Wankanki and Pitjantjatjara Supersuites themselves, represent the most isotopically juvenile felsic components of Proterozoic central Australia (e.g. Wade et al., 2008).

Figure 42 illustrates the Nd-isotopic evolution trends for a range of central Australian crustal components. Rocks of the Arunta Orogen show a range in T_{DM2}(Nd) values of ~2200–2050 Ma (Foden et al., 1995; Sun et al., 1995; Zhao and McCulloch, 1995) and are less radiogenic than the crustal component that we suggest dominates the isotopic budget of the Wankanki and Pitjantjatjara Supersuites. Furthermore, the ages of magmatic zircons, rare zircon xenocrysts in granites, and detrital zircons from the west Musgrave Province (Fig. 5) include no significant components between 2200 and 1650 Ma, with the exception of detrital age peaks at c. 1770 and 1730 Ma in geographically restricted paragneisses in the far southeast of the west Musgrave Province (Evins et al., in prep.). Rocks of the Warumpi Province and of the Biranup Zone have protolith ages that do overlap known age peaks in detrital and xenocrystic zircon data from the west Musgrave Province, but have Nd-isotopic compositions

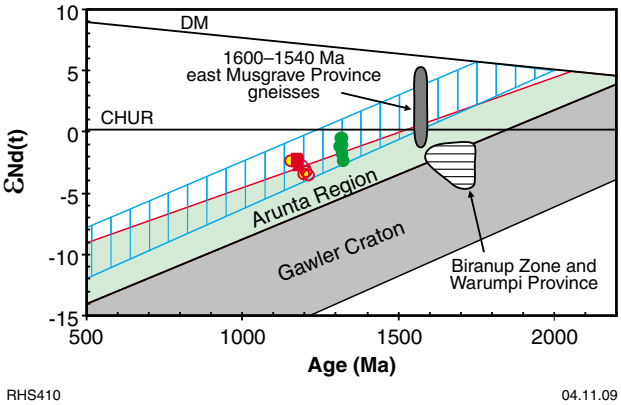

Figure 42. ε_{Nd} evolution diamgram comparing granites of the west Musgrave Province with potential regional source regions (additional data from Wade et al., 2006, 2008; Foden et al., 1995; Sun et al., 1995; Zhao and McCulloch, 1995; Spaggiari et al., 2009; Close et al., 2003).

that are even less radiogenic than rocks of the northern part of the Arunta Orogen (Fig. 42). The only regionally available material that matches the isotopic signature of the source for the Wankanki and Pitjantjatjara Supersuites is c. 1600 and 1540 Ma felsic crust, or the more widely exposed metasedimentary rocks derived largely from such crust.

Accordingly, and in agreement with Wade et al. (2008), we suggest that the geochemically and isotopically homogeneous crustal component that dominated the Nd- and Hf-isotopic budgets of the bulk source for the Wankanki and Pitjantjatjara Supersuites was c. 1600–1540 Ma juvenile felsic (?andesitic) crust. The compositions of granites of the Pitjantjatjara Supersuite reflect a K-, REE-, and HFSE-rich source with La/Nb and Th/Nb ratios significantly above chondritic values, making a subduction-related origin for that source a plausible proposition. Old T_{DM2}(Nd) values require that small amounts of crustal material of Archean age (but not necessarily Archean crust itself) were also incorporated into, and homogenized within, this source to produce felsic crust that was only weakly to moderately radiogenic with respect to depleted mantle. This crust was remobilized, and incorporated into intraplated and underplated mafic magmas during the Mount West and Musgrave Orogenies, to form the bulk source of the Wankanki and Pitjantjatjara Supersuites.

The tectonic setting of the Wankanki Supersuite is unclear. Several studies suggest that the evolution of the Albany–Fraser Orogen, to the southwest, between c. 1345 and 1290 Ma involved the convergence, collision, and suturing of the West Australian Craton (to the northwest) and the Mawson Craton, with the subducting slab dipping to the south (Fig. 43; e.g. Clark et al., 2000; Bodorkos and Clark, 2004; Cawood and Korsch, 2008). The only lines of evidence pointing to a subduction setting for the Wankanki Supersuite are a subduction-like geochemistry closely matching Andean-style continental arc-magmatism and the relatively juvenile isotopic compositions. Although

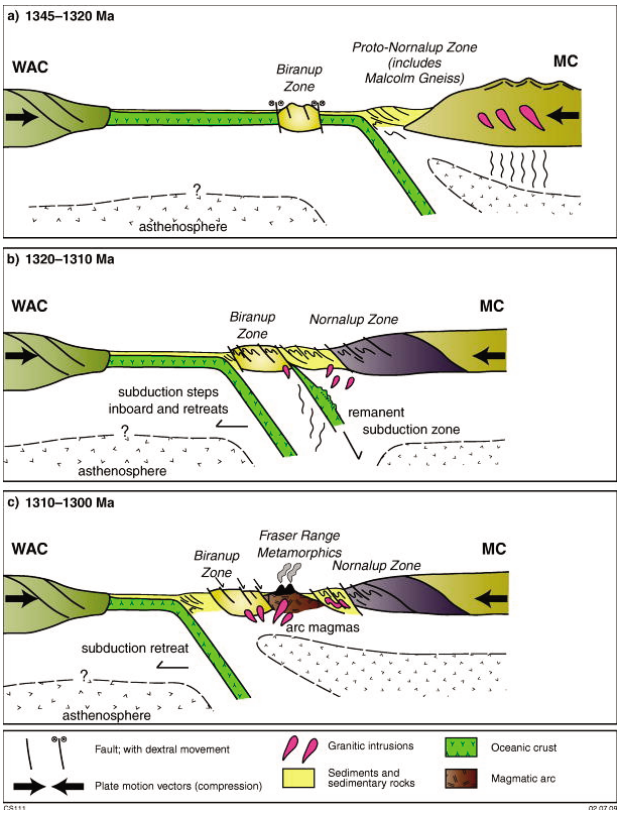

Figure 43. Schematic diagrams showing tectonic evolution of the Albany–Fraser Orogeny from 1345 to 1300 Ma (after Spaggiari et al., 2009).

Wankanki Supersuite magmatism is absent to the north of the Tjuni Purlka Tectonic Zone, this alone provides no firm basis for inferring a subduction-related suture.

Although it is tempting to relate the Wankanki Supersuite to a continental arc setting, and to correlate the province, at that time, with the Albany–Fraser Orogen (e.g. Clark et al., 2000), it must also be stressed that the subduction-setting interpreted for the latter, between c. 1345 and 1290 Ma, is itself based mainly on fundamentally ambiguous geochemical signatures. In addition, a southerly dipping slab, as proposed for the Albany–Fraser Orogen (e.g. Bodorkos and Clark, 2004) is difficult to accommodate with the Mount West Orogeny if granites in both the Wankanki Supersuite and the Pitjantjatjara Supersuite (i.e. on both sides of a suture) share a common crustal source component. If the Wankanki granites are arc-related then a north-dipping slab, and overriding juvenile 1600–1540 Ma crust, is required (Fig. 44). In this scenario, the Tjuni Purlka Tectonic Zone may have also been initiated during the Mount West Orogeny as an incipient back-arc rift. If the Wankanki Supersuite is directly related to subduction, then Proterozoic central Australia is characterized by a progressively southwards younging series of subduction-related tectonic slices, and the c. 1345 to c. 1293 Ma Mount West Orogeny reflects the final convergence of northern and southern cratonic elements.

Whether a subduction suture or the site of back-arc (or intracontinental) rifting during the Mount West Orogeny, the Tjuni Purlka Tectonic Zone was clearly a crustal-

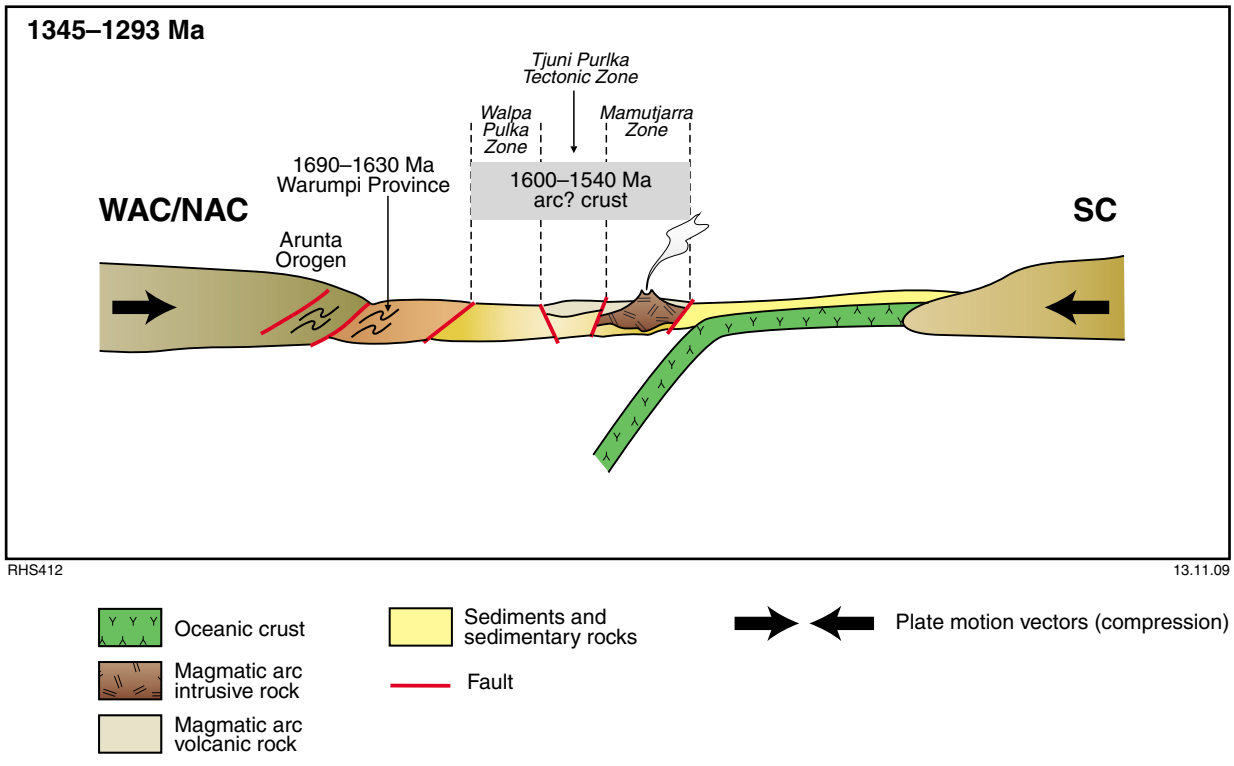

Figure 44. Schematic diagrams showing tectonic evolution of the west Musgrave Province during the Mount West Orogeny. WAC/NAC = combined West and North Australian Craton; SC = a southern cratonic mass.

scale shear zone that was active throughout the Musgrave Orogeny. Transtensional movement within the Tjuni Purlka Tectonic Zone, and along its boundaries, had a major control on the style of intrusion and also ultimately on magma compositions and compositional zonations within Pitjantjatjara granite suites. The Tjuni Purlka Tectonic Zone was also the locus of voluminous mantle-derived magmas at various stages during the Giles Event, from >1078 to c. 1026 Ma.

The c. 100 Ma of high-temperature magmatism and of UHT metamorphism recorded in the lower to middle crust of the Musgrave Province throughout the Musgrave Orogeny, likely makes this region unique amongst hot orogens. This duration, however, is possibly a minimum. Given that the upper age constraint on the Giles Event (>1078 Ma) is a minimum (Smithies et al., 2009a), the time interval separating the Musgrave Orogeny and the Giles Event may be short (Fig. 5), with at least punctuated episodes of high-heat flow, mantle underplating, intraplating, and crustal melting extending from c. 1120 Ma to perhaps c. 1026 Ma. There is no suggestion that the prevailing intracontinental tectonic setting during the Giles Event fundamentally differed from that of the Musgrave Orogeny, and so it is possible that the two events could justifiably be viewed as a continuum. Significant lithological differences between the two include the greater abundance of mafic magmatism, including upper crustal dyke emplacement and extrusion, during the Giles Event and the lack of Ti- and P-enriched charnockite-series granites. These differences could relate to a combination of progressive crustal and lithospheric thinning and a gradual reduction in the amount of fusible components within the lower crust (i.e. progressive melt-depletion), leading to a decreasing volume of felsic melt and a trend to more brittle tectonic styles.

Both the Musgrave Orogeny and the Giles Event almost certainly reflect a period of intracratonic extension, and in this respect, analogies with the Mesozoic break-up of Gondwana, the associated HPT latites of the Karoo and Paraná-Etendeka Provinces, and the felsic magmas of the Chon Aike Province, might be relevant. The difference is that magmatism related to the Early Cretaceous break-up of Gondwana covered periods of only a few millions of years (for most of the basaltic volcanism; Duncan et al., 1997) to 30 Ma (Chon Aike; Pankhurst et al., 2000), rather than the 100 Ma period over which the Pitjantjatjara Supersuite evolved. In addition, although the thermal conditions that might be expected to immediately precede, or initiate, break-up prevailed for c. 100 Ma, and possibly as much as 200 Ma, break-up never actually occurred.

Active continental rifting is commonly ascribed to mantle plumes impinging on the base of the lithosphere, with the Mesozoic break-up of Gondwana (for example) attributed to the effects of several plumes (Tristan da Cunha – Discovey–Shona–Bouvet)(e.g. Pankhurst et al., 2000: Riley et al., 2001; Ewart, et al, 2004b). The duration of magmatism attributed to a single plume can be arguably stretched to ~50 Ma (e.g. Ernst and Buchan, 2001), and so the duration of the Musgrave Orogeny and the Giles Event (individually and collectively) does not favour simple plume magmatism. In addition, crustal plates typically move with respect to a specific mantle heat source. Hence, while the total duration of plume magmatism might be as much as 50 Ma, the duration of magmatism in a given place should be much shorter. In the case of the Musgrave Province, it is possible that the locus of maximum heat flux did not move at all with respect to the lower crust. Magmatic temperature estimates indicate a south-westerly increase in temperature, but this is not linked to age. In addition, the trend to successively younger intrusion ages to the southwest of the Fanny Fault is better interpreted as a migration in the locus of intrusion and not in the locus of maximum heat flux. This locus of intrusion switches back to the north of the Fanny Fault for a period within the late Musgrave Orogeny. Thus, during the Musgrave Orogeny, it is possible that the locus of maximum heat flow was strongly coupled to the lithospheric architecture.

If this is the case, then the position of the Musgrave Province itself, at the triple-point of Proterozoic Australia, explains the prolonged thermal history in a tectonic scenario akin to a 'stagnant-lid' tectonothermal regime (e.g. Sears et al., 2005; Stern, 2008) overlying a mantle superswell (e.g. Hoffman, 1989; McNutt, 1998). McNutt (1998) describes superswells as large-scale (thousands of kms) dynamic mantle upwellings from the low-viscosity zone immediately beneath a plate. In oceanic environments (e.g. South Pacific Superswell), this can cause a four-fold increase in the rate of volcanism, not immediately attributable to plate separation or convergence or to deep-mantle plumes (McNutt, 1998). Hoffman (1989) applied the concept of superswells to Laurentia, whereby this stationary Proterozoic supercontinent insulated the underlying mantle, inducing convective upwellings, decompression melting, and invasion and ponding of resulting melts at or within the crust. This, in turn, resulted in anhydrous partial melting of the lower crust and the production of widespread anorogenic magmatism; including massif anorthosites and temporally related granites (e.g. the anorthosite–mangerite–charnockite–granite (AMCG) suite).

In developing our model, we suggest that boundaries of ancient crustal blocks remain fundamental features of lithospheric structural architecture (e.g. Begg et al., 2009), and correspondingly remain the sites of geological activity for long periods after collisional orogeny. According to Begg et al. (2009), the lithospheric architecture of the African continent comprises a number of dominantly Archean cratonic blocks with deep, rigid, and steep-sided sub-continental lithospheric mantle roots. Junctions between cratonic blocks remain areas of weaker, thinner, and hotter lithosphere. These provide pathways for heat, either through the direct focussing of ascending magmas, or through channelling convecting mantle into thinner lithospheric regimes where decompression melting becomes possible. Lying at the triple junction of three older cratonic blocks, the base of the sub-Musgrave lithosphere was potentially one region where voluminous mantle melts may have been focussed throughout a long period of time — channelled into a regional low-pressure melt-trap (Fig. 45). Crustal-scale shear zones, like those that bound the Tjuni Purlka Tectonic Zone, define second-order crustal blocks, and provide conduits for the ascent

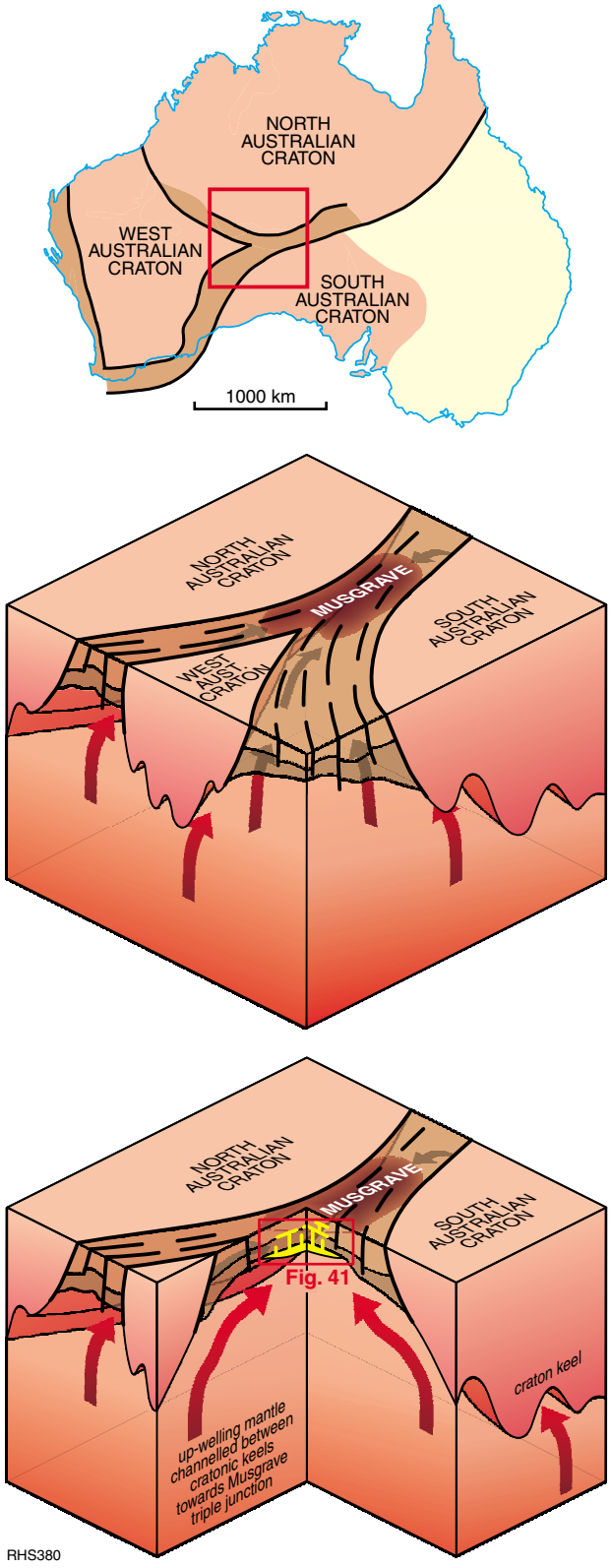

Figure 45. Block diagram showing the influence of crustal blocks on tectonothermal evolution during the Musgrave Orogeny (see text for details).

of mantle magmas into the lower crust and the ascent of felsic magmas out of the lower crust.

According to Sears et al. (2005), drift stagnation of supercontinental masses, and thermal insulation and subsequent expansion of the underlying mantle (superswell), lead to a specific geometric pattern (truncated icosahedral tessellations) of lithospheric fracturing. Decompression melting of asthenosphere along these fractures ultimately results in anorogenic magmatism, with long-lived magmatic regions occurring near triple points. However, in the case of the Musgrave Province, the triple-point configuration that drives the UHT metamorphism and anorogenic magmatism was established during amalgamation of the larger continental mass, not during an attempt to dismantle that mass.

If it is this lithospheric architecture that specifically controls UHT heat-flux beneath the Musgrave Province during the Musgrave Orogeny, and given that the Mount West Orogeny does not reflect UHT conditions, then this architecture must have been established within the c. 70 Ma separating the two orogenies. This provides a further line of evidence favouring subduction, collisional orogeny and final amalgamation of the North and South Australian Cratons during, or shortly before, the Mount West Orogeny.

References

Anderson, IC, Frost, CD and Frost, BR 2003, Petrogenesis of the Red Mountain pluton, Laramie anorthosite complex, Wyoming: implications for the origin of A-type granite: Precambrian Research, v. 124, p. 243–267.

Annen, C and Sparks, RSJ 2002, Effects of repetitive emplacement of basaltic intrusions on thermal evolution and melt generation in the crust: Earth and Planetary Science Letters, v. 203, p. 937–955.

Annen, C, Blundy, JD and Sparks, RSJ 2006, The Genesis of Intermediate and Silicic Magmas in Deep Crustal Hot Zones: Journal of Petrology, v. 47, p. 505–539.

Ashwal, LD, Tucker, RD and Zinner, EK 1999, Slow cooling of deep crustal granulites and Pb-loss in zircon: Geochimica et Cosmochimica Acta, v. 63, p. 2839–2851

Bachmann, O and Bergantz, GW 2008, Rhyolites and their Source Mushes across Tectonic Settings: Journal of Petrology, v. 49, p. 2277–2285.

Bea, F 1996, Residence of REE, Y, Th and U in granites and crustal protoliths; implications for the chemistry of crustal melts: Journal of Petrology, v. 37, p. 521–552.

Beard, JS, Abitz, RJ and Lofgren, GE 1993, Experimental melting of crustal xenoliths from Kilbourne Hole, New Mexico and implications for the contamination and genesis of magmas: Contributions to Mineralogy and Petrology, v. 115, p. 88–102.

Begg, GC, Griffin, WL, Natapov, LM, O'Reilly, SY, Grand, SP, O'Neill, CJ, Hronsky, JMA, Poudjom Djomani, Y, Swain, CJ, Deen, T and Bowden, P 2009, The lithospheric architecture of Africa: Seismic tomography, mantle petrology, and tectonic evolution: Geosphere, v. 5, p. 23–50.

Bodorkos, S and Clark, DJ 2004, Evolution of a crustal-scale transpressive shear zone in the Albany Fraser Orogen, SW Australia: 2. Tectonic history of the Coramup Gneiss and a kinematic framework for Mesoproterozoic collision of the West Australian and Mawson cratons: Journal of Metamorphic Geology, v. 22, p. 713–731.

Bodorkos, S and Wingate, MTD 2008a, 174594: metamorphosed leucogabbro, Mirturtu Camp: Geological Survey of Western Australia, Geochronology Record 716 4p.

Bodorkos, S and Wingate, MTD 2008b, 174589: quartz syenite dyke, Amy Giles Hill: Geological Survey of Western Australia, Geochronology Record 715: 4p.

Bodorkos, S, Wingate, MTD and Kirkland, CL 2008a, 174538: metamonzogranite, Mount Daisy Bates: Geological Survey of Western Australia, Geochronology Record 712: 4p.

Bodorkos, S, Wingate, MTD and Kirkland, CL 2008b, 174558: metamorphosed quartz diorite, Mount Fanny: Geological Survey of Western Australia, Geochronology Record 713: 4p.

Bodorkos, S, Wingate, MTD and Kirkland, CL 2008c, 174736: granofelsic metasyenogranite, Mount Fanny: Geological Survey of Western Australia, Geochronology Record 717: 4p.

Bodorkos, S, Wingate, MTD and Kirkland, CL 2008d, 174737: foliated metamonzogranite, Mount Fanny: Geological Survey of Western Australia, Geochronology Record 718: 5p.

Bodorkos, S, Wingate, MTD and Kirkland, CL 2008e, 174747: metagabbro, Mount Fanny: Geological Survey of Western Australia, Geochronology Record 719: 4p.

Bonin, B 2007, A-type granites and related rocks: Evolution of a concept, problems and prospects: Lithos, v. 97, p. 1–29.

Brown, M 2007a, Metamorphic Conditions in Orogenic Belts: A Record of Secular Change: International Geology Review, v. 49, p. 193–234.

Brown, M 2007b, Crustal melting and melt extraction, ascent and emplacement in orogens: mechanisms and consequences: Journal of the Geological Society, London, v. 164, p. 709–730.

Brown, M 2008, Characteristic thermal regimes of plate tectonics and their metamorphic imprint throughout Earth history: When did Earth first adopt a plate tectonics mode of behaviour?, *in* When did plate tectonics begin on planet Earth? *edited by* KC Condie and V Pease: Geological Society of America, Special Paper 440, p. 97–128.

Bryan, SE, Ferrari, L, Reiners, PW, Allem, CM, Petrone, CM, Ramos-Rosique, A and Campbell, IH 2008, New Insights into Crustal Contributions to Large-volume Rhyolite Generation in the Mid-Tertiary Sierra Madre Occidental Province, Mexico, Revealed by U–Pb Geochronology: Journal of Petrology, v. 49, p. 47–77.

Camacho, A 1989, The Woodroffe Thrust, eastern Musgrave Block, NT: A problem of large scale melting during thrusting: Geological Society of Australia, Abstracts 24, p. 14–15.

Camacho, A 1997, An isotopic study of deep-crustal orogenic processes: Musgrave Block, Central Australia: The Australian National University, PhD Thesis (unpublished).

Camacho, A, Compston, W, McCulloch, M and McDougall, I 1997, Timing and exhumation of eclogite facies shear zones, Musgrave Block, central Australia: Journal of Metamorphic Geology, v. 15, p. 735–751.

Cawood, PA and Korsch, RJ 2008, Assembling Australia: Proterozoic building of a continent: Precambrian Research, v. 166, p. 1–38.

Cherniak, DJ and Watson, EB 2001, Pb diffusion in zircon: Chemical Geology, v. 172, p. 5–24.

Clark, DJ, Hensen, BJ and Kinny, PD 2000, Geochronological constraints for a two-stage history of the Albany–Fraser Orogen, Western Australia: Precambrian Research, v. 102, p. 155–183.

Clarke, GL, Sun, S-S and White, RW 1995, Grenville age belts and associated older terranes in Australia and Antarctica: Australian Geological Survey Organisation, Journal of Australian Geology and Geophysics, v. 16, p. 25–39.

Clemens, JD, Holloway, JR and White, AJR 1986, Origin of an A-type granite: experimental constraints: American Mineralogist, v. 71, p. 317–324.

Close, D, Scrimgeour, I, Edgoose, C, Cross, A, Claoue-Long, J, Kinny, P and Meixner, A 2003, Redefining the Warumpi Province: Annual GeoScience Exploration Seminar (AGES) 2003. Record of Abstracts, Northern Territory Geological Survey, Record 2003–001.

Close, D, Scrimgeour, I and Edgoose, C 2006, Evolution and mineral potential of the Paleoproterozoic Warumpi Province: Geoscience Australia, Record 2006/16, p. 9–10.

Collins, WJ, Beams, SD, White, AJR and Chappell, BW 1982, Nature and origin of A-type granites with particular reference to southeastern Australia: Contributions to Mineralogy and Petrology, v. 80, p. 189–200.

Condie, KC and Myers, JS 1999, Mesoproterozoic Fraser Complex: geochemical evidence for multiple subduction-related sources of lower crustal rocks in the Albany–Fraser Orogen, Western Australia: Australian Journal of Earth Sciences, v. 46, p. 875–882.

Daniels, JL 1974, The Geology of the Blackstone region, Western Australia: Geological Survey of Western Australia, Bulletin 123, 257p.

Dawson, GC, Krapez, B, Fletcher, IR, McNaughton, NJ and Rasmussen, B 2002, 1.2 Ga thermal metamorphism in the Albany–Fraser Orogen of Western Australia: consequence of collision or regional heating by dyke swarms?: Journal of the Geological Society, London, v. 160, p. 29–37.

Deer, WA, Howie, RA and Zussman, J 1966, An introduction to the rock-forming minerals: Longman, London, 528p.

Degeling, H, Eggins, S and Ellis, DJ 2001, Zr budgets for metamorphic reactions, and the formation of zircon from garnet breakdown: Mineralogical Magazine, v. 65, p. 749–758.

Dufek, J and Bergantz, GW 2005, Lower crustal magma genesis and preservation: a stochastic framework for the evaluation of basalt-crust interaction: Journal of Petrology, v. 46, p. 2167–2195.

Duncan, RA, Hooper, PR, Rehacek, J, Marsh, JS and Duncan, AR 1997, The timing and duration of the Karoo igneous event, southern Gondwana: Journal of Geophysical Research, v. 102B, p. 18127–18138.

Edgoose, CJ, Scrimgeour, IR and Close, DF 2004, Geology of the Musgrave Block, Northern Territory: Northern Territory Geological Survey, Report 15, 48p.

Ernst, RE and Buchan, KL 2001, Large mafic magmatic events through time and links to mantle plume heads, *in* Mantle Plumes. Their Identification Through Time; *edited by* RE Ernst and KL Buchan: Geological Society of America, Special Paper 352, p. 483–575.

Evins, PM, Smithies, RH, Maier, WD and Howard, HM 2009, Holt, WA Sheet 4546: Geological Survey of Western Australia, 1:100 000 Geological Series.

Evins, PM, Smithies, H, Howard, HM, Kirkland, CL, Wingate, MTD and Bodorkos, S in press, Devil in the detail; the structural evolution and chronology of a Mesoproterozoic mafic-felsic intrusive province: Precambrian Research.

Ewart, A, Marsh, JS, Milner, SC, Duncan, AR, Kamber, BS and Armstrong, RA 2004a, Petrology and Geochemisrty of Early Cretaceous Bimodal Continental Flood Volcanism of the NW Etendeka, Namibia. Part 2: Characteristics and Petrogenesis of the High-Ti Latite and High-Ti and Low-Ti Voluminous Quartz Latite Eruptives: Journal of Petrology, v. 45, p. 107–138.

Ewart, A, Marsh, JS, Milner, SC, Duncan, AR, Kamber, BS and Armstrong, RA 2004b, Petrology and Geochemisrty of Early Cretaceous Bimodal Continental Flood Volcanism of the NW Etendeka, Namibia. Part 1: Introduction, Mafic Lavas and Re-evaluation of Mantle Source Components: Journal of Petrology, v. 45, p. 59–105.

Flöttmann, T and Hand, M 1999, Folded basement-cored tectonic wedges along the northern edge of the Amadeus Basin, central Australia; evaluation of orogenic shortening: Journal of Structural Geology, v. 21, p. 399–412.

Foden, J, Mawby, J, Kelley, S, Turner, S and Bruce, D 1995, Metamorphic events in the eastern Arunta Inlier. Part 2: Nd–Sr–Ar isotopic constraints, *in* Time Limits on Tectonic Events and Crustal Evolution using Geochronology; Some Australian Examples *edited by* WJ Collins and RD Shaw: Precambrian Research, Elsevier, Amsterdam, International, p. 207–227.

Foley, S, Tiepolo, M and Vannucci, R 2002, Growth of early continental crust controlled by melting of amphibole in subduction zones: Nature, v. 417, p. 837–840.

Fraser, G, Ellis, D and Eggins, S 1997, Zirconium abundance in granulite-facies minerals, with implications for zircon geochronology in high-grade rocks: Geology, v. 25, p. 607–610.

Frost, CD and Frost, BR 1997, Reduced rapakivi-type granites: the tholeiitic connection: Geology, v. 25, p. 647–650.

Frost, BR and Frost, CD 2008, On Charnockites: Gondwana Research, v. 13, p. 30–44.

Frost, BR, Barnes, CG, Collins, WJ, Arculus, RJ, Ellis, DJ and Frost, CD 2001, A Geochemical Classification for Granite Rocks: Journal of Petrology, v. 42, p. 2033–2048.

Garland, F, Hawkesworth, CJ and Mantovani, MSM 1995, Description and Petrogenesis of the Paraná Rhyolites, Southern Brazil: Journal of Petrology, v. 36, p. 1193–1227.

Glikson, AY, Stewart, AT, Ballhaus, GL, Clarke, GL, Feeken, EHT, Level, JH, Sheraton, JW and Sun, S-S 1996, Geology of the western Musgrave Block, central Australia, with reference to the mafic–ultramafic Giles Complex: Australian Geological Survey Organisation, Bulletin 239, Australian Government Publishing Service, Canberra, 206p.

Goode, ADT 1970, The petrology and structure of the Kalka and Ewarara layered basic intrusions, Giles Complex, central Australia: University of Adelaide, PhD thesis (unpublished).

Gray, CM 1971, Strontium isotope studies on granulites: Australian National University, PhD thesis (unpublished).

Gray, CM 1978, Geochronology of granulite-facies gneisses in the western Musgrave Block, central Australia: Journal of the Geological Society of Australia, v. 25, p. 403–414.

Gray, CM and Compston, W 1978, A Rb-Sr chronology of the metamorphism and prehistory of central Australian granulites: Geochimica et Cosmochimica Acta, v. 42, p. 1735–1748.

Guidotti, CV 1984, Micas in metamorphic rocks, *in* Micas (Reviews in Mineralogy vol. 13) *edited by* SW Bailey: Mineralogical Society of America, Washington DC, p. 357–467.

Harley, SL 1998, On the occurrence and characterization of ultrahigh-temperature crustal metamorphism, *in* What Drives Metamorphism and Metamorphic Relations? *edited by* PJ Treloar and PJ O'Brien: Geological Society, London, Special Publication, p. 81–107.

Hawkesworth, C, Mantovani, M and Peate, D 1988, Lithosphere Remobilization during Parana CFB Magmatism: Journal of Petrology, Special Lithosphere Issue, p. 205–223.

Hildreth, W 1981, Gradients in silicic magma chambers: implications for lithospheric magmatism: Journal of Geophysical Research, v. 86, p. 10153–10192.

Hildreth, W and Moorbath, S 1988, Crustal contributions to arc magmatism in the Andes of Central Chile: Contributions to Mineralogy and Petrology, v. 98, p. 455–489.

Hildreth, W and Wilson, CJN 2007, Compositional Zoning of the Bishop Tuff: Journal of Petrology, v. 48, p. 951–999.

Hoffman, PF 1989, Speculation on Laurentia's first gigayear (2.0 to 1.0 Ga): Nature, v. 17, p. 135–138.

Hoskin, PWO and Black, LP 2000, Metamorphic zircon formation by solid-state recrystallization of protolith igneous zircon: Journal of Metamorphic Geology v. 18, p. 423–439.

Howard, HM, Smithies, RH, Pirajno, F and Skwarnecki, MS 2006, Bates, W.A. Sheet 4646: Geological Survey of Western Australia, 1:100 000 Geological Series.

Howard, HM, Smithies, RH, Pirajno, F and Skwarnecki, MS 2007, Bell Rock, W.A. Sheet 4645: Geological Survey of Western Australia, 1:100 000 Geological Series.

Icenhower, JP and London, D 1997, Partitioning of fluorine and chlorine between biotite and granitic melt: experimental calibration at 200 MPa H_2O: Contributions to Mineralogy and Petrology, v. 127, p. 17–29.

Kelsey, DE 2008, On ultrahigh-temperature crustal metamorphism: Gondwana Research, v. 13, p. 1–29.

Kelsey, DE, White, RW, Powell, R and Holland, TJB 2004, Calculated phase equilibria in K_2O–FeO–MgO–Al_2O_3–SiO_2–H_2O for sapphirine-quartz-bearing mineral assemblages: Journal of Metamorphic Geology, v. 22, p. 559–578.

Kelsey, DE, Hand, M, Evins, P, Clark, C and Smithies, H 2009, High temperature, high geothermal gradient metamorphism in the Musgrave Province, central Australia; potential constraints on tectonic setting. Kangaroo Island 2009 conference. Specialist Group in Geochemistry, Mineralogy and Petrology, Geological Society of Australia.

Kemp, AIS, Wormald, RJ, Whitehouse, MJ and Price, RC 2005, Hf isotopes in zircon reveal contrasting sources and crystallization histories for alkaline to peralkaline granites of Temora, southeastern Australia: Geology, v. 33, p. 797–800.

King, RJ 2008, Using calculated pseudosections in the system NCKFMASHTO and SHRIMP II U–Pb zircon dating to constrain the metamorphic evolution of paragneisses in the Latitude Hills, West Musgrave Province, Western Australia: Geological Survey of Western Australia, Record 2009/15, 116p.

Kilpatrick, JA and Ellis, DJ 1992, C-type magmas: igneous charnockites and their extrusive equivalents: Transactions of the Royal Society of Edinburgh, Earth Sciences, v. 83, p. 155–164.

Kirkland, CL, Wingate, MTD and Bodorkos, S 2008a, 183496: orthogneiss, Mount West: Geological Survey of Western Australia, Geochronology Record 747, 5p.

Kirkland, CL, Wingate, MTD and Bodorkos, S 2008b, 183459: charnockite, Latitude Hill: Geological Survey of Western Australia, Geochronology Record 722, 5p.

Kirkland, CL, Wingate, MTD and Bodorkos, S 2008c, 183509: leucogranite dyke, Mount West: Geological Survey of Western Australia, Geochronology Record 724: 4p.

Kirkland, CL, Wingate, MTD and Bodorkos, S 2008d, 193850: leucogranite dyke, Mount Fanny: Geological Survey of Western Australia, Geochronology Record 748: 4p.

Kirkland, CL, Wingate, MTD and Bodorkos, S 2008e, 174761: porphyritic granite dyke, Charnockite Flats: Geological Survey of Western Australia, Geochronology Record 721: 4p.

Kirkland, CL, Wingate, MTD and Bodorkos, S 2008f, 185509: leucogranite, Mount Aloysius: Geological Survey of Western Australia, Geochronology Record 725: 4p.

Kirkland, CL, Wingate, MTD and Bodorkos, S 2008g, 183474: hornblende syenogranite, South Hill: Geological Survey of Western Australia, Geochronology Record 723: 4p.

Kirkland, CL, Whitehouse, MJ and Slagstad, T 2009, Fluid-assisted zircon and monazite growth within a shear zone: a case study from Finnmark, Arctic Norway: Contributions to Mineralogy and Petrology, v. 158, 5, p. 637–657.

Landenberger, B and Collins, WJ 1996, Derivation of A-type granites from a dehydrated charnockitic lower crust: evidence from the Chaelundi Complex, eastern Australia: Journal of Petrology, v. 37, p. 145–170.

Liew, TC and Hofmann, AW 1988, Precambrian crustal components, plutonic associations, plate environment of the Hercynian Fold Belt of Central Europe: indications from a Nd and Sr isotopic study: Contributions to Mineralogy and Petrology, v. 98, p. 129–138

Maboko, MAH 1988, Metamorphic and geochronological evolution in the Musgrave Ranges, central Australia: Canberra, Australian National University, PhD thesis (unpublished).

Major, RB and Conor, CHH 1993, Musgrave Block, *in* The Geology of South Australia *edited by* JF Drexel, WV Preiss, and AJ Parker: Geological Survey of South Australia, Bulletin 54, p. 156–167.

McNutt, MK 1998, Superswells: Reviews of Geophysics, v. 36, p. 211–244.

Miller, JA and Harris, C 2007, Petrogenesis of the Swaziland and Northern Natal Rhyolites of the Lembombo Rifted Volcanic Margin, South East Africa: Journal of Petrology, v. 48, p. 185–218.

Moeller, A, O'Brien, PJ, Kennedy, A and Kroner, A 2003, Linking growth episodes of zircon and metamorphic textures to zircon chemistry: An example from the ultrahigh-temperature granulites of Rogaland (SW Norway), *in* Geochronology: Linking the Isotopic Record with Petrology and Textures *edited by* D Vance, W Muller, and IM Villa: Geological Society of London Special Publication 220, p. 65– 81.

Morris, PA and Pirajno, F 2005, Geology, geochemistry, and mineralization potential of Mesoproterozoic sill complexes of the Bangemall Supergroup, Western Australia: Geological Survey of Western Australia, Report 99.

Murakami, T, Chakoumakos, BC, Ewing, RC, Lumpkin, GR and Weber, WJ 1991, Alpha-decay event damage in zircon: American Mineralogist, v. 76, p. 1510–1532.

Muñoz, JL 1984, F-OH and Cl-OH exchange in micas with applications to hydrothermal ore deposits, *in* Micas *edited by* SW Bailey: Mineralogical Society of America, Washington DC: Reviews in Mineralogy, v. 13. p. 469–493

Muñoz, JL and Ludington, SD 1974, Fluoride-hydroxyl exchange in biotite: American Journal of Science, v. 274, p. 396–413.

Myers, JS, Shaw, RD and Tyler, IM 1996, Tectonic evolution of Proterozoic Australia: Tectonics, 16, p. 1431–1446

Pankhurst, RJ, Leat, PT, Sruoga, P, Rapela, CW, Marquez, M, Storey, BC and Riley, TR 1998, The Chon Aike silicic igneous province of Patagonia and related rocks in Antarctica: a silicic LIP: Journal of Volcanology and Geothermal Research, v. 81, p. 113–136.

Pankhurst, RJ, Riley, TR, Fanning, CM and Kelley, SP 2000, Episodic Silicic Volcanism in Patagonia and the Antarctic Peninsula: Chronology of Magmatism Associated with the Break-up of Gondwana: Journal of Petrology, v. 41, p. 605–625.

Pearce, JA, Harris, NBW and Tindle, AG 1984, Trace element discrimination diagrams for the tectonic interpretation of granitic rocks: Journal of Petrology, v. 25, p. 956–983.

Peterson, JW, Chacko, T and Kuehner, SM 1991, The effects of fluorine on the vapour-absent melting of phlogopite + quartz: implications for deep-crustal processes: American Mineralogist, v. 76, p. 470–476.

Petford, N and Gallagher, K 2001, Partial melting of mafic (amphibolitic) lower crust by periodic influx of basaltic magma: Earth and Planetary Science Letters, v. 193, p. 483–489.

Powell, R and Holland, TJB 1988, An internally consistent thermodynamic dataset with uncertainties and correlations: 3. Application methods, worked examples and a computer program: Journal of Metamorphic Geology, v. 6, p. 173–204.

Raimondo, T, Collins, AS, Hand, M, Walker-Hallam, A, Smithies, RH, Evins, PM and Howard, HM 2009, Ediacaran intracontinental channel flow: Geology, v. 37, p. 291–294.

Rapp, R and Watson, EB 1995, Dehydration melting of metabasalt at 8–32 kbar: implications for continental growth and crust-mantle recycling: Journal of Petrology, v. 36, p. 891–931.

Riley, TR, Leat, PT, Pankhurst, RJ and Harris, C 2001, Origins of Large Volume Rhyolitic Volcanism in the Antarctic Peninsula and Patagonia by Crustal Melting: Journal of Petrology, v. 42, p. 1043–1065.

Rollinson, HR and Tarney, J 2005, Adakites — the key to understanding LILE depletion in granulites: Lithos, v. 79, p. 61–81.

Rowe, MC, Wolff, JA, Gardner, JN, Ramos, FC, Teasdale, R and Heikoop, CE 2007, Development of a Continental Volcanic Field: Petrogenesis of Pre-caldera Intermediate and Silicic Rocks and Origin of the Bandelier Magmas, Jemez Mountains (New Mexico, USA): Journal of Petrology, v. 48, p. 2063–2091.

Schaltegger, UM, Fanning, M, Günther, D, Maurin, JC, Schulmann, K and Gebauer, D 1999, Growth, annealing and recrystallization of zircon and preservation of monazite in high-grade metamorphism: conventional and in-situ U–Pb isotope, cathodoluminescence and microchemical evidence: Contributions to Mineralogy and Petrology, v. 134, p. 186–201.

Scrimgeour, IR and Close, DF 1999, Regional high pressure metamorphism during intracratonic deformation: the Petermann orogeny, central Australia: Journal of Metamorphic Geology, v. 17, p. 557–572.

Scrimgeour, IR, Kinny, PD, Close, DF and Edgoose, CJ 2005, High-T granulites and polymetamorphism in the southern Arunta Region, central Australia: Evidence for a 1.64 Ga accretionary event: Precambrian Research, v. 142, p. 1–27.

Sears, JW, St. George, GM and Winne, JC 2005, Continental rift systems and anorogenic magmatism: Lithos, v. 80, p. 147–154.

Seat, Z 2008, Geology, Petrology, Mineral and Whole-rock Chemistry, Stable and Radiogenic Isotope Systematics and Ni–Cu–PGE Mineralisation of the Nebo-Babel Intrusion, west Musgrave, Western Australia: University of Western Australia, PhD thesis (unpublished).

Shaw, SE, and Flood, RH 2009, Zircon Hf Isotopic Evidence for Mixing of Crustal and Silicic Mantle-derived Magmas in a Zoned Granite Pluton, Eastern Australia; Journal of Petrology, v. 50, p. 147–168.

Skjerlie, KP and Johnston, AD 1993, Fluid-Absent Melting Behaviour of an F-Rich Tonalitic Gneiss at Mid-Crustal Pressures: Implications for the Generation of Anorogenic Granites: Journal of Petrology, v. 34, p. 785–815.

Smith, DR, Noblett, J, Wobus, RA, Unruh, D, Douglass, J, Beane, R, Davis, C, Goldman, S, Kay, G, Gustavson, B, Saltoun, B and Stewart, J 1999, Petrology and geochemistry of late-stage intrusions of the A-type, mid-Proterozoic Pikes Peak batholith (Central Colorado, USA): implications for petrogenetic models: Precambrian Research, v. 98, p. 271–305.

Smithies, RH, Howard HM, Evins PM, Kirkland CL, Bodorkos, S and Wingate, MTD 2009a, The west Musgrave Complex — some new geological insights from recent mapping, geochronology, and geochemical studies: Geological Survey of Western Australia Record 2008/19, 20p.

Smithies, RH, Howard HM, Maier, WD and Evins PM 2009b, Blackstone, WA Sheet 4545: Geological Survey of Western Australia 1:100 000 Geological Series.

Spaggiari, CV, Bodorkos, S, Barquero-Molina, M, Tyler, IM and Wingate, MDT 2009, Interpreted bedrock geology of the South Yilgarn and central Albany–Fraser Orogen, Western Australia: Geological Survey of Western Australia, Record 2009/10, 84p.

Stern, RJ 2008, Neoproterozoic Crustal Growth: The Solid Earth System During A Critical Time of Earth History: Gondwana Research, v.14, p. 33–50.

Stewart, AJ 1995, Resolution of conflicting structures and deformation history of the Mount Aloysius granulite massif, western Musgrave Block, central Australia: Australian Geological Survey Organisation, Journal of Australian Geology and Geophysics, v. 16, p. 91–105.

Stüwe, K 2002, Geodynamics of the lithosphere. An introduction: Springer-Verlag, 449p.

Sun, S-S, Warren, RG and Shaw, RD 1995, Nd isotope study of granites from the Arunta Inlier, central Australia; constraints on geological models and limitation of the method, *in* Time Limits on Tectonic Events and Crustal Evolution using Geochronology Some Australian Examples *edited by* WJ Collins and RD Shaw: Precambrian Research, Elsevier, Amsterdam, p. 310–314.

Sun, S-S, Sheraton, JW, Glikson, AY and Stewart, AJ 1996, A major magmatic event during 1050–1080 Ma in central Australia, and an emplacement age for the Giles Complex: Australian Geological Survey Organisation, Journal of Australian Geology and Geophysics, v. 24, p. 13–15.

Thompson, AB, 1992, Metamorphism and fluids *in* Understanding the Earth *edited by* G Brown, C Hawkesworth and C Wilson: Cambridge University Press, 542p.

Tollo, RP, Aleinikoff, JN, Bartholomew, MJ and Rankin, DW 2004, Neoproterozoic A-type granitoids of the central and southern Appalachians: intraplate magmatism associated with episodic rifting of the Rodinian supercontinent: Precambrian Research, v. 128, p. 3–38.

Turner, SP, Foden, JD and Morrison, RS 1992, Derivation of some A-type magmas by fractionation of basaltic magma: an example from the Padthaway Ridge, South Australia: Lithos, v. 28, p. 151–179.

Vander Auwera, J, Bogaerts, M, Bolle, O and Longhi, J 2008, Genesis of intermediate igneous rocks at the end of the Sveconorwegian (Grenvillian) orogeny (S Norway) and their contribution to intracrustal differentiation: Contribution to Mineralogy and Petrology, v. 156, p. 721–743.

Vavra, G, Schmid, R and Gebauer, D 1999, Internal morphology, habit, and U–Th–Pb microanalysis of amphibolite-to-granulite facies zircons: Geochronology of the Ivrea zone (Southern Alps): Contributions to Mineralogy and Petrology, v. 134, p. 380– 404.

Wade, BP, Barovich, K, Hand, M, Scrimgeour, IR and Close, DF 2006, Evidence for early Mesoproterozoic arc magmatism in the Musgrave Block, central Australia: implications for Proterozoic crustal growth and tectonic reconstructions of Australia: Journal of Geology, v. 114(1), p. 43–63.

Wade, BP, Kelsey, DE, Hand, M and Barovich, KM 2008, The Musgrave Province: Stitching north, west and south Australia: Precambrian Research, v. 166, p. 370–386.

Watson, EB and Harrison, MT 1983, Zircon saturation revisited: temperature and composition effects in a variety of crustal magma types: Earth and Planetary Science Letters, v. 64, p. 295–304.

Whalen, JB, Currie, KL and Chappell, BW 1987, A-type granites: geochemical characteristics, discrimination and petrogenesis: Contributions to Mineralogy and Petrology. v. 95, p. 407–418.

White, RW 1997, The pressure–temperature evolution of a granulite facies terrain, western Musgrave Block, central Australia: School of Earth Sciences, Macquarie University, PhD thesis (unpublished).

White, RW, Clarke, GL and Nelson, DR 1999, SHRIMP U–Pb zircon dating of Grenville-age events in the western part of the Musgrave Block, central Australia: Journal of Metamorphic Geology, v. 17, p. 465–481.

Williams, IS 1992, Some observations on the use of zircon U–Pb geochronology on the study of granitic rocks: Transactions Royal Society of Edinburgh: Earth Science, v. 83, p. 447–458.

Windley, BF 1977, The Evolving Continents (2nd edition): John Wiley and Sons Ltd, 399p.

Wingate, MTD, Campbell, IH and Harris, LB 2000, SHRIMP baddeleyite age for the Fraser Dyke Swarm, southeast Yilgarn Craton Western Australia: Australian Journal of Earth Science, v. 47, p. 309–313.

Wingate, MTD, Pirajno, F and Morris, PA 2004, Warakurna large igneous province: a new Mesoproterozoic large igneous province in west-central Australia: Geology, v. 32, p. 105–108.

Wingate, MTD, Morris, PA, Pirajno, F and Pidgeon, RT 2005, Two Large Igneous Provinces in late Mesoproterozoic Australia: Supercontinents and Earth Evolution Symposium, Perth: Geological Society of Australia, Abstracts**,** 81**,** p. 151.

Wolf, MB and Wyllie, PJ 1994, Dehydration-melting of amphibolite at 10 kbar: the effects of temperature and time: Contributions to Mineralogy and Petrology, v. 115, p. 369–383.

Zhao, J-x and McCulloch, MT 1995, Geochemical and Nd isotopic systematics of granites from the Arunta Inlier, central Australia: implications for Proterozoic crustal evolution: Precambrian Research, v. 71, p. 265–299.

Appendix 1

Geochronological results

Sample	Supersuite/unit	Suite	MGA Zone 52 Easting	Northing	Crystallization age (Ma)	Metamorphic age (Ma)	Source
Mamutjarra Zone							
184149	Wirku Metamorphics	–	408773	7081530	–	1184 ± 5	GSWA
189540	Wirku Metamorphics	–	380563	7088966	–	1175 ± 8	GSWA
194422	Wirku Metamorphics	–	361180	7113890	–	1119 ± 7	GSWA
194433	Wirku Metamorphics	–	368553	7115610	–	1156 ± 8	GSWA
184150	Wankanki	–	408801	7081555	1317 ± 9	1185 ± 20	GSWA
184158	Wankanki	–	407493	7076919	1321 ± 5	–	GSWA
185581	Wankanki	–	433456	7090442	1314 ± 9	–	GSWA
185606	Wankanki	–	412136	7088141	1326 ± 10	1171 ± 8	GSWA
194379	Wankanki	–	364597	7115730	1306 ± 11	1127 ± 9	GSWA
194381	Wankanki	–	365166	7116451	1316 ± 38	–	GSWA
189522	Pitjantjatjara	Waratjarra	378194	7117326	1148 ± 6	–	GSWA
189523	Pitjantjatjara	Waratjarra	378038	7117710	1157 ± 9	–	GSWA
184146	Pitjantjatjara	unassigned	408788	7081514	1202 ± 7	–	GSWA
184147	Pitjantjatjara	unassigned	408863	7081534	1189 ± 11	–	GSWA
185610	Pitjantjatjara	unassigned	405758	7083884	1197 ± 8	–	GSWA
194376	Pitjantjatjara	norite	364775	7115309	1149 ± 10	–	GSWA
183474	Warakurna	–	467560	7071861	1072 ± 8	–	GSWA
183847	Warakurna	–	439840	7079281	1076 ± 6	–	GSWA
185583	Warakurna	–	435796	7100732	1073 ± 6	–	GSWA
187177	Warakurna	–	436662	7116045	1026 ± 26	–	GSWA
1478534	Warakurna	–	477572	7091980	1078 ± 3	–	GA
Tjuni Purlka Tectonic Zone							
183466	Wirku Metamorphics	–	496227	7080263	–	1221 ± 7	GSWA
183466	Wirku Metamorphics	–	496227	7080263	–	1083 ± 64	GSWA
185590	Wirku Metamorphics	–	494528	7081977	–	1198 ± 5	GSWA
185592	Wirku Metamorphics	–	496785	7077622	–	1211 ± 95	GSWA
185593	Wirku Metamorphics	–	497287	7087129	–	1207 ± 5	GSWA
185593	Wirku Metamorphics	–	497287	7087129	–	1180 ± 5	GSWA
187113	Wirku Metamorphics	–	466258	7121620	–	1193 ± 5	GSWA
185508	Wirku Metamorphics	–	471367	7120871	–	1028 ± 23	GSWA
185508	Wirku Metamorphics	–	471367	7120871	–	1038 ± 24	GSWA
185508	Wirku Metamorphics	–	471367	7120871	–	1050 ± 53	GSWA
185508	Wirku Metamorphics	–	471367	7120871	–	1069 ± 29	GSWA
185508	Wirku Metamorphics	–	471367	7120871	–	1071 ± 17	GSWA
185508	Wirku Metamorphics	–	471367	7120871	–	1078 ± 29	GSWA
185508	Wirku Metamorphics	–	471367	7120871	–	1088 ± 23	GSWA
185508	Wirku Metamorphics	–	471367	7120871	–	1143 ± 27	GSWA
185508	Wirku Metamorphics	–	471367	7120871	–	1158 ± 23	GSWA
185508	Wirku Metamorphics	–	471367	7120871	–	1165 ± 23	GSWA
185508	Wirku Metamorphics	–	471367	7120871	–	1185 ± 30	GSWA
185508	Wirku Metamorphics	–	471367	7120871	–	1216 ± 16	GSWA
187105	Wirku Metamorphics	–	458052	7119017	–	1163 ± 40	GSWA
187109	Wirku Metamorphics	–	464816	7122705	–	1182 ± 5	GSWA
187109	Wirku Metamorphics	–	464816	7122705	–	1212 ± 6	GSWA
187115	Wirku Metamorphics	–	466258	7121620	–	1163 ± 40	GSWA
187195	Wirku Metamorphics	–	405582	7140874	–	1179 ± 4	GSWA
187195	Wirku Metamorphics	–	405582	7140874	–	1196 ± 4	GSWA
187195	Wirku Metamorphics	–	405582	7140874	–	1298 ± 26	GSWA
187289	Wirku Metamorphics	–	417531	7160221	–	1185 ± 10	GSWA
155712	Wankanki	–	482229	7108125	1303 ± 54	1198 ± 24	GSWA
155750	Wankanki	–	482077	7108096	1305 ± 11	1191 ± 10	GSWA
180867	Wankanki	–	424133	7146395	1319 ± 7	1180 ± 12	GSWA
183492	Wankanki	–	479065	7108230	1322 ± 7	1189 ± 13	GSWA
183496	Wankanki	–	479680	7106191	1321 ± 7	1178 ± 21	GSWA
183726	Wankanki	–	481944	7106528	1293 ± 9	1223 ± 8	GSWA
187151	Wankanki	–	432774	7126315	1312 ± 15	–	GSWA
194393	Wankanki	–	364754	7171517	1345 ± 7	1196 ± 9	GSWA
m053	Wankanki	–	Mount West		1324 ± 12	1233 ± 21	White et al., 1999
m057	Wankanki	–	Mount West		1309 ± 7	–	White et al., 1999
m096	Wankanki	–	Mount West		1296 ± 8	–	White et al., 1999
m107	Wankanki	–	Mount West		1324 ± 4	1211 ± 5	White et al., 1999
m175	Wankanki	–	Mount West		1312 ± 16	–	White et al., 1999
187103	Pitjantjatjara	Local melt sheet	456819	7121725	1197 ± 5	1165 ± 6	GSWA
187172	Pitjantjatjara	Local melt sheet	418328	7162109	1183 ± 7	–	GSWA
187174	Pitjantjatjara	Local melt sheet	419242	7161799	1201 ± 6	1178 ± 7	GSWA
187179	Pitjantjatjara	Local melt sheet	420644	7161885	1197 ± 10	–	GSWA
187196	Pitjantjatjara	Local melt sheet	419397	7161586	1200 ± 5	–	GSWA
187171	Pitjantjatjara	Ilurpa	418389	7162276	1188 ± 4	–	GSWA

Appendix 1 (continued)

Sample	Supersuite/unit	Suite	MGA Zone 52 Easting	Northing	Crystallization age (Ma)	Metamorphic age (Ma)	Source
187166	Pitjantjatjara	Pirntirri	431128	7157580	1217 ± 12	1175 ± 10	GSWA
187274	Pitjantjatjara	Pirntirri	430194	7166342	1205 ± 6	–	GSWA
183459	Pitjantjatjara	Punuwarra	494495	7080625	1195 ± 4	–	GSWA
155710	Pitjantjatjara	Tjuni Purlka	482201	7108123	1166 ± 13	–	Belperio, 2009/GSWA
183509	Pitjantjatjara	Tjuni Purlka	478093	7108943	1165 ± 10	–	GSWA
185339	Pitjantjatjara	Tjuni Purlka	490651	7107248	1200 ± 5	–	GSWA
185339	Pitjantjatjara	Tjuni Purlka	407398	7146377	1191 ± 14	–	GSWA
180860	Pitjantjatjara	Waratjarra	421079	7132084	1162 ± 16	–	GSWA
1478487	Pitjantjatjara	unassigned	492537	7107502	1188 ± 4	–	GA
1488329	Pitjantjatjara	unassigned	491538	7107723	1176 ± 6	–	GA
m215b	Pitjantjatjara	unassigned	Mount West		1189 ± 18	–	White et al., 1999
174589	Warakurna	–	451114	7133869	1074 ± 3	–	GSWA
174761	Warakurna	–	473626	7116039	1075 ± 7	–	GSWA
185509	Warakurna	–	471391	7120896	1075 ± 3	–	GSWA
187256	Warakurna	–	436323	7160678	1061 ± 9	–	GSWA
194354	Warakurna	Gabbro	354869	7163642	1067 ± 8	–	GSWA
194367	Warakurna	–	369783	7166857	1058 ± 9	–	GSWA
1478434	Warakurna	–	458263	7104889	1078 ± 5	–	GA
1478472	Warakurna	–	473425	7118330	1073 ± 5	–	GA
1478477	Warakurna	–	474029	7116448	1052 ± 11	–	GA
1478481	Warakurna	–	488738	7108828	1068 ± 6	–	GA
1478519	Warakurna	–	490142	7103735	1058 ± 14	–	GA
1478523	–	Mafic dyke	493040	7101854	824 ± 4	–	GA
187175	–	Pegamatite	445835	7137334	622 ± 10	–	GSWA
Walpa Pulka Zone							
187154	Wirku Metamorphics	–	485245	7139388		1199 ± 19	GSWA
174588	Wirku Metamorphics	–	494327	7134425		1193 ± 10	GSWA
174748	Wirku Metamorphics	–	463945	7150771		1170 ± 8	GSWA
174748	Wirku Metamorphics	–	463945	7150771		1214 ± 7	GSWA
174736	Pitjantjatjara	Local melt sheet	460565	7147986	1180 ± 7		GSWA
174797	Pitjantjatjara	Local melt sheet	498605	7137890	1173 ± 8		GSWA
180262	Pitjantjatjara	Kapi-Parra	488835	7141487	1180 ± 4		GSWA
174538	Pitjantjatjara	Mirturtu	479442	7142104	1178 ± 8		GSWA
180256	Pitjantjatjara	Mirturtu	488577	7143422	1176 ± 6		GSWA
180299	Pitjantjatjara	Mirturtu	499043	7138416	1175 ± 15		GSWA
180300	Pitjantjatjara	Mirturtu	499039	7138293	1181 ± 6		GSWA
174558	Pitjantjatjara	Walpa	466891	7148636	1215 ± 13	1174 ± 11	GSWA
174737	Pitjantjatjara	Walpa	460511	7147960	1219 ± 12	1171 ± 12	GSWA
155735	Pitjantjatjara	unassigned	486644	7146037	1121 ± 11	570 ± 25	Walker-Hallam, 2009/GSWA
155737	Pitjantjatjara	unassigned	486710	7146062	1137 ± 13		Walker-Hallam, 2009/GSWA
180270	Pitjantjatjara	unassigned	490721	7138388	1183 ± 9		GSWA
187323	Pitjantjatjara	unassigned	480390	7157417		1170 ± 6	Raimondo, 2009/GSWA
187323	Pitjantjatjara	unassigned	480390	7157417		541 ± 4	Raimondo, 2009/GSWA
187325	Pitjantjatjara	unassigned	480234	7153921		1178 ± 13	Raimondo, 2009/GSWA
193847	Pitjantjatjara	unassigned	484831	7161377	1166 ± 2		GSWA
193850	Pitjantjatjara	unassigned	469806	7150168	1181 ± 9		GSWA
155731	Pitjantjatjara	unassigned	486733	7146105		523 ± 14	Walker-Hallam, 2009/GSWA
155731	Pitjantjatjara	unassigned	486733	7146105		552 ± 12	Walker-Hallam, 2009/GSWA
187323	Pitjantjatjara	unassigned	480390	7157417		572 ± 7	Raimondo, 2009/GSWA
187337	Pitjantjatjara	unassigned	486861	7149675		573 ± 14	Raimondo, 2009/GSWA
174594	Pitjantjatjara	gabbro	490563	7133432	1190 ± 9		GSWA
183597	–	late aplite vien	460482	7147973	1004 ± 8		GSWA

NOTES: Summary U–Pb geochronology table for the west Musgraves. GSWA data is available online as pdfs of the Geochronology Record Series at http://www. dmp.wa.gov.au/geochron. These records document the sample details, citation information, and provide the individual spot level SHRIMP U–Pb data for each sample. Multiple dates given for 195508 reflect the apparent age of individual metamorphic overgrowths and indicate a prolonged event. All other ages are weighted mean dates or concordia ages

Appendix 2

Geochemical and isotopic analytical techniques

Major and trace elements

Major elements were determined by wavelength-dispersive XRF on fused disks using methods similar to those of Norrish and Hutton (1969). Precision is better than ±1% of the reported values. Loss on Ignition (LOI) was determined by gravimetry after combustion at 1100°C. Iron abundances were determined by digestion and electrochemical titration using a modified methodology based on Shapiro and Brannock (1962). The trace elements Ba, Cr, Cu, Ni, Sc, V, Zn, and Zr were determined by wavelength-dispersive XRF on a pressed pellet using methods similar to those of Norrish and Chappell (1977), whereas Cs, Ga, Nb, Pb, Rb, Sr, Ta, Th, U, Y, and the REE were analysed by ICP-MS (Agilent 7500) using methods similar to those of Eggins et al. (1997), but on solutions obtained by dissolution of fused glass disks (Pyke, 2000). Precision for trace elements is better than ±10% of the reported values. Details of standards used for major and trace element analysis are given in Morris and Pirajno (2005).

Whole Rock Nd isotopes

Sm–Nd isotopic analyses were determined by isotope dilution at VIEPS Radiogenic Isotope Laboratory, Department of Earth Sciences, La Trobe University, Victoria. Analytical techniques follow the methodology reported in Waight et al. (2000).

LA-MC-ICP-MS zircon Lu–Hf analyses

Hafnium isotope analyses were conducted in situ using a New Wave/Merchantek LUV213 laser-ablation microprobe, attached to a Nu Plasma multi-collector inductively coupled plasma mass spectrometer (LA-MC-ICPMS). The analyses employed a beam diameter of ~55 µm and a 5 Hz repetition rate. Typical ablation times were 100–120 seconds, resulting in pits 40–60 µm deep. The ablated sample material was transported from the laser-ablation cell, via a mixing chamber, to the ICP-MS torch by a helium carrier gas.

Interference of ^{176}Lu on ^{176}Hf was corrected by measuring the intensity of the interference-free ^{175}Lu isotope, and by using ^{176}Lu/^{175}Lu = 1/40.02669 (DeBievre and Taylor, 1993) to calculate ^{176}Lu/^{177}Hf. Similarly, interference of ^{176}Yb on ^{176}Hf was corrected by measuring the interference-free ^{172}Yb isotope, and using ^{176}Yb/^{172}Yb to calculate ^{176}Yb/^{177}Hf. The appropriate value of ^{176}Yb/^{172}Yb was determined by spiking the JMC475 hafnium standard with ytterbium, and finding the value of ^{176}Yb/^{172}Yb (0.58669) required to yield the value of ^{176}Hf/^{177}Hf obtained on the pure hafnium solution. Analyses of standard zircons (Griffin et al., 2000, 2004) illustrate the precision and accuracy obtainable on the ^{176}Hf/^{177}Hf ratio, despite corrections to ^{176}Hf. The typical 2σ precision of the ^{176}Hf/^{177}Hf ratios is +0.00002, equivalent to +0.7 εHf unit. The accuracy and precision of this method are discussed in more detail by Griffin et al. (2000, 2004), and detailed discussions regarding the overlap corrections for ^{176}Lu and ^{176}Yb are provided by Griffin et al. (2006, 2007).

Zircon grains from the Mud Tank carbonatite locality were analysed, together with the samples, as an independent control on reproducibility and instrument stability (one Mud Tank analysis for every 10 unknown analyses). Most of the data and the mean ^{176}Hf/^{177}Hf value (0.282527 ± 0.000028; n = 10) are within 2 standard deviations of the recommended value (0.282522 ± 0.000042 (2σ); Griffin et al., 2007). A single analysis of the 91500 zircon standard analysed during this study indicated ^{176}Hf/^{177}Hf = 0.282304 ± 0.000042 (2σ), which is well within the range of values reported by Griffin et al. (2006).

Calculation of ε_{Hf} values employed the chondritic values of Scherer et al. (2001). Calculation of model ages (T_{DM}) based on a depleted-mantle source used a model with (^{176}Hf/^{177}Hf)$_i$ = 0.279718 at 4.56 Ga and ^{176}Lu/^{177}Hf = 0.0384; this produces a present-day value of ^{176}Hf/^{177}Hf of 0.28325, similar to that of average mid-ocean ridge basalt (MORB; Griffin et al., 2000, 2004). T_{DM} ages, which are calculated using the measured ^{176}Lu/^{177}Hf of the zircon, can only give a minimum age for the source material of the magma from which the zircon crystallized. Therefore, for each zircon, a 'crustal' model age was calculated, which assumes that its parental magma was produced from a volume of average Precambrian continental crust with a ^{176}Lu/^{177}Hf ratio of 0.015 (Griffin et al., 2002).

SIMS (SHRIMP) zircon U–Pb analyses

Zircon U–Pb analyses were performed using the SHRIMP ion microbrobes at the John de Laeter Centre of Mass Spectrometry, Curtin University. Procedures for zircon separation, mount manufacture, ion-probe setup, and analysis and data reduction follow those detailed in Wingate and Kirkland (2009).

References

DeBievre, P and Taylor, PDP 1993, Table of the isotopic composition of the elements: International Journal of Mass Spectrometry and Ion Processes, v. 123, p. 149.

Eggins, SM, Woodhead, JD, Kinsley, LPJ, Mortimer, GE, Sylvester, P, McCulloch, MT, Hergt, JM and Handler, MR 1997, A simple method for the precise determination of >40 trace elements in geological samples by ICPMS using enriched isotope internal standardisation: Chemical Geology, v. 134, p. 311–326.

Griffin, WL, Pearson, NJ, Belousova, EA, Jackson, SE, O'Reilly, SY, van Achterberg, E and Shee, SR 2000, The Hf isotope composition of cratonic mantle: LAM-MC-ICPMS analysis of zircon megacrysts in kimberlites: Geochimica et Cosmochimica Acta, v. 64, p. 133–147.

Griffin, WL, Wang, X, Jackson, SE, Pearson, NJ, O'Reilly, SY, Xu, X and Zhou, X 2002, Zircon chemistry and magma genesis, SE China: in-situ analysis of Hf isotopes, Pingtan and Tonglu igneous complexes: Lithos, v. 61, p. 237–269.

Griffin, WL, Belousova, EA, Shee, SR, Pearson, NJ and O'Reilly, SY 2004, Archean crustal evolution in the northern Yilgarn Craton: U–Pb and Hf-isotope evidence from detrital zircons: Precambrian Research, v. 127, p. 19–41.

Griffin, WL, Pearson, NJ, Belousova, EA and Saeed, A 2006, Comment: Hf-isotope heterogeneity in standard zircon 91500: Chemical Geology, v. 233, p. 358–363.

Griffin, WL, Pearson, NJ, Belousova, EA and Saeed, A 2007, Reply to 'Comment to short-communication 'Comment: Hf-isotope heterogeneity in zircon 91500' by WL Griffin, NJ Pearson, EA Belousova, A Saeed (Chemical Geology 233 (2006) p. 358–363)' by F Corfu: Chemical Geology, v. 244, p. 354–356.

Jackson, SE, Pearson, NJ, Griffin, WL and Belousova, EA 2004, The application of laser ablation-inductively coupled plasma-mass spectrometry to in-situ U–Pb zircon geochronology: Chemical Geology, v. 211, p. 47–69.

Kirkland, CL, Wingate, MTD and Smithies, RH 2010a, 194422: quartzite, Cohn Hill; Geochronology Record 864: Geological Survey of Western Australia, 5p.

Kirkland, CL, Wingate, MTD and Smithies, RH 2010b, 189540: pelitic gneiss, Mount Blyth; Geochronology Record 865: Geological Survey of Western Australia, 6p.

Norrish, K and Chappell, BW 1977, X-ray fluorescence spectrometry, *in* Physical Methods in Determinative Mineralogy, 2nd Edition *edited by* J Zussman: Academic press, London, p. 201–272.

Norrish, K and Hutton, JT 1969, An accurate X-ray spectrographic method for the analysis of a wide range of geological samples: Geochemica et Cosmochimica Acta, v. 33, p. 431–453.

Pyke, J 2000, Minerals laboratory staff develops new ICP-MS preparation method: Australian Geological Survey Organisation Newsletter v. 33, p. 12–14.

Scherer, E, Münker, C and Mezger, K 2001, Calibration of the lutetium–hafnium clock: Science, v. 293, p. 683–687.

Shapiro, L and Brannock, WW 1962, Rapid analysis of silicate, carbonate and phosphate rocks: United States Geological Survey, Bullitin, v. 1144-A, p. A1–A56.

Waight, TE, Maas, R and Nicholls, IA 2000, Fingerprinting feldspar phenocrysts using crystal isotopic composition stratigraphy: implications for crystal transfer and magma mingling in S-type granites, Contributions to Mineralogy and Petrology, v. 139, p. 227–239.

Wingate, MTD and Kirkland, CL 2009, Introduction to geochronology information released in 2009: Geological Survey of Western Australia, 5p.

Appendix 3

Whole rock geochemical data

Series name	*Warakurna Supersuite*										
Sample no.	*174589*	*174760*	*174761*	*174765*	*174766*	*174769*	*174771*	*183721*	*185509*	*185511*	*189463*
Easting	*451114*	*473626*	*473626*	*474450*	*476272*	*474376*	*473114*	*480005*	*471391*	*471343*	*476032*
Northing	*7133869*	*7116039*	*7116039*	*7116550*	*7115792*	*7119326*	*7119072*	*7111487*	*7120896*	*7119620*	*7134121*
						Weight percent					
SiO_2	74.70	71.20	70.86	75.89	67.96	77.10	70.76	73.28	72.51	70.30	72.65
TiO_2	0.27	0.46	0.52	0.10	0.76	0.12	0.46	0.43	0.81	0.67	0.30
Al_2O_3	12.12	12.61	13.05	11.51	13.54	11.81	13.22	12.70	12.25	12.98	12.85
Fe_2O_3T	2.81	2.91	3.84	1.23	4.78	1.03	4.43	2.50	2.38	3.64	3.40
FeO	0.97	1.41	1.73	0.49	2.47	0.17	1.39	1.10	0.88	2.06	0.23
MnO	0.07	0.05	0.07	0.01	0.07	0.01	0.09	0.04	0.03	0.04	0.04
MgO	0.16	0.34	0.42	0.03	1.21	0.10	0.25	0.37	0.16	0.47	0.05
CaO	0.88	1.14	1.55	0.53	2.43	0.88	1.46	1.09	1.29	1.78	0.86
Na_2O	2.96	2.67	2.64	1.82	2.65	1.48	2.13	2.94	2.07	2.27	3.36
K_2O	5.69	6.13	5.97	6.66	5.57	6.81	6.68	6.01	6.28	6.13	5.55
P_2O_5	0.04	0.08	0.11	0.02	0.13	0.03	0.07	0.07	0.11	0.15	0.02
LOI	-0.02	2.22	0.74	2.11	0.68	0.52	0.16	0.42	1.83	1.23	0.55
Total	**99.68**	**99.80**	**99.75**	**99.91**	**99.77**	**99.87**	**99.70**	**99.85**	**99.72**	**99.67**	**99.63**
						Parts per million					
Cr	11	9	7	11	37	7	10	9	18	28	1
Ni	db	db	3	db	15	3	db	10	8	12	5
V	6	12	13	bd	53	3	6	14	20	60	1
Cu	5	17	20	2	27	bd	12	4	3	5	1
Zn	87	50	71	20	52	7	105	36	37	42	75
F	468	829	721	77	1 092	127	140	1 221	273	235	237
Cs	0.5	0.21	0.27	0.15	0.15	0.14	0.11	0.5	0.19	0.14	0.28
Ba	822	561	865	143	585	387	993	434	1 627	1 794	1 887
Rb	205.4	266.3	219.6	219.2	226.8	224.8	195.4	331.2	182	174.1	184.7
Sr	39.9	46.9	71.8	18.6	91.8	68.1	55.5	48.5	144.3	193.8	83.7
Pb	44	44	45	43	40	41	43	39	38	31	22
Th	32.40	49.00	46.90	16.30	46.60	42.70	44.40	56.80	80.70	3.90	20.15
U	2.07	4.45	1.59	1.06	2.60	1.10	2.02	4.77	2.69	0.33	1.93
Ga	18.9	18.6	21.0	17.8	19.3	14.7	20.8	19.1	12.2	16.3	23.2
Sn	2.0	5.0	4.2	2.1	3.2	1.3	2.0	3.3	0.6	0.7	9.0
Nb	20.3	24.3	22.9	7.0	21.8	0.6	23.0	19.2	27.8	5.5	65.8
Ta	0.7	0.7	bd	bd	bd	bd	bd	1.1	1.3	0.2	4.05
Zr	366	415	457	127	464	140	677	382	518	335	803
Hf	11.60	13.70	16.60	5.80	13.90	5.80	20.30	11.40	15.00	9.70	22.18
Y	93.0	80.0	79.0	37.0	59.0	3.0	74.0	54.0	88.0	17.0	158.7
La	80.31	127.70	88.34	43.46	72.45	37.95	130.80	72.94	448.70	26.04	118.90
Ce	186.50	180.80	237.00	86.70	125.90	62.04	247.90	143.70	747.70	46.70	355.20
Pr	20.03	22.17	21.09	8.80	14.43	6.16	27.90	15.69	83.89	5.00	30.37
Nd	72.65	77.22	80.37	31.71	52.78	20.32	103.50	53.12	265.40	18.22	121.20
Sm	17.17	13.43	15.71	6.37	9.75	2.66	18.91	10.27	38.55	3.83	29.39
Eu	2.397	1.359	2.185	0.595	1.380	1.203	3.001	1.084	3.449	2.848	4.385
Gd	13.82	11.57	14.06	6.21	8.75	1.59	15.66	8.39	24.67	2.99	29.23
Tb	2.45	2.07	2.43	1.13	1.54	0.18	2.53	1.55	3.42	0.47	4.88
Dy	15.28	12.67	13.84	6.93	9.20	0.83	14.05	8.85	16.61	2.82	29.40
Ho	2.97	2.75	2.84	1.45	1.96	0.16	2.83	1.92	3.33	0.60	6.09
Er	9.41	8.32	8.12	4.16	5.91	0.46	7.79	5.69	8.00	1.71	15.36
Yb	8.23	7.02	6.80	3.42	5.27	0.44	6.01	4.89	6.34	1.43	13.15
Lu	1.19	1.07	1.06	0.50	0.80	0.07	1.01	0.75	1.11	0.20	1.81
Rb/Sr	5.15	5.68	3.06	11.78	2.47	3.30	3.52	6.83	1.26	0.90	2.21
K/Rb	230	191	225	252	204	251	284	151	287	292	250
Sr/Ba	0.05	0.08	0.08	0.13	0.16	0.18	0.06	0.11	0.09	0.11	0.04
La/Nb	4.0	5.3	3.9	6.2	3.3	63.3	5.7	3.8	16.1	4.7	1.8
La/Yb	9.76	18.19	12.99	12.71	13.75	86.25	21.76	14.92	70.77	18.21	9.04
La/Gd	5.81	11.04	6.28	7.00	8.28	23.87	8.35	8.69	18.19	8.71	4.07
La/Sm	4.68	9.51	5.62	6.82	7.43	14.27	6.92	7.10	11.64	6.80	4.05
Th/U	15.65	11.01	29.50	15.38	17.92	38.82	21.98	11.91	30.00	11.82	10.44
Eu/Eu*	0.46	0.33	0.44	0.29	0.45	1.65	0.52	0.35	0.32	2.48	0.45
Mg#	10	19	18	5	33	16	10	23	11	20	3
MALI	7.77	7.66	7.06	7.94	5.79	7.41	7.35	7.86	7.06	6.62	8.06
ASI	0.96	0.96	0.96	1.03	0.91	1.04	0.99	0.95	0.98	0.95	0.98

Appendix 3 (continued)

Series name	*Warakurna Supersuite*										
Sample no.	*194342*	*194346*	*183473*	*183474*	*180853*	*185557*	*185558*	*185583*	*185585*	*185586*	*187191*
Easting	*369670*	*362920*	*467466*	*467560*	*436912*	*425811*	*426584*	*435796*	*430940*	*434339*	*404197*
Northing	*7165032*	*7168609*	*7173271*	*7171861*	*7160794*	*7113830*	*7114360*	*7100732*	*7102442*	*7102115*	*7141054*
						Weight percent					
SiO_2	64.77	68.91	70.79	72.09	73.03	73.22	72.97	73.34	75.01	73.42	73.30
TiO_2	1.00	0.77	0.40	0.42	0.47	0.31	0.29	0.25	0.14	0.23	0.44
Al_2O_3	13.10	12.94	12.08	12.27	12.81	12.94	12.54	12.32	12.40	12.45	12.09
Fe_2O_3T	6.66	4.21	4.71	4.39	3.48	2.71	2.58	2.22	1.68	2.05	2.62
FeO	3.84	2.14	2.46	2.42	1.34	1.17	1.25	0.38	0.58	0.14	0.84
MnO	0.12	0.08	0.11	0.10	0.06	0.06	0.06	0.04	0.04	0.03	0.04
MgO	0.73	0.57	0.22	0.31	0.25	0.24	0.22	0.17	0.08	0.17	0.24
CaO	2.58	1.76	1.38	1.58	1.26	1.09	1.05	1.07	0.83	1.14	0.99
Na_2O	2.33	2.34	3.15	3.13	3.11	3.32	3.21	2.84	3.07	2.98	2.23
K_2O	5.41	6.02	5.29	5.25	5.93	5.54	5.45	5.79	5.58	5.66	6.69
P_2O_5	0.27	0.16	0.06	0.07	0.10	0.04	0.04	0.04	0.02	0.04	0.09
LOI	2.67	1.95	1.46	0.09	-0.74	0.34	1.40	1.78	1.02	1.68	1.07
Total	**99.61**	**99.70**	**99.66**	**99.70**	**99.74**	**99.80**	**99.81**	**99.85**	**99.87**	**99.85**	**99.80**
						Parts per million					
Cr	3	3	7	13	bd	9	17	17	19	9	3
Ni	4	3	8	9	6	9	8	7	7	7	6
V	15	12	9	10	5	8	5	4	1	5	7
Cu	3	7	7	9	8	14	13	2	2	1	1
Zn	161	97	127	119	62	66	62	41	36	30	43
F	849	85	1 750	1 523	bd	2 571	2 562	5 671	6 013	6 088	67
Cs	0.23	0.11	1.56	1.56	0.11	3.66	3.47	2.44	4.08	4.57	0.29
Ba	860	858	1 808	1 620	804	731	704	312	80	352	456
Rb	254	224.4	189.3	173.8	179.6	306.5	308.7	405.6	552.8	425.7	296.5
Sr	85.2	88.4	65.4	73.5	53	57.9	59.7	47.7	20.7	47.4	47.3
Pb	63	46	41	38	43	43	48	66	84	63	51
Th	4.93	0.93	28.00	27.90	41.35	43.83	44.59	110.00	114.40	98.52	58.16
U	0.68	0.28	6.66	3.39	2.18	9.35	8.75	11.06	16.43	9.64	4.90
Ga	21.9	22.2	21.6	21.2	23.8	21.0	19.8	19.6	20.1	19.2	17.3
Sn	3.1	1.2	5.1	4.9	3.4	6.6	7.3	10.0	20.3	9.7	10.5
Nb	34.1	29.9	34.0	29.8	15.7	35.0	34.7	19.5	20.3	19.3	17.5
Ta	1.21	1.14	1.8	1.7	0.7	2.51	2.49	1.73	2.68	2.49	1.49
Zr	1 405	932	711	646	488	408	388	276	198	242	354
Hf	44.52	35.27	19.80	19.00	14.83	10.82	10.34	8.57	7.54	8.09	11.49
Y	110.4	38.3	138.0	92.0	85.8	88.1	88.8	82.5	79.8	83.5	93.8
La	121.00	65.72	109.20	101.30	97.41	83.27	84.68	140.90	115.40	120.50	73.42
Ce	319.40	188.70	231.80	212.30	199.70	164.20	158.80	249.40	196.40	213.00	155.10
Pr	37.45	17.78	27.08	23.70	23.05	18.53	18.22	24.35	17.48	21.03	16.50
Nd	158.20	76.09	104.20	88.44	83.88	67.92	65.93	75.47	51.33	66.45	64.44
Sm	35.22	16.42	22.47	17.34	16.21	13.15	13.37	12.41	8.21	10.94	14.06
Eu	3.970	2.796	3.693	3.324	1.971	1.605	1.500	0.957	0.447	0.937	1.209
Gd	30.95	14.59	20.48	15.34	14.67	13.46	12.73	10.58	7.80	9.89	14.27
Tb	4.61	2.25	3.76	2.73	2.40	2.18	2.01	1.75	1.36	1.65	2.39
Dy	25.91	12.04	22.30	15.61	14.47	12.90	12.31	10.83	9.33	10.18	14.70
Ho	5.09	2.34	4.99	3.40	2.87	2.80	2.66	2.44	2.22	2.28	3.19
Er	12.84	5.76	14.56	9.90	7.96	7.64	7.38	7.09	7.18	7.07	8.89
Yb	10.37	4.73	13.05	9.28	6.86	7.20	7.17	7.71	9.41	8.36	8.16
Lu	1.41	0.69	2.12	1.46	1.07	1.06	1.01	1.20	1.51	1.27	1.21
Rb/Sr	2.98	2.54	2.89	2.36	3.39	5.29	5.17	8.50	26.71	8.98	6.27
K/Rb	177	223	232	251	274	150	147	119	84	110	187
Sr/Ba	0.10	0.10	0.04	0.05	0.07	0.08	0.08	0.15	0.26	0.13	0.10
La/Nb	3.5	2.2	3.2	3.4	6.2	2.4	2.4	7.2	5.7	6.2	4.2
La/Yb	11.67	13.89	8.37	10.92	14.20	11.57	11.81	18.27	12.26	14.41	9.00
La/Gd	3.91	4.50	5.33	6.60	6.64	6.19	6.65	13.32	14.79	12.18	5.15
La/Sm	3.44	4.00	4.86	5.84	6.01	6.33	6.33	11.35	14.06	11.01	5.22
Th/U	7.25	3.32	4.20	8.23	18.97	4.69	5.10	9.95	6.96	10.22	11.87
Eu/Eu*	0.36	0.54	0.52	0.61	0.38	0.37	0.35	0.25	0.17	0.27	0.26
Mg#	18	21	8	12	12	15	15	13	9	14	15
MALI	5.16	6.60	7.06	6.80	7.77	7.77	7.62	7.56	7.82	7.49	7.93
ASI	0.91	0.95	0.90	0.90	0.93	0.96	0.96	0.96	0.98	0.95	0.95

Appendix 3 (continued)

Series name	*Warakurna Supersuite*										
Sample no.	*187198*	*187256*	*187286*	*189404*	*189405*	*189409*	*189491*	*190218*	*185664*	*189419*	*190255*
Easting	*402032*	*436323*	*425922*	*403745*	*414888*	*399841*	*362519*	*440259*	*410655*	*410084*	*400673*
Northing	*7181675*	*7160678*	*7177644*	*7183699*	*7175196*	*7188757*	*7139512*	*7170951*	*7105842*	*7183809*	*7192968*
						Weight percent					
SiO_2	73.55	74.25	70.32	74.07	72.24	73.94	74.30	74.19	71.81	74.00	76.64
TiO_2	0.30	0.33	0.50	0.36	0.37	0.34	0.26	0.19	0.40	0.18	0.04
Al_2O_3	12.05	12.10	12.64	11.97	12.08	12.32	11.82	12.32	13.33	12.00	12.45
Fe_2O_3T	3.01	2.77	4.38	3.20	3.80	3.05	2.73	2.02	3.05	1.94	0.74
FeO	1.88	1.19	2.56	1.01	1.60	1.60	1.00	0.19	1.42	0.92	0.05
MnO	0.06	0.06	0.09	0.06	0.08	0.07	0.06	0.02	0.07	0.05	0.03
MgO	0.05	0.15	0.57	0.07	0.13	0.15	0.12	-0.01	0.49	0.12	-0.01
CaO	0.87	1.01	1.47	0.97	1.11	1.01	0.75	0.18	1.54	0.56	0.63
Na_2O	3.41	3.01	3.03	3.36	3.35	3.35	3.30	3.26	3.26	3.03	3.58
K_2O	5.49	5.68	5.41	5.48	5.36	5.53	5.05	5.27	5.14	5.59	4.60
P_2O_5	0.07	0.08	0.10	0.08	0.08	0.08	0.03	0.03	0.08	0.02	0.02
LOI	0.86	0.34	1.23	0.14	1.09	-0.10	–	2.29	0.63	2.35	1.19
Total	99.72	99.76	99.73	99.74	99.70	99.72	98.42	99.75	99.80	99.84	99.90
						Parts per million					
Cr	1	2	3	2	bd	5	bd	bd	3	1	bd
Ni	5	6	9	5	7	8	4	7	10	3	4
V	bd	4	31	1	2	3	3	3	18	2	3
Cu	11	5	18	9	11	12	2	11	34	7	4
Zn	113	80	110	101	111	110	94	50	56	73	12
F	1 932	63	300	1 292	952	1 360	bd	bd	683	1 771	bd
Cs	1.49	0.32	0.25	0.78	0.77	1.19	0.06	0.13	3.65	1.22	2.48
Ba	930	776	1 142	768	1 085	1 011	1 078	880	594	550	18
Rb	228.7	204.8	170.1	209.4	202.1	222.8	123.4	140.8	346.6	262.9	532
Sr	34.7	42.5	71.8	38.4	59.4	41.6	34.1	55.8	77.3	24.2	6.6
Pb	46	40	40	37	38	43	24	28	45	47	116
Th	35.82	27.85	26.10	33.86	32.94	37.20	20.76	16.83	45.19	44.49	30.60
U	8.99	3.71	2.73	4.78	4.54	4.48	1.51	1.63	13.81	6.04	5.16
Ga	23.6	26.1	18.6	22.8	23.1	22.9	19.5	24.9	25.5	20.6	14.8
Sn	5.5	1.4	1.6	5.7	4.6	4.1	2.6	2.8	7.4	5.0	2.5
Nb	38.3	19.1	20.3	39.2	31.4	34.5	40.8	4.9	34.8	40.2	9.5
Ta	2.37	0.8	0.83	2.41	1.8	2.07	1.28	0.23	2.18	2.43	0.54
Zr	494	344	453	547	604	503	461	275	417	310	69
Hf	14.96	12.30	12.47	16.85	17.88	14.66	18.59	8.59	11.89	9.72	2.88
Y	107.7	81.1	93.8	99.9	100.0	106.9	153.1	82.6	65.3	92.2	16.9
La	101.78	72.02	82.78	139.62	104.28	111.31	191.20	68.12	75.47	107.80	6.29
Ce	213.60	166.80	155.58	310.70	224.30	231.10	286.20	174.41	158.60	201.50	20.91
Pr	22.93	19.69	18.54	30.04	23.55	24.66	58.96	18.53	17.37	22.57	1.49
Nd	90.70	76.59	72.26	115.80	93.94	97.49	240.40	69.80	62.11	79.41	5.36
Sm	18.83	16.12	15.55	21.62	18.96	19.49	48.73	15.07	12.26	15.76	1.08
Eu	2.585	2.474	3.218	2.206	2.916	2.774	5.479	2.473	1.549	1.586	0.146
Gd	18.33	15.05	15.73	19.99	18.59	18.91	41.86	14.95	10.95	14.27	1.42
Tb	2.84	2.56	2.68	3.07	2.87	2.91	6.24	2.67	1.81	2.40	0.31
Dy	17.51	15.20	15.43	18.29	17.13	17.75	35.73	15.46	10.87	14.41	2.08
Ho	3.65	3.10	3.17	3.72	3.56	3.72	6.59	3.16	2.24	3.14	0.52
Er	10.00	8.39	8.68	10.07	9.71	10.15	16.95	8.25	6.28	8.42	1.65
Yb	9.18	7.58	7.68	9.00	8.63	9.02	14.10	6.47	6.00	8.23	2.12
Lu	1.38	1.16	1.24	1.32	1.30	1.37	2.06	0.88	0.90	1.23	0.34
Rb/Sr	6.59	4.82	2.37	5.45	3.40	5.36	3.62	2.52	4.48	10.86	80.61
K/Rb	199	230	264	217	220	206	340	310	123	176	72
Sr/Ba	0.04	0.05	0.06	0.05	0.05	0.04	0.03	0.06	0.13	0.04	0.37
La/Nb	2.7	3.8	4.1	3.6	3.3	3.2	4.7	13.9	2.2	2.7	0.7
La/Yb	11.09	9.50	10.78	15.51	12.08	12.34	13.56	10.53	12.58	13.10	2.97
La/Gd	5.55	4.79	5.26	6.98	5.61	5.89	4.57	4.56	6.89	7.55	4.43
La/Sm	5.41	4.47	5.32	6.46	5.50	5.71	3.92	4.52	6.16	6.84	5.82
Th/U	3.98	7.51	9.56	7.08	7.26	8.30	13.75	10.33	3.27	7.37	5.93
Eu/Eu*	0.42	0.48	0.62	0.32	0.47	0.44	0.36	0.50	0.40	0.32	0.36
Mg#	3	10	21	4	6	9	8	0	24	11	0
MALI	8.03	7.68	6.97	7.87	7.60	7.87	7.61	8.34	6.86	8.06	7.54
ASI	0.92	0.94	0.94	0.91	0.91	0.92	0.96	1.08	0.97	0.99	1.04

Appendix 3 (continued)

Series name	*Tjuni Purlka suite*										
Sample no.	*180805*	*180871*	*183404*	*183407*	*183408*	*183412*	*183414*	*183415*	*183416*	*183464*	*183477*
Easting	*442746*	*424717*	*473783*	*473302*	*473143*	*474765*	*475573*	*475612*	*475576*	*495198*	*458685*
Northing	*7150803*	*7146327*	*7103214*	*7103055*	*7103024*	*7101229*	*7101754*	*7101545*	*7101622*	*7079767*	*7097253*
Weight percent											
SiO_2	74.32	59.26	73.88	72.59	76.83	56.51	68.30	70.16	72.84	69.61	71.89
TiO_2	0.36	1.61	0.22	0.32	0.13	0.22	0.47	0.33	0.28	0.55	0.40
Al_2O_3	12.13	15.05	11.51	12.47	10.74	24.61	13.61	13.30	11.89	13.72	13.00
Fe_2O_3T	2.65	9.57	2.25	3.01	1.21	3.22	4.30	3.10	2.65	3.99	2.61
FeO	0.35	5.74	1.16	1.23	0.56	1.20	2.77	2.03	1.86	2.46	1.30
MnO	0.06	0.15	0.03	0.05	0.01	0.05	0.08	0.06	0.04	0.07	0.04
MgO	0.22	1.65	0.09	0.16	0.06	0.15	0.28	0.16	0.12	0.44	0.28
CaO	0.95	4.20	0.78	1.24	0.64	4.06	1.85	1.35	1.03	1.95	1.58
Na_2O	2.78	2.95	2.58	2.92	2.53	1.73	3.01	2.91	2.50	3.09	2.74
K_2O	5.97	4.20	5.60	5.50	4.84	8.14	5.66	6.05	5.70	5.79	6.08
P_2O_5	0.08	0.73	0.03	0.06	0.02	0.02	0.12	0.07	0.05	0.16	0.07
LOI	0.25	0.12	2.89	1.43	2.89	1.07	2.05	2.27	2.69	0.35	1.13
Total	99.77	99.48	99.85	99.75	99.90	99.77	99.71	99.75	99.79	99.71	99.81
Parts per million											
Cr	2	12	18	16	41	9	16	8	32	24	18
Ni	8	11	db	db	db	db	db	db	db	9	8
V	5	84	bd	bd	bd	bd	4	bd	bd	17	9
Cu	9	15	bd	bd	bd	bd	3	2	2	3	1
Zn	80	200	55	76	25	72	101	68	62	77	48
F	513	3 944	2 878	2 813	162	487	1 247	792	1 474	525	7 233
Cs	0.49	1.42	0.14	0.1	0.03	2.64	0.8	0.82	0.76	0.07	9.39
Ba	585	1 320	123	805	91	135	856	742	480	1028	578
Rb	262.1	224.7	361.5	309.7	206.9	863.4	308.3	316.3	323.1	216	412.1
Sr	36.5	192.8	25.4	77.5	20.7	74.3	93	77.4	56	114.1	98.6
Pb	47	59	64	56	66	130	60	60	59	37	64
Th	51.93	75.48	89.70	21.30	14.40	165.90	53.10	69.80	83.30	6.70	130.20
U	3.93	3.80	13.30	3.16	1.57	18.67	5.92	6.60	11.26	1.13	15.96
Ga	24.1	33.1	20.4	21.4	22.0	44.5	24.1	22.2	20.6	22.5	21.1
Sn	2.8	4.9	1.1	2.3	1.1	25.7	6.4	3.5	3.1	0.7	13.6
Nb	31.2	49.5	21.8	11.6	4.9	73.2	32.9	27.7	22.0	22.8	29.0
Ta	1.32	1.93	0.7	0.7	0.3	5.4	3	2.1	1.5	1	2.8
Zr	492.6	1 742	306.2	388.3	147.4	407.5	569.3	369.3	358.6	572.2	457.5
Hf	12.87	36.88	12.30	13.90	6.30	23.30	17.30	13.50	12.90	15.80	15.10
Y	103.4	210.7	166.0	99.0	35.0	208.0	132.0	104.0	119.0	91.0	108.0
La	98.69	221.34	138.00	88.48	34.97	166.90	117.70	128.90	144.80	89.58	183.00
Ce	215.60	540.90	275.00	190.40	55.65	350.50	243.00	253.60	283.60	191.60	375.50
Pr	24.73	67.62	30.75	22.02	6.25	35.43	27.35	28.20	32.42	23.26	39.17
Nd	89.45	264.50	109.40	84.69	23.56	122.40	103.00	101.40	115.60	92.11	132.30
Sm	17.76	51.18	23.38	17.04	5.38	25.32	21.27	19.55	22.57	20.66	23.65
Eu	1.932	4.248	0.601	2.030	0.593	0.458	2.566	2.168	1.700	3.416	1.946
Gd	16.66	39.26	20.90	14.67	4.69	23.97	18.04	16.06	18.74	18.87	17.34
Tb	2.79	5.82	4.09	2.60	0.87	4.77	3.31	2.86	3.45	3.35	3.18
Dy	17.04	31.64	26.98	15.47	5.60	32.05	21.31	17.61	21.08	17.89	16.96
Ho	3.60	6.14	5.62	3.21	1.14	7.04	4.53	3.62	4.27	3.67	3.72
Er	10.36	16.05	16.84	9.29	3.51	22.00	13.83	10.63	12.36	9.78	11.02
Yb	9.74	13.84	14.40	6.92	2.83	20.28	12.66	9.16	9.78	7.10	10.49
Lu	1.51	2.09	2.11	0.96	0.42	3.06	1.94	1.33	1.35	1.08	1.63
Rb/Sr	7.18	1.17	14.23	4.00	10.00	11.62	3.32	4.09	5.77	1.89	4.18
K/Rb	189	155	129	147	194	78	152	159	146	222	122
Sr/Ba	0.06	0.15	0.21	0.10	0.23	0.55	0.11	0.10	0.12	0.11	0.17
La/Nb	3.2	4.5	6.3	7.6	7.1	2.3	3.6	4.7	6.6	3.9	6.3
La/Yb	10.13	15.99	9.58	12.79	12.36	8.23	9.30	14.07	14.81	12.62	17.45
La/Gd	5.92	5.64	6.60	6.03	7.46	6.96	6.52	8.03	7.73	4.75	10.55
La/Sm	5.56	4.32	5.90	5.19	6.50	6.59	5.53	6.59	6.42	4.34	7.74
Th/U	13.21	19.86	6.74	6.74	9.17	8.89	8.97	10.58	7.40	5.93	8.16
Eu/Eu*	0.34	0.28	0.08	0.38	0.35	0.06	0.39	0.36	0.25	0.52	0.28
Mg#	14	25	8	9	9	8	11	9	8	18	17
MALI	7.80	2.96	7.40	7.18	6.74	5.81	6.82	7.62	7.18	6.93	7.23
ASI	0.95	0.88	0.98	0.96	1.02	1.29	0.94	0.97	0.98	0.92	0.93

Appendix 3 (continued)

Series name	*Tjuni Purlka suite*										
Sample no.	*183509*	*183703*	*183720*	*183872*	*185339*	*187105*	*187140*	*187199*	*187200*	*190216*	*190228*
Easting	*478093*	*477282*	*482835*	*493681*	*490651*	*458052*	*439611*	*402857*	*401868*	*441657*	*407398*
Northing	*7108943*	*7100317*	*7109946*	*7106981*	*7107248*	*7119017*	*7144730*	*7181465*	*7181332*	*7172313*	*7146377*
						Weight percent					
SiO_2	73.06	78.09	73.75	71.87	67.47	65.42	68.38	68.51	69.35	69.63	67.52
TiO_2	0.09	0.18	0.41	0.21	0.68	0.57	0.77	0.67	0.82	0.75	0.84
Al_2O_3	14.23	10.93	12.54	13.49	14.34	14.85	14.57	13.21	12.51	12.56	13.31
Fe_2O_3T	2.09	1.79	2.50	2.24	4.61	5.37	4.90	6.71	5.92	4.96	5.40
FeO	0.56	1.03	0.20	1.04	2.44	4.32	2.74	2.94	3.00	1.65	3.44
MnO	0.03	0.03	0.03	0.04	0.08	0.11	0.06	0.12	0.10	0.07	0.09
MgO	0.10	0.07	0.31	0.33	0.75	0.29	0.78	0.25	0.45	0.56	0.63
CaO	1.52	0.73	1.06	1.32	2.02	2.28	2.08	1.97	2.21	2.95	1.84
Na_2O	2.72	2.41	2.27	3.13	3.24	3.49	3.17	3.90	3.73	1.16	2.66
K_2O	6.25	5.51	6.71	5.16	5.05	6.11	5.48	4.32	3.71	4.07	5.84
P_2O_5	0.03	0.02	0.07	0.07	0.19	0.13	0.25	0.12	0.23	0.24	0.19
LOI	-0.32	0.13	0.20	1.95	1.33	0.97	-0.75	-0.11	0.68	2.81	1.37
Total	**99.81**	**99.87**	**99.83**	**99.81**	**99.74**	**99.59**	**99.69**	**99.68**	**99.69**	**99.76**	**99.67**
						Parts per million					
Cr	3	51	19	32	7	bd	4	bd	bd	3	bd
Ni	9	8	10	8	9	6	7	5	5	10	5
V	4	bd	11	11	27	5	31	11	5	32	19
Cu	bd	4	7	bd	13	5	5	10	23	2	5
Zn	81	55	42	54	109	104	94	84	170	39	123
F	221	2263	369	825	bd	312	bd	622	243	1402	2781
Cs	1.79	0.92	0.19	0.49	0.42	0.11	0.16	1.03	5.18	0.55	0.19
Ba	489	166	688	748	897	1 605	674	1 258	1 156	1 088	976
Rb	556.3	317.6	232.9	269.1	297.3	209	263.3	163.2	131.2	234.4	264.7
Sr	122	25.9	73.7	122.2	140.7	139.3	103.5	141.5	110.1	122.9	101.9
Pb	143	53	41	59	47	42	50	36	30	58	60
Th	44.20	64.60	49.50	111.20	149.20	6.01	107.90	26.02	25.79	215.50	7.33
U	4.60	9.91	1.45	10.28	10.63	0.80	4.98	4.40	4.36	30.31	0.72
Ga	32.1	17.2	17.5	22.4	17.4	30.1	28.2	23.7	20.2	15.3	21.8
Sn	15.3	1.0	1.9	0.7	1.1	0.7	0.3	5.2	2.7	5.4	1.5
Nb	63.7	11.7	18.0	19.7	27.9	37.9	15.9	33.0	27.8	29.1	44.1
Ta	3.9	0.29	0.8	0.5	1.35	1.5	0.428	2.01	1.57	1.63	1.67
Zr	259.4	250.7	355.2	287.2	542.7	1 086	857.1	729.5	517.4	515.8	1104
Hf	10.60	9.18	10.40	9.70	12.66	23.25	20.61	17.56	12.46	13.71	26.85
Y	135.0	85.0	51.0	43.0	352.0	87.6	35.5	96.4	71.6	98.5	138.4
La	155.40	110.50	103.60	132.30	219.60	93.52	222.40	85.69	84.74	148.50	134.90
Ce	268.90	227.00	215.30	215.60	333.10	235.60	433.30	184.90	177.80	247.39	303.97
Pr	34.81	26.07	23.12	26.44	48.96	28.72	44.30	19.83	19.02	30.50	39.88
Nd	128.20	89.99	80.41	83.11	179.60	111.70	148.30	81.50	75.18	107.20	159.40
Sm	28.79	20.05	14.51	13.71	38.79	21.65	21.38	17.17	14.65	19.79	32.86
Eu	1.812	0.879	1.908	1.330	1.984	4.576	1.456	3.266	2.581	2.636	3.509
Gd	23.79	17.15	11.29	9.83	41.93	19.73	13.84	17.34	13.38	17.38	28.26
Tb	3.85	3.16	1.90	1.36	7.34	3.11	1.68	2.71	2.01	2.81	4.58
Dy	20.86	17.19	9.86	7.79	45.63	18.12	7.87	16.49	11.85	15.02	24.16
Ho	4.24	3.53	2.02	1.55	9.32	3.60	1.38	3.40	2.45	3.03	4.63
Er	12.05	8.93	5.18	4.27	23.90	9.82	3.33	9.38	6.67	8.27	11.95
Yb	10.24	6.00	3.86	3.46	16.18	9.10	2.68	8.12	6.07	7.02	9.63
Lu	1.45	0.86	0.58	0.54	1.88	1.39	0.42	1.24	0.91	1.11	1.48
Rb/Sr	4.56	12.26	3.16	2.20	2.11	1.50	2.54	1.15	1.19	1.91	2.60
K/Rb	93	144	239	159	141	243	173	220	235	144	183
Sr/Ba	0.25	0.16	0.11	0.16	0.16	0.09	0.15	0.11	0.10	0.11	0.10
La/Nb	2.4	9.4	5.8	6.7	7.9	2.5	14.0	2.6	3.0	5.1	3.1
La/Yb	15.18	18.42	26.84	38.24	13.57	10.28	83.05	10.55	13.96	21.15	14.01
La/Gd	6.53	6.44	9.18	13.46	5.24	4.74	16.08	4.94	6.33	8.54	4.77
La/Sm	5.40	5.51	7.14	9.65	5.66	4.32	10.40	4.99	5.78	7.50	4.11
Th/U	9.61	6.52	34.14	10.82	14.04	7.51	21.65	5.91	5.92	7.11	10.18
Eu/Eu*	0.21	0.14	0.44	0.33	0.15	0.66	0.24	0.57	0.55	0.42	0.34
Mg#	8	7	19	23	24	10	24	7	13	18	19
MALI	7.45	7.20	7.91	6.96	6.27	7.32	6.58	6.25	5.23	2.28	6.66
ASI	1.02	0.97	0.97	1.03	0.99	0.90	0.98	0.90	0.88	1.08	0.95

Appendix 3 (continued)

Series name	*Tjuni Purlka suite*				*Kapi-Parra suite*						*Mirturtu suite*
Sample no.	*190229*	*190231*	*193870*	*194367*	*174704*	*174706*	*174710*	*180262*	*180263*	*180294*	*174538*
Easting	*407031*	*402399*	*488387*	*369783*	*483093*	*486074*	*485600*	*488835*	*488812*	*486458*	*479442*
Northing	*7146402*	*7155044*	*7108316*	*7166857*	*7151840*	*7150389*	*7148732*	*7141487*	*7141428*	*7136884*	*7142104*
						Weight percent					
SiO_2	67.21	67.96	76.38	67.87	64.14	65.72	69.54	72.87	71.70	66.68	62.38
TiO_2	0.73	0.54	0.27	0.70	1.26	1.14	0.65	0.44	0.41	0.92	1.41
Al_2O_3	13.14	13.63	13.51	13.12	13.21	13.21	12.95	12.93	12.31	13.24	13.26
Fe_2O_3T	5.26	4.26	2.37	4.32	7.09	6.16	3.92	2.87	2.67	5.64	8.60
FeO	3.44	2.60	0.90	2.48	3.91	3.36	2.20	1.60	1.52	3.26	5.41
MnO	0.10	0.09	0.04	0.09	0.13	0.12	0.08	0.05	0.05	0.11	0.17
MgO	0.54	0.33	0.30	0.61	1.34	1.14	0.65	0.44	0.36	0.85	1.19
CaO	1.72	1.56	1.01	1.84	3.25	2.87	1.89	1.46	1.29	2.64	4.18
Na_2O	2.58	2.51	2.37	2.44	2.69	2.70	2.31	2.55	2.31	2.83	2.85
K_2O	5.88	6.22	6.76	6.05	4.50	4.74	5.55	5.98	5.89	4.82	3.84
P_2O_5	0.14	0.13	0.05	0.14	0.36	0.32	0.19	0.11	0.10	0.41	0.64
LOI	2.38	2.50	-3.31	2.55	1.76	1.64	2.06	-0.06	2.60	1.38	1.00
Total	99.68	99.73	99.76	99.73	99.73	99.75	99.78	99.63	99.69	99.51	99.50
						Parts per million					
Cr	bd	2	9	bd	11	8	5	8	18	14	4
Ni	6	5	8	4	5	5	bd	4	4	4	bd
V	10	9	22	10	79	66	31	19	16	35	54
Cu	4	4	2	2	11	9	3	2	2	3	6
Zn	137	115	48	122	95	78	56	43	42	105	143
F	2 810	5 670	486	1 971	2 382	2 147	1 686	867	821	1 354	737
Cs	0.12	1.55	0.15	0.26	0.48	0.43	2.29	0.59	0.46	0.22	0.52
Ba	861	832	1059	590	869	852	741	544	519	1238	1321
Rb	282	401.9	240.6	305.4	216	224.1	352.6	326.4	342.3	213.3	133.9
Sr	88.2	100.6	165.5	71.7	193.3	186.2	130.7	108.8	103.4	205.6	304.9
Pb	66	99	58	74	41	42	54	47	47	44	36
Th	21.64	103.40	216.90	24.96	31.50	33.80	61.80	86.50	91.40	15.90	4.30
U	1.15	4.94	23.41	1.38	1.70	1.16	5.78	6.10	4.86	1.08	0.83
Ga	16.7	18.2	18.7	16.7	20.1	19.1	18.1	16.2	15.4	21.1	23.1
Sn	2.1	10.0	0.8	3.1	4.0	3.3	2.7	1.2	1.4	2.5	2.5
Nb	63.4	61.5	13.1	68.9	29.0	27.1	20.0	11.9	10.9	21.0	24.5
Ta	2.15	3.11	0.4	2.58	1.9	2	1.3	1	0.9	1.3	1.4
Zr	1 197	875.9	382.1	1 331	363.9	369.3	305.8	277.4	266.9	428.8	441
Hf	30.46	24.91	9.10	36.97	13.20	12.40	9.60	8.50	8.10	12.00	15.10
Y	160.4	180.7	43.0	131.5	78.0	68.0	74.0	42.0	42.0	71.0	75.0
La	264.60	402.30	240.20	218.80	89.59	76.03	99.14	121.90	137.50	100.60	73.42
Ce	589.65	1006.79	435.20	633.00	184.30	157.10	176.70	225.60	244.70	202.00	155.40
Pr	65.71	90.37	46.94	65.73	21.80	18.76	21.82	23.83	26.02	25.66	18.92
Nd	243.70	311.30	147.20	262.90	84.56	72.27	80.71	72.36	79.08	94.16	80.78
Sm	46.17	52.28	20.45	52.45	15.55	13.50	14.42	11.94	12.15	16.54	15.74
Eu	3.682	3.967	1.494	3.195	2.488	2.339	1.845	1.441	1.459	3.157	3.763
Gd	37.56	40.30	11.08	43.11	13.25	11.19	11.76	8.31	8.41	14.00	13.86
Tb	6.06	6.55	1.57	6.61	2.20	1.87	2.00	1.30	1.29	2.08	2.21
Dy	31.78	35.54	7.88	36.38	12.84	10.98	11.80	7.75	7.45	12.53	12.87
Ho	6.19	7.11	1.48	7.06	2.61	2.20	2.41	1.55	1.43	2.42	2.56
Er	15.52	19.10	4.06	17.93	7.89	6.66	7.28	4.41	4.16	7.03	7.23
Yb	12.34	17.09	3.40	14.23	6.64	5.92	6.05	3.46	3.38	5.94	6.20
Lu	1.87	2.67	0.47	1.96	1.02	0.96	0.93	0.47	0.46	0.84	0.93
Rb/Sr	3.20	4.00	1.45	4.26	1.12	1.20	2.70	3.00	3.31	1.04	0.44
K/Rb	173	129	233	165	173	176	131	152	143	188	238
Sr/Ba	0.10	0.12	0.16	0.12	0.22	0.22	0.18	0.20	0.20	0.17	0.23
La/Nb	4.2	6.5	18.3	3.2	3.1	2.8	5.0	10.2	12.6	4.8	3.0
La/Yb	21.44	23.54	70.65	15.38	13.49	12.84	16.39	35.23	40.68	16.94	11.84
La/Gd	7.04	9.98	21.68	5.08	6.76	6.79	8.43	14.67	16.35	7.19	5.30
La/Sm	5.73	7.70	11.75	4.17	5.76	5.63	6.88	10.21	11.32	6.08	4.66
Th/U	18.82	20.93	9.27	18.09	18.53	29.14	10.69	14.18	18.81	14.72	5.18
Eu/Eu*	0.26	0.25	0.27	0.20	0.52	0.57	0.42	0.42	0.42	0.62	0.76
Mg#	17	13	20	22	27	27	25	23	21	23	22
MALI	6.74	7.18	8.12	6.65	3.93	4.58	5.97	7.07	6.91	5.02	2.51
ASI	0.96	1.00	1.04	0.94	0.87	0.89	0.98	0.97	0.98	0.90	0.81

Appendix 3 (continued)

Series name	*Mirturtu suite*										
Sample no.	*174701*	*174722*	*174723*	*174795*	*174800*	*180248*	*180254*	*180256*	*180295*	*180298*	*180299*
Easting	*499270*	*486804*	*487410*	*498843*	*482158*	*490914*	*491184*	*488577*	*486459*	*499022*	*499043*
Northing	*7137883*	*7145930*	*7145923*	*7138019*	*7162624*	*7142134*	*7143126*	*7143422*	*7139741*	*7138427*	*7138416*
						Weight percent					
SiO_2	63.34	63.11	63.17	68.90	71.81	78.02	61.59	61.74	61.94	63.23	67.87
TiO_2	1.42	1.23	1.19	0.62	0.41	0.09	1.21	1.35	0.75	1.42	0.93
Al_2O_3	13.95	14.02	14.02	13.42	12.95	11.74	15.32	13.96	17.25	13.87	13.74
Fe_2O_3T	8.04	7.17	6.75	3.90	2.72	0.98	7.18	7.94	4.89	7.65	4.97
FeO	4.45	4.48	3.94	2.31	1.46	0.78	4.37	4.84	2.52	4.17	2.49
MnO	0.16	0.12	0.14	0.08	0.07	0.04	0.13	0.15	0.12	0.15	0.08
MgO	1.54	1.26	1.19	0.64	0.52	0.07	1.22	1.51	0.88	1.54	0.76
CaO	3.94	3.66	3.42	2.09	1.58	0.62	4.50	4.21	3.04	3.85	2.20
Na_2O	2.88	2.89	2.84	2.82	2.65	2.97	3.10	2.86	4.42	2.82	2.55
K_2O	4.28	4.31	4.59	5.23	5.35	5.01	4.21	4.04	5.97	4.59	6.02
P_2O_5	0.46	0.54	0.48	0.19	0.09	0.01	0.54	0.55	0.27	0.43	0.21
LOI	-0.50	1.43	1.91	1.89	1.66	0.20	0.37	1.07	0.02	-0.04	0.19
Total	**99.50**	**99.74**	**99.70**	**99.77**	**99.79**	**99.75**	**99.36**	**99.39**	**99.54**	**99.50**	**99.51**
						Parts per million					
Cr	14	5	5	13	22	18	23	15	14	21	27
Ni	9	3	bd	bd	bd	5	5	7	6	13	5
V	90	58	57	33	30	bd	56	79	27	90	36
Cu	12	4	bd	5	4	bd	6	11	bd	11	2
Zn	111	110	103	58	35	19	120	118	77	102	79
F	1 165	1 339	1 591	1 857	328	886	643	560	1 042	2 046	1 088
Cs	0.44	0.76	0.67	0.51	0.65	1.41	1.2	0.79	0.28	0.28	0.5
Ba	1 178	842	1 147	735	752	33	1 133	1 367	1 011	1 171	1 009
Rb	162.2	177.9	175.5	332.6	204.5	639.3	169.1	141	247.8	175.2	247.9
Sr	245.1	194.1	225.2	149.6	78.4	15	269.5	279.5	209.9	246.9	160.7
Pb	36	40	39	44	32	67	39	36	52	40	44
Th	3.60	6.10	5.20	9.60	2.90	3.40	4.20	3.60	64.80	3.20	2.10
U	0.47	1.04	0.85	1.03	0.61	1.74	0.72	0.66	3.76	0.44	1.37
Ga	20.4	22.4	21.8	19.4	15.3	16.6	22.6	20.2	21.7	19.8	19.1
Sn	3.0	3.6	2.8	2.6	1.0	1.4	2.5	2.9	5.1	3.0	2.5
Nb	25.7	25.8	30.3	16.0	7.7	2.3	25.5	23.1	24.9	28.8	16.0
Ta	1.6	1.6	1.7	1.4	0.5	0.2	1.5	1.4	2.2	1.7	0.9
Zr	425	462	441	290	181.9	88.7	568.4	459.1	354	448	885.4
Hf	11.00	13.80	14.40	9.80	5.70	4.50	14.70	11.90	10.30	11.80	23.40
Y	64.0	83.0	73.0	54.0	26.0	81.0	75.0	65.0	72.0	72.0	62.0
La	78.62	73.64	77.33	79.78	33.93	37.79	78.75	73.91	111.30	77.81	56.53
Ce	164.40	169.10	171.00	151.90	51.20	49.53	172.30	155.90	223.20	168.10	116.50
Pr	20.11	20.34	20.05	16.99	6.33	6.07	21.94	19.62	25.99	22.14	16.77
Nd	72.83	85.23	81.18	63.06	24.68	21.29	83.23	73.28	86.97	81.01	65.43
Sm	13.50	17.06	15.35	11.60	4.87	4.96	16.36	14.11	15.38	14.59	12.86
Eu	3.141	3.392	3.773	1.944	1.270	0.305	4.122	3.489	2.563	2.868	3.344
Gd	11.61	14.37	13.20	9.11	4.30	6.28	14.62	12.11	12.26	12.41	11.24
Tb	1.70	2.39	2.13	1.52	0.70	1.00	2.22	1.83	1.97	2.07	1.86
Dy	10.57	13.96	12.14	9.39	4.18	5.92	12.74	10.62	11.54	11.23	9.83
Ho	2.15	2.79	2.46	1.90	0.86	1.26	2.51	2.07	2.36	2.28	2.06
Er	6.22	8.11	7.25	5.59	2.53	3.86	7.09	6.04	7.28	6.76	5.83
Yb	5.66	6.88	6.28	4.74	2.12	2.84	6.26	5.41	7.04	6.20	5.24
Lu	0.83	1.02	0.95	0.74	0.34	0.42	0.96	0.76	1.06	0.90	0.79
Rb/Sr	0.66	0.92	0.78	2.22	2.61	42.62	0.63	0.50	1.18	0.71	1.54
K/Rb	219	201	217	130	217	65	207	238	200	218	202
Sr/Ba	0.21	0.23	0.20	0.20	0.10	0.45	0.24	0.20	0.21	0.21	0.16
La/Nb	3.1	2.9	2.6	5.0	4.4	16.4	3.1	3.2	4.5	2.7	3.5
La/Yb	13.89	10.70	12.31	16.83	16.00	13.31	12.58	13.66	15.81	12.55	10.79
La/Gd	6.77	5.12	5.86	8.76	7.89	6.02	5.39	6.10	9.08	6.27	5.03
La/Sm	5.82	4.32	5.04	6.88	6.97	7.62	4.81	5.24	7.24	5.33	4.40
Th/U	7.66	5.87	6.12	9.32	4.75	1.95	5.83	5.45	17.23	7.27	1.53
Eu/Eu*	0.75	0.64	0.79	0.56	0.83	0.17	0.80	0.80	0.55	0.63	0.83
Mg#	27	26	26	24	27	12	25	27	26	29	23
MALI	3.22	3.53	4.01	5.95	6.41	7.35	2.81	2.68	7.34	3.56	6.37
ASI	0.84	0.87	0.88	0.95	0.99	1.03	0.86	0.83	0.90	0.84	0.93

Appendix 3 (continued)

Series name	*Mirturtu suite*		*Waratjarra suite*								
Sample no.	*180300*	*193874*	*180860*	*187145*	*187190*	*189451*	*189452*	*189496*	*189501*	*189502*	*189515*
Easting	*499039*	*474215*	*421079*	*436867*	*404593*	*378478*	*377895*	*366521*	*374371*	*374842*	*383101*
Northing	*7138293*	*7159728*	*7132084*	*7128140*	*7132533*	*7127566*	*7126144*	*7129056*	*7121185*	*7119338*	*7117803*
Weight percent											
SiO_2	62.35	73.35	63.26	63.60	61.18	73.41	64.11	63.28	59.04	62.96	63.63
TiO_2	1.52	0.56	1.47	1.60	1.75	0.21	1.15	1.12	1.19	0.82	0.89
Al_2O_3	13.90	13.43	12.79	12.78	13.57	13.79	13.39	14.43	15.66	16.03	15.47
Fe_2O_3T	8.41	3.78	9.40	9.63	8.64	1.97	6.99	6.72	6.15	5.48	4.41
FeO	4.69	2.09	6.43	6.70	5.28	1.03	4.34	6.57	2.94	2.97	0.16
MnO	0.17	0.07	0.20	0.20	0.14	0.03	0.12	0.18	0.11	0.13	0.10
MgO	1.67	0.55	0.97	1.14	1.79	0.37	1.10	0.96	1.55	0.76	0.82
CaO	4.03	1.90	3.79	4.16	4.22	1.80	3.32	4.18	4.00	5.21	3.35
Na_2O	2.80	2.72	2.55	2.64	2.90	3.26	2.70	2.59	3.12	2.90	3.54
K_2O	4.22	5.50	4.58	4.19	3.80	4.34	4.46	4.11	4.90	3.44	4.66
P_2O_5	0.46	0.16	0.67	0.74	0.58	0.06	0.51	0.55	0.41	0.55	0.38
LOI	-0.07	-2.21	-0.25	-1.22	1.09	0.64	1.86	–	–	–	–
Total	**99.46**	**99.80**	**99.43**	**99.45**	**99.66**	**99.87**	**99.70**	**98.13**	**96.13**	**98.27**	**97.24**
Parts per million											
Cr	8	4	2	bd	14	6	3	bd	4	bd	3
Ni	12	10	5	5	12	5	2	3	3	2	16
V	97	28	24	35	111	12	64	34	73	16	45
Cu	12	4	4	5	12	bd	6	4	6	1	85
Zn	123	60	162	154	125	42	121	139	108	124	82
F	1 780	1 505	627	bd	1 686	677	1 318	970	2 601	583	865
Cs	0.31	1.84	0.3	0.25	1.35	2.18	0.25	0.21	0.24	0.24	1.1
Ba	1 050	621	2 185	1 806	1 315	429	1 467	1 808	4 110	1 829	2 370
Rb	175.3	327.9	121.9	113.1	139.4	244.6	152.8	121	129.7	86.7	115.9
Sr	236.4	112.8	264.1	281.7	275.9	134.3	206.6	255.1	600.9	407	367.9
Pb	40	41	30	27	34	48	40	36	45	30	31
Th	10.00	83.40	4.46	3.36	19.54	26.05	14.11	4.01	21.80	3.42	12.06
U	0.55	10.61	0.55	0.44	2.66	4.53	0.66	0.35	0.93	0.45	0.79
Ga	20.4	20.0	28.1	25.3	21.9	22.0	19.8	21.4	19.6	26.3	21.3
Sn	3.8	1.4	2.6	2.4	3.5	1.6	2.7	1.9	3.3	1.2	5.2
Nb	28.4	22.0	23.6	20.9	22.1	7.4	22.5	31.8	19.5	20.5	25.0
Ta	1.9	1.8	1.11	0.894	1.38	0.85	1.13	1.46	1.02	0.94	1.16
Zr	417.3	354	699.5	580.1	556.4	163.1	620.3	759.9	828.4	709.5	621.7
Hf	11.50	12.00	15.89	13.50	12.91	5.20	14.78	18.23	19.07	16.30	14.06
Y	72.0	68.0	114.3	90.9	72.7	14.8	71.1	72.1	56.8	64.9	59.6
La	81.16	103.60	62.76	64.29	85.61	29.71	85.23	88.46	155.00	73.28	107.80
Ce	170.40	213.50	149.60	130.40	175.50	55.20	168.50	209.90	301.40	149.50	203.80
Pr	22.61	24.42	19.14	16.63	20.01	5.80	20.76	23.95	35.15	18.55	23.75
Nd	80.53	79.04	82.42	69.66	82.77	20.74	80.61	96.97	128.30	77.19	89.89
Sm	15.09	14.76	18.56	16.15	16.33	3.56	16.72	19.85	20.28	16.28	16.88
Eu	2.997	1.906	5.053	4.032	3.281	0.879	3.415	4.235	4.267	5.701	4.184
Gd	12.72	12.92	19.19	16.28	14.95	3.21	15.06	18.23	14.70	15.59	14.24
Tb	2.11	2.07	3.23	2.68	2.14	0.46	2.23	2.81	2.03	2.38	2.12
Dy	11.37	12.74	19.06	15.74	12.16	2.83	13.63	16.55	11.50	13.63	12.02
Ho	2.30	2.69	4.02	3.27	2.46	0.62	2.58	3.08	2.13	2.57	2.22
Er	6.79	7.59	11.00	9.18	6.42	1.71	6.94	8.27	5.48	6.80	5.82
Yb	6.46	7.56	10.09	8.26	5.60	1.63	5.89	7.38	4.89	5.92	5.13
Lu	0.92	1.12	1.60	1.34	0.84	0.25	0.90	1.08	0.76	0.88	0.75
Rb/Sr	0.74	2.91	0.46	0.40	0.51	1.82	0.74	0.47	0.22	0.21	0.32
K/Rb	200	139	312	307	226	147	242	282	313	329	334
Sr/Ba	0.23	0.18	0.12	0.16	0.21	0.31	0.14	0.14	0.15	0.22	0.16
La/Nb	2.9	4.7	2.7	3.1	3.9	4.0	3.8	2.8	7.9	3.6	4.3
La/Yb	12.56	13.70	6.22	7.78	15.29	18.23	14.47	11.99	31.70	12.38	21.01
La/Gd	6.38	8.02	3.27	3.95	5.73	9.26	5.66	4.85	10.54	4.70	7.57
La/Sm	5.38	7.02	3.38	3.98	5.24	8.35	5.10	4.46	7.64	4.50	6.39
Th/U	18.18	7.86	8.11	7.71	7.35	5.75	21.38	11.46	23.44	7.60	15.27
Eu/Eu*	0.64	0.41	0.81	0.75	0.63	0.78	0.65	0.67	0.72	1.08	0.80
Mg#	28	22	17	19	29	27	24	22	33	21	27
MALI	2.99	6.32	3.33	2.67	2.48	5.79	3.84	2.52	4.02	1.13	4.84
ASI	0.84	0.97	0.80	0.78	0.82	1.03	0.88	0.89	0.88	0.89	0.91

Appendix 3 (continued)

Series name	*Waratjarra suite*						*Ilurpa suite*				
Sample no.	*189519*	*189523*	*190278*	*190333*	*194394*	*194395*	*155685*	*180872*	*187138*	*187139*	*187155*
Easting	*380541*	*378038*	*396327*	*398697*	*363904*	*361885*	*448682*	*424951*	*447572*	*444841*	*429471*
Northing	*7118961*	*7117710*	*7137608*	*7131159*	*7120133*	*7118091*	*7119736*	*7145016*	*7155390*	*7159394*	*7146136*
						Weight percent					
SiO_2	67.15	65.39	62.15	64.76	69.39	64.17	71.00	67.84	63.92	66.60	65.86
TiO_2	0.67	0.69	1.26	1.21	0.67	1.15	0.33	0.84	1.37	1.05	1.04
Al_2O_3	14.52	14.50	13.15	13.63	13.01	14.23	13.59	14.86	14.11	13.85	14.02
Fe_2O_3T	4.48	4.63	7.69	7.12	3.36	5.98	2.50	3.99	7.15	5.31	6.49
FeO	2.61	2.00	5.13	1.65	1.79	3.48	1.17	0.41	4.78	2.27	4.45
MnO	0.12	0.13	0.13	0.12	0.05	0.09	0.05	0.07	0.11	0.08	0.11
MgO	0.55	0.57	1.19	1.20	0.63	1.34	0.47	0.84	1.20	1.02	0.75
CaO	3.37	3.34	3.67	3.38	1.69	3.17	1.61	2.58	4.10	2.77	3.63
Na_2O	2.54	2.61	2.58	2.68	2.72	2.64	2.84	3.32	3.00	2.73	2.82
K_2O	4.79	4.85	4.38	4.59	5.56	4.01	5.56	5.27	4.41	5.63	4.94
P_2O_5	0.33	0.34	0.57	0.46	0.16	0.44	0.08	0.32	0.58	0.28	0.51
LOI			2.91	0.57	2.54	2.51	1.75	-0.28	-0.42	0.34	-0.57
Total	**98.53**	**97.05**	**99.68**	**99.72**	**99.78**	**99.73**	**99.77**	**99.65**	**99.52**	**99.65**	**99.59**
						Parts per million					
Cr	1	1	bd	8	7	12	5	1	5	10	bd
Ni	3	3	2	6	6	10	6	6	9	14	4
V	10	10	67	68	29	71	17	34	61	52	25
Cu	bd	bd	5	6	8	19	2	3	8	26	4
Zn	121	135	131	113	74	106	44	79	120	82	136
F	914	1 387	1 592	1 609	2 489	2 286	1 222	1 124	bd	bd	bd
Cs	0.76	1.42	0.89	0.81	1.37	3.25	1.81	0.49	0.6	0.35	0.19
Ba	1 917	1 606	1 502	1 317	872	1 085	952	1 605	991	1 280	1 673
Rb	159.8	194.4	155.4	172.5	191.1	201.4	285.9	175.8	195.2	227.5	155.5
Sr	297	279.3	219.1	202	157.6	221	141.1	310.2	240.1	158.2	254.9
Pb	42	51	38	40	34	45	50	41	43	47	45
Th	21.43	30.48	13.16	26.97	16.25	41.55	46.83	23.92	14.84	18.67	6.02
U	1.96	2.82	1.45	1.31	3.43	2.60	4.25	1.16	2.33	1.78	0.63
Ga	20.8	20.9	19.7	17.4	21.5	18.8	23.4	24.0	25.3	23.4	27.6
Sn	2.5	4.0	3.6	2.7	3.7	4.4	5.8	4.4	3.1	3.4	2.6
Nb	24.6	33.9	22.6	22.6	42.9	28.2	23.2	20.8	37.6	35.4	41.6
Ta	1.38	1.89	1.2	1.27	3.13	1.68	1.01	1.32	1.813	1.65	1.807
Zr	666.2	633.6	618.3	528.3	643.6	598.5	394.4	404.1	589.9	734.8	779.4
Hf	16.42	16.05	15.42	13.30	15.67	14.43	10.69	9.30	13.91	16.07	17.89
Y	67.2	92.2	84.6	82.8	34.5	72.2	44.0	59.3	98.2	70.2	96.8
La	87.90	125.20	82.64	82.63	128.70	127.10	109.04	93.16	125.40	99.85	128.90
Ce	165.30	230.30	197.60	182.60	302.20	246.20	280.50	200.80	257.80	189.10	255.30
Pr	20.74	28.65	23.05	21.77	28.41	26.91	26.65	22.42	30.73	22.34	31.40
Nd	82.51	111.40	90.27	84.21	96.70	96.95	85.75	82.57	113.20	81.30	121.10
Sm	17.21	21.93	18.48	17.18	16.63	17.93	13.83	15.94	22.20	15.37	24.38
Eu	4.887	4.722	3.754	3.150	2.530	2.764	1.487	3.140	3.380	2.571	4.718
Gd	16.26	20.05	15.67	14.78	11.88	14.94	10.83	13.23	18.89	13.21	20.49
Tb	2.50	3.02	2.52	2.45	1.77	2.23	1.65	2.08	3.00	2.10	3.18
Dy	14.85	18.40	14.30	13.95	9.46	12.44	9.34	11.66	17.18	11.95	17.63
Ho	2.77	3.43	2.83	2.80	1.83	2.49	1.82	2.25	3.45	2.49	3.45
Er	7.38	9.28	7.59	7.62	4.82	6.52	5.00	6.02	9.62	7.02	9.19
Yb	6.74	8.49	6.48	6.64	4.09	5.32	4.34	5.06	9.02	6.56	8.24
Lu	1.01	1.36	0.96	0.95	0.59	0.76	0.60	0.74	1.29	1.02	1.24
Rb/Sr	0.54	0.70	0.71	0.85	1.21	0.91	2.03	0.57	0.81	1.44	0.61
K/Rb	249	207	234	221	241	165	161	249	187	205	264
Sr/Ba	0.15	0.17	0.15	0.15	0.18	0.20	0.15	0.19	0.24	0.12	0.15
La/Nb	3.6	3.7	3.7	3.7	3.0	4.5	4.7	4.5	3.3	2.8	3.1
La/Yb	13.04	14.75	12.75	12.44	31.47	23.89	25.12	18.41	13.91	15.21	15.65
La/Gd	5.41	6.24	5.27	5.59	10.83	8.51	10.07	7.04	6.64	7.56	6.29
La/Sm	5.11	5.71	4.47	4.81	7.74	7.09	7.88	5.84	5.65	6.50	5.29
Th/U	10.93	10.81	9.08	20.59	4.74	15.98	11.02	20.62	6.37	10.51	9.57
Eu/Eu*	0.88	0.68	0.66	0.59	0.52	0.50	0.36	0.64	0.49	0.54	0.63
Mg#	20	20	23	25	27	31	27	29	25	28	19
MALI	3.95	4.12	3.30	3.89	6.59	3.48	6.79	6.00	3.31	5.58	4.14
ASI	0.94	0.93	0.84	0.88	0.96	0.99	1.00	0.94	0.82	0.89	0.85

Appendix 3 (continued)

Series name	*Ilurpa suite*			*Pirntirri suite*							*Punuwarra suite*
Sample no.	*187158*	*187171*	*190358*	*187165*	*187166*	*187168*	*187181*	*187185*	*187274*	*190244*	*183459*
Easting	*429085*	*418389*	*442533*	*431782*	*431128*	*429251*	*426417*	*427669*	*430194*	*429896*	*494495*
Northing	*7145476*	*7162276*	*7152839*	*7157344*	*7157580*	*7157176*	*7165736*	*7157996*	*7166342*	*7163055*	*7080625*
						Weight percent					
SiO_2	69.28	70.38	67.33	72.82	72.31	72.58	71.17	71.25	73.76	70.55	63.15
TiO_2	0.86	0.70	0.85	0.42	0.41	0.41	0.47	0.44	0.23	0.30	0.86
Al_2O_3	13.14	13.85	13.68	13.43	13.70	14.04	13.84	14.01	13.56	13.82	16.23
Fe_2O_3T	5.22	4.85	4.95	2.75	2.44	2.59	2.76	2.91	1.60	2.96	6.02
FeO	3.38	3.59	2.73	1.37	1.19	1.66	1.43	1.66	0.59	1.33	3.51
MnO	0.09	0.09	0.07	0.04	0.03	0.03	0.04	0.03	0.02	0.05	0.11
MgO	0.53	0.82	0.77	0.38	0.41	0.46	0.46	0.51	0.18	0.30	0.71
CaO	2.18	2.28	2.50	1.45	1.51	1.71	1.57	1.73	0.84	0.99	4.72
Na_2O	2.58	3.24	2.73	3.01	3.02	3.08	2.93	2.95	2.92	2.84	3.41
K_2O	5.97	4.31	5.30	5.46	5.64	5.64	5.73	5.69	5.72	5.79	4.05
P_2O_5	0.27	0.19	0.27	0.12	0.13	0.14	0.15	0.15	0.05	0.11	0.53
LOI	-0.48	-1.03	1.33	-0.08	0.21	-0.88	0.66	0.10	0.99	2.11	-0.22
Total	**99.63**	**99.69**	**99.77**	**99.79**	**99.79**	**99.79**	**99.77**	**99.77**	**99.87**	**99.83**	**99.56**
						Parts per million					
Cr	bd	7	2	3	2	3	4	5	3	3	8
Ni	5	9	5	6	5	7	7	5	5	6	7
V	12	34	36	13	13	16	16	17	7	16	19
Cu	3	11	9	1	2	3	2	4	bd	2	3
Zn	110	68	85	53	47	51	51	53	31	58	125
F	bd	bd	2730	bd	bd	bd	628	bd	bd	127	660
Cs	0.3	0.17	0.38	0.16	0.23	0.05	0.3	0.11	0.38	0.18	0.11
Ba	1 150	672	801	531	598	553	648	623	371	639	1 865
Rb	206.8	238.4	295.9	287.2	300.8	248.6	312.2	250.5	300.3	288.1	96.5
Sr	161.4	86.9	165.1	84.1	92	90.1	101.2	98.6	75.9	100	392.5
Pb	53	51	67	62	62	59	55	60	61	63	28
Th	7.39	24.92	172.25	116.10	105.00	111.90	100.80	107.50	79.99	133.10	2.00
U	0.78	1.60	21.91	6.54	4.36	6.33	6.18	7.18	5.60	7.37	0.34
Ga	25.3	23.5	17.6	22.9	23.4	22.0	20.6	22.2	21.3	20.0	26.7
Sn	2.3	0.7	2.8	0.4	0.5	0.4	3.8	0.5	0.7	0.5	1.1
Nb	35.1	20.1	26.8	9.7	10.0	15.9	10.1	8.6	5.7	8.1	21.6
Ta	1.751	1.374	1.31	0.236	0.28	0.239	0.41	0.15	0.16	0.19	1
Zr	995.9	351.4	522.8	312.4	310.7	284.2	413	360.7	200.1	311.4	614.4
Hf	22.80	9.55	14.30	8.47	8.41	7.59	10.93	9.85	6.07	8.76	16.30
Y	82.3	33.1	93.3	21.9	23.8	27.7	23.0	29.2	15.3	28.9	74.0
La	110.50	71.66	136.10	131.20	129.60	127.40	129.91	131.85	98.47	130.60	74.23
Ce	206.80	134.10	264.70	251.60	252.00	236.60	268.10	279.00	192.50	254.16	164.50
Pr	25.46	14.16	28.02	27.41	26.96	25.88	25.58	27.53	19.80	26.42	19.45
Nd	97.38	50.09	96.64	91.54	91.30	87.31	90.42	99.83	67.17	89.28	78.67
Sm	19.17	9.18	17.72	15.14	15.31	14.87	13.36	17.43	11.54	14.80	16.59
Eu	4.597	1.634	2.709	1.150	1.206	1.262	1.329	1.406	1.103	1.292	5.408
Gd	16.98	8.04	14.16	9.81	10.19	10.24	9.26	12.27	7.41	10.79	14.29
Tb	2.66	1.16	2.37	1.19	1.32	1.36	1.10	1.48	0.89	1.41	2.41
Dy	14.73	6.37	13.84	5.33	5.97	6.21	5.36	6.76	3.74	6.08	13.10
Ho	2.85	1.27	2.77	0.84	0.93	0.99	0.84	1.05	0.55	0.97	2.75
Er	7.65	3.35	7.66	1.84	1.90	2.18	1.90	2.24	1.20	2.14	7.68
Yb	7.00	3.02	7.05	1.30	1.34	1.60	1.35	1.45	0.95	1.54	6.46
Lu	1.06	0.52	1.02	0.22	0.19	0.23	0.22	0.22	0.15	0.26	1.01
Rb/Sr	1.28	2.74	1.79	3.41	3.27	2.76	3.08	2.54	3.96	2.88	0.25
K/Rb	240	150	149	158	156	188	152	189	158	167	349
Sr/Ba	0.14	0.13	0.21	0.16	0.15	0.16	0.16	0.16	0.20	0.16	0.21
La/Nb	3.1	3.6	5.1	13.5	13.0	8.0	12.9	15.3	17.3	16.1	3.4
La/Yb	15.80	23.75	19.30	100.61	96.57	79.58	96.23	90.93	103.65	84.81	11.49
La/Gd	6.51	8.92	9.61	13.37	12.72	12.44	14.03	10.75	13.29	12.10	5.19
La/Sm	5.76	7.81	7.68	8.67	8.47	8.57	9.72	7.56	8.53	8.82	4.47
Th/U	9.51	15.55	7.86	17.76	24.11	17.67	16.31	14.97	14.28	18.06	5.88
Eu/Eu*	0.76	0.57	0.51	0.27	0.28	0.30	0.35	0.28	0.34	0.30	1.05
Mg#	17	25	23	22	25	26	25	26	18	17	19
MALI	6.37	5.27	5.53	7.01	7.15	7.00	7.09	6.92	7.80	7.63	2.75
ASI	0.90	0.98	0.93	0.99	0.99	0.98	1.00	0.99	1.08	1.08	0.87

Appendix 3 (continued)

Series name	*Punuwarra suite*		*Walpa suite*								
Sample no.	*183488*	*183713*	*174554*	*174558*	*174716*	*174717*	*174726*	*174728*	*174737*	*174752*	*174756*
Easting	*495534*	*493689*	*463881*	*466891*	*474185*	*476087*	*472486*	*468649*	*460511*	*466969*	*460121*
Northing	*7082535*	*7085227*	*7153080*	*7148636*	*7147627*	*7147852*	*7153181*	*7152919*	*7147960*	*7150179*	*7163554*
						Weight percent					
SiO_2	62.97	62.86	73.80	60.55	59.41	63.80	58.94	65.64	61.86	69.36	65.92
TiO_2	0.82	1.13	0.54	1.68	1.86	1.18	1.50	0.91	1.24	0.68	0.95
Al_2O_3	16.60	15.09	13.05	14.53	13.12	12.90	13.74	14.15	15.58	13.70	13.58
Fe_2O_3T	5.73	7.17	3.99	10.37	10.48	7.56	9.99	5.70	6.84	4.16	5.98
FeO	3.68	4.69	1.92	5.68	6.47	4.83	6.97	3.89	2.90	2.29	3.36
MnO	0.10	0.13	0.07	0.17	0.19	0.20	0.20	0.14	0.10	0.07	0.15
MgO	0.75	0.92	0.53	1.86	1.76	0.99	1.31	0.74	1.74	0.81	0.79
CaO	4.94	4.51	1.77	5.55	4.33	3.66	4.88	3.66	3.95	2.39	3.15
Na_2O	3.53	3.11	2.51	2.96	2.69	2.52	2.83	3.02	3.31	2.89	2.93
K_2O	3.73	4.01	5.83	3.13	3.77	3.95	3.54	4.06	4.48	4.99	4.19
P_2O_5	0.58	0.65	0.11	0.73	0.65	0.64	0.93	0.44	0.44	0.21	0.42
LOI	-0.17	-0.03	-2.39	-2.22	1.43	2.28	1.60	1.25	-0.09	0.49	1.62
Total	**99.58**	**99.54**	**99.81**	**99.30**	**99.69**	**99.66**	**99.44**	**99.69**	**99.45**	**99.75**	**99.69**
						Parts per million					
Cr	7	12	13	4	11	bd	3	5	5	8	5
Ni	7	8	10	10	3	bd	bd	bd	4	bd	bd
V	23	38	23	117	99	28	44	15	76	46	30
Cu	3	4	2	13	11	5	4	3	14	8	7
Zn	106	139	57	152	154	130	191	114	93	62	124
F	655	927	291	975	772	755	916	488	1987	1206	1135
Cs	0.08	0.25	0.2	0.33	0.58	0.31	0.42	0.21	0.07	0.48	1.68
Ba	1845	1 700	689	1 830	1 101	1 751	1 511	1 457	2 971	925	1 366
Rb	76.2	114.6	228.3	84.9	127.8	104.4	107.8	102.2	109.7	227.4	147.6
Sr	400	344.2	78.6	402	253.6	277.2	365.4	313.1	672.1	176.9	270.6
Pb	22	30	28	25	31	30	36	33	41	45	41
Th	1.80	6.60	13.20	2.60	3.10	0.80	5.40	1.10	3.60	8.70	9.70
U	0.32	0.84	0.63	0.60	0.63	0.11	0.93	0.13	0.42	1.82	1.02
Ga	26.7	25.5	16.4	23.3	21.9	19.8	25.2	21.0	21.2	19.3	20.7
Sn	0.8	1.9	1.8	2.3	2.8	1.6	2.5	1.7	4.2	2.5	2.9
Nb	13.9	30.0	11.0	23.9	31.5	16.3	28.6	16.2	24.1	23.3	24.1
Ta	0.6	1.4	0.4	1	2.2	0.8	1.6	0.9	bd	0.6	0.1
Zr	531	730.5	366.4	590.2	444.7	265.4	509.4	322	618	308.3	358.3
Hf	12.40	17.60	9.30	11.40	13.40	6.80	18.10	10.70	15.60	10.00	10.90
Y	60.0	97.0	49.0	73.0	85.0	64.0	101.0	55.0	71.0	58.0	65.0
La	59.33	92.76	60.16	90.74	72.92	51.95	98.51	58.61	166.90	62.67	81.89
Ce	120.60	193.50	114.80	178.50	165.00	113.40	217.40	120.30	314.50	133.00	159.30
Pr	15.09	24.28	13.03	23.51	20.19	14.30	26.96	14.54	35.31	15.75	19.31
Nd	61.69	98.19	46.94	95.25	85.28	63.02	115.00	61.30	129.90	62.42	76.40
Sm	13.03	20.96	9.27	17.45	16.72	12.87	22.39	11.70	20.08	11.86	14.43
Eu	5.648	5.334	1.344	3.824	3.382	4.084	5.204	3.327	4.002	1.840	3.108
Gd	11.81	18.40	7.60	14.00	15.43	12.49	20.21	10.88	14.46	9.87	12.18
Tb	1.95	3.08	1.21	2.04	2.49	1.96	3.17	1.69	2.24	1.68	1.95
Dy	10.53	16.69	7.72	10.72	14.13	11.26	17.62	9.78	12.36	9.70	10.81
Ho	2.21	3.58	1.61	2.14	2.83	2.32	3.52	1.94	2.39	2.01	2.24
Er	6.11	9.61	4.69	6.00	8.24	6.55	9.81	5.65	6.85	5.74	6.51
Yb	4.84	7.94	4.16	5.68	6.71	5.39	7.59	4.55	5.22	4.79	5.38
Lu	0.79	1.27	0.61	0.84	1.07	0.87	1.18	0.72	0.78	0.72	0.87
Rb/Sr	0.19	0.33	2.90	0.21	0.50	0.38	0.30	0.33	0.16	1.29	0.55
K/Rb	407	290	212	306	245	314	273	330	339	182	236
Sr/Ba	0.22	0.20	0.11	0.22	0.23	0.16	0.24	0.21	0.23	0.19	0.20
La/Nb	4.3	3.1	5.5	3.8	2.3	3.2	3.4	3.6	6.9	2.7	3.4
La/Yb	12.26	11.68	14.46	15.98	10.87	9.64	12.98	12.88	31.97	13.08	15.22
La/Gd	5.02	5.04	7.92	6.48	4.73	4.16	4.87	5.39	11.54	6.35	6.72
La/Sm	4.55	4.43	6.49	5.20	4.36	4.04	4.40	5.01	8.31	5.28	5.67
Th/U	5.63	7.86	20.95	4.33	4.92	7.27	5.81	8.46	8.57	4.78	9.51
Eu/Eu*	1.37	0.81	0.47	0.72	0.63	0.97	0.73	0.89	0.68	0.51	0.70
Mg#	21	20	21	26	25	21	21	20	34	28	21
MALI	2.32	2.61	6.56	0.54	2.13	2.80	1.49	3.42	3.85	5.50	3.97
ASI	0.88	0.86	0.96	0.79	0.80	0.86	0.79	0.88	0.89	0.94	0.90

Appendix 3 (continued)

Series name	*Walpa suite*			*Wankanki Supersuite*							
Sample no.	*174791*	*174794*	*180461*	*183439*	*183440*	*183492*	*183494*	*183496*	*183564*	*183706*	*183716*
Easting	*454949*	*458053*	*477630*	*472530*	*472469*	*479065*	*479616*	*479680*	*487416*	*477351*	*476216*
Northing	*7147686*	*7146949*	*7133554*	*7111334*	*7111282*	*7108230*	*7108345*	*7106191*	*7095596*	*7102952*	*7108773*
Weight percent											
SiO_2	61.06	56.87	59.64	73.27	67.34	69.77	68.22	60.33	71.78	70.20	66.54
TiO_2	1.44	1.82	1.15	0.21	0.57	0.52	0.57	0.79	0.24	0.41	0.57
Al_2O_3	15.63	14.93	17.21	13.31	14.31	14.20	14.62	16.36	13.82	14.63	15.46
Fe_2O_3T	6.86	8.92	7.42	1.41	3.80	3.49	3.90	7.36	1.94	2.64	4.60
FeO	3.03	3.69	2.75	0.57	1.76	1.10	1.70	3.81	0.92	0.93	2.18
MnO	0.07	0.14	0.16	0.02	0.09	0.07	0.08	0.15	0.03	0.05	0.09
MgO	1.47	2.35	1.01	0.35	1.45	1.16	1.43	3.01	0.28	0.91	1.52
CaO	3.48	5.35	6.18	1.54	3.22	2.74	3.19	6.29	1.46	2.78	4.23
Na_2O	3.09	3.04	3.45	3.22	3.15	3.03	3.33	3.51	2.88	3.38	3.42
K_2O	4.82	4.09	2.85	5.23	4.13	4.92	4.43	1.90	5.70	4.45	2.83
P_2O_5	0.47	0.83	0.81	0.06	0.19	0.17	0.19	0.20	0.03	0.09	0.17
LOI	1.10	0.80	-0.30	1.21	1.51	-0.32	-0.19	-0.14	1.56	0.26	0.35
Total	**99.48**	**99.14**	**99.57**	**99.80**	**99.76**	**99.74**	**99.76**	**99.75**	**99.73**	**99.78**	**99.79**
Parts per million											
Cr	14	11	10	10	34	31	33	27	16	17	21
Ni	2	4	bd	bd	7	16	16	13	8	9	8
V	67	110	25	14	54	56	59	150	9	42	77
Cu	10	21	3	2	3	2	3	16	bd	bd	3
Zn	135	128	140	17	47	40	48	79	30	22	49
F	2 984	2 514	991	589	960	1 004	1 754	793	446	952	679
Cs	0.08	0.02	0.26	0.58	0.15	0.11	0.08	0.03	0.51	0.12	0.05
Ba	1 798	1 926	1 406	975	1 108	1 209	1 281	752	1 539	1 232	1 113
Rb	174	119.5	65.6	171.4	123.9	145.4	120.7	45.5	208.5	141.8	76.8
Sr	291.9	611	444.2	237.5	365.9	340.7	384.6	371.2	192.6	243.4	345.2
Pb	36	36	25	38	32	25	25	15	41	21	19
Th	13.90	3.30	3.20	46.50	33.90	23.60	19.20	0.70	27.50	16.70	3.00
U	0.46	0.30	0.61	0.80	0.58	0.62	0.42	bd	1.29	0.58	0.25
Ga	24.8	22.9	25.0	14.6	16.9	16.9	17.6	19.6	15.0	13.4	17.8
Sn	3.0	4.9	1.3	1.0	3.3	2.6	2.5	1.9	1.9	5.6	1.8
Nb	30.7	38.3	23.1	1.2	9.3	8.8	9.3	6.1	5.9	8.3	6.9
Ta	1.4	2.2	1.2	bd	0.7	0.4	0.5	0.1	bd	0.54	0.2
Zr	1 013	684	509.8	115	214	208	228	180	225	194	192
Hf	31.40	20.10	11.30	3.80	6.30	6.20	6.60	4.90	8.90	5.36	5.20
Y	41.0	67.0	82.0	4.0	41.0	38.0	37.0	26.0	9.0	39.0	27.0
La	223.70	164.40	69.42	40.31	49.63	46.86	49.53	21.25	50.34	37.47	30.78
Ce	442.40	336.00	140.60	65.12	102.60	97.64	101.10	45.08	86.52	85.42	59.26
Pr	49.39	38.67	20.09	6.12	11.77	10.70	11.76	5.47	10.32	9.35	6.63
Nd	181.80	143.40	88.66	19.18	44.09	38.48	43.46	21.72	32.87	34.24	25.14
Sm	26.95	22.03	18.89	2.51	8.18	7.35	8.52	4.73	5.11	7.10	5.10
Eu	3.296	4.110	4.724	0.824	1.507	1.393	1.627	1.453	1.167	1.199	1.202
Gd	14.89	14.87	17.14	1.29	6.56	5.80	6.53	4.37	3.16	5.54	4.45
Tb	1.87	2.20	2.42	0.15	1.11	1.03	1.12	0.75	0.38	0.98	0.74
Dy	8.80	11.99	13.80	0.67	6.53	5.91	6.16	4.29	2.04	5.68	4.34
Ho	1.52	2.29	2.68	0.13	1.35	1.27	1.31	0.97	0.36	1.31	0.95
Er	3.54	6.38	7.44	0.34	4.05	3.82	3.76	2.76	1.08	3.94	2.70
Yb	2.30	5.08	6.19	0.33	3.60	3.53	3.31	2.56	1.06	3.67	2.59
Lu	0.31	0.72	0.89	0.05	0.55	0.56	0.50	0.39	0.19	0.59	0.40
Rb/Sr	0.60	0.20	0.15	0.72	0.34	0.43	0.31	0.12	1.08	0.58	0.22
K/Rb	230	284	360	253	277	281	304	346	227	260	306
Sr/Ba	0.16	0.32	0.32	0.24	0.33	0.28	0.30	0.49	0.13	0.20	0.31
La/Nb	7.3	4.3	3.0	33.6	5.3	5.3	5.3	3.5	8.5	4.5	4.5
La/Yb	97.26	32.36	11.21	122.15	13.79	13.27	14.96	8.30	47.49	10.21	11.88
La/Gd	15.02	11.06	4.05	31.25	7.57	8.08	7.58	4.86	15.93	6.76	6.92
La/Sm	8.30	7.46	3.67	16.06	6.07	6.38	5.81	4.49	9.85	5.28	6.04
Th/U	30.22	11.00	5.25	58.13	58.45	38.06	45.71	0.00	21.32	28.79	12.00
Eu/Eu*	0.46	0.66	0.79	1.25	0.61	0.63	0.64	0.96	0.83	0.56	0.75
Mg#	30	34	21	33	43	40	42	45	22	40	40
MALI	4.42	1.78	0.12	6.91	4.06	5.20	4.57	-0.88	7.12	5.04	2.02
ASI	0.94	0.78	0.86	0.97	0.92	0.93	0.91	0.85	1.02	0.95	0.94

Appendix 3 (continued)

Series name	*Wankanki Supersuite*										
Sample no.	*183719*	*183725*	*183727*	*185515*	*155694*	*180867*	*184149*	*184150*	*184156*	*184158*	*185552*
Easting	*480467*	*481963*	*481508*	*471081*	*453313*	*424133*	*408773*	*408801*	*408177*	*407493*	*438850*
Northing	*7108966*	*7106542*	*7108033*	*7115713*	*7123244*	*7146395*	*7081530*	*7081555*	*7077587*	*7076919*	*70889977*
						Weight percent					
SiO_2	60.17	58.96	72.07	65.79	66.67	68.21	55.64	73.12	66.72	68.38	74.49
TiO_2	0.80	0.98	0.38	0.37	0.45	0.64	0.94	0.23	0.58	0.49	0.19
Al_2O_3	17.57	17.78	13.70	16.72	15.99	15.57	17.28	13.48	15.36	14.73	12.81
Fe_2O_3T	6.05	7.65	2.45	3.31	3.81	3.44	10.11	1.72	3.92	3.53	1.24
FeO	2.38	2.81	0.95	0.28	2.14	1.39	6.20	0.50	1.68	1.35	0.30
MnO	0.13	0.15	0.05	0.07	0.06	0.10	0.18	0.04	0.10	0.11	0.04
MgO	2.26	2.84	0.77	0.33	1.15	1.00	3.80	0.30	1.25	0.98	0.24
CaO	5.68	6.49	2.22	2.21	3.24	2.98	7.30	1.21	3.48	2.93	1.06
Na_2O	3.95	3.83	3.00	3.82	3.96	3.72	2.98	2.40	3.56	3.44	3.51
K_2O	2.66	1.76	5.01	6.70	3.14	4.47	0.63	6.63	3.69	3.88	4.72
P_2O_5	0.26	0.29	0.11	0.12	0.16	0.24	0.19	0.03	0.19	0.16	0.05
LOI	0.20	-1.16	0.06	0.24	0.96	-0.66	0.80	0.57	0.91	1.16	1.52
Total	**99.72**	**99.56**	**99.80**	**99.66**	**99.59**	**99.70**	**99.85**	**99.72**	**99.77**	**99.78**	**99.86**
						Parts per million					
Cr	24	23	29	18	9	3	11	1	2	-1	17
Ni	14	13	12	7	11	6	8	5	6	5	7
V	112	143	32	6	52	30	213	7	36	26	10
Cu	17	22	bd	bd	26	2	3	2	2	2	1
Zn	79	91	30	47	68	55	99	36	49	50	29
F	1 474	1 046	654	166	679	609	601	227	635	566	740
Cs	0.11	0.03	0.15	0.08	0.43	0.49	0.43	0.74	0.15	0.36	4.14
Ba	1 118	925	966	2 118	2 044	1 281	635	1 706	1 339	1 263	461
Rb	80.9	44.2	145.8	155.1	107.9	122.7	22.5	229.5	110	133.2	175.1
Sr	518.1	492.2	269.1	171.5	643.9	356.3	390.8	198.7	298	262.9	217.4
Pb	21	16	29	20	23	21	11	53	20	23	46
Th	2.30	5.60	28.40	1.40	24.11	8.45	7.80	26.76	10.12	19.17	27.21
U	0.30	0.13	0.49	0.37	1.24	0.40	0.54	0.77	0.58	1.18	2.04
Ga	20.4	21.6	14.6	25.5	22.1	21.0	23.5	15.8	19.5	19.1	17.8
Sn	3.1	2.8	1.6	bd	2.0	5.3	2.5	1.8	3.0	3.0	2.5
Nb	8.8	10.1	5.7	6.2	9.7	10.0	13.1	4.9	11.8	10.9	8.9
Ta	0.4	0.4	0.23	0.2	0.51	0.62	0.37	bd	0.47	0.5	0.99
Zr	260	275	168	342	212	208	118	179	206	180	136
Hf	7.30	6.80	4.57	9.00	6.08	5.89	3.43	6.81	7.04	6.85	3.90
Y	37.0	37.0	26.0	19.0	23.4	37.0	30.3	12.7	47.6	36.7	14.8
La	33.54	34.74	39.46	23.74	64.28	45.60	27.74	44.55	44.51	43.30	43.08
Ce	74.84	70.73	77.60	45.30	136.70	88.16	62.55	97.63	102.10	97.32	68.07
Pr	8.58	8.51	8.87	5.49	13.97	9.77	7.26	10.36	11.37	10.46	6.12
Nd	34.18	33.64	31.97	20.96	45.79	35.86	28.07	36.57	43.01	38.65	19.03
Sm	7.17	7.26	6.05	4.72	7.36	6.75	6.18	6.46	9.23	7.84	2.75
Eu	1.890	1.892	1.239	5.016	1.487	1.747	1.521	1.626	1.851	1.670	0.410
Gd	5.97	6.30	4.53	3.78	5.38	5.84	6.21	4.46	8.11	6.92	2.08
Tb	1.07	1.05	0.72	0.63	0.79	0.89	0.96	0.55	1.26	1.14	0.32
Dy	5.85	5.98	4.25	3.52	4.32	5.32	5.78	2.53	7.79	6.42	1.81
Ho	1.29	1.24	0.88	0.78	0.83	1.13	1.13	0.44	1.70	1.32	0.43
Er	3.78	3.72	2.62	2.18	2.24	2.98	3.15	1.06	4.88	3.71	1.31
Yb	3.41	3.50	2.22	1.94	2.04	2.77	2.90	0.90	4.82	3.77	1.62
Lu	0.56	0.54	0.25	0.29	0.31	0.42	0.40	0.14	0.71	0.60	0.25
Rb/Sr	0.16	0.09	0.54	0.90	0.17	0.34	0.06	1.16	0.37	0.51	0.81
K/Rb	273	330	285	358	242	302	231	240	278	242	224
Sr/Ba	0.46	0.53	0.28	0.08	0.32	0.28	0.62	0.12	0.22	0.21	0.47
La/Nb	3.8	3.4	6.9	3.8	6.6	4.6	2.1	9.1	3.8	4.0	4.8
La/Yb	9.84	9.93	17.77	12.24	31.51	16.46	9.57	49.50	9.23	11.49	26.59
La/Gd	5.62	5.51	8.71	6.28	11.95	7.81	4.47	9.99	5.49	6.26	20.71
La/Sm	4.68	4.79	6.52	5.03	8.73	6.76	4.49	6.90	4.82	5.52	15.67
Th/U	7.67	43.08	57.96	3.78	19.44	21.13	14.44	34.75	17.45	16.25	13.34
Eu/Eu*	0.86	0.84	0.69	3.51	0.69	0.83	0.74	0.88	0.64	0.68	0.50
Mg#	43	42	38	16	37	36	43	26	39	36	28
MALI	0.92	-0.90	5.79	8.31	3.87	5.20	-3.69	7.82	3.76	4.38	7.17
ASI	0.89	0.89	0.95	0.95	1.01	0.95	0.92	1.01	0.95	0.97	1.00

Appendix 3 (continued)

Series name	*Wankanki Supersuite*											
Sample no.	*185581*	*185582*	*185606*	*185613*	*185614*	*185621*	*185625*	*187120*	*187161*	*187173*	*190328*	*194393*
Easting	*433456*	*434785*	*412136*	*404323*	*403820*	*419574*	*408427*	*441603*	*435289*	*418944*	*391736*	*364754*
Northing	*090442*	*7093910*	*7088141*	*7083605*	*7084120*	*7084917*	*7091264*	*7146641*	*7146269*	*7161733*	*7144893*	*7171517*
						Weight percent						
SiO_2	74.72	75.60	74.50	66.04	67.16	65.78	69.87	51.23	69.70	65.85	69.56	66.10
TiO_2	0.22	0.14	0.10	0.55	0.56	0.59	0.38	1.19	0.54	0.59	0.36	0.73
Al_2O_3	12.86	12.95	13.18	15.32	15.18	16.17	14.67	15.38	14.90	16.38	14.23	14.28
Fe_2O_3T	1.25	1.06	1.00	5.01	4.85	4.28	2.75	11.26	2.68	4.57	2.64	4.65
FeO	0.04	0.09	0.22	2.36	2.38	1.83	1.16	8.51	0.95	3.14	1.05	3.01
MnO	0.06	0.04	0.05	0.10	0.10	0.10	0.08	0.17	0.10	0.12	0.06	0.07
MgO	0.27	0.17	0.15	1.52	1.44	1.23	0.83	7.37	0.73	1.48	0.57	0.81
CaO	1.01	0.92	1.26	4.33	4.09	4.11	2.86	11.25	2.31	3.75	2.21	2.49
Na_2O	3.37	3.35	3.09	3.49	3.49	3.72	3.44	2.50	3.78	3.67	3.51	2.75
K_2O	5.13	5.32	5.41	2.78	2.86	3.18	3.93	0.81	4.71	3.91	4.20	5.34
P_2O_5	0.06	0.03	0.03	0.15	0.14	0.17	0.11	0.17	0.18	0.25	0.11	0.24
LOI	0.94	0.30	1.12	0.50	-0.08	0.43	0.87	-1.86	0.09	-0.88	2.36	2.27
Total	**99.88**	**99.87**	**99.88**	**99.78**	**99.79**	**99.75**	**99.77**	**99.48**	**99.72**	**99.68**	**99.81**	**99.73**
						Parts per million						
Cr	6	11	20	20	12	3	2	300	bd	3	bd	3
Ni	7	7	6	7	7	6	5	118	6	5	4	5
V	9	7	4	63	62	48	27	282	20	49	19	25
Cu	bd	bd	1	4	4	5	3	163	2	5	bd	9
Zn	21	22	20	43	46	59	39	81	39	56	44	60
F	1 043	542	174	461	707	546	259	bd	bd	bd	497	284
Cs	2.08	3.11	0.53	0.13	0.17	0.27	0.29	0.12	0.09	0.06	0.34	0.18
Ba	292	357	382	1 254	1 104	1 419	1 161	271	1 242	1 403	950	1 147
Rb	353	214	220.5	80.4	96.9	93	140.5	23.2	135.4	152	134.1	199.4
Sr	80.5	191.3	90.2	267.4	246.9	364.8	235.6	175.3	311.3	323	212.4	146.8
Pb	51	50	56	14	18	25	25	6	20	35	30	38
Th	46.09	33.29	29.41	2.60	4.22	10.02	18.95	4.55	1.72	1.68	15.36	7.90
U	8.14	3.24	11.94	0.50	0.46	0.56	0.80	0.57	0.25	0.42	0.52	1.35
Ga	17.7	17.5	16.0	18.0	18.9	19.9	17.9	17.4	18.8	17.5	15.6	16.5
Sn	1.2	1.3	0.8	1.5	1.4	2.6	2.5	0.9	7.3	0.8	1.7	1.1
Nb	13.5	7.8	1.9	5.4	6.0	9.9	9.5	5.6	9.9	7.2	5.1	20.4
Ta	0.92	0.58	bd	0.21	0.21	0.42	0.55	0.208	0.675	0.267	0.21	0.97
Zr	131	112	75	159	154	224	137	112	195	159	192	435
Hf	3.79	3.21	2.51	4.00	4.17	6.41	4.73	3.03	5.66	4.28	5.45	13.34
Y	13.0	6.8	13.9	20.8	26.6	50.6	25.9	27.1	26.7	22.2	28.6	55.5
La	54.14	42.93	19.03	20.48	36.01	40.12	36.80	18.81	45.34	31.10	65.47	103.20
Ce	75.87	63.00	32.37	35.11	56.23	80.82	78.27	34.99	74.97	50.37	126.90	207.40
Pr	6.62	5.41	3.46	3.98	6.54	10.06	8.17	4.32	7.88	5.68	12.98	21.70
Nd	19.23	14.79	11.76	15.35	23.55	39.68	27.38	17.38	28.35	20.42	44.18	78.21
Sm	2.94	1.79	2.42	3.19	4.26	8.36	5.08	4.16	5.12	4.30	7.01	14.59
Eu	0.558	0.310	0.504	1.182	1.273	1.934	1.214	1.209	1.456	1.317	1.457	2.362
Gd	2.01	1.24	2.22	3.41	4.16	8.11	4.43	4.65	4.44	3.70	5.58	12.13
Tb	0.31	0.18	0.32	0.53	0.60	1.29	0.67	0.77	0.66	0.57	0.86	1.84
Dy	1.69	0.92	1.91	3.20	3.73	7.42	4.11	4.80	4.41	3.43	4.97	10.48
Ho	0.37	0.20	0.42	0.69	0.80	1.62	0.87	1.03	0.85	0.71	0.97	2.01
Er	1.12	0.68	1.30	1.92	2.16	4.37	2.57	2.85	2.55	2.17	2.66	5.16
Yb	1.43	0.86	1.53	1.85	2.05	4.10	2.75	2.69	2.20	2.29	2.37	4.20
Lu	0.26	0.14	0.26	0.28	0.32	0.64	0.43	0.42	0.35	0.39	0.35	0.61
Rb/Sr	4.39	1.12	2.44	0.30	0.39	0.25	0.60	0.13	0.43	0.47	0.63	1.36
K/Rb	121	206	204	287	245	284	232	290	289	213	260	222
Sr/Ba	0.28	0.54	0.24	0.21	0.22	0.26	0.20	0.65	0.25	0.23	0.22	0.13
La/Nb	4.0	5.5	10.0	3.8	6.0	4.1	3.9	3.4	4.6	4.3	12.8	5.1
La/Yb	37.86	49.92	12.44	11.07	17.57	9.79	13.38	6.98	20.61	13.57	27.62	24.57
La/Gd	26.94	34.62	8.57	6.01	8.66	4.95	8.31	4.04	10.22	8.41	11.73	8.51
La/Sm	18.41	23.98	7.86	6.42	8.45	4.80	7.24	4.52	8.86	7.23	9.34	7.07
Th/U	5.66	10.27	2.46	5.20	9.17	17.89	23.69	7.94	6.83	3.98	29.54	5.85
Eu/Eu*	0.66	0.60	0.65	1.09	0.91	0.71	0.76	0.84	0.91	0.99	0.69	0.53
Mg#	30	24	22	38	37	36	37	56	35	39	30	26
MALI	7.49	7.75	7.24	1.94	2.27	2.79	4.50	-7.93	6.19	3.83	5.50	5.61
ASI	0.99	1.00	1.00	0.92	0.93	0.95	0.97	0.60	0.96	0.96	0.99	0.96

Appendix 4

Whole rock Nd isotopic data

GSWA sample no.	*Supersuite/suite*	*Easting*	*Northing*	*Age (Ma)*	*Method*	*Sm (ppm)*	*Nd (ppm)*	$^{147}Sm/^{144}Nd$	$^{143}Nd/^{144}Nd$	$^{143}Nd/^{144}Nd^{(a)}$	$^{143}Nd/^{144}Nd$ *initial*	T_{CHUR}	ε_{Nd}	T_{DM2}
Warakurna Supersuite														
174589		451114	7133869	1074	SHRIMP	14.980	71.590	0.1265	0.511959	0.511971	0.511079	0.511264	-3.61	1.92
174761		473626	7116039	1075	SHRIMP	16.410	84.790	0.1170	0.511901	0.511913	0.511088	0.511262	-3.42	1.91
174765		474450	7116550	1075	assumed	6.550	33.040	0.1198	0.511902	0.511914	0.511069	0.511262	-3.78	1.94
174766		476272	7115792	1075	assumed	10.500	55.470	0.1145	0.511908	0.511920	0.511112	0.511262	-2.94	1.87
183474		467560	7071861	1073	SHRIMP	16.390	86.840	0.1141	0.511834	0.511846	0.511042	0.511265	-4.35	1.98
185583		435796	7100732	1073	SHRIMP	12.340	74.131	0.1006	0.511835	0.511847	0.511138	0.511265	-2.48	1.84
Pitjantjatjara Supersuite														
183408	Tjuni Purlka suite	473143	7103024	1180	assumed	5.420	24.820	0.1321	0.511992	0.512004	0.510981	0.511126	-2.85	1.95
183509	Tjuni Purlka suite	478093	7108943	1156	SHRIMP	28.250	129.410	0.1320	0.512024	0.512036	0.511034	0.511157	-2.41	1.90
185339	Tjuni Purlka suite	490651	7107248	1200	SHRIMP	41.273	194.438	0.1284	0.511919	0.511931	0.510920	0.511100	-3.52	2.02
180262	Kapi-Parra suite	488835	7141487	1180	SHRIMP	13.160	84.370	0.0943	0.511706	0.511718	0.510987	0.511126	-2.71	1.94
180294	Kapi-Parra suite	486458	7136884	1180	assumed	15.800	86.690	0.1101	0.511845	0.511857	0.511004	0.511126	-2.39	1.92
174800	Mirturtu suite	482158	7162624	1180	assumed	4.580	23.820	0.1162	0.511876	0.511888	0.510988	0.511126	-2.71	1.94
180256	Mirturtu suite	488577	7143422	1176	SHRIMP	16.910	88.590	0.1154	0.511897	0.511909	0.511018	0.511131	-2.22	1.90
180299	Mirturtu suite	499043	7138416	1175	SHRIMP	13.580	66.370	0.1237	0.511948	0.511960	0.511006	0.511133	-2.48	1.92
180300	Mirturtu suite	499039	7138293	1181	SHRIMP	15.400	80.440	0.1138	0.511874	0.511886	0.511004	0.511125	-2.37	1.92
174538	Mirturtu suite	479442	7142104	1178	SHRIMP	16.810	85.410	0.1190	0.511920	0.511932	0.511012	0.511129	-2.29	1.91
183459	Punuwarra suite	494495	7080625	1195	SHRIMP	14.740	71.300	0.1250	0.511931	0.511943	0.510962	0.511107	-2.83	1.96
174737	Walpa suite	460511	7147960	1207	SHRIMP	20.580	128.270	0.0970	0.511679	0.511691	0.510922	0.511091	-3.30	2.01
174558	Walpa suite	466891	7148636	1215	SHRIMP	17.630	93.120	0.1145	0.511799	0.511811	0.510898	0.511081	-3.59	2.04
174726	Walpa suite	472486	7153181	1210	assumed	22.920	116.780	0.1187	0.511914	0.511926	0.510983	0.511087	-2.04	1.92
Wankanki Supersuite														
183440		472469	7111282	1320	assumed	8.440	44.930	0.1136	0.511873	0.511885	0.510900	0.510945	-0.87	1.92
183492		479065	7108230	1322	SHRIMP	7.070	37.690	0.1134	0.511855	0.511867	0.510882	0.510942	-1.17	1.95
183496		479680	7106191	1321	SHRIMP	4.390	20.460	0.1296	0.512027	0.512039	0.510914	0.510943	-0.56	1.90
180867		424133	7146395	1319	SHRIMP	6.156	32.807	0.1135	0.511887	0.511899	0.510916	0.510946	-0.59	1.90
184150		408801	7081555	1317	SHRIMP	5.268	32.487	0.0981	0.511717	0.511729	0.510881	0.510948	-1.33	1.95
184158		407493	7076919	1321	SHRIMP	6.547	34.207	0.1157	0.511841	0.511853	0.510849	0.510943	-1.85	2.00
185581		433456	7090442	1314	SHRIMP	2.839	19.760	0.0869	0.511626	0.511638	0.510889	0.510952	-1.25	1.94
185606		412136	7088141	1326	SHRIMP	2.318	11.422	0.1227	0.511871	0.511883	0.510815	0.510937	-2.39	2.04

NOTES: (a) Normalized against measured value of the La Jolla standard

Appendix 5

Zircon Hf isotopic data

	Analysis no.	Age (Ma)	$^{176}Hf/^{177}Hf$	1 standard error	$^{176}Lu/^{177}Hf$	$^{176}Yb/^{177}Hf$	$^{176}Hf/^{177}Hf$ initial	ε Hf	1σ error	T(DM) crustal
180256	1.2	1172	0.282094	0.000014	0.000735	0.02930	0.282078	1.4	0.5	1.91
	2.1	1152	0.282135	0.000015	0.000807	0.03836	0.282117	2.4	0.52	1.83
	3.1	1116	0.282120	0.000012	0.000523	0.02381	0.282109	1.3	0.4	1.88
	4.1	1145	0.282075	0.000016	0.000491	0.02201	0.282064	0.3	0.6	1.96
	5.1	1191	0.282034	0.000020	0.000546	0.02866	0.282022	-0.2	0.7	2.02
	7.1	1155	0.282181	0.000017	0.000805	0.04362	0.282163	4.1	0.6	1.73
	8.1	1151	0.282068	0.000024	0.000703	0.02427	0.282053	0.0	0.8	1.98
	9.1	1149	0.282125	0.000025	0.000619	0.03436	0.282112	2.1	0.9	1.85
	10.1	1154	0.282040	0.000075	0.000879	0.02774	0.282021	-1.0	2.6	2.05
	11.1	1204	0.282080	0.000010	0.000753	0.03491	0.282063	1.6	0.4	1.92
	12.1	1183	0.282104	0.000013	0.000503	0.02300	0.282093	2.2	0.5	1.87
	13.1	1115	0.282121	0.000018	0.001264	0.04612	0.282094	0.7	0.6	1.91
	14.1	1154	0.282118	0.000008	0.000670	0.03103	0.282103	1.9	0.3	1.86
	15.1	1207	0.282101	0.000009	0.000832	0.03986	0.282082	2.3	0.3	1.88
	16.1	1032	0.282102	0.000012	0.000598	0.02796	0.282090	-1.3	0.4	1.97
	17.1	1147	0.282072	0.000022	0.001042	0.03711	0.282049	-0.2	0.8	1.99
	18.1	1234	0.282125	0.000014	0.000732	0.01963	0.282108	3.9	0.5	1.80
	19.1	1096	0.282113	0.000015	0.000671	0.02798	0.282099	0.4	0.5	1.91
	20.1	1161	0.282111	0.000020	0.000821	0.02394	0.282093	1.7	0.7	1.88
	21.1	1084	0.282133	0.000014	0.000532	0.02308	0.282122	1.0	0.5	1.87
	24.1	1170	0.282097	0.000010	0.000571	0.02188	0.282084	1.6	0.4	1.90
	22.1	1187	0.282114	0.000015	0.000865	0.03964	0.282095	2.3	0.5	1.86
	25.1	1134	0.282071	0.000012	0.000652	0.02040	0.282057	-0.2	0.4	1.98
	26.1	1179	0.282042	0.000017	0.000772	0.02311	0.282025	-0.3	0.6	2.03
	27.1	1157	0.282092	0.000023	0.000722	0.02259	0.282076	1.0	0.8	1.92
	28.2	1132	0.282098	0.000023	0.000461	0.02065	0.282088	0.9	0.8	1.91
	29.1	1137	0.282100	0.000037	0.000596	0.02437	0.282087	0.9	1.3	1.91
	30.1	1119	0.282111	0.000011	0.000466	0.02061	0.282101	1.0	0.4	1.89
174558	1.1	1150	0.281995	0.000011	0.000376	0.01646	0.281987	-2.3	0.4	2.13
	2.1	1157	0.282012	0.000009	0.000497	0.02190	0.282001	-1.7	0.33	2.09
	3.1	1209	0.282003	0.000008	0.000462	0.02139	0.281992	-0.8	0.3	2.08
	4.1	1206	0.282013	0.000016	0.000635	0.01963	0.281999	-0.7	0.6	2.07
	6.1	1189	0.282027	0.000011	0.000386	0.01738	0.282018	-0.3	0.4	2.03
	7.1	1191	0.282034	0.000011	0.000428	0.01970	0.282024	-0.1	0.4	2.02
	7.2	1146	0.281992	0.000017	0.000400	0.01871	0.281983	-2.5	0.6	2.14
	8.1	1191	0.282044	0.000014	0.000763	0.02553	0.282027	0.0	0.5	2.01
	8.2	1183	0.281982	0.000018	0.000531	0.01787	0.281970	-2.2	0.6	2.15
	9.1	1174	0.282020	0.000016	0.000442	0.02202	0.282010	-0.9	0.6	2.06
	10.1	1148	0.282026	0.000015	0.000404	0.01782	0.282017	-1.3	0.5	2.06
	10.2	1203	0.282010	0.000011	0.000659	0.03107	0.281995	-0.8	0.4	2.08
	11.2	1207	0.282008	0.000015	0.000495	0.02342	0.281997	-0.7	0.5	2.07
	11.1	1203	0.282016	0.000012	0.000409	0.01858	0.282007	-0.4	0.4	2.05
	12.1	1188	0.282059	0.000012	0.000438	0.01921	0.282049	0.7	0.4	1.96
	12.2	1224	0.282001	0.000014	0.000468	0.02170	0.281990	-0.5	0.5	2.07
	13.2	1215	0.282016	0.000011	0.000458	0.01942	0.282006	-0.2	0.4	2.05
	14.1	1153	0.282001	0.000011	0.000445	0.01918	0.281991	-2.1	0.4	2.12
	14.2	1162	0.282012	0.000011	0.000560	0.01940	0.282000	-1.6	0.4	2.09
	15.1	1242	0.282016	0.000010	0.000524	0.02398	0.282004	0.3	0.3	2.03
	19.1	1168	0.282026	0.000014	0.000374	0.01713	0.282018	-0.8	0.5	2.05
	20.1	1217	0.282033	0.000010	0.000509	0.02556	0.282021	0.4	0.3	2.01
	20.2	1200	0.282026	0.000011	0.000559	0.02720	0.282013	-0.3	0.4	2.04
	24.1	1145	0.282004	0.000013	0.000389	0.01741	0.281996	-2.1	0.5	2.11
	25.1	1154	0.282017	0.000015	0.000585	0.01946	0.282004	-1.6	0.5	2.09
	26.2	1200	0.281985	0.000019	0.000568	0.02082	0.281972	-1.7	0.7	2.13
183496	1.1	1322	0.282070	0.000006	0.000900	0.03828	0.282048	3.7	0.2	1.88
	2.1	1330	0.282100	0.000016	0.000961	0.03050	0.282076	4.9	0.6	1.81
	3.1	1311	0.282059	0.000009	0.001055	0.04426	0.282033	2.9	0.3	1.92
	3.2	1168	0.282085	0.000011	0.000336	0.01189	0.282078	1.3	0.4	1.91
	4.1	1342	0.282088	0.000010	0.001050	0.03756	0.282061	4.6	0.3	1.84
	5.1	1315	0.282059	0.000009	0.000881	0.03684	0.282037	3.2	0.3	1.91
	7.1	1299	0.282061	0.000008	0.000753	0.03231	0.282043	3.0	0.0	1.91
	9.2	1306	0.282108	0.000009	0.000678	0.02815	0.282091	4.9	0.3	1.79
	11.1	1319	0.282035	0.000009	0.000622	0.02756	0.282020	2.6	0.3	1.95
	14.2	1344	0.282086	0.000011	0.000783	0.03580	0.282066	4.9	0.4	1.82
	15.1	1308	0.282044	0.000008	0.000549	0.01559	0.282030	2.8	0.3	1.93
	15.2	1177	0.282059	0.000011	0.000758	0.03202	0.282042	0.3	0.4	1.99
	16.1	1163	0.282086	0.000010	0.000375	0.01380	0.282078	1.2	0.3	1.92
	16.2	1321	0.282070	0.000009	0.000573	0.02351	0.282056	4.0	0.3	1.86
	16.3	1319	0.282067	0.000012	0.000733	0.03274	0.282049	3.7	0.4	1.88
	17.2	1336	0.282078	0.000008	0.000791	0.03447	0.282058	4.4	0.3	1.85

Appendix 5 (continued)

	Analysis no.	Age (Ma)	$^{176}Hf/^{177}Hf$	1 standard error	$^{176}Lu/^{177}Hf$	$^{176}Yb/^{177}Hf$	$^{176}Hf/^{177}Hf$ initial	ε Hf	1σ error	T(DM) crustal
183496 (cont.)	18.1	1230	0.282089	0.000012	0.000379	0.01652	0.282080	2.8	0.4	1.87
	18.2	1310	0.282064	0.000010	0.000818	0.03702	0.282044	3.3	0.3	1.90
	19.2	1359	0.282090	0.000008	0.000832	0.03688	0.282069	5.3	0.3	1.81
	20.1	1313	0.282062	0.000012	0.000776	0.03510	0.282043	3.3	0.4	1.90
	24.2	1311	0.282055	0.000007	0.000591	0.02366	0.282040	3.2	0.3	1.90
	25.2	1315	0.282065	0.000008	0.001063	0.04344	0.282039	3.2	0.3	1.91
	26.2	1307	0.282055	0.000008	0.000880	0.03652	0.282033	2.9	0.3	1.92
	27.1	1153	0.282133	0.000012	0.000503	0.01680	0.282122	2.5	0.4	1.82
	27.2	1354	0.282060	0.000010	0.000702	0.02900	0.282042	4.2	0.3	1.87
	30.1	1208	0.282076	0.000006	0.000361	0.01415	0.282068	1.9	0.2	1.91
	30.2	1355	0.282084	0.000009	0.001111	0.04800	0.282056	4.7	0.3	1.84
183509	2.1	1167	0.282107	0.000007	0.001349	0.06275	0.282077	1.3	0.2	1.92
	7.1	1199	0.282094	0.000009	0.000621	0.03268	0.282080	2.1	0.3	1.89
	8.1	1175	0.282114	0.000013	0.000807	0.04169	0.282096	2.1	0.5	1.87
	9.1	1157	0.282095	0.000008	0.000484	0.02460	0.282084	1.3	0.3	1.91
	11.1	1166	0.282020	0.000013	0.000850	0.02652	0.282001	-1.5	0.5	2.09
	13.1	1169	0.282083	0.000006	0.000530	0.02106	0.282071	1.1	0.2	1.93
	15.1	1124	0.282094	0.000007	0.000445	0.02072	0.282085	0.6	0.3	1.93
	16.1	1165	0.282081	0.000009	0.001197	0.05718	0.282055	0.4	0.3	1.97
	18.1	1183	0.282082	0.000009	0.000183	0.00933	0.282078	1.7	0.3	1.90
	21.1	1163	0.282105	0.000009	0.001490	0.07257	0.282072	1.0	0.3	1.93
	22.1	1114	0.281905	0.000009	0.000378	0.01721	0.281897	-6.3	0.3	2.35
	26.1	1170	0.282089	0.000011	0.000452	0.02399	0.282079	1.4	0.4	1.91
	28.1	1098	0.282072	0.000016	0.000941	0.03060	0.282053	-1.2	0.6	2.02
185339	3.1	1221	0.282043	0.000009	0.001105	0.05949	0.282018	0.4	0.3	2.01
	12.1	1220	0.282022	0.000007	0.000363	0.01684	0.282014	0.2	0.2	2.02
	14.1	1189	0.282059	0.000010	0.000698	0.03031	0.282043	0.6	0.3	1.98
	16.1	1222	0.282073	0.000015	0.000960	0.03597	0.282051	1.6	0.5	1.94
	18.1	1227	0.282042	0.000012	0.001671	0.08158	0.282003	0.0	0.4	2.04
	21.1	1223	0.282037	0.000013	0.001118	0.03335	0.282011	0.2	0.5	2.03
	23.1	1204	0.282046	0.000008	0.000410	0.01978	0.282037	0.7	0.3	1.98
	40.1	1191	0.282056	0.000012	0.000704	0.03597	0.282040	0.5	0.4	1.98
	45.1	1195	0.282035	0.000011	0.000687	0.03498	0.282020	-0.2	0.4	2.03
	9.1	1286	0.282077	0.000011	0.000866	0.03698	0.282056	3.2	0.4	1.88
	11.1	1303	0.282088	0.000011	0.000858	0.04226	0.282067	4.0	0.4	1.85
	20.1	1342	0.282067	0.000009	0.000556	0.02777	0.282053	4.3	0.3	1.85
	31.1	1296	0.282103	0.000012	0.001020	0.04845	0.282078	4.2	0.4	1.83
	36.1	1303	0.282052	0.000010	0.000738	0.03883	0.282034	2.8	0.3	1.92

The report outlines the felsic rocks of the west Musgrave Province that were formed and metamorphosed during several distinct events within the late Mesoproterozoic; including the 1345–1293 Ma Mount West Orogeny (Wankanki Supersuite), the 1220–1150 Ma Musgrave Orogeny (Pitjantjatjara Supersuite), and the >1078–1026 Ma Giles Event (Warakurna Supersuite). The felsic rocks were derived from similar and regionally homogeneous sources but the compositions of granites from each supersuite differ significantly. Different geographical distribution patterns for these supersuites are also consistent with the recent subdivision of the Musgrave Province, in Western Australia (i.e. the west Musgrave Province), into three zones; the Walpa Pulka Zone, Mamutjarra Zone, and the Tjuni Purlka Tectonic Zone.

Smithies, et al.

Geochemistry, Geochronology, and Petrogenesis of Mesoproterozoic Felsic Rocks in the West Musgrave Province, Central Australia, and implications for the Mesoproterozoic Tectonic evolution of the region

REPORT 106

Further details of geological publications and maps produced by the Geological Survey of Western Australia are available from:

Information Centre
Department of Mines and Petroleum
100 Plain Street
East Perth, WA 6004
Phone: (08) 9222 3459 Fax: (08) 9222 3444

www.dmp.wa.gov.au/GSWApublications